NUREG/CR-1631

Lateral Loads on Vent Pipe in Steam Chugging

Prepared by I. Catton, C. K. Chan, V. K. Dhir, T. Risch

School of Engineering and Applied Science
University of California, Los Angeles

Prepared for
U.S. Nuclear Regulatory
Commission

Available from

GPO Sales Program
Division of Technical Information and Document Control
U. S. Nuclear Regulatory Commission
Washington, D. C. 20555

Printed copy price: $5.00

and

National Technical Information Service
Springfield, Virginia 22161

NUREG/CR-1631

Lateral Loads on Vent Pipe in Steam Chugging

Manuscript Completed: December 1979
Date Published: August 1980

Prepared by
I. Catton, C. K. Chan, V. K. Dhir, T. Risch

School of Engineering and Applied Science
University of California, Los Angeles
Los Angeles, CA 90024

Prepared for
Division of Reactor Safety Research
Office of Nuclear Regulatory Research
U.S. Nuclear Regulatory Commission
Washington, D.C. 20555
NRC FIN No. B5875

Abstract

The quasi-steady injection of steam into a pool of subcooled water was investigated. The resulting phenomenon was studied with emphasis on structural loading on the steam downcommer. From experimental data at a single steam mass flux it was found that pressure pulsations in the pool were temperature dependent. At low pool temperatures pressure pulsations were found to have high magnitudes and occur at low frequencies. At higher pool temperatures smaller, high frequency pressure pulses were observed.

Three types of pressure pulsations were observed to occur within the pool. Pressure pulsations from 1) bubble growth and bubble shape changes 2) bubble collapse and 3) water slug movement within the downcommer were observed and recorded. Loadings on the steam downcommer were seen to be influenced only by bubble collapse and the magnitudes were independent of pool temperature.

Executive Summary

The dynamic forces experienced on a vent pipe inside a BWR pressure suppression pool during the steam injection portion of a LOCA were examined. Saturated steam was allowed to flow in a quasi-steady manner into a pool of water at different temperatures. Based on experimental data at a single mass flux it was determined that the frequency of loading on the downcommer was dependent on the pool temperature. At low pool temperatures (53°C) pressure loading was characterized by large pressure peaks with a low frequency while at high pool temperatures, smaller high frequency pressure pulse were observed. The magnitude of the loading on the downcommer was found to be independent of pool temperature.

From the experimental movies it was found that pressure forces could be classified into three categories 1) due to the change of bubble shape 2) due to bubble collapse and 3) due to water slug movement within the downcommer. Lateral loading on the downcommer was seen only to be significantly dependent on the bubble collapse.

TABLE OF CONTENTS

List of Figures

List of Figures (Con't.)

List of Figures (Con't.)

List of Figures (Con't.)

List of Figures (Con't.)

List of Tables

Preface

This report was prepared as an account of work sponsored by the United States Government. Neither the United States nor the United States Nuclear Regulatory Commission, nor any of their employees, nor the University of California or their employees, makes any warranty, express or implied, or assumes any legal liability or responsibility for the accuracy, completeness, or usefulness of any information, apparatus, product or process disclosed, or represents that its use would not infringe privately owned rights.

Acknowledgments

The support by the U. S. Nuclear Regulatory Commission through contract No. AT(48-24)-0342 is gratefully acknowledged.

1. INTRODUCTION

The Boiling Water Reactor (BWR) systems have been designed with a pressure suppression containment or wet well to condense any steam released in the dry well during a Loss of Coolant Accident (LOCA) Fig. 1.1. In addition the pressure suppression containment acts as a heat sink for Hot Standby and Relief Valve Operation and provides a source of water for the Emergency Core Cooling. Because of these critical functions, the integrity of the suppression pool is essential from the view of public safety. Recent experimental tests and analyses have revealed potential dynamic loadings onto the containment structure during the LOCA transient [1].

At the onset of a LOCA, the pressure rise in the drywell pushes the water initially standing in the vent pipe into the wet well. The vent clearing is followed by the air-stream mixture. The steam portion is condensed leaving the air which is initially at drywell pressure to expand and to rise up in the pool. The dynamics of the air transients have been extensively reported [1,2,3,4,5]. This report focuses on the dynamical forces during the later period of the accident, when the steam flow is decreasing and the water can re-enter the vent pipe and condense the remaining steam inside the pipe. This phenomenon, known as steam chugging, can impose forces onto the downcommer pipe and the containment structure. Non-axisymmetric steam condensation at the exit can also impose a lateral loading on the downcommer.

This report presents the results of laboratory scaled tests conducted at UCLA to study the lateral loading on the downcommer during steam chugging. The main objectives of these tests are 1) to better understand the effects of pool subcooling on lateral loading and 2) to examine whether there is a directional preference of loadings produced by bubble collapses at the pipe exit.

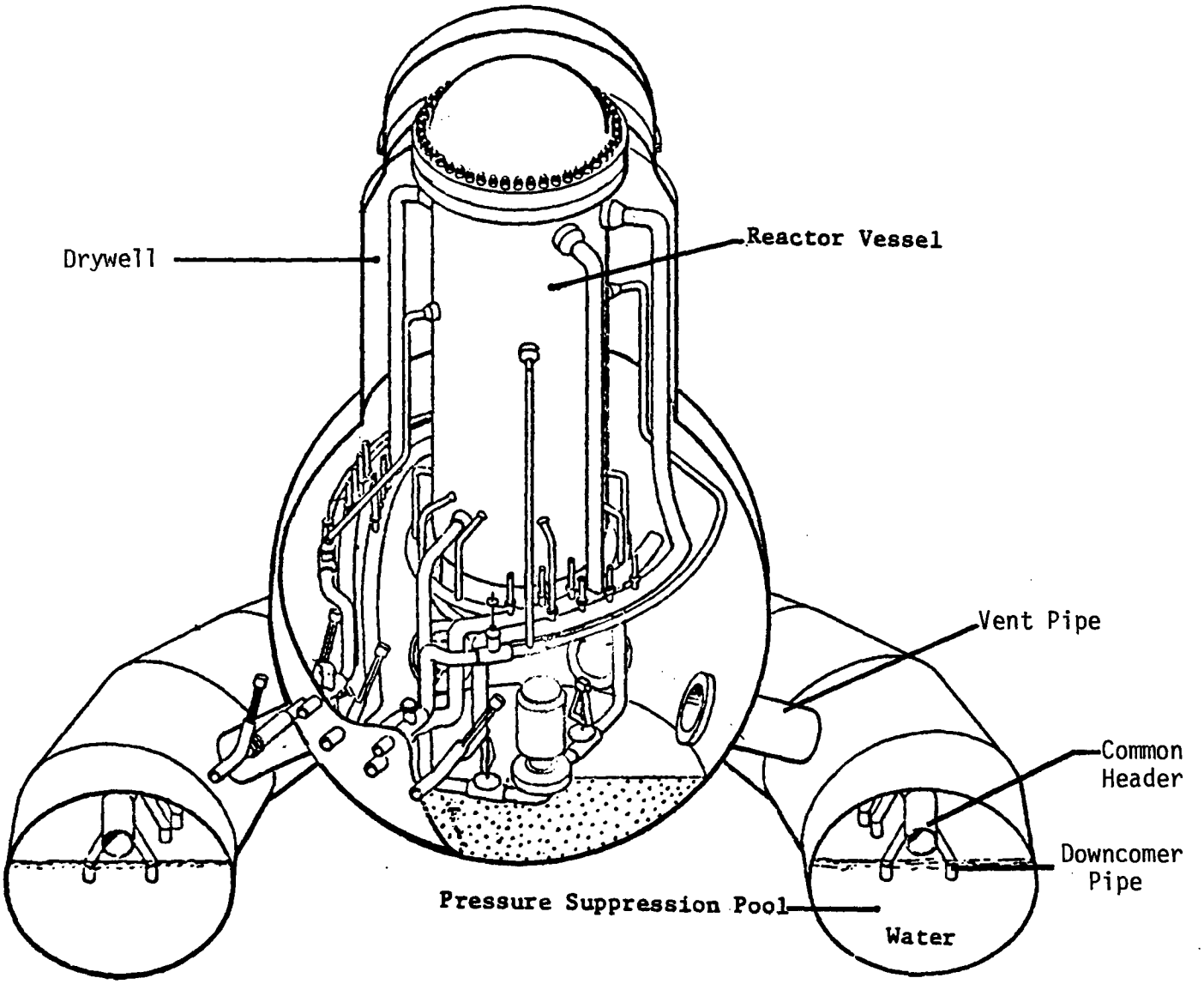

Figure 1.1 BWR Mark-I Primary Containment

The test basically involves the injection of saturated steam vertically into a pool of subcooled water under controlled conditions.

Detailed experimental procedure is presented in section 2 and the results of the tests are discussed in section 3.

2. APPARATUS AND PROCEDURE

2.1 Apparatus

The primary function of the system is to allow controlled verticle injection of steam into subcooled water at varying subcooling levels. The major components of the system consist of a steam supply loop, suppression test chamber, and verticle steam injection tube.

2.1.1 Main Steam Supply

A schematic diagram of the system arrangement is shown in Fig. 2.1 and photographs of some major system components are illustrated in Figs. 2.2 and 2.3. The steam supply loop is a closed loop, recyclable system in which the main components consist of a boiler, superheater, and surge tank. Every component of the main steam channel is either lined or constructed from 304 stainless steel in order to inhibit corrosion. The central component of the steam supply system is a 220V, 17kw, three phase Chromalox boiler. The boiler has a maximum steam generation rate of 7.56 gm/sec. Saturated steam exits from the boiler and flows through a 1.5kw Chromalox superheater, where its temperature increased to a maximum of 200° C. After exiting from the superheater the steam flows through a 1.0 m horizontal section of 5.1 cm diameter pipe which contains an isolation solenoid valve (V1). Downstream of the valve the steam channel makes a 90° band upward into a 1.5 m verticle 5.1cm diameter pipe. The channel then makes two short 90° bends before the steam exits vertically downward into the 0.044 m^3 surge tank shown in Fig. 2.4. The surge tank performs dual function: as a damping capacitor for spurious pressure transients in the boiler and as an accumulator of steam at high pressures. The surge tank is capable of supporting pressures as high as 1185 Kpa. Under control of second solenoid valve downstream of the surgetank, supply steam flows through a 2 m section of horizontal pipe. One 90° bend directs the steam vertically downward where it converges into

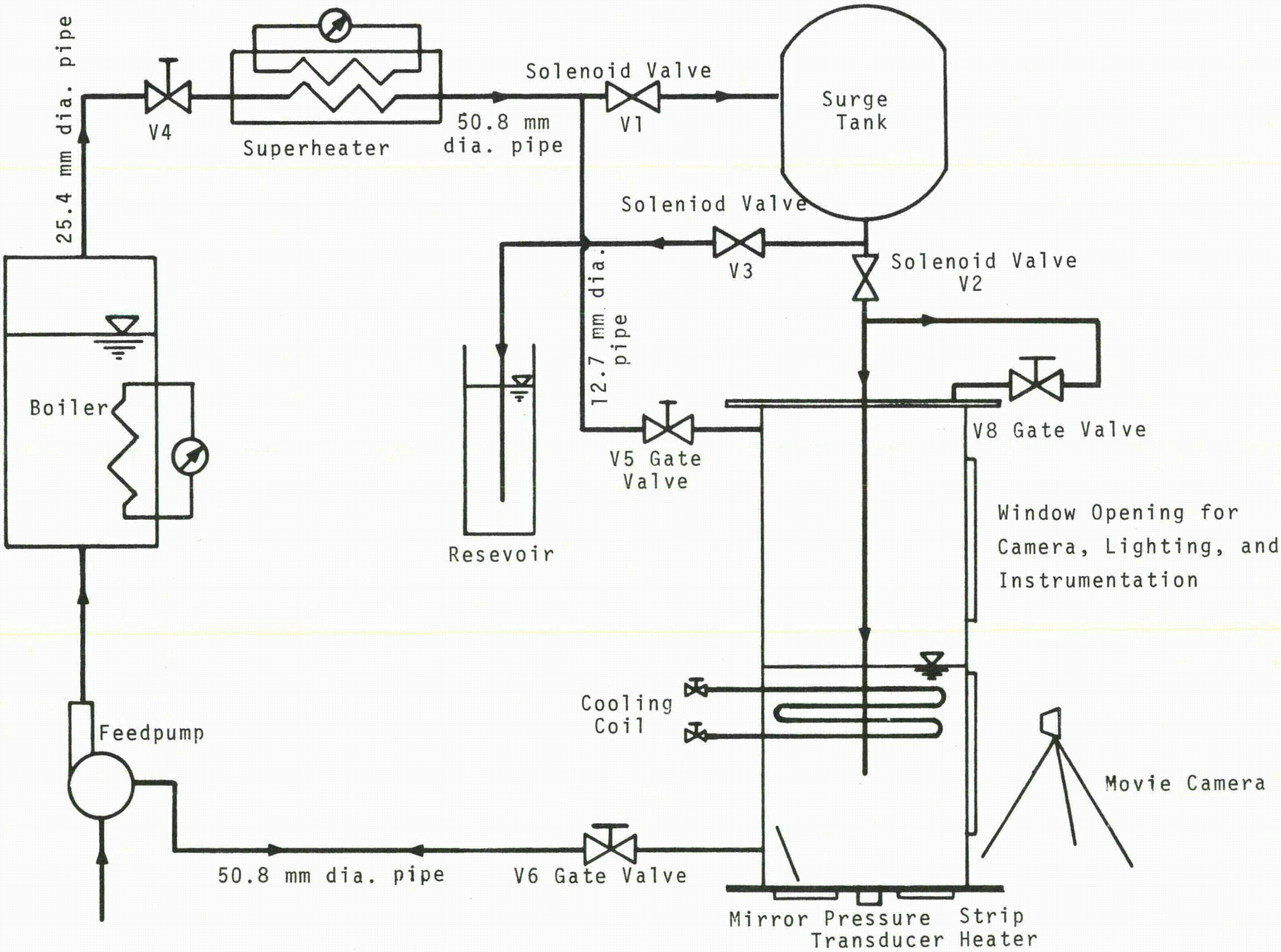

Figure 2.1 Steam Injection System

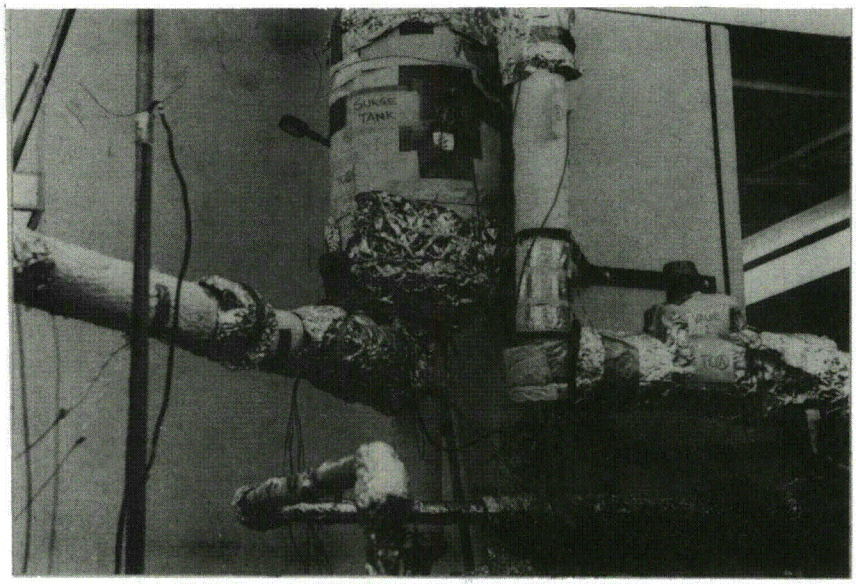

Figure 2.2 Surge Tank and Steam Supply Line

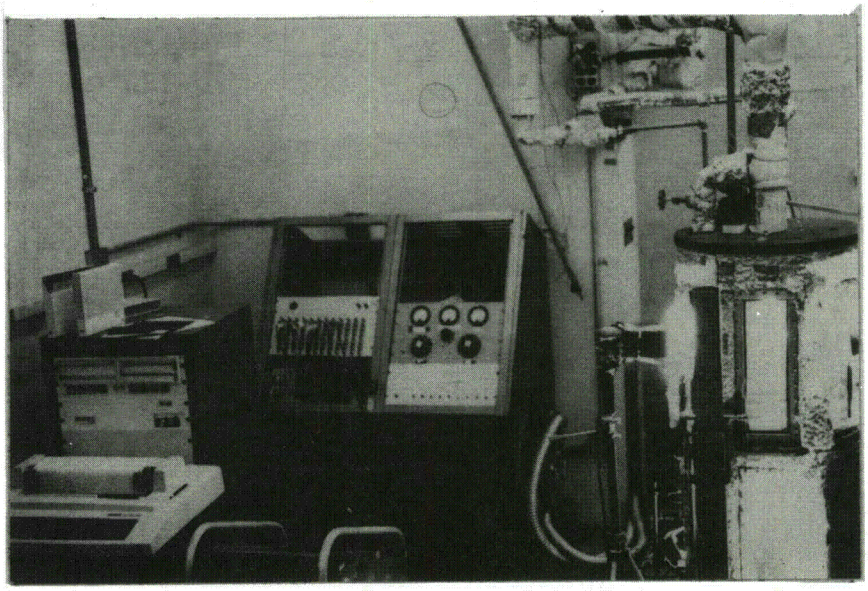

Figure 2.3 Test Chamber, Computer, and Operator's Console

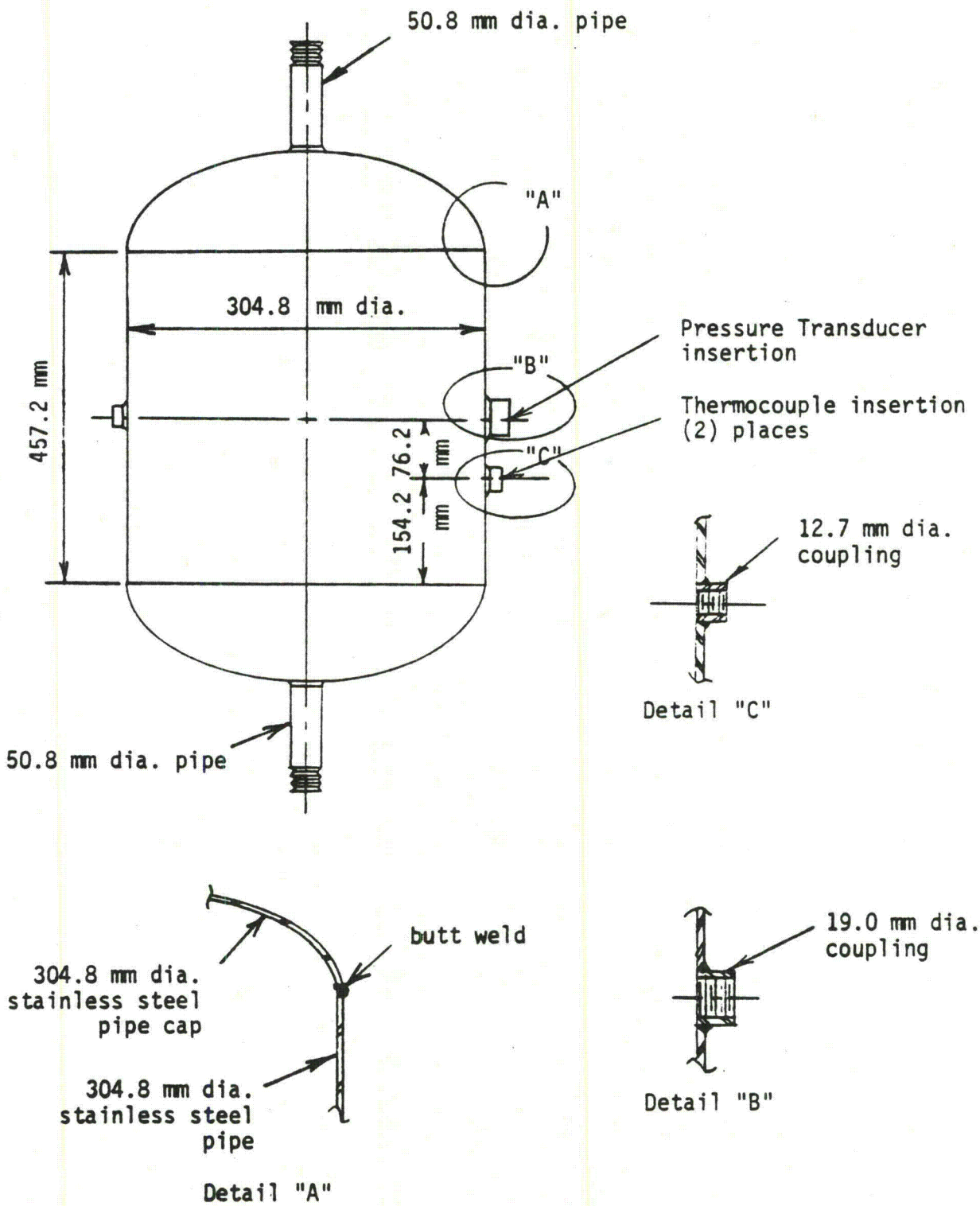

Figure 2.4 Surge Tank

a 5 cm tubing downcommer.Steam flows through the downcommer and is injected into the test chamber completing the main system circuit.

To prevent condensation in the main steam circuit the entire main steam channel is kept at an elevated temperature. Steam pipes are wrapped with electrical heating tape and 2.5 cm fiberglass insulation. High pipe wall temperatures are therefore achieved.

2.1.2 Test Chamber

The suppression test chamber consists of two hexagonal sections, one stacked on top of the other and is symmetrical about the center injection tube. As illustrated in Fig. 2.5 each section has a cross-sectional flat-to-flat dimension of 457 mm and a height of 602 mm. Each flat surface of the hexagon has a 101 mm x 229 mm opening for either windows or steel plates. A photograph of the test chamber is shown in Fig. 2.6. The windows allow visual observation of the phenomenon under study and permit photographic recording. The steel plates serve as mounting supports for insertion of various measuring devices. The temperature of the water located in the test section is controlled by eight electrically strip heaters and a single cooling coil. The strip heaters are located on the underside of the test chamber while the cooling coil is attached to the inside surface of the hexagon and mounted in the center. The coil consists of four turns of 50 mm pitch, 12.7 mm stainless steel tubing. Coolant is circulated through the tubing via an external pump. Two bottom ports on the hexagon connect the test chamber to a fresh water supply line and to a drain located on the bottom of the chamber directly in the center is a pressure transducer which transmits pressure variations in the pool.

2.1.3 Injection Tube

The steam injection tube is located in the center of the test section

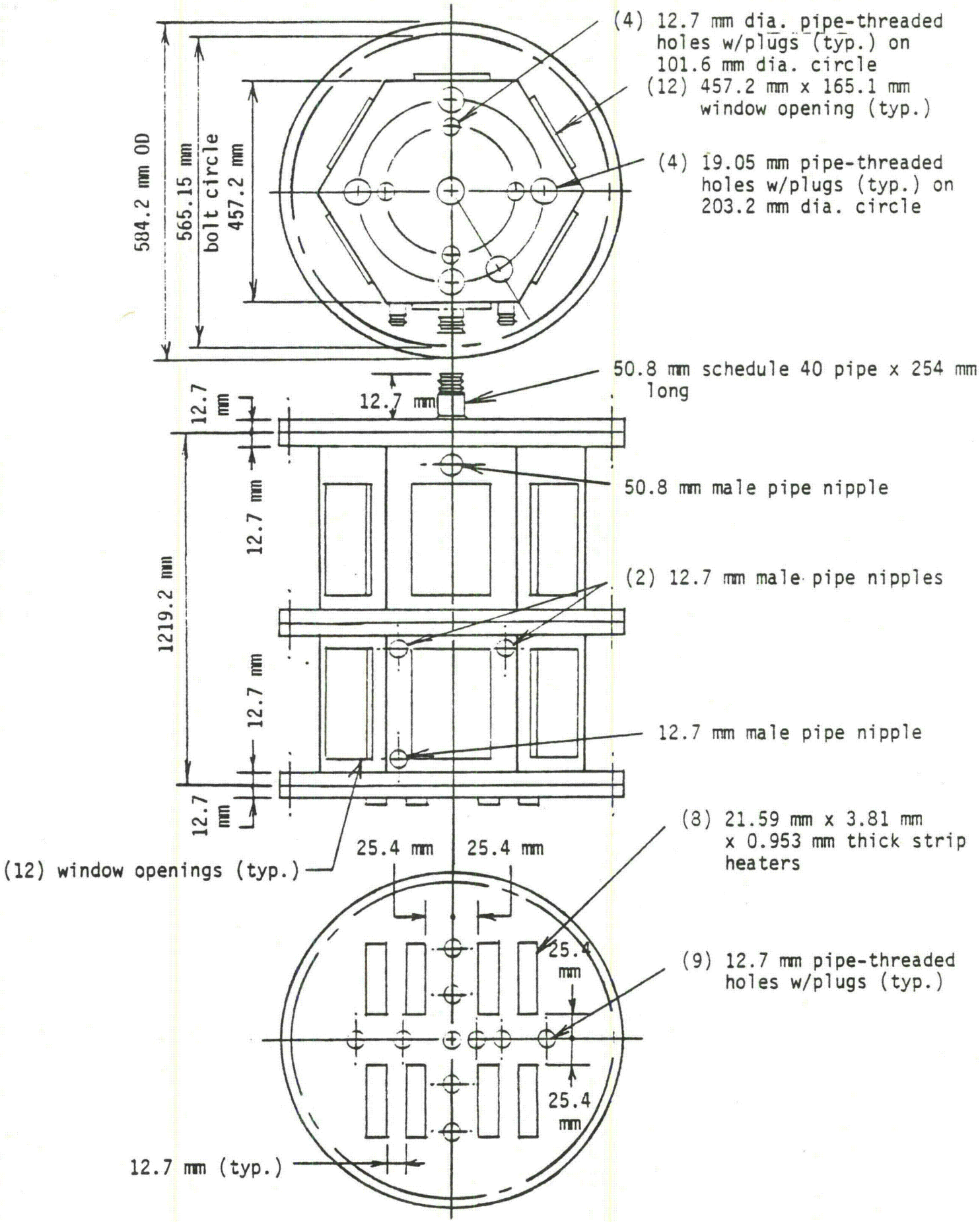

Figure 2.5 Test Chamber Dimensions

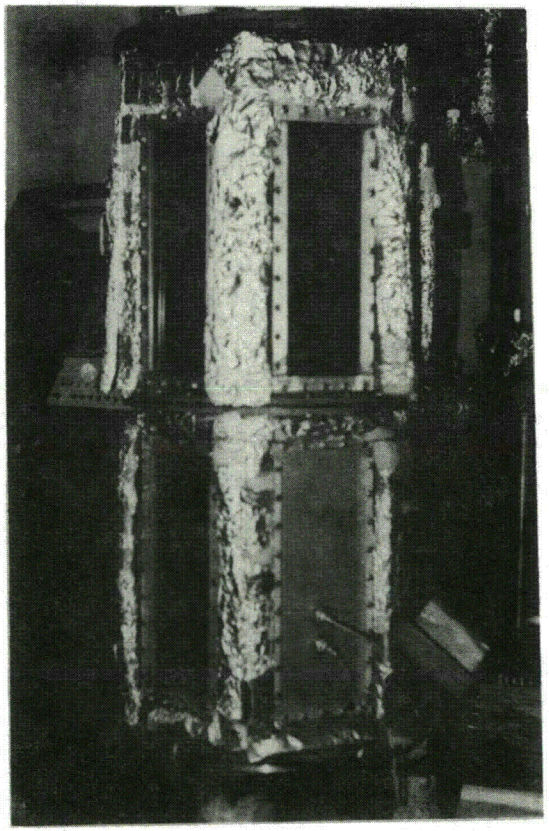

Figure 2.6
Test Chamber

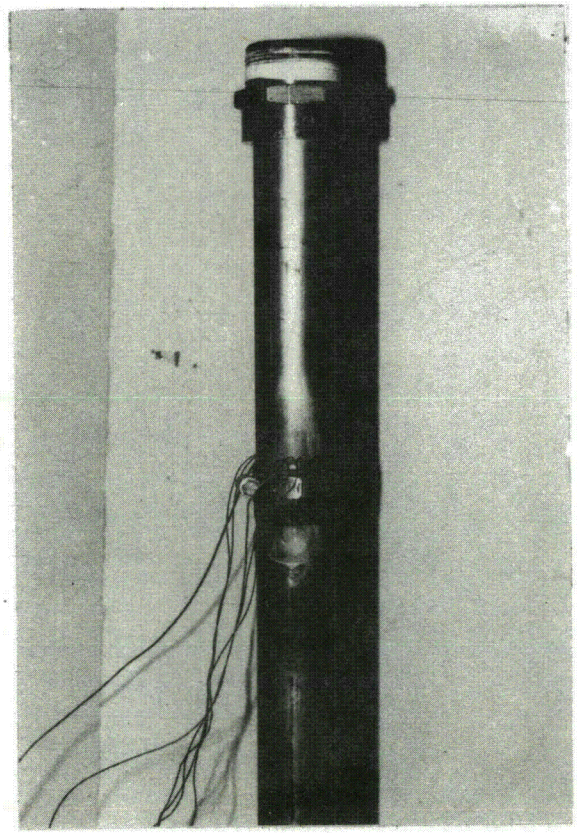

Figure 2.7
Injection Tube

supported vertically from the top. A photograph of the injection tube is shown in Fig. 2.7 and an illustration of the injection tube inside the test chamber is shown in Fig. 2.8. The tube is a 855 cm long section of thin walled 304 stainless tubing, with an outside diameter of 50.8 mm and an inside diameter of 47.5 mm (1.65 mm wall). Welded to one end of the tubing is a standard two inch pipe reducer which permits threaded connection to the steam supply line entering the test chamber from the top. The tube is fastened tightly to the steam supply coupling and to assure rigidity is horizontally supported by three metal crossmembers. The crossmembers are braced tightly against the test section sides and converge on the tube near the top. The tube is left unsupported at the exit and hence can be modelled as a simply supported cantilever beam.

The tube extends down through the test chamber into the water pool. The tube exit is submerged 25.4 cm from the pool surface and is 25.4 cm from the pool bottom. Located 25.4 cm from the mounting section on the tube are two vertically aligned strain gauges, mounted at right angles to each other. Also located near each gauge is a single Chromel Alumel thermocouple.

2.1.4 Auxiliary Mechanical Support Systems

The majority of electromechanical components of the system are operated by controls that are centralized on an operators console and remotely situated from the system hardware. Meters and signal lamps on the console indicate boiler power, tape heater power and the operating status of pumps and valves.

Supporting the main steam generation and control, auxiliary systems are needed to recycle feedwater to the boiler, discharge and recirculate water in the test chamber, and discharge unwanted steam pressure. The feedwater system consists of a 0.75kw high pressure pump with a flow capacity

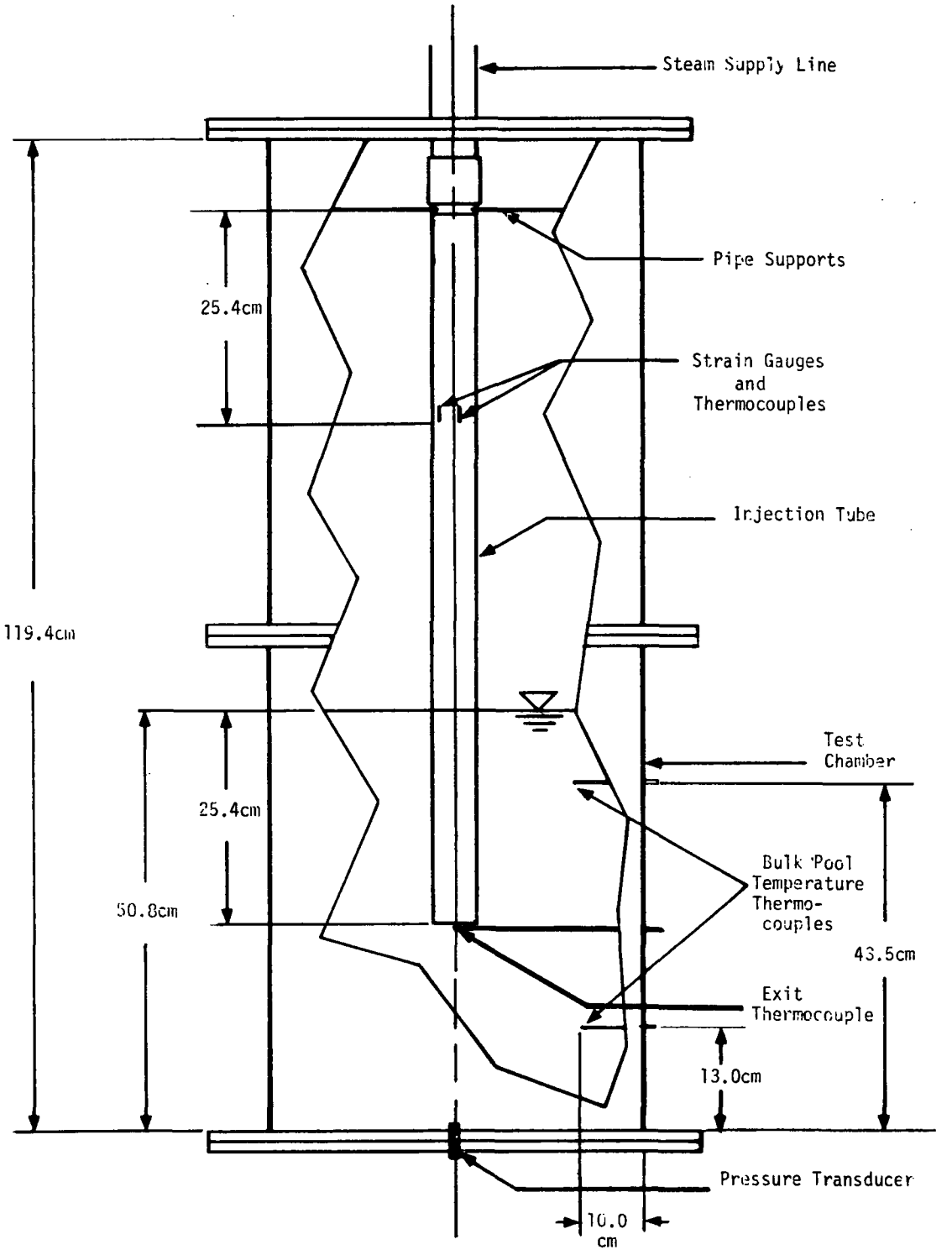

Figure 2.8 Instrumentation Locations Inside Test Chamber

of 7.56 ml/sec mounted in a 1.27 cm diameter water line between the chamber and boiler. The pump draws suction from either the test chamber or an external source of demineralized water. Manually operated valves are capable of isolating the feedwater section from the system when desired. An auxiliary vapor injection system consists of a 1.27 cm steam line connecting the surge tank to a standby water resevoir. A third solenoid valve controls steam flow in the 1.27 cm diameter line for the dumping of unwanted steam during normal operation and emergencies. A 1.1kw pump is designed into a network of valves and plumbing to provide circulation for the cooling coil. The pump is also capable of transferring water between the test chamber and resevoir and providing drainage for the test chamber.

2.1.5 Data Acquisition System

High speed movie photography and digital samplings of instrumentation signals comprise the complimentary techniques of data acquisition used in the experiments.

The central component of photographic equipment is a Red Lake, high speed 100 ft. film movie camera with a variable frame rate up to 3000 frames/sec. Additional photographic equipment includes 1.0kw high intensity lighting fixtures, a film speed controller, and an internal strobe film timing device and a signal lamp that is triggered by activating the data acquisition system.

Also incorporated into the photographic recording technique is a mirror located inside the test chamber below the vent exit. The mirror is oriented such that within the field two separate views were recorded. Fig. 2.9 illustrates the mirror placement inside the test chamber. The high speed camera is placed horizontally level with the injection tube exit. The camera directly records the front of the steam bubble and also, through the reflection in

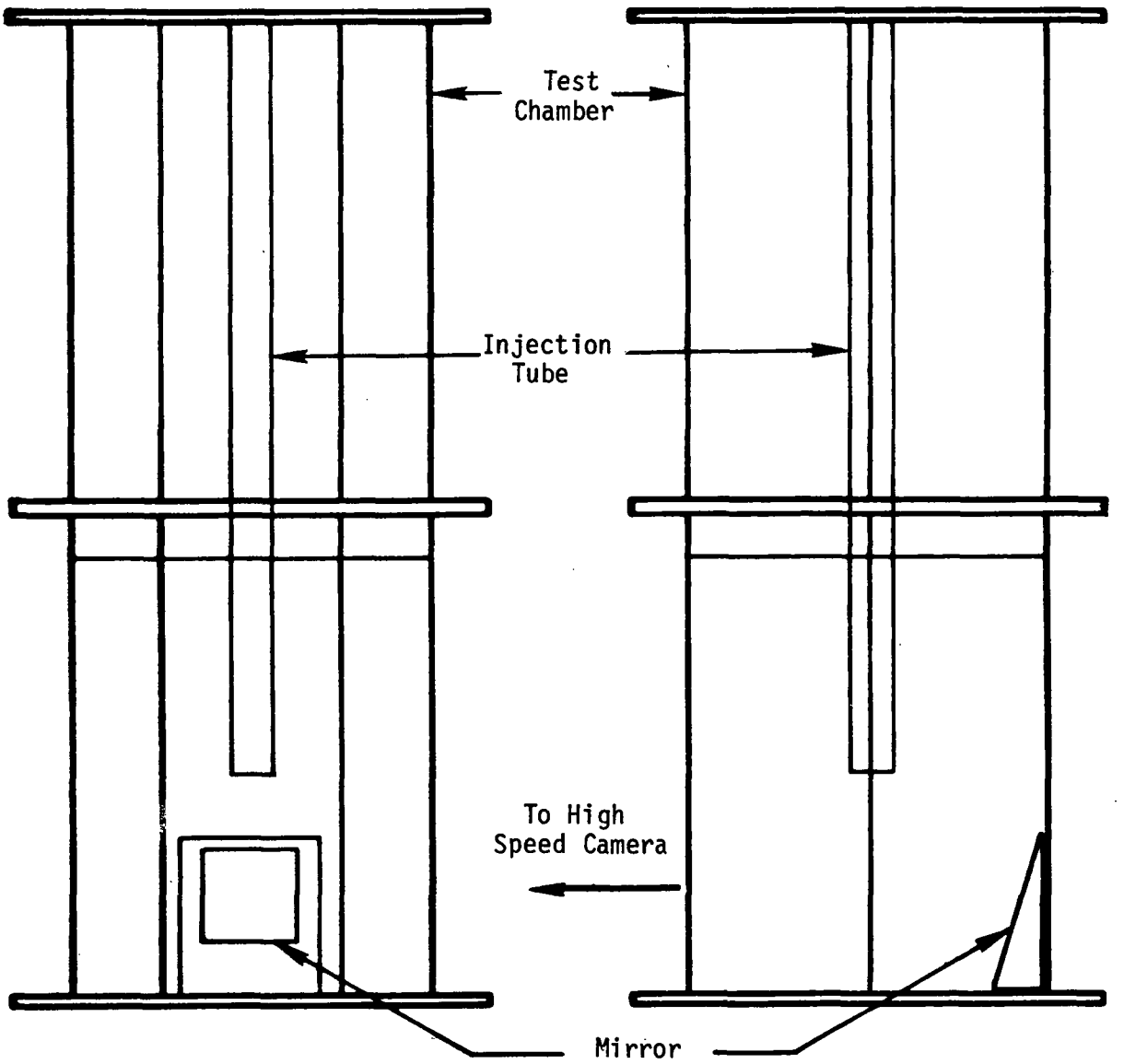

Figure 2.9 Photographic Mirror Placement
Within Test Chamber

the mirror, simultaneously captures the back underside view. From this it is possible to determine whether radial symmetry of the steam bubble exists around the injection tube exit.

The digital sampling system consists of a sixteen channel, 1000 gain amplifier bank, sixteen channels of analog-digital/(A-D) converters, and a LSI-11 microcomputer which monitors the sampling process via user written software. The arrangement of signal input to the digitizing system is optional. Any number of the sixteen A-D channels operate simultaneously as specified by the user. The maximum sample frequency of the A-D converter is 10^4 sec^{-1}. The maximum storage capacity of the computer memory is 9000 independent digital samples divisible between any number of the sixteen signal channels. The signal acceptance criterion of the A-D converter is a $\pm$ 10V range.

Digital numbers corresponding to this voltage range are stored in raw form in the computer memory with values between 0-4096. The discretization of the input signals is therefore on the order of 5mV steps. The purpose of the signal amplification stage is to avoid losses in resolution of the low-level instrument signals.

2.1.6 Instrumentation

A diagram of system instrumentation points is shown in Fig. 2.8. Pertinent system variables measured in the experiment include transient pressure and temperature variations and dynamic loadings. Instrumentation therefore consists of devices capable of measuring such system variations. Semiconductor strain gauges, Statham pressure transducers, and standard thermocouple wire are used in the experimental procedure.

Transient pressure measurements are accomplished by using Statham, unbonded, differential pressure transducers. Model PL 131TC in two pressure

ranges is used: one in a 0-100 psid range of natural frequency 11,000 Hz the other in a 0-15 psid range with natural frequency of 6000 Hz. The stated accuracy of the transducer is $\pm$ 0.75% of the full-scale reading. The pressure transducer is mounted directly below the vent exit on the bottom of the pool. Pool pressure variations caused by the chugging phenomenon are recorded by the transducer.

Five thermocouples are positioned in strategic positions throughout the test chamber. Directly below the vent exit a single 25.4 μm diameter Chromel-Alumel junction is horizontally mounted through a port from the side of the test chamber. The response time of this thermocouple is on the order of 4.5 msec. Situated near each strain gauge, in direct contact with the outside surface of the pipe, is a thermocouple designed to measure the strain gauge temperature. There are also two other thermocouples protruding through sealed ports in the side of the chamber to measure the bulk pool water temperature. Two thermocouples are mounted 13 cm and 43 cm from the bottom of the chamber and are extended inward into the pool by approximately 10 cm.

Two BLH self temperature compensating semiconductor strain gauges are mounted vertically on the steam injection tube 25.4 cm from the top. The gauges themselves are mounted at right angles to each other on the outside surface of the tube. Placement of the gauges in this manner allows the direction of the tube deflection to be determined if only pure bending of the tube is considered.

A single component, highly nonconductive, polymide adhesive bonds the strain gauges firmly to the tube. The adhesive is capable of withstanding temperatures greater than 375°C and is resistant to both water and steam. Two thin wire cables are soldered to each gauge. The wires pass up through the test section and exit at the top where they connect to a single shielded

cable. To insure high reliability each strain gauge and thermocouple is covered with a thin layer of silicon sealer which provides an impermeable layer to moisture.

All low level instrument signals are transmitted by a shielded cable to a reception panel on the operators console. From there the signals are routed to the amplification stage of the digital sampling system. Pressure transducers and thermocouples are self contained instruments. Their signal is amplified and recorded directly by the digital sampling system. Strain gauges, however, are interfaced into the sampling system via external fully active bridges constructed especially for this purpose.

2.2.1 Experimental Procedure

Before any experimental test, the air present in the system was eliminated by steam purging while the air dissolved in the water was eliminated by heaters.

First the air initially in the system was driven out by the steam generated in the boiler. This was achieved by turning on the boiler until it reaches steady state. Then valves V4, V1, and V3 were opened and valve V2 was closed. The air-steam mixture was discharged into the steam resevoir. Subsequently, valve V5 was opened so that the air initially in the pipe was driven into the test chamber atmosphere. Finally the air initially in the vent pipe was driven into the pool by turning on valve V2 and turning off valves V3 and V5. Actuation of valve V6 allowed water to flow into the test chamber. By turning on the test chamber heater, the air initially dissolved in the water could be purged. Air was prevented from being re-absorbed into the water by maintaining a steady steam flow over the water surface through the line controlled by valve V5. This process was continued long enough to insure that all of the dissolved air was driven out of the water.

At the end of the degas process, valve V2 was closed so that no more steam was injected into the pool. Then, after the surge tank reached the desired pressure valve V1 was closed and the boiler was adjusted to a lower power level to maintain a small steam generation rate. The pool was allowed to sit while the bottom heaters were turned off and cold water was allowed to run through the cooling coil to reduce the pool temperature to the desired subcooling. Steam generated in the boiler was continuously fed into the test section over the pool surface to keep the test section's pressure above atmospheric pressure for the prevention of a backflow of air into the test section.

After the pool temperature reached the desired temperature by the use of either the cooling coil or the heater, the camera and the data acquisition were placed in standby mode. Steam was injected into the pool by varying power to the boiler until a steady state flow of 5.0 kg/m^2-sec was achieved. The high speed movie camera was started. Then with a manually operated control switch the data acquisition system and a signal lamp placed within view of the camera were activated simultaneously. Appearance of the signal lamp on the photo-film marked the onset of data collection by the LSI-11. Cross correspondence between the data and movies was therefore achieved.

Each run is 5.625 sec. long and consists of 4 channels of 2250 data points. The interval of each sample is therefore 2.5 ms. In all tests the pool water level was 50.8 cm which corresponds to a submergence depth of 25.4 cm.

A total of eight separate tests were performed at four levels of pool subcooling ranging from 53°C to 74°C. Two independent sets of data were obtained. To test the directional response of the pipe the two sets of runs correspond to a radial rotation of the pipe by 90°. Ambient conditions

remain the same for each run with the pressure inside the test chamber atmospheric.

2.2.2 Data Acquisition Procedure

Prior to injection of steam, the data acquisition system was calibrated, zero- referenced, and programmed for the upcoming experimental event. To calibrate the digital sampling system, a standard 1mV square wave signal was amplified into the 1V range, and recorded by each channel of the A-D converter. A 1mV amplitude was chosen for its order of magnitude relation to actual instrumentation signal amplitudes. The peak values of the amplified square wave signal were recorded by the converter and differenced by the computer, creating an internal data scale factor for future experimental records of each channel. To complete the calibration excercise, samples of the instrument outputs were taken at known reference values, (e.g., 0° or 0 psid). Computer numbers corresponding to the real reference values, provide a computer recognized reference for future data reduction.

After calibrating the digitizing channels, the preliminary stage of a sampling software program was run to specify the sample frequency, number of signal channels, and the total number of discretized data points for the experiment. The sampling system was then put into a standby mode until a manually operated switch was used to actuate the sampling event.

From preliminary test movies which were made to test the lighting arrangement in the subject area, it was found that optimal results were achieved with large camera lens aperature openings and low to moderate levels of external lighting. It was found in some cases that excessive external lighting was being dispersed in the liquid pool, producing a loss of contrast in the image. Hence the camera was positioned approximately 0.5 meters from the vent exit, the aperature was set at f2.8, and two high intensity

lamps were used for direct and background lighting.

2.2.3 Data Reduction from Data Acquisition System

One of the advantages of a digital sampling system is the flexibility that it has in the data reduction process. Once raw data is stored in files of software devices, the task of converting them into a useful form can usually be accomplished quickly by additional computer software. Two data reduction programs have been written for the present work. The first is a conversion routine which manipulates raw computer records into units of interest, like temperature, pressure and strain. All three devices used in the experiment respond linearly to system changes. Correlation factors for the instruments are incorporated into the software, along with the reference samples and calibration factors established at run time. The calibration factors are used to convert computer records back into voltage values, and useful data are then calculated. A second program has been written to interface with the digital-analog (D-A) function of the converter. After specifying several parameters for the program control, digital reproductions of the original analog signals are output by the converter. The output frequency can be different from the original sample frequency allowing expansion of the event timescale. The signal reproductions are used as inputs to oscilloscopes and X-Y plotters, to create graphic representation of the results.

2.2.4 Data Reduction from High Speed Movies

The purpose of high speed movies is to correlate interfacial motion of the steam bubble with numerical data obtained from the data acquisition system. Interfacial movements were analyzed by projecting the image on a screen. Each portion of interest was divided into a suitable number of time steps. A tracing of the interfacial outline was acquired at each step from the movie. As mentioned before, an internal strobe device in the camera

marked real time intervals of 0.1 sec on the film. Along with projector equipment implemented with frame counters the exact time for each frame could be dtermined. Some reduced movie data showing bubble interfacial history as a function of time is shown in Fig. 3.99 and 3.100.

3.1 Lateral Load Experimental Results

This section presents the data obtained from the lateral load experiments preformed. A total of eight sets of experiments at four pool subcoolings (53.3°C, 57.2°C, 67.2°, and 73.9°C) are presented. Two distinct groups of experiments were performed each having four runs at each of the pool subcodings previously mentioned. The experiments were performed at a single mass flux of 5.0 kg/m^2sec. while the pool temperature was varied between 53° and 74°C.

The two groups of experiments correspond to the two orientations of the injection tube as shown in Figs. 3.1 and 3.2. A summary of each experiment and its corresponding test conditions are presented in Table 3.1

Run	Bulk Pool Temperature (°C)	Steam Generation Rate at Boiler g/sec	Strain Gauge Orientation (° from N)	
			Gauge #1	Gauge #2
A1	53.3	5.7	13.5	103.5
A2	57.2	5.7	13.5	103.5
A3	67.2	5.7	13.5	103.5
A4	73.9	5.7	13.5	103.5
B1	53.3	5.7	103.5	193.5
B2	57.2	5.7	103.5	193.5
B3	67.2	5.7	103.5	193.5
B4	73.9		103.5	193.5

Ambient Conditions: Pressure at Pool Surface 101.325 kPa

Table 3.1 Experimental Conditions

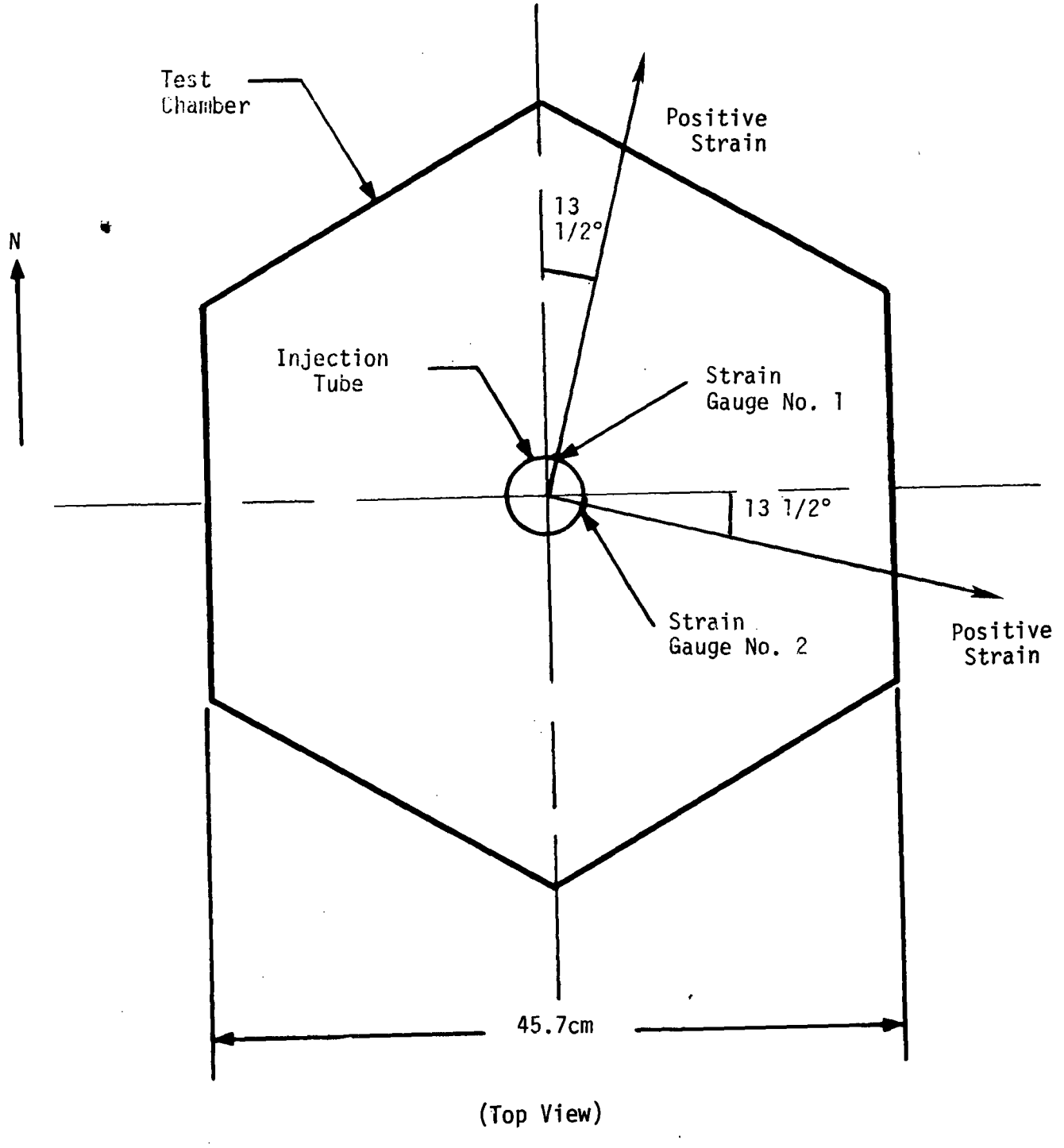

Figure 3.1 Strain Gauge Orientation Relative to Test Chamber
Runs Set A

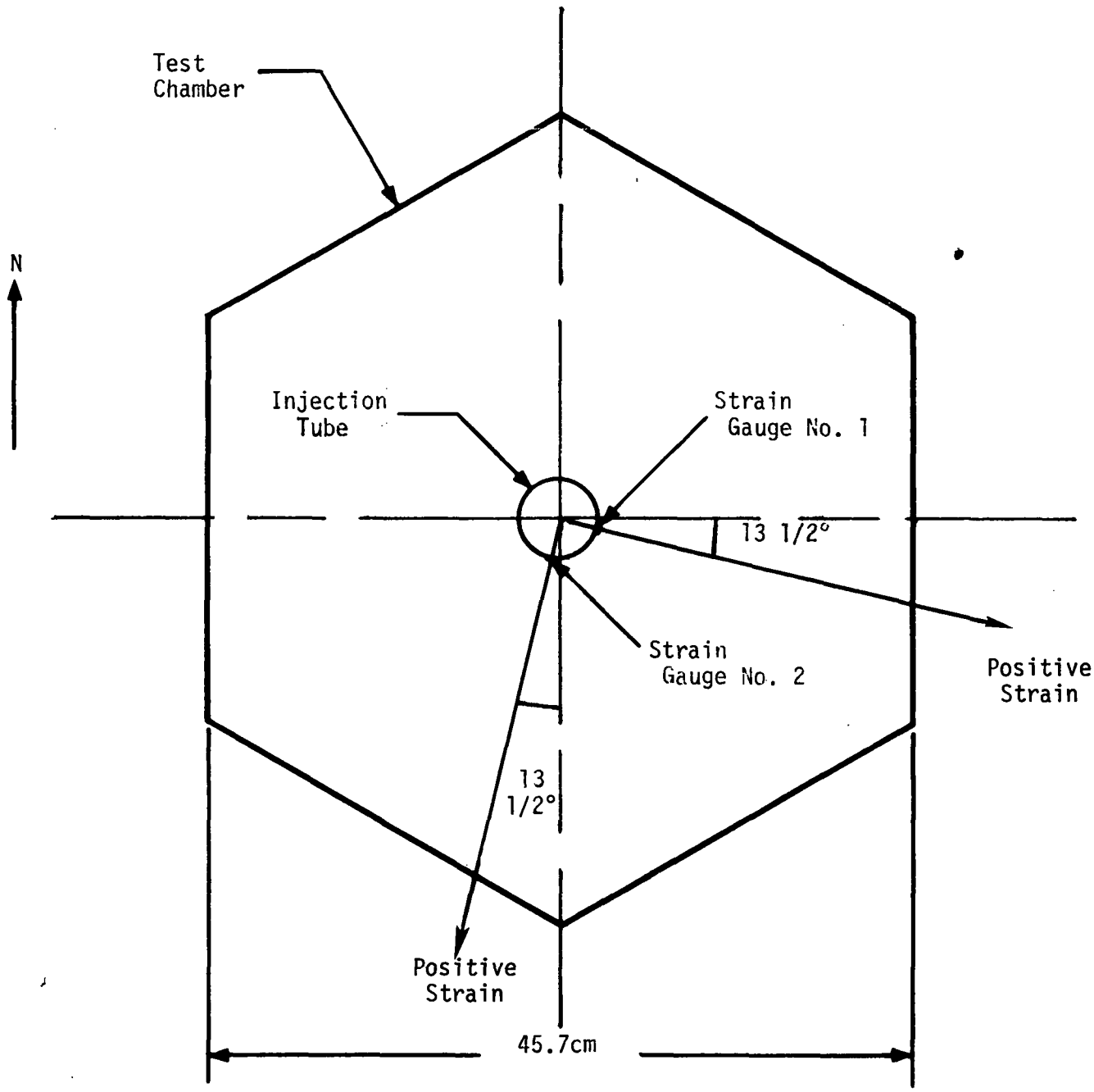

(Top View)

Figure 3.2 Strain Gauge Orientation Relative to Test Chamber
Runs Set B

Data plots for each experimental run are shown in Fig. 3.3 thru 3.98. Each run consists of eight plots representing the four instruments used. Each plot displays the data recorded by the instrument over one half the sampling time for the run (2.8125 secs.). Also included for each run is a detailed set of plots for a pressure pulse and beam loading transient typical to that run. These detailed plots present the transient over an expanded time scale of 187.5 m secs. Additional information on each run is presented in appendix A which contains some pertinent numerical data.

From the experimental data it was observed that the outside pipe wall temperature near the strain gauges was nearly constant. The temperature on the tube surface deviated no more than one percent from the initial value recorded. This temperature data is therefore not shown in the report. The signals obtained from the strain gauges were assumed to be taken from a constant temperature environment and were therefore not subject to any transient temperature compensation in data reduction.

Preliminary analysis of the data for the experiments on the injection tube load experiments revealed different tube response characteristics induced by the phenomenon depending on the relative orientation of the tube to the test chamber. Shown in Figs. 3.3 through 3.98. are the test data for both experiments. Run set A, Runs A1 through A4, Figs. 3.3 through 3.50, correspond to an injection tube orientation shown in Fig. 3.1. Run set B, Runs B1 through B4, which corresponds to an orientation shown in Fig. 3.2. is presented in Figs. 3.51 through 3.98. In both cases the tube's response to the chugging input consisted of a damped oscillatory motion with a natural vibration frequency of about 36 Hz. As it can be seen damping effects for the two cases differed significantly. The injection tube motion in an orientation

corresponding to run set B was significantly more damped than in an orientation corresponding to run set A.

The different tube responses attributable to the simplistic pipe coupling used to mount the injection tube to the steam supply line at the top of the test chamber. For runs set A the beam was more securely fastened by the coupling than in set B, hence less energy dissipated through the pipe supports in run set A. Observation of the data shows this to be an important consideration in data analysis. Definite tube response variations can be observed between the two sets for similar experimental conditions.

Comparing the two sets of runs, set A and set B, corresponding to the two orientations of the strain gauges in the test chambers, it appears that some individual strain gauge influence on the data was present. Definite variations can be detected between the general shapes of the two strain gauge curves. In run set A strain gauge number one seems to be more damped than strain gauge number two. In run set B the opposite effect is observed, strain gauge number two is more damped than strain gauge number one.

Possible explanations for this effect are: 1) structural differences in the hexagonally symmetric rather than rectangularly symmetric test chamber which would allow deflection to occur more easily in certain directions. 2) Non-identical strain gauge placement and orientation along the pipe. 3) Radially nonsymmetric and non-uniform loading characteristics from the bubble collapse with the test chamber. Since the same type of irregularity was observed in both gauges depending on orientation, differences in gauge mountings are unlikely. Either explanation No. (1) or (3) seem probable, the relative effects of each, however,are unknown at this time.

With regards to peak magnitudes of strain recorded no oberservable trend existed which suggests a preferential loading direction. Peak

magnitudes of loading were not associated consistently with any single directions and the loading direction from each bubble collapse appeared to be distributed throughout all directions.

Presented in Figs. 3.99 and 3.100 is a typical interfacial history for a developing steam bubble. Drawings (a) and (b) represent two different views captured by photography of the bubble. Drawing (a) is a straight and level view from the front of the developing bubble, while drawing (b) shows the bubble from a view looking up from the back underside. Figs. 3.101 through 3.104 show the recorded data of the four instruments plotted over a similar time scale. The pressure pulsations are those recorded on the bottom of the pool, the two strains are those recorded along the axis of the pipe, and the temperature is that of the fluid immediately adjacent to the tube exit. The pressure pulsations can be described by dividing them into three types depending upon their origin within the pool. The first few ripples in the pressure vs. time plot are due to bubble growth with changing bubble shapes at the vent exit. The first large pressure oscillation is due to the relatively fast bubble collapse at the tube exit. It can be seen that the pressure peak follows immediately after the bubble has collapsed. Figs. 3.101 and 3.102 show the corresponding strain-time plots over the same interval. Unlike pressure variations with the pool the strain in the pipe is not effected in the same way. The small pressure variations caused by bubble shape changes do not significantly effect the recorded strain. In a similar manner the rush of water up the pipe vent after the bubble collapse also imposes only minor loading onto the pipe. The bubble collapse, on the other hand, is responsbible for almost all of the transient loading observable. As can be deduced from Fig. 3.101 the recorded strain peak occurs simultaneously with the first large pressure peak in the pool. Forces, therefore,

are generated on the pipe during the bubble collapse and are removed when the bubble disappears. Similar behavior is observable in the other runs.

In Figs. 3.3 through 3.14 and 3.51 through 3.62 show the data for the low temperature runs A1 and B1. Pressure oscillations at this pool temperature are widely spaced with a frequency of about 1.5 sec^{-1}. Recorded pressure peaks at this temperature are between 115 to 120 kPa with an occasional peak to 125 kPa. At this pool temperature chugging is common as can be seen from Figs. 3.7 and 3.8 and 3.55 and 3.56 which shows vent exit temperature vs. time. All large lateral loadings on the pipe are caused by bubble collapse at the vent.

At intermediate pool temperatures the average frequency of pressure pulses increased to 2.5 sec^{-1} at 56.3°C and 5 sec^{-1} at 67.2°C. The data for runs are presented in Figs. 3.15 through 3.38 and 3.63 through 3.86. At pool temperatures of 57.2°C steam chugging is still a common occurrence while at pool temperatures of 67.2°C steamwater transitions at the vent exit are reduced and the vent exit temperature remains primarily that of the steam. Observed pressure peaks decrease from the 115-120 kPa range at 53°C to 105-110 kPa at 67.2°C. Data for these pool temperatures are presented in Figs. 3.15 through 3.38 and 3.63 through 3.86. At pool temperatures of 73.9°C the average pressure pulse frequency increases to about 6.5 sec^{-1}, with a corresponding decrease in pressure peaks observed to 104-106 kPa. From Figs. 3.43 and 3.44 it can be seen that the vent exit temperature undergoes variations of only about 10°C from the predominant steam temperature.

As discussed it is seen that the general trend in pressure pulses with increasing temperature is increased frequency and decreased peak magnitude. Recorded strains along the pipe do not follow this observed trend. Peak strains recorded on the pipe are seen to be essentially independent of pool

temperature. With increasing pool temperature, however, the general trend was an increase in the number of strain peaks, corresponding to an increase in the number of observable pressure oscillations. The average R.M.S. strain value increased with increasing pool temperature, indicating a greater input of energy into the beam.

Finally, it should be mentioned that the peak pressures and strain (positive and negative) measured in the various runs may not be representative of the actual highest and lowest values that occurred. Because of the 2.5 msec. recording time span used, sampling intervals may be too long compared to the duration of the pressure transient.

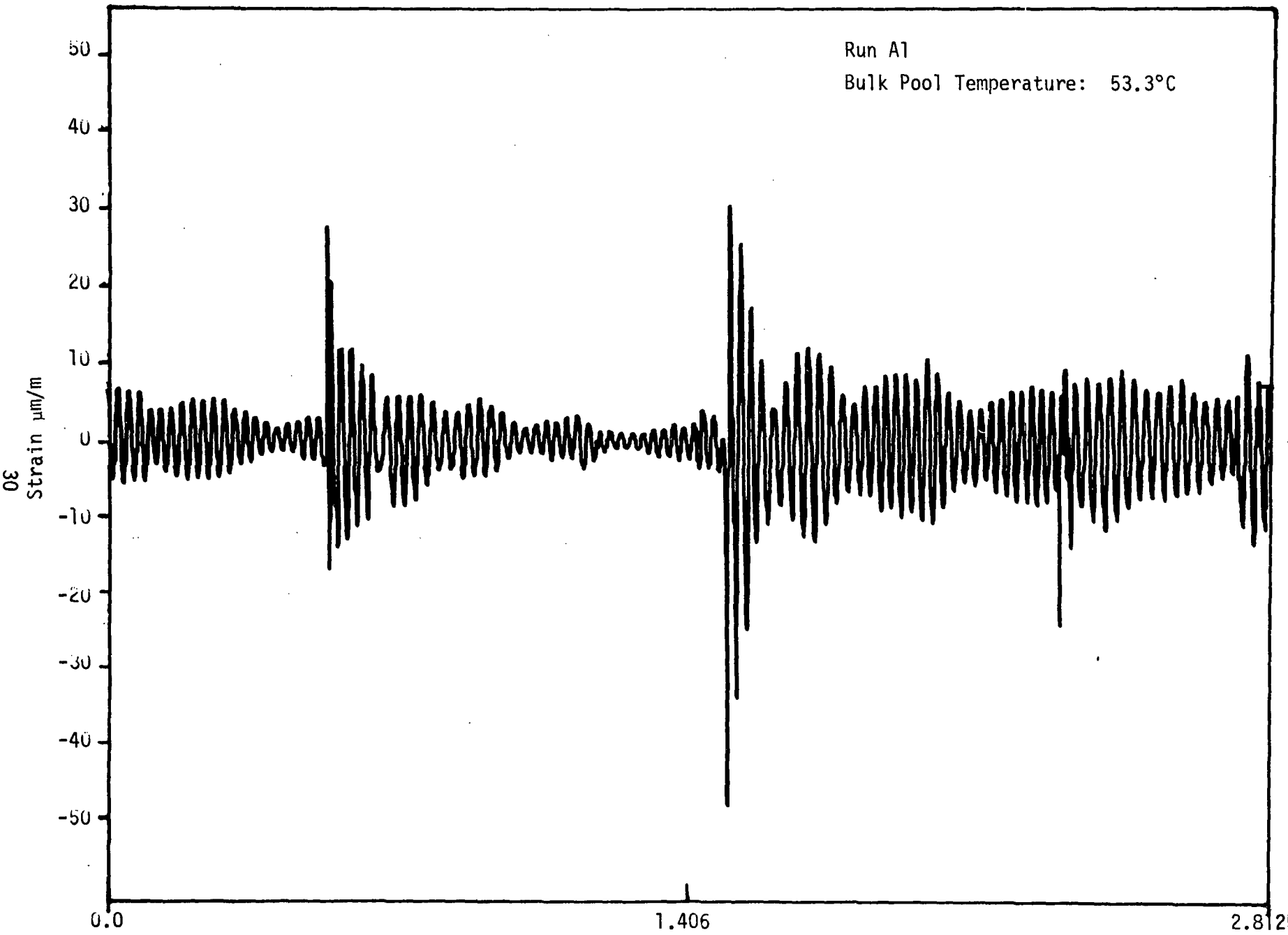

Figure 3.3 Strain (Gauge #1) vs Time for Run A1

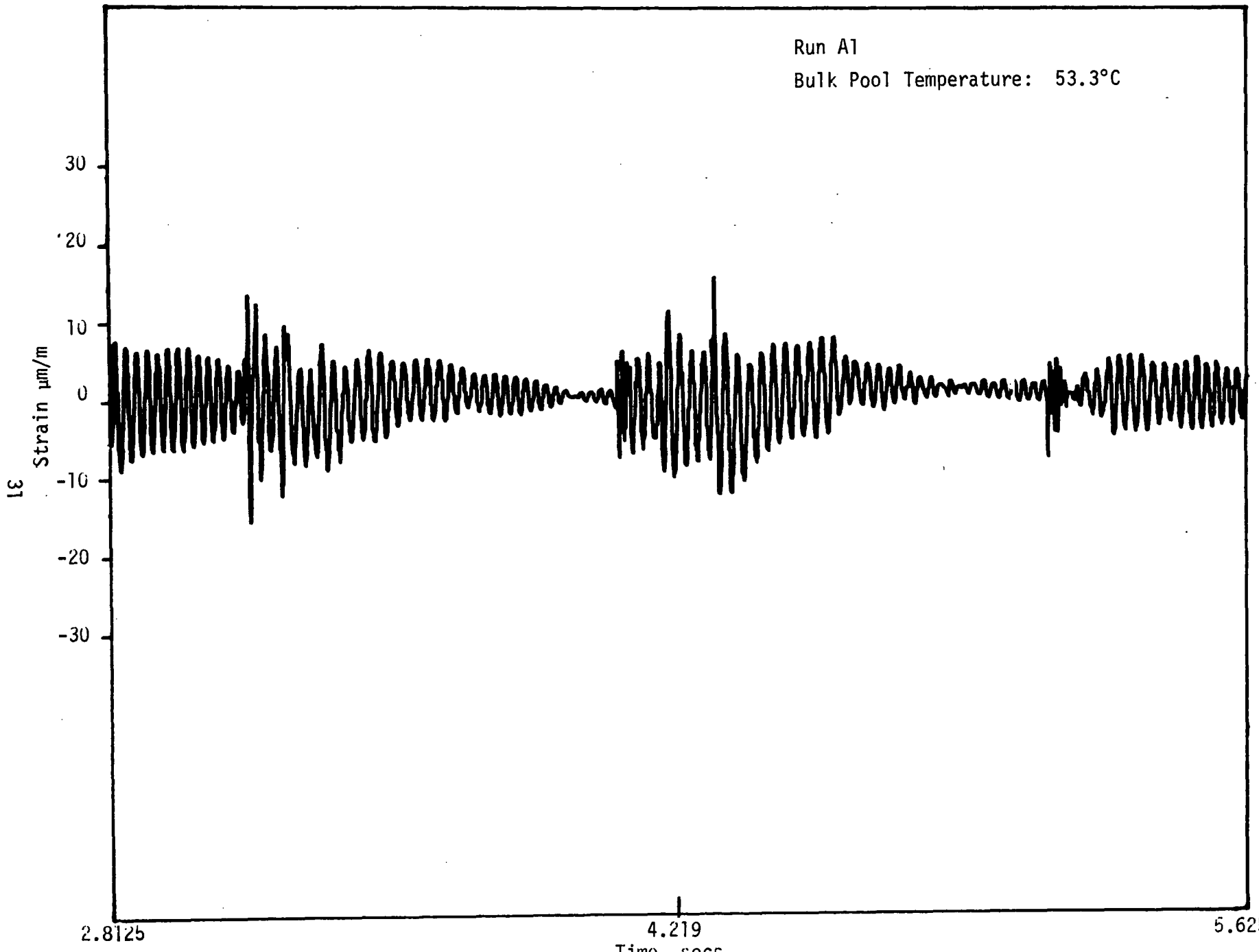

Figure 3.4 Strain (Gauge #1) vs Time for Run A1

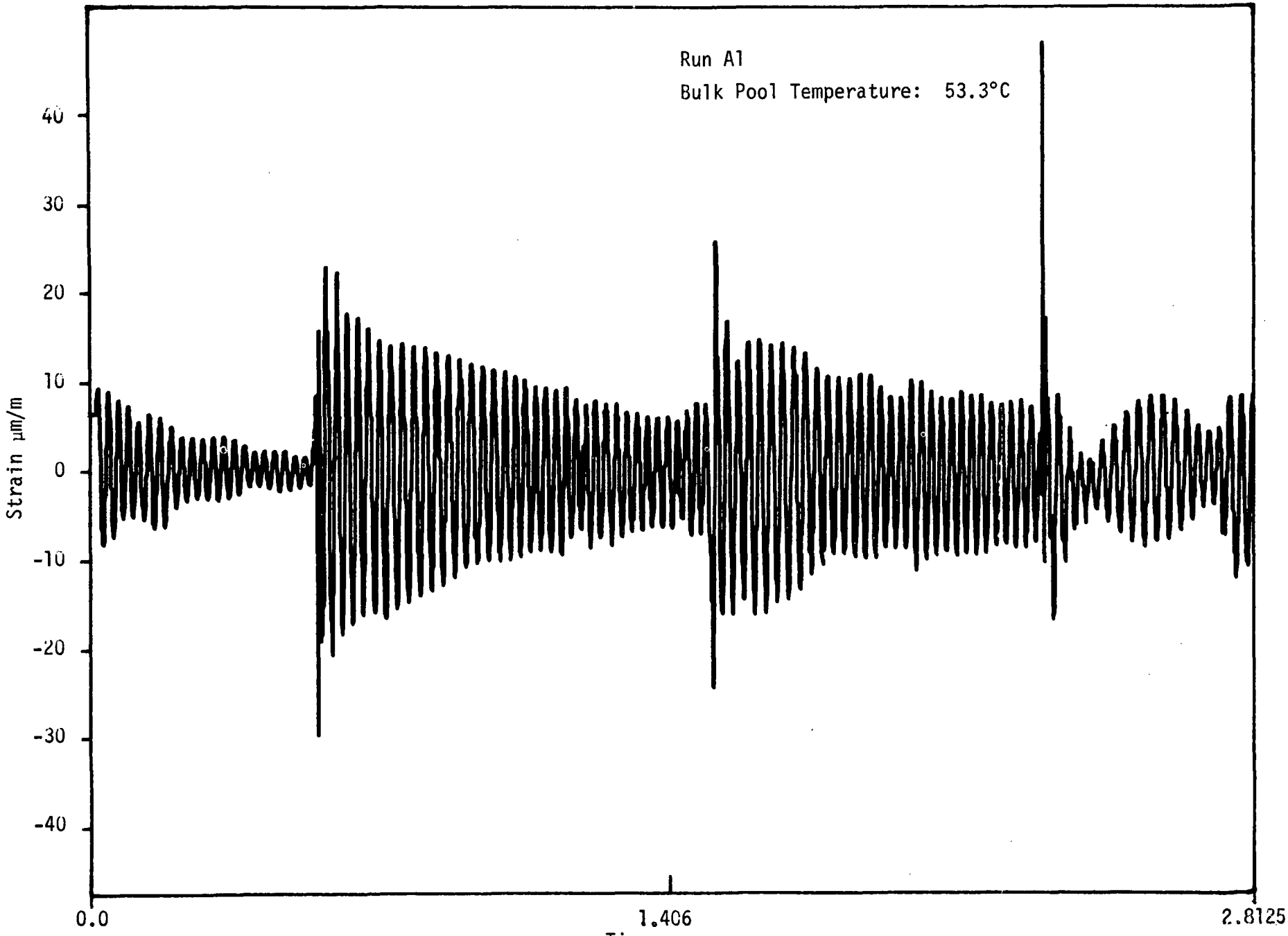

Figure 3.5 Strain (Gauge #2) vs Time for Run A1

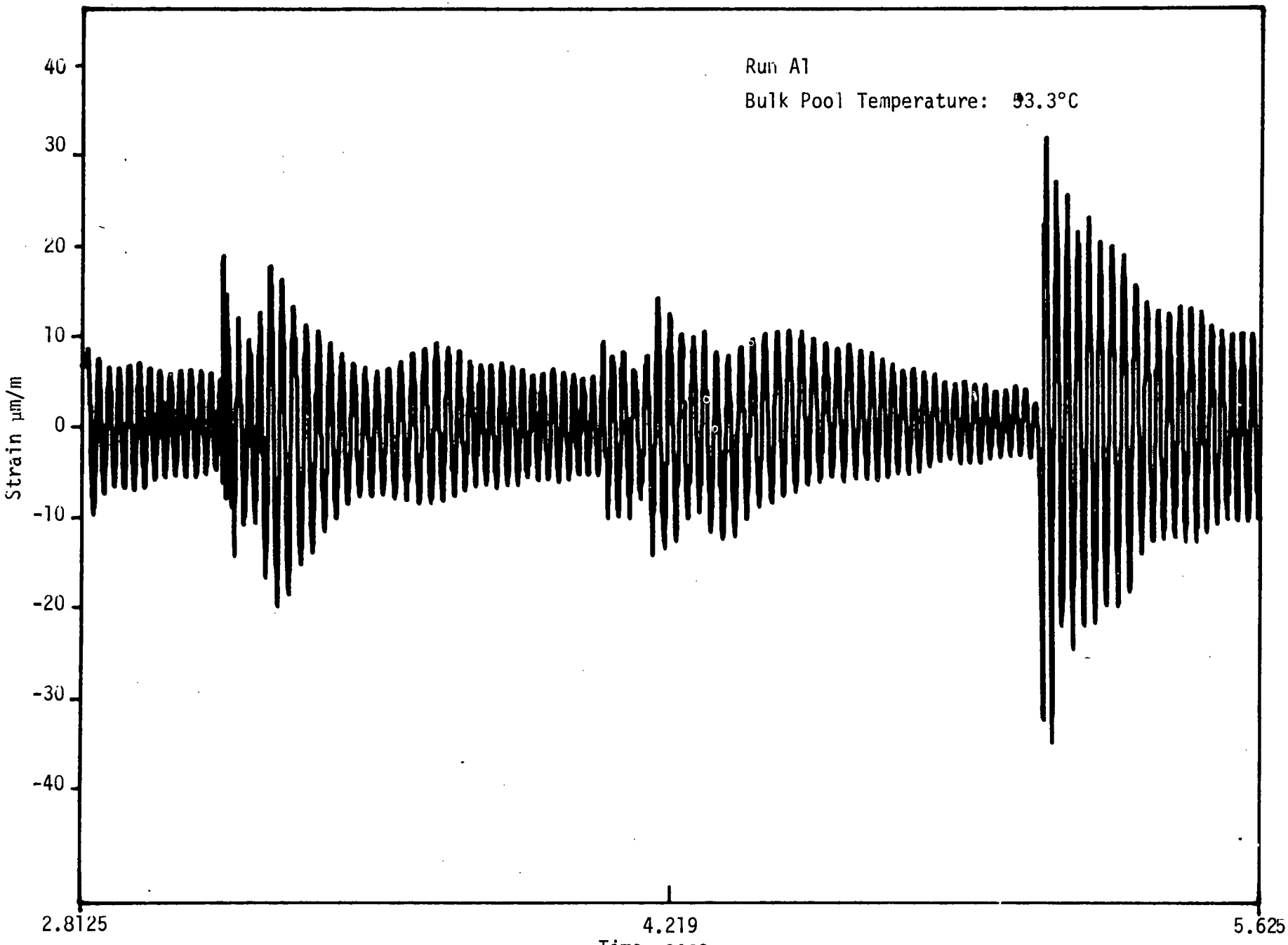

Figure 3.6 Strain (Gauge #2) vs Time for Run A1

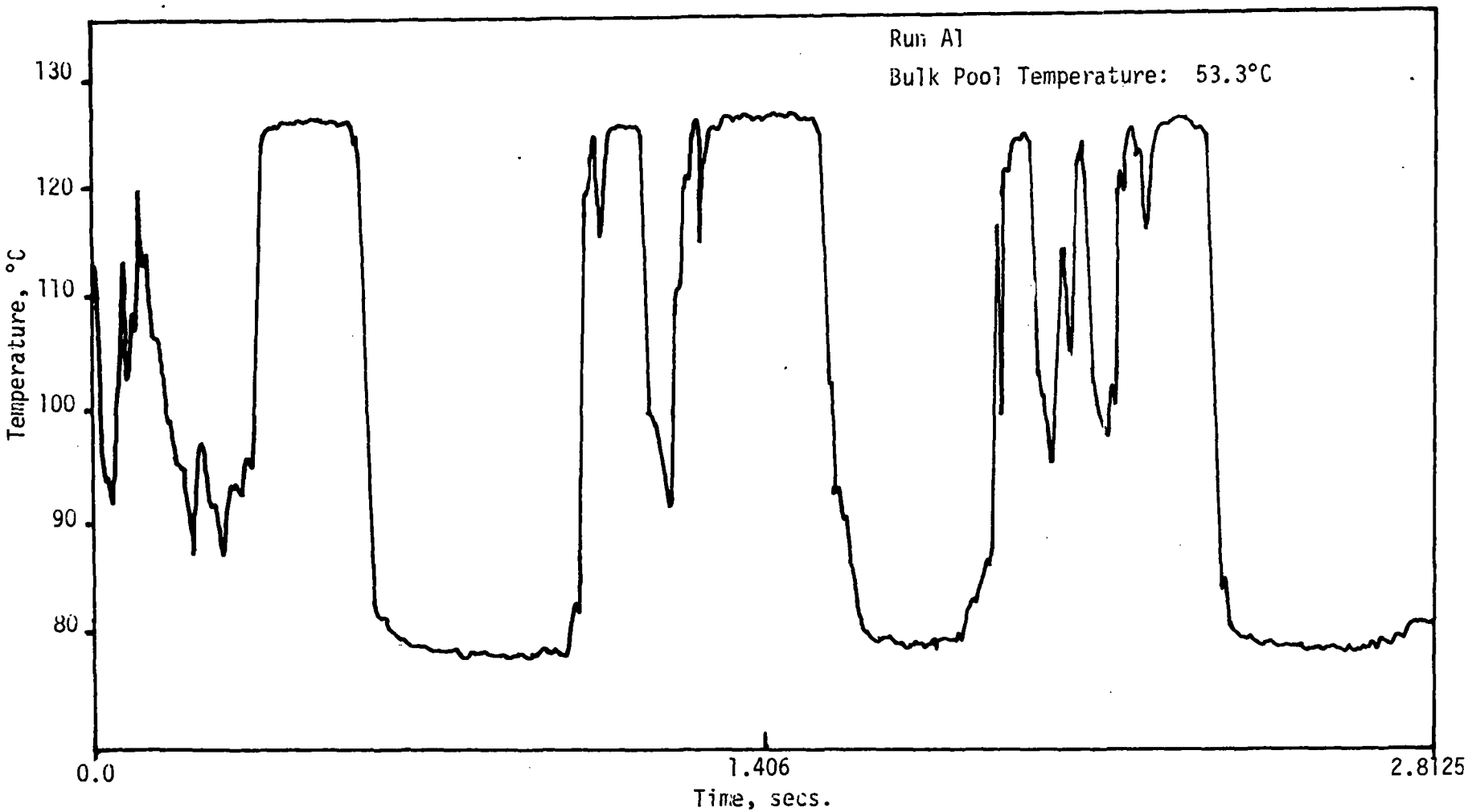

Figure 3.7 Vent Exit Temperature vs. Time Run A1

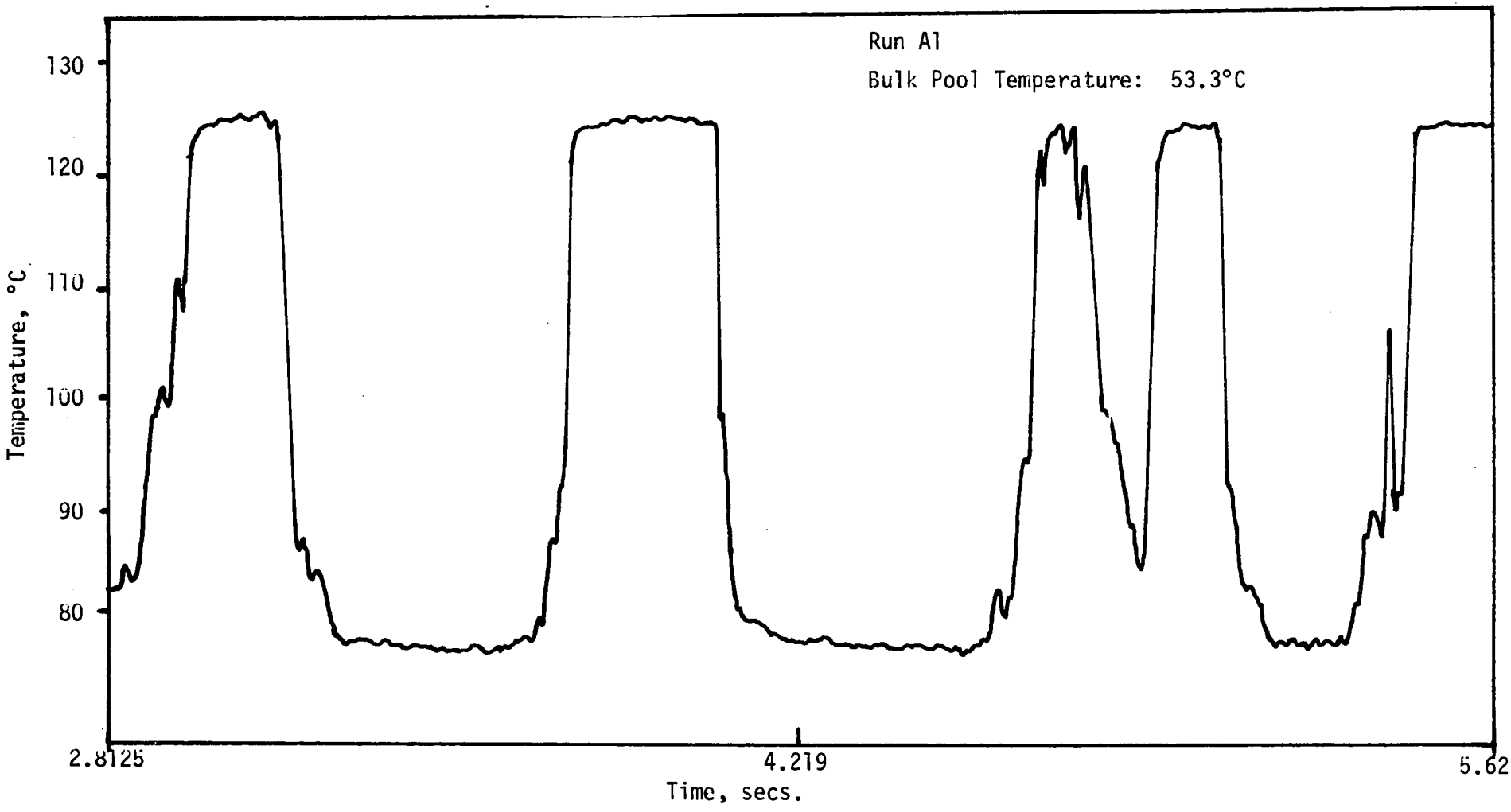

Figure 3.8 Vent Exit Temperature vs Time for Run A1

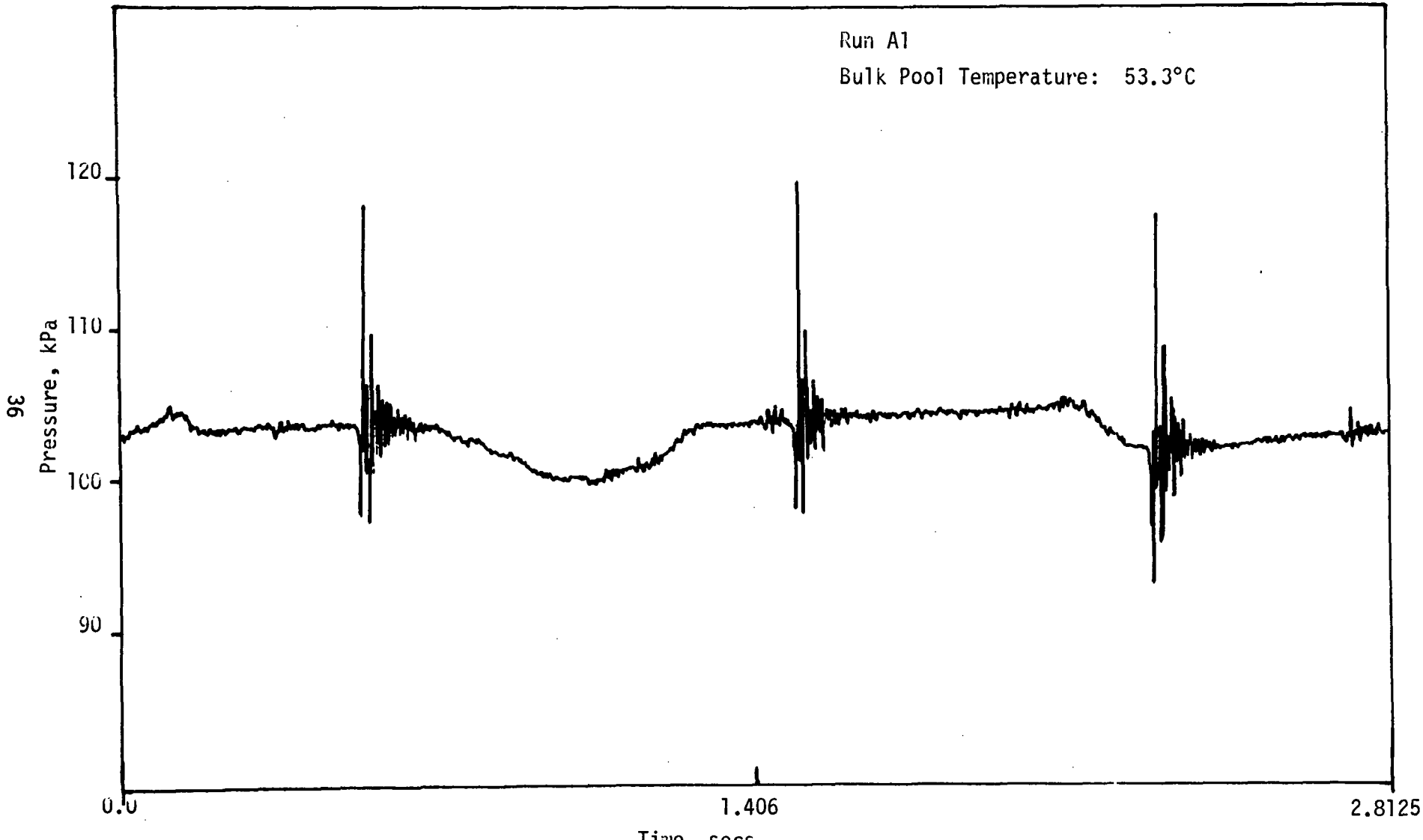

Figure 3.9 Bottom Pressure vs. Time for Run A1

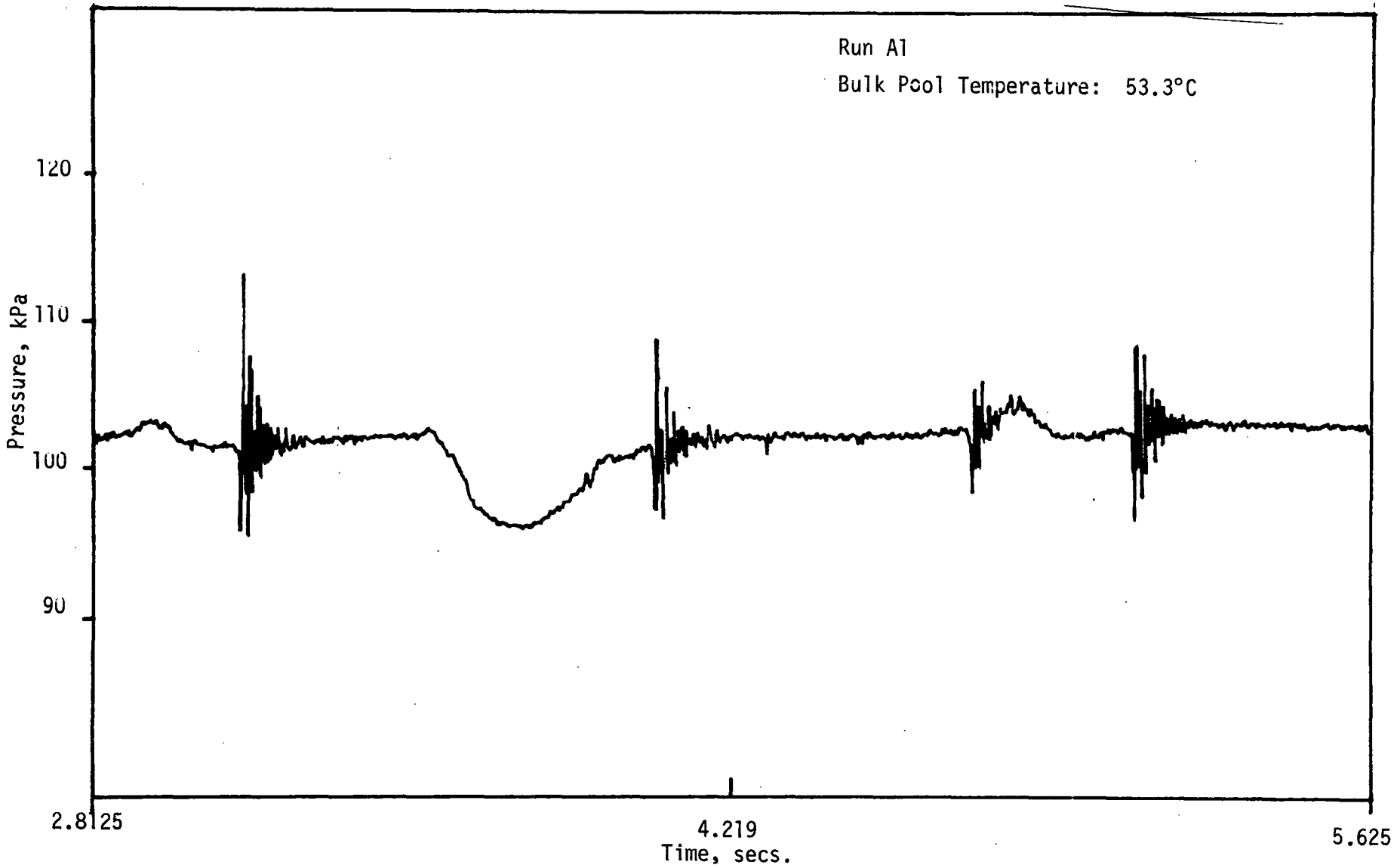

Figure 3.10 Bottom Pressure vs. Time for Run A1

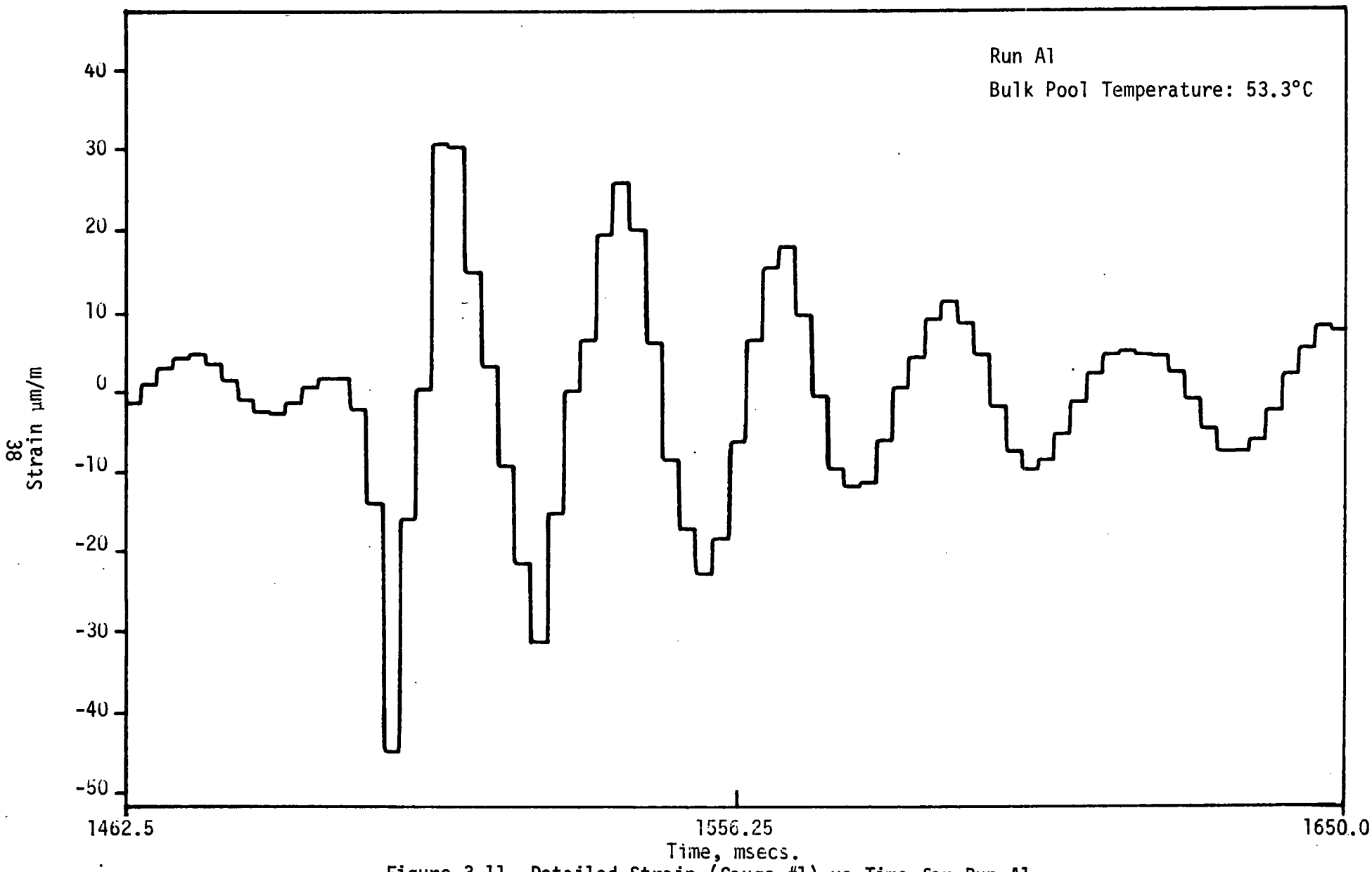

Figure 3.11 Detailed Strain (Gauge #1) vs Time for Run A1

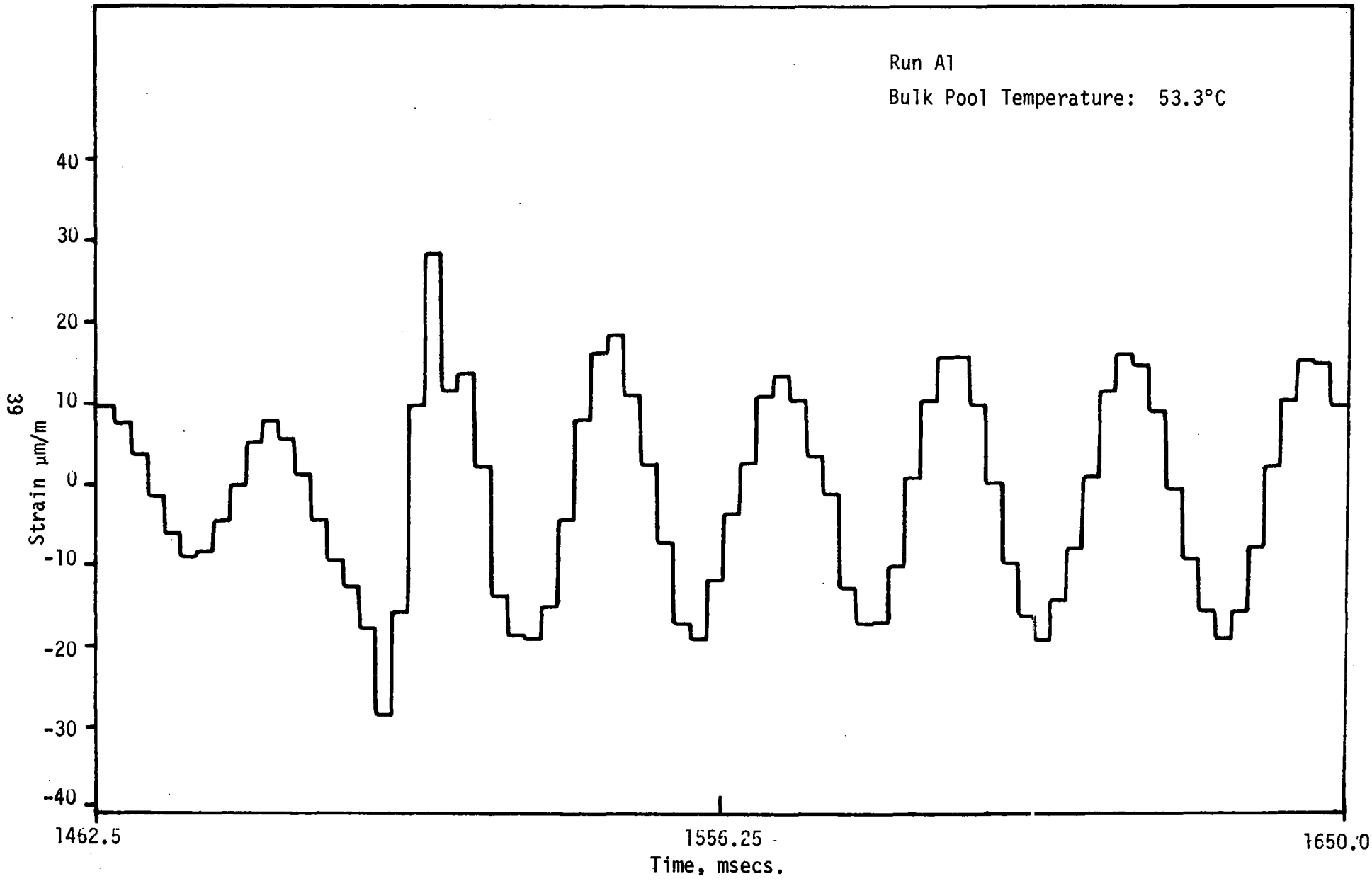

Figure 3.12 Detailed Strain (Gauge #2) vs Time for Run A1

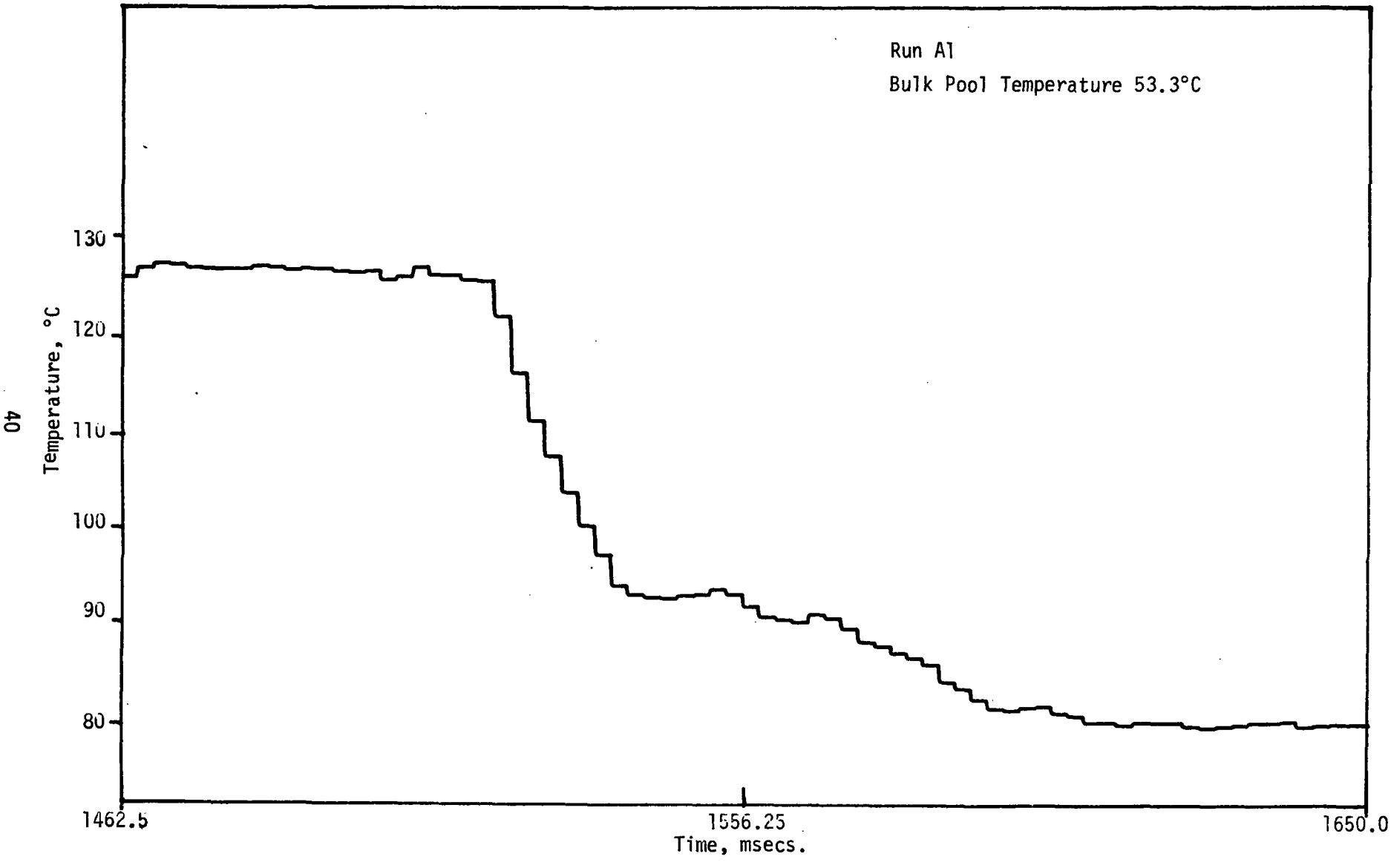

Figure 3.13 Detailed Vent Exit Temperature vs Time for Run A1

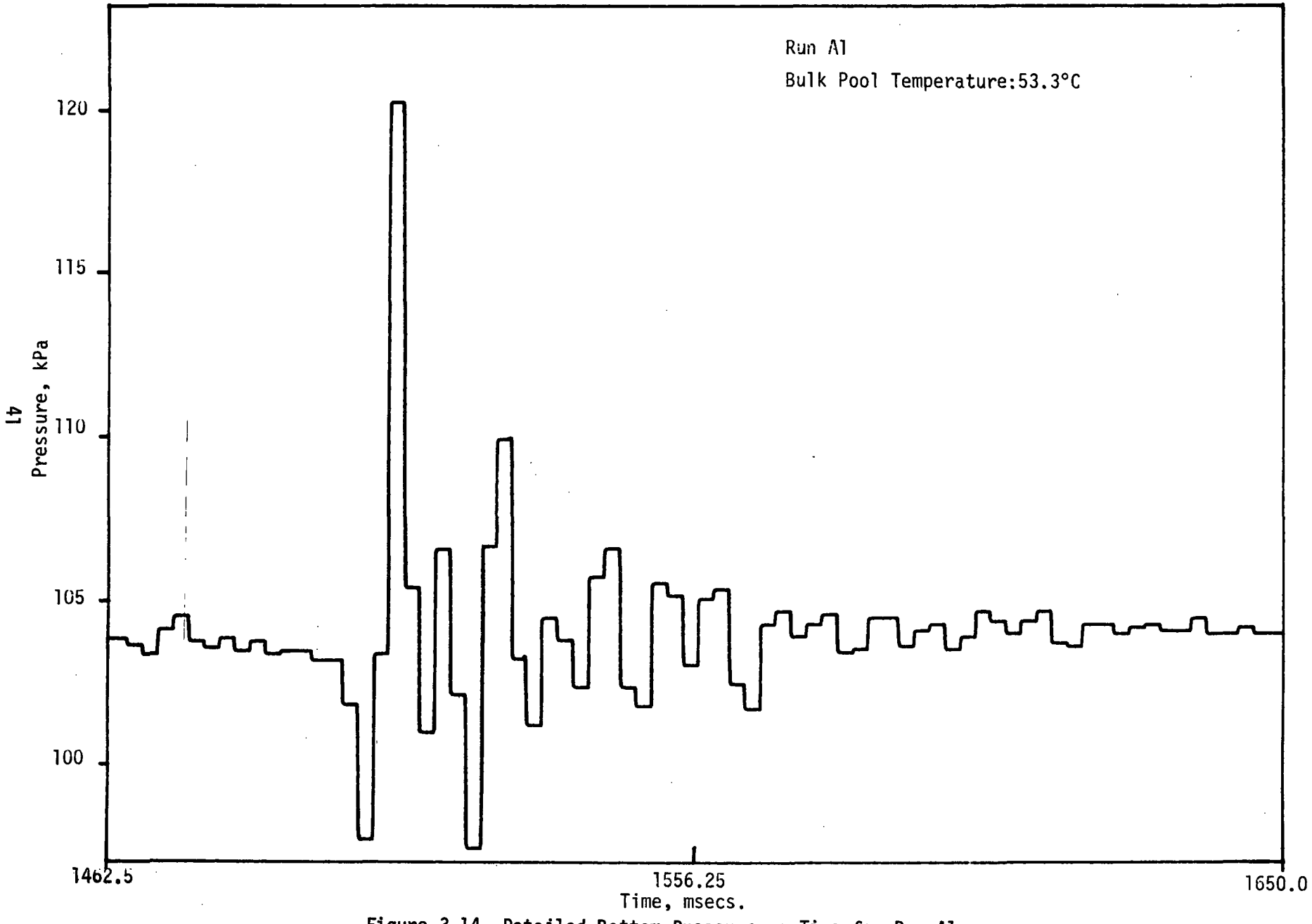

Figure 3.14 Detailed Bottom Pressure vs Time for Run A1

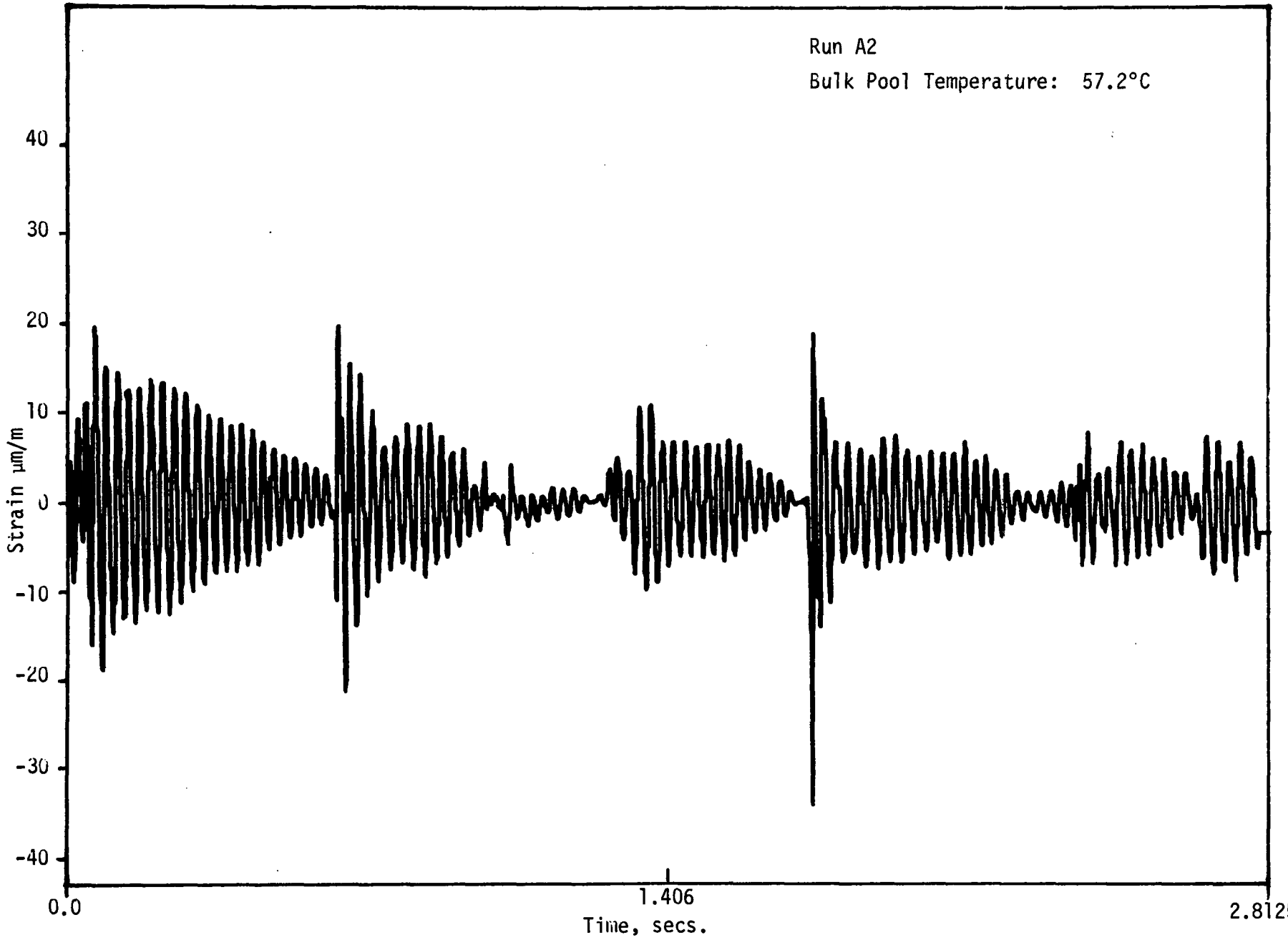

Figure 3.15 Strain (Gauge #1) vs Time for Run A2

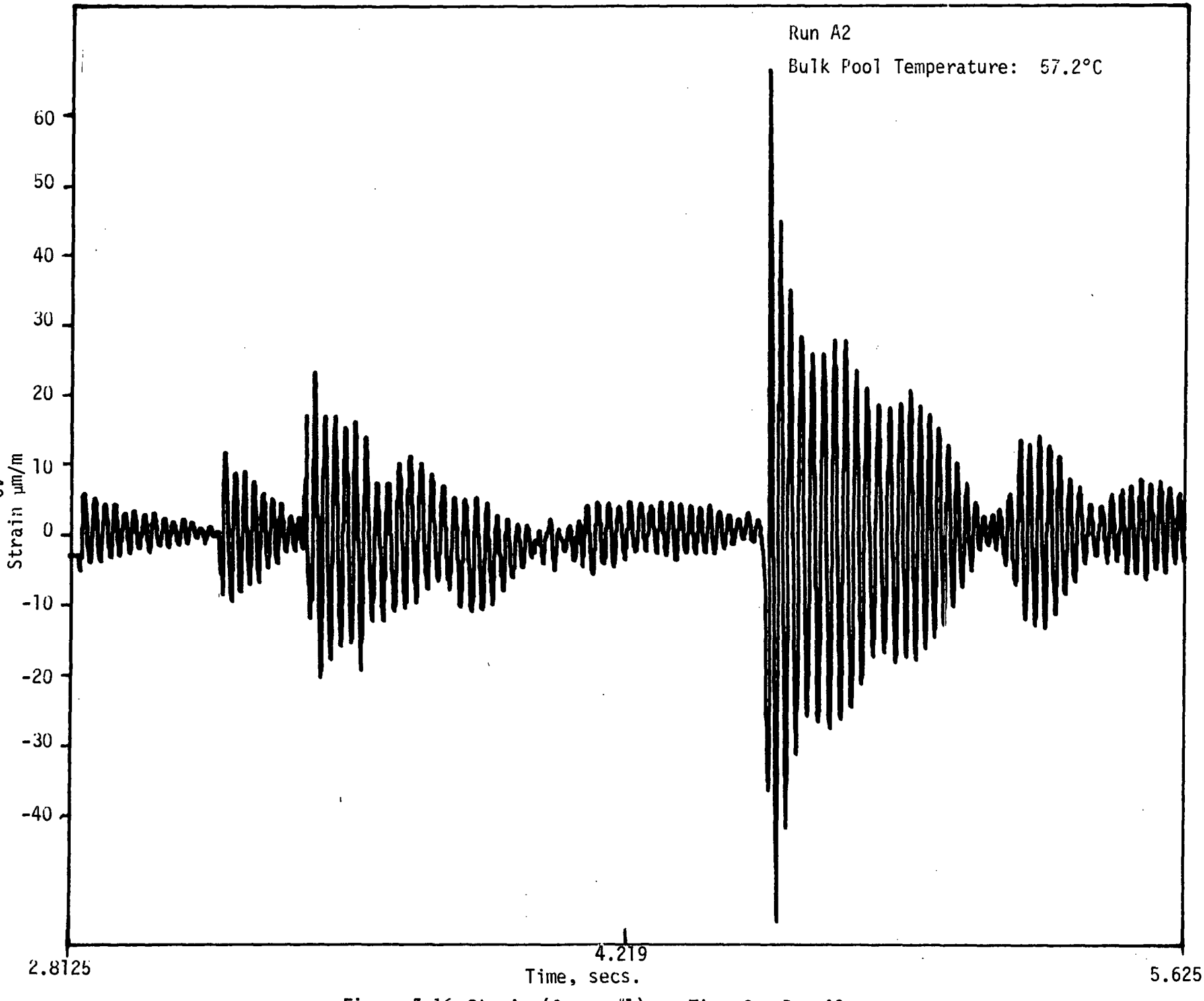

Figure 3.16 Strain (Gauge #1) vs Time for Run A2

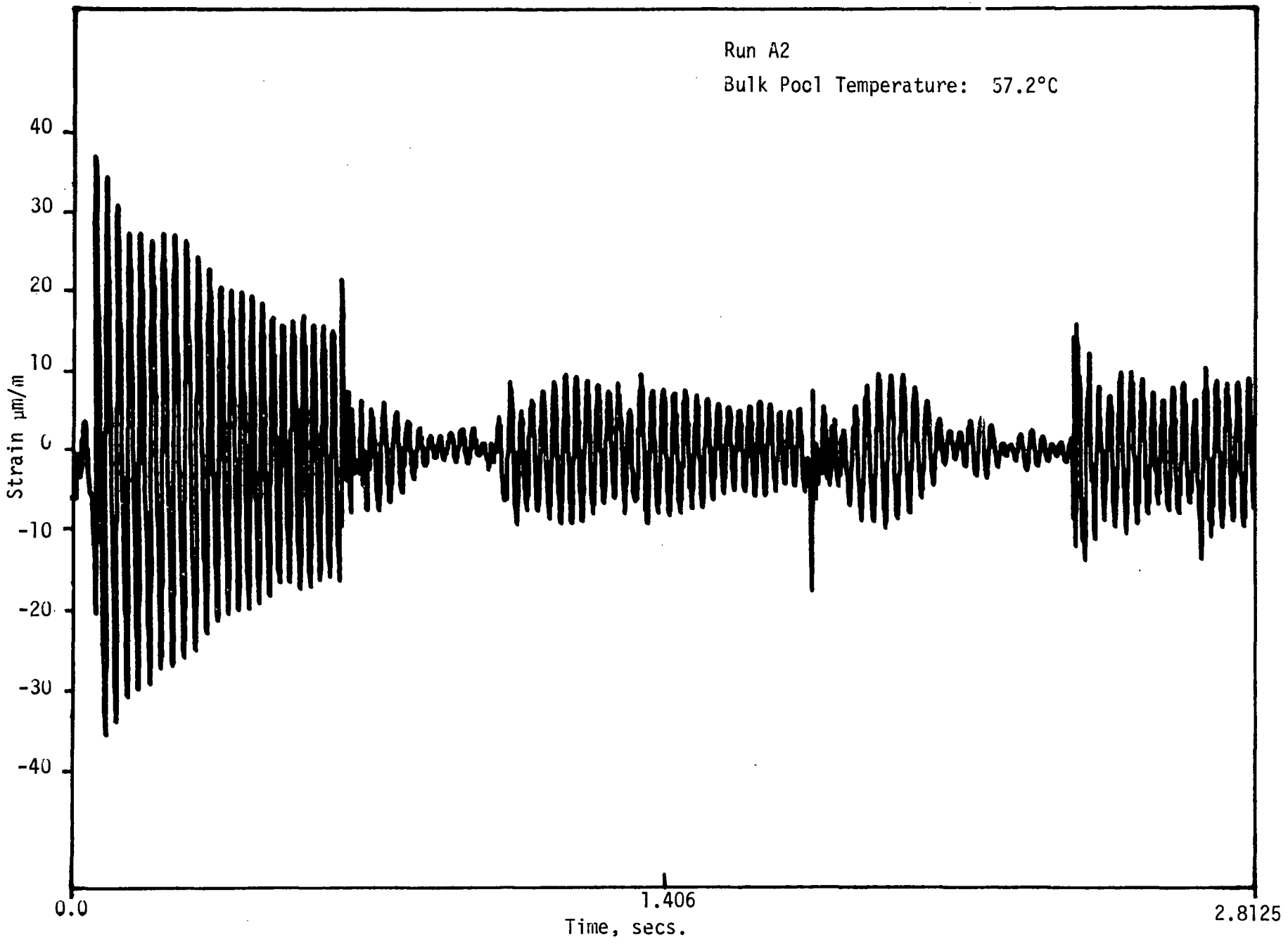

Figure 3.17 Strain (Gauge #2) vs Time for Run A2

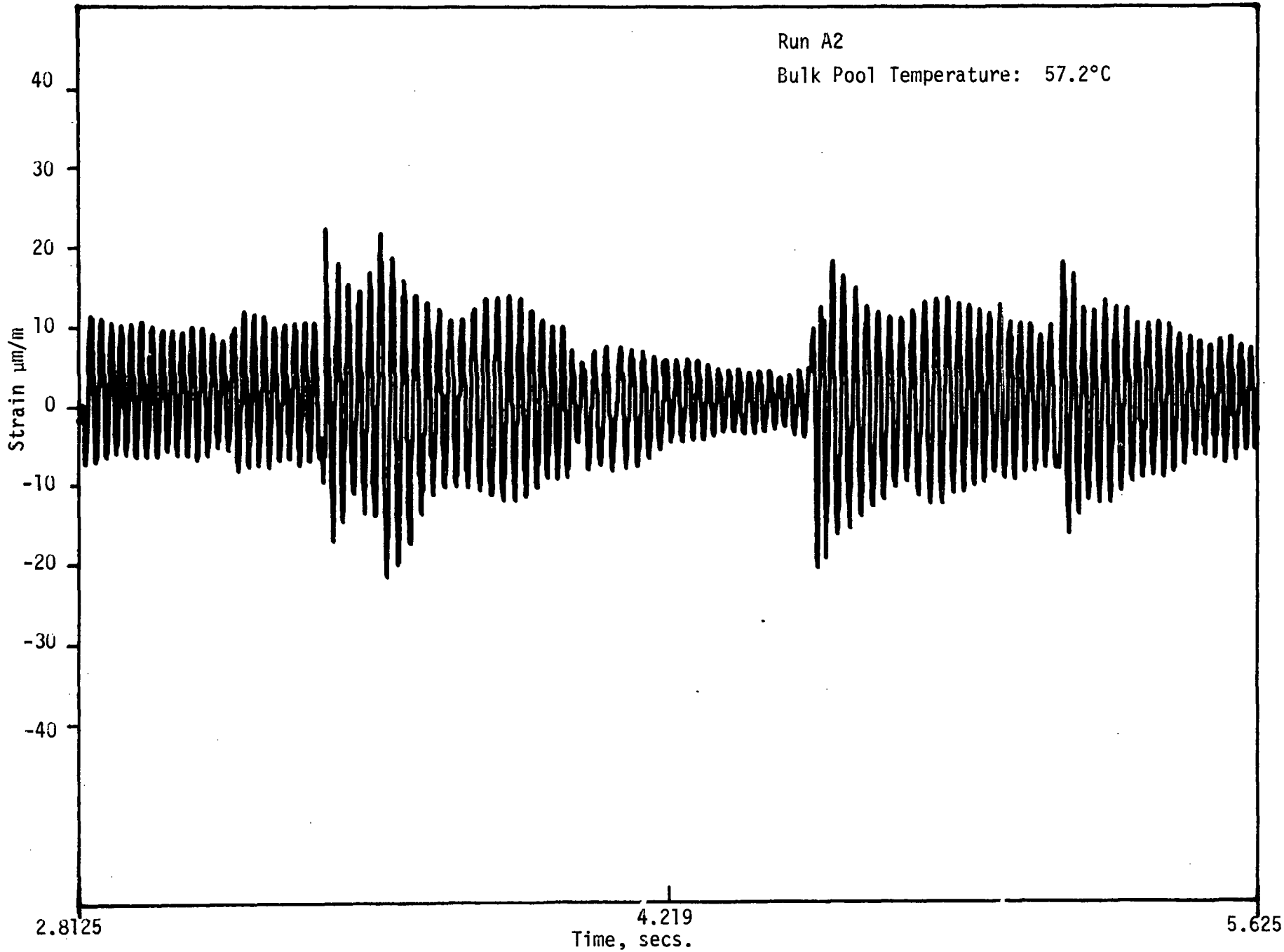

Figure 3.18 Strain (Gauge #2) vs Time for Run A2

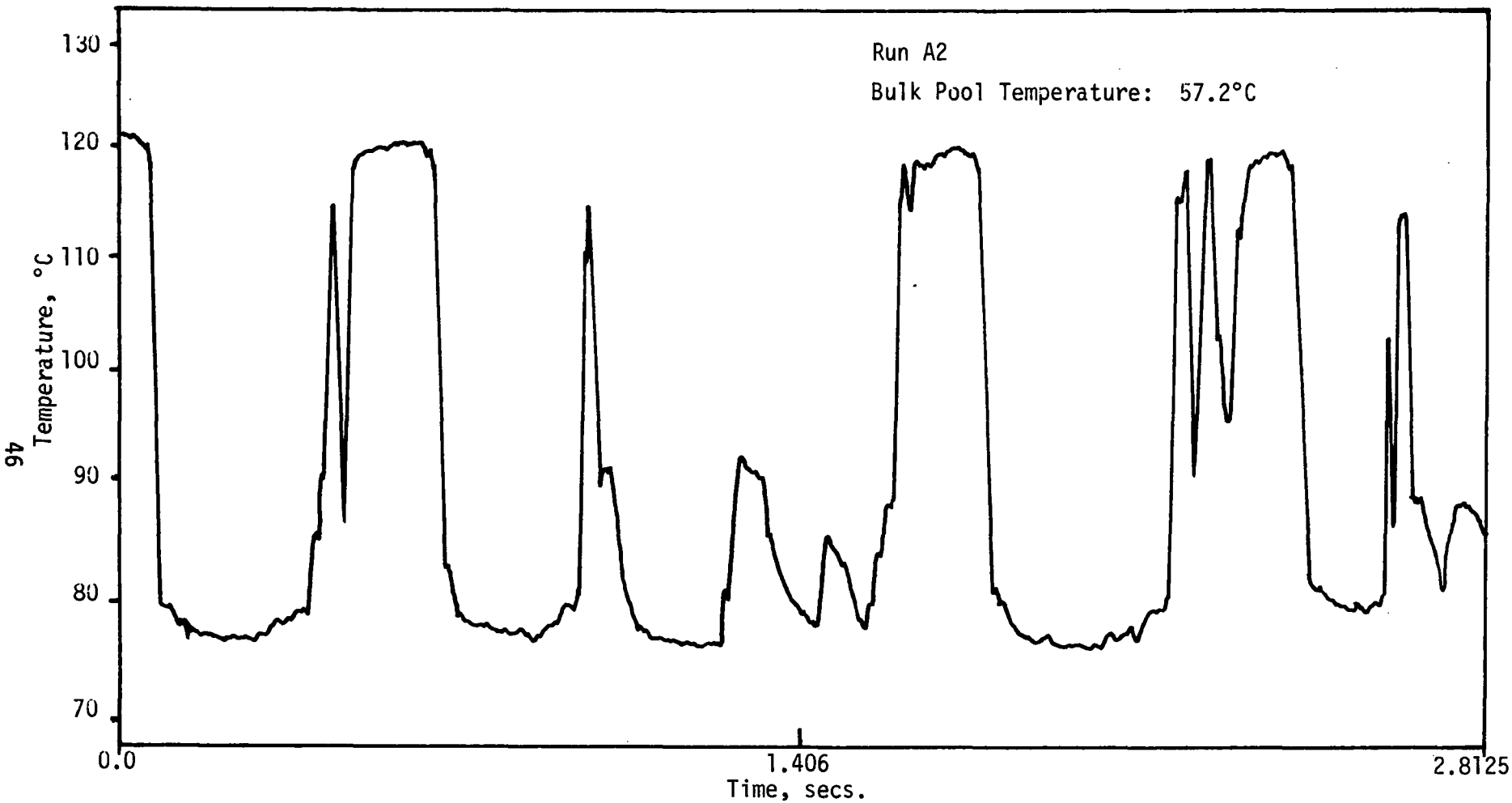

Figure 3.19 Vent Exit Temperature vs Time for Run A2

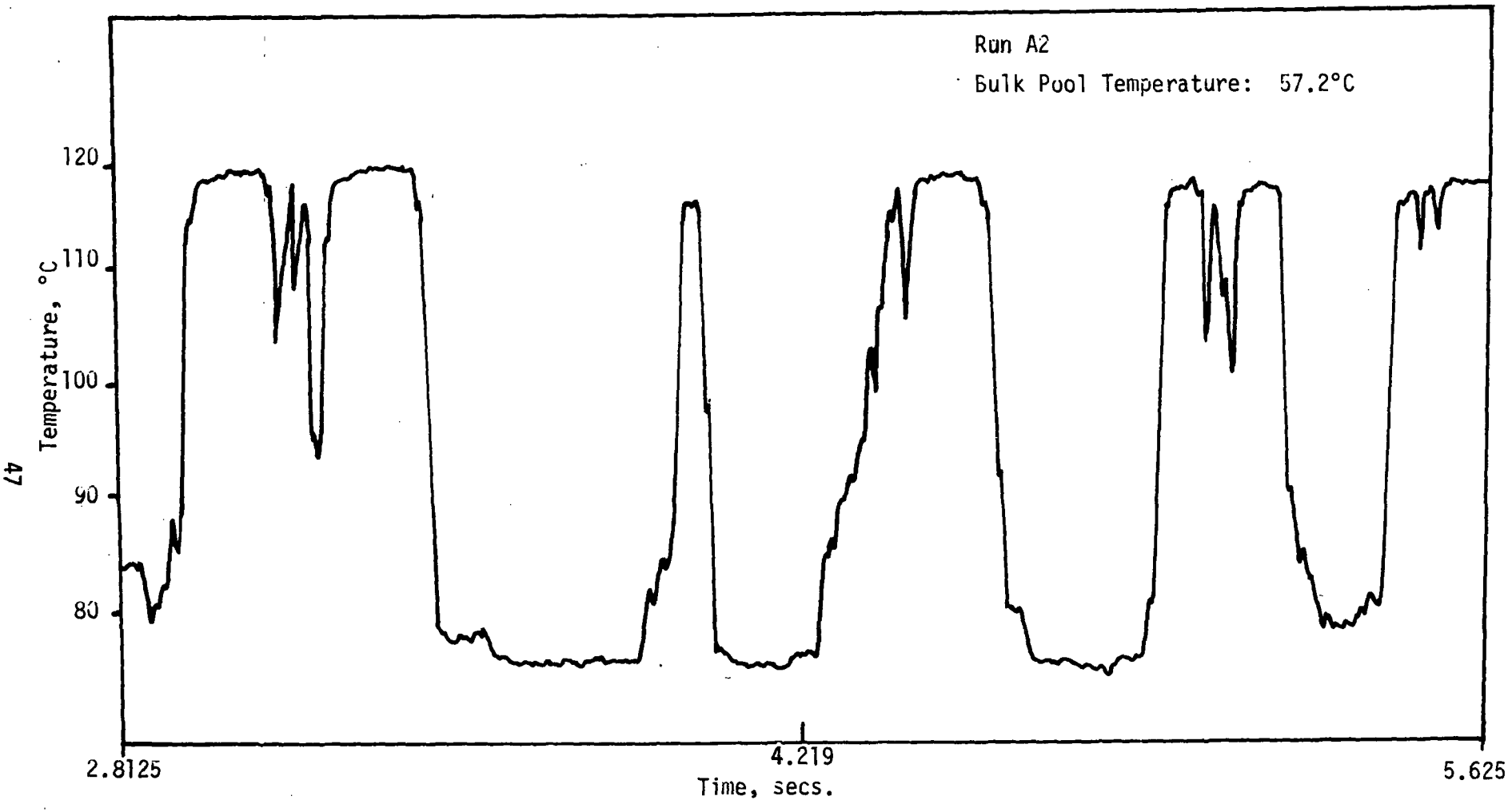

Figure 3.20 Vent Exit Temperature vs Time for Run A2

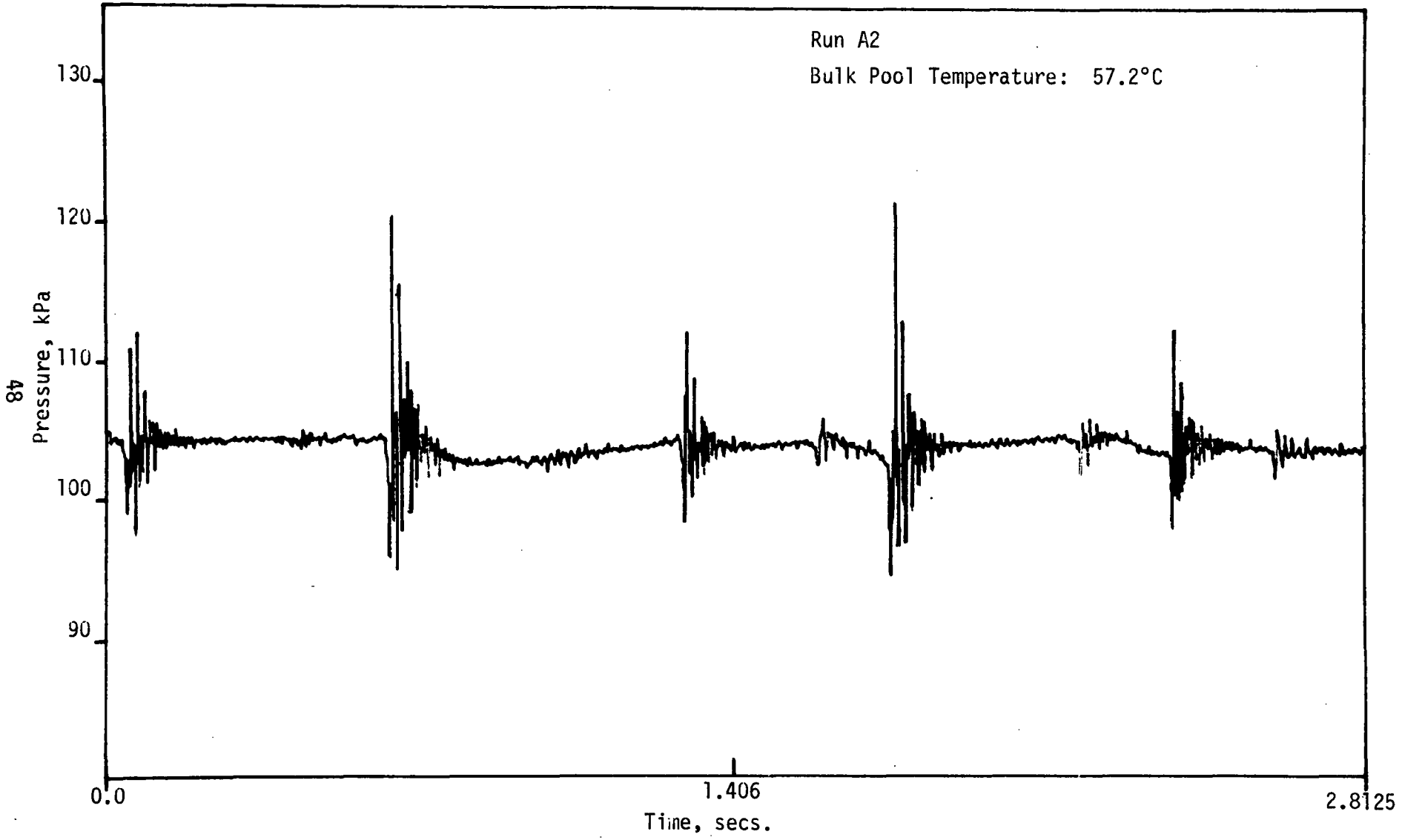

Figure 3.21 Bottom Pressure vs Time for Run A2

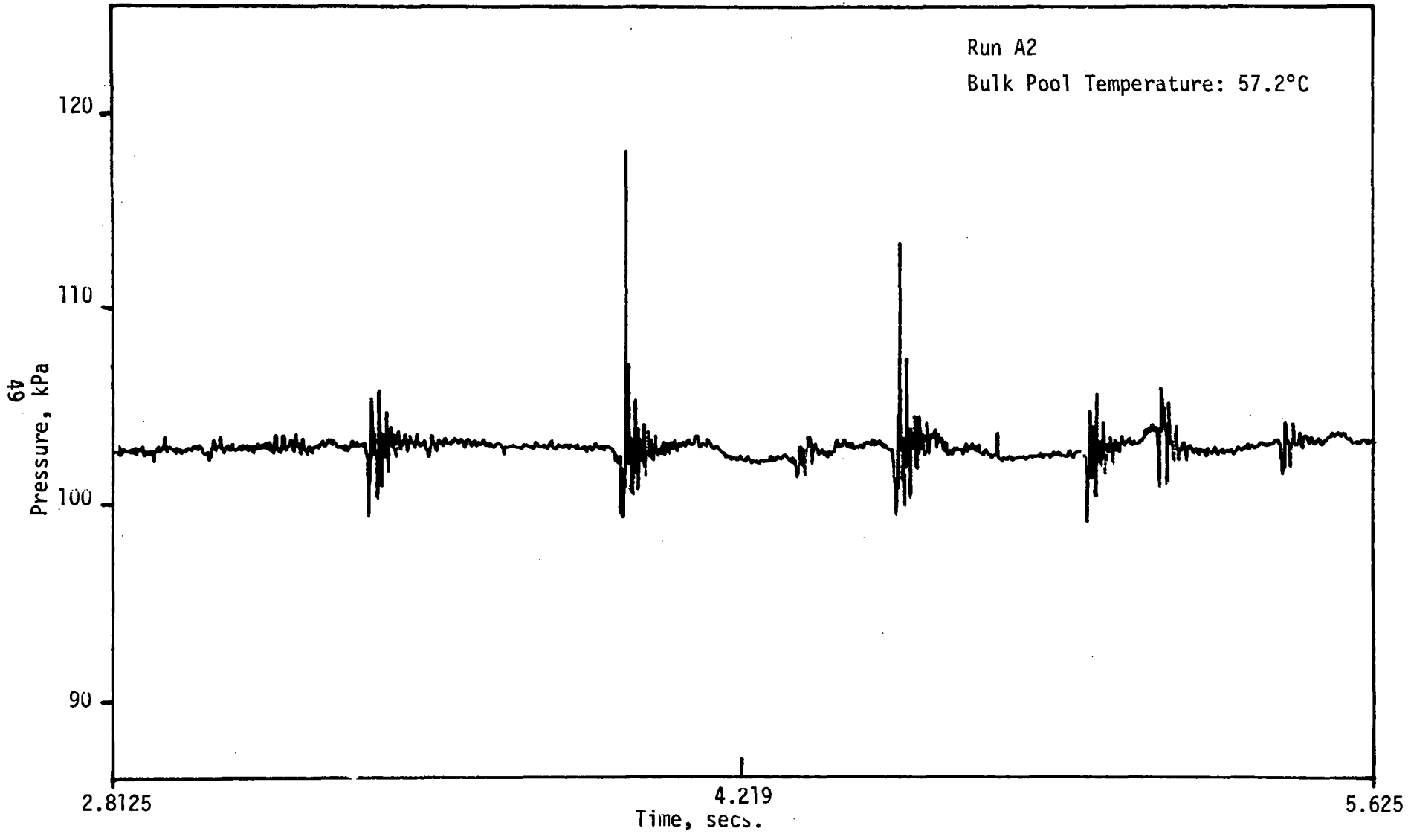

Figure 3.22 Bottom Pressure vs Time for Run A2

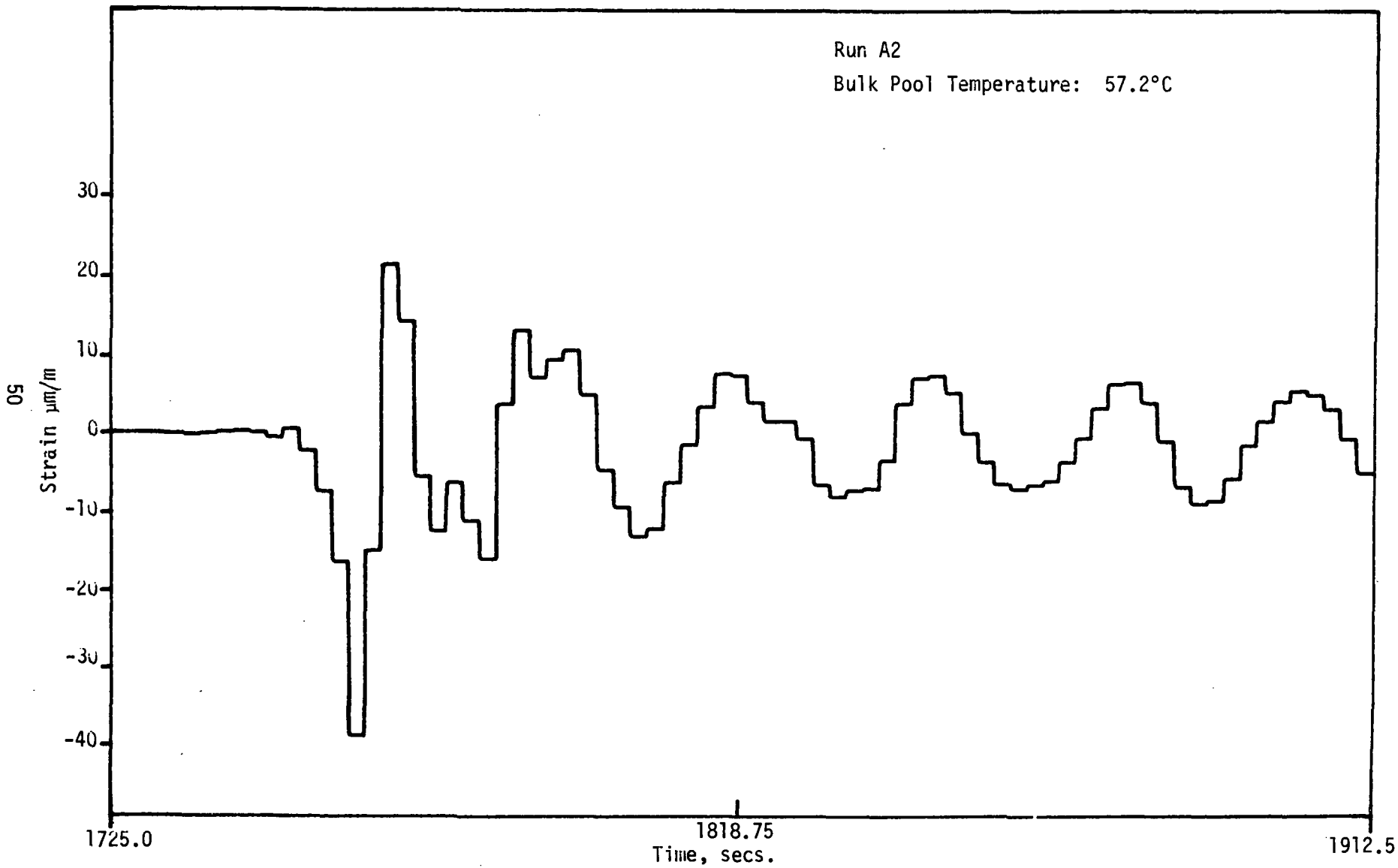

Figure 3.23 Detailed Strain (Gauge #1) vs Time for Run A2

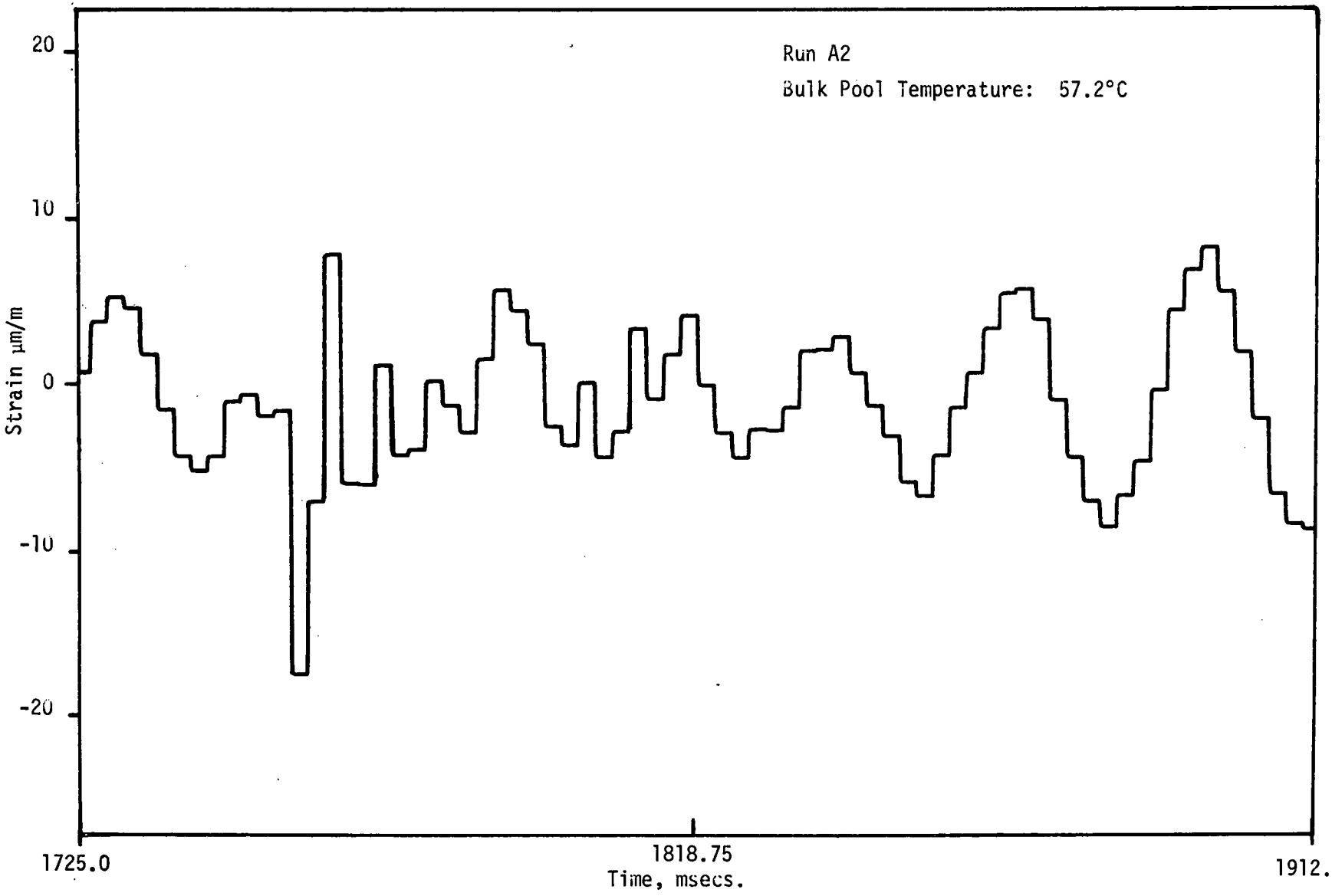

Figure 3.24 Detailed Strain (Gauge #2) vs Time for Run A2

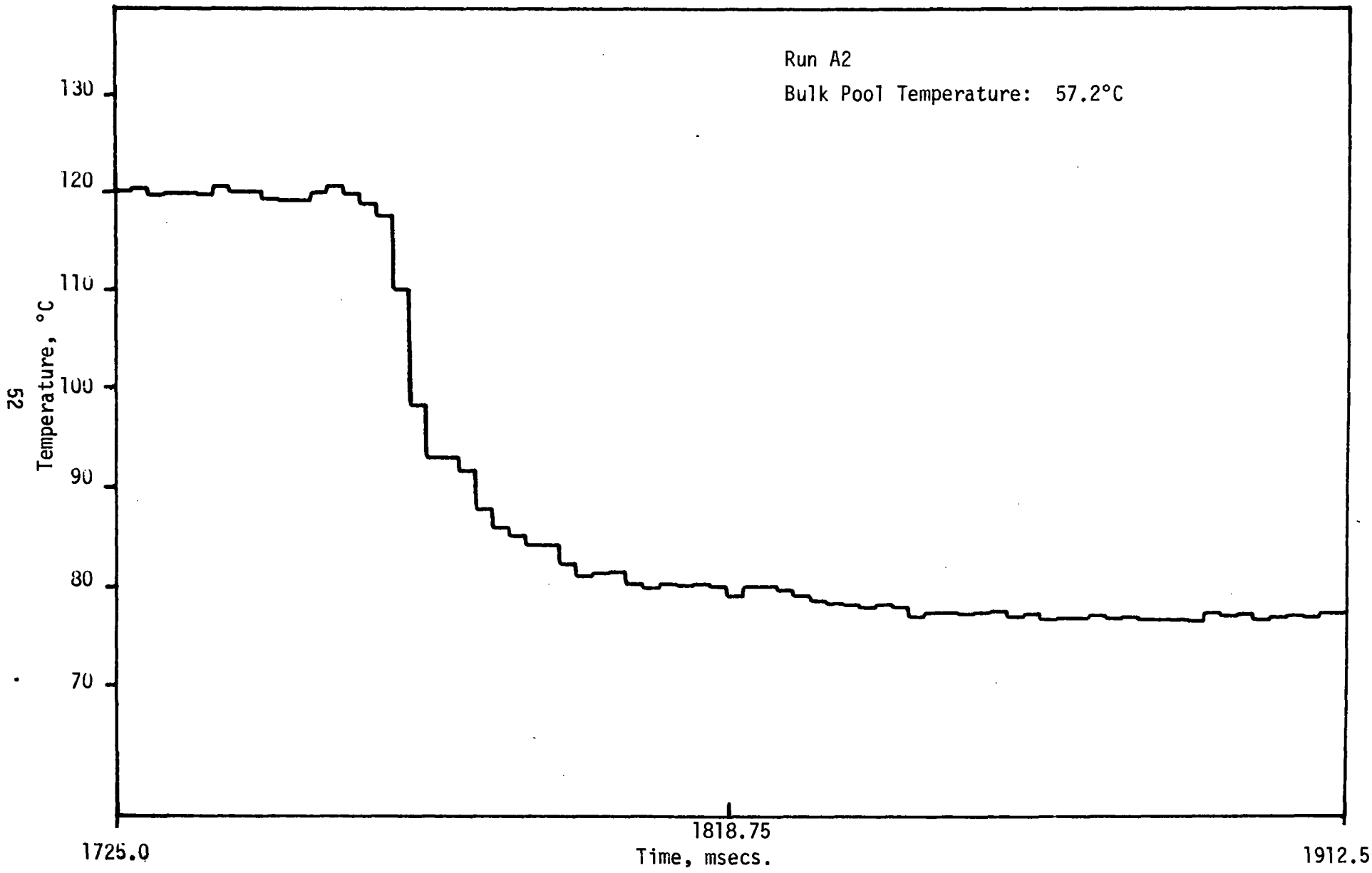

Figure 3.25 Detailed Vent Exit Temperature vs Time for Run A2

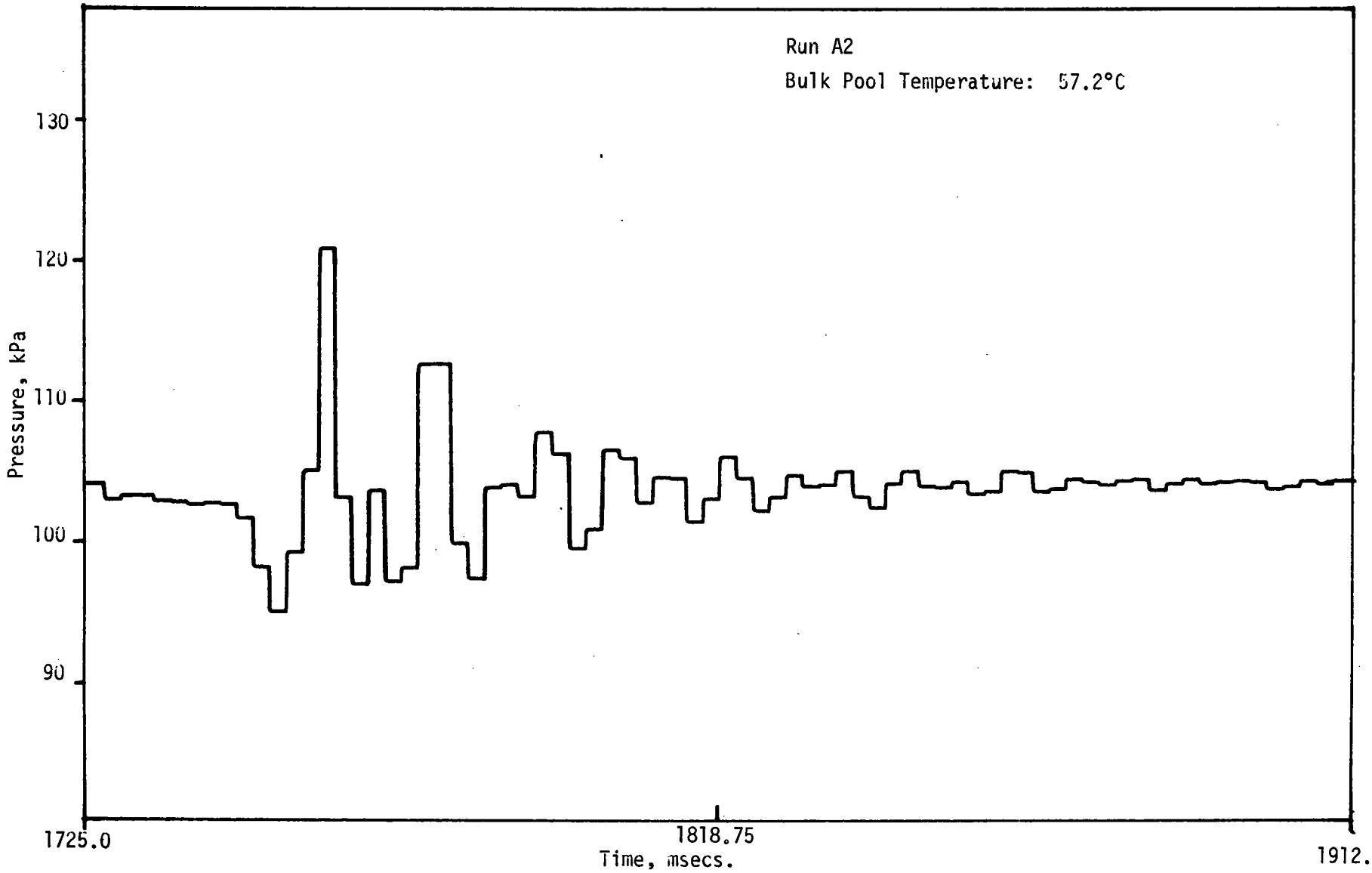

Figure 3.26 Detailed Bottom Pressure vs Time for Run A2

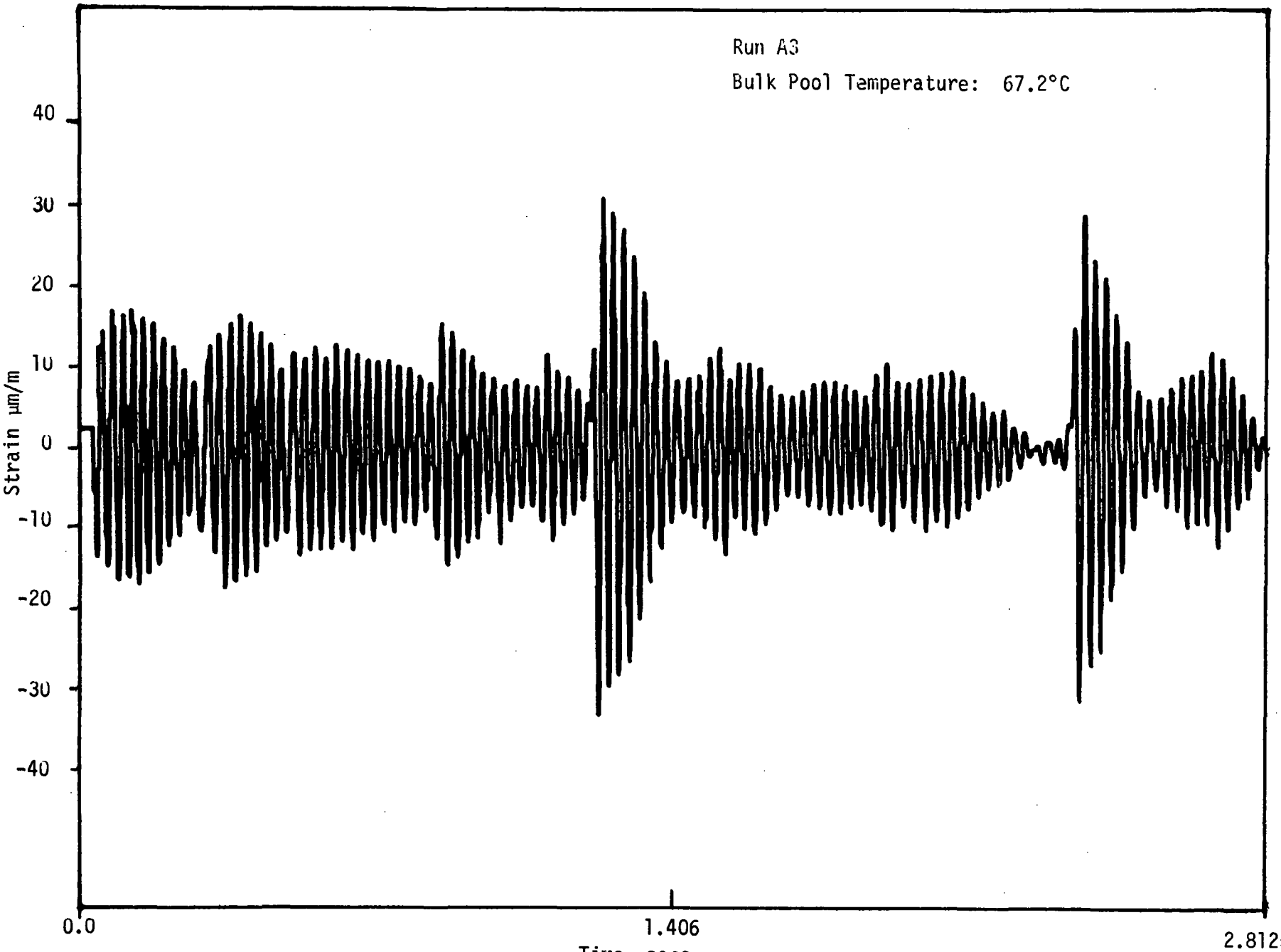

Figure 3.27 Strain (Gauge #1) vs Time for Run A3

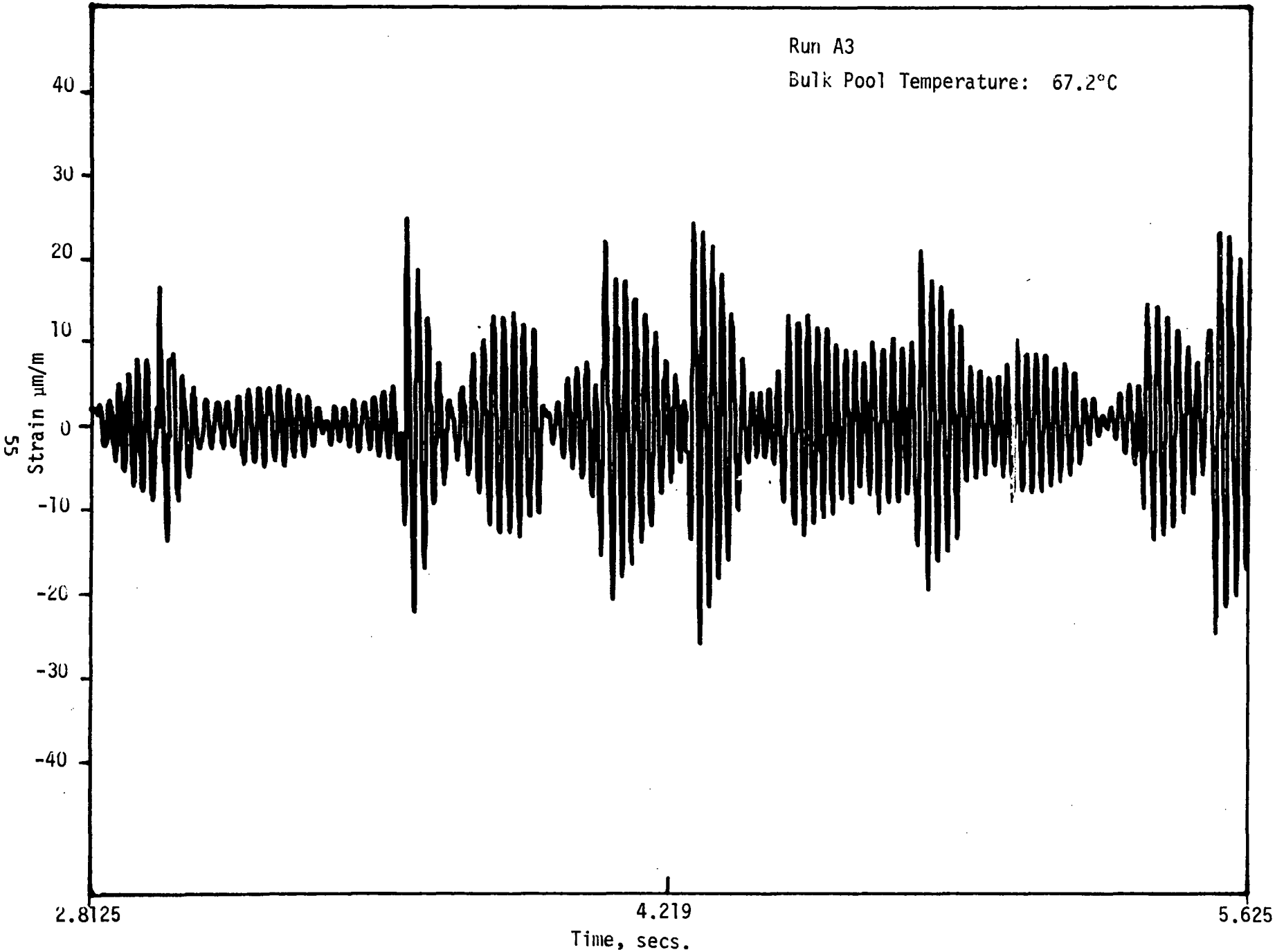

Figure 3.28 Strain (Gauge #1) vs Time for Run A3

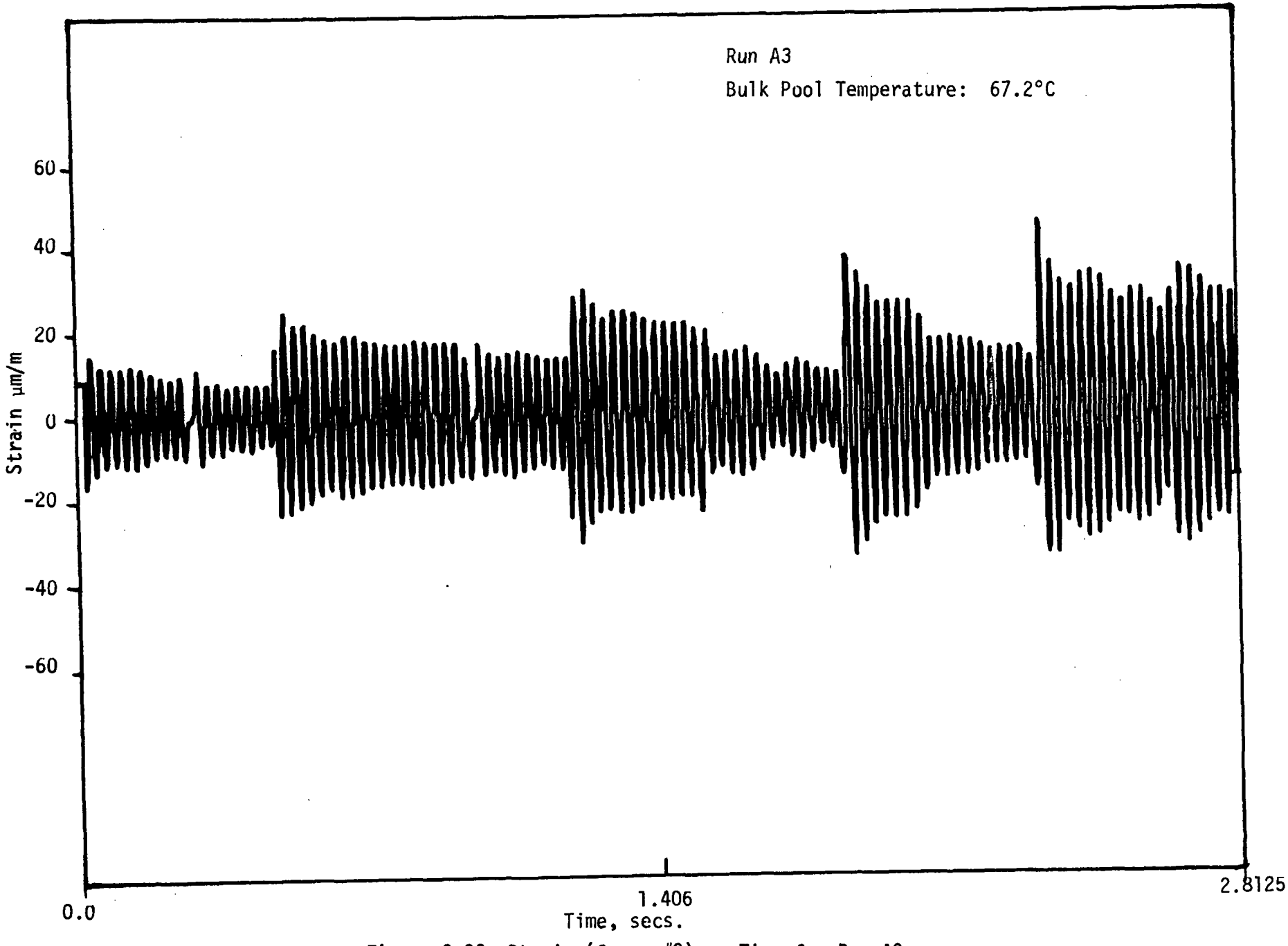

Figure 3.29 Strain (Gauge #2) vs Time for Run A3

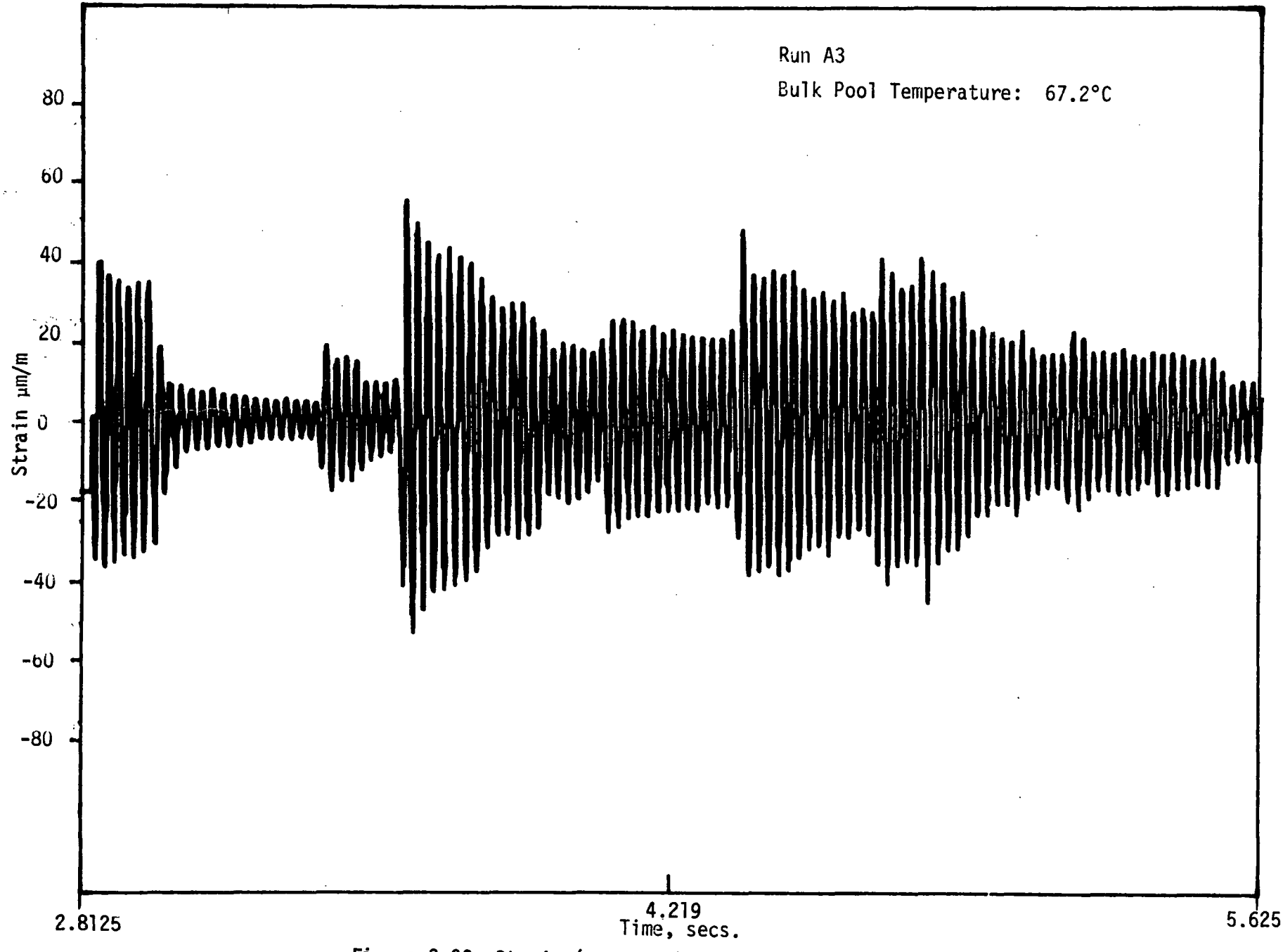

Figure 3.30 Strain (Gauge #2) vs Time for Run A3

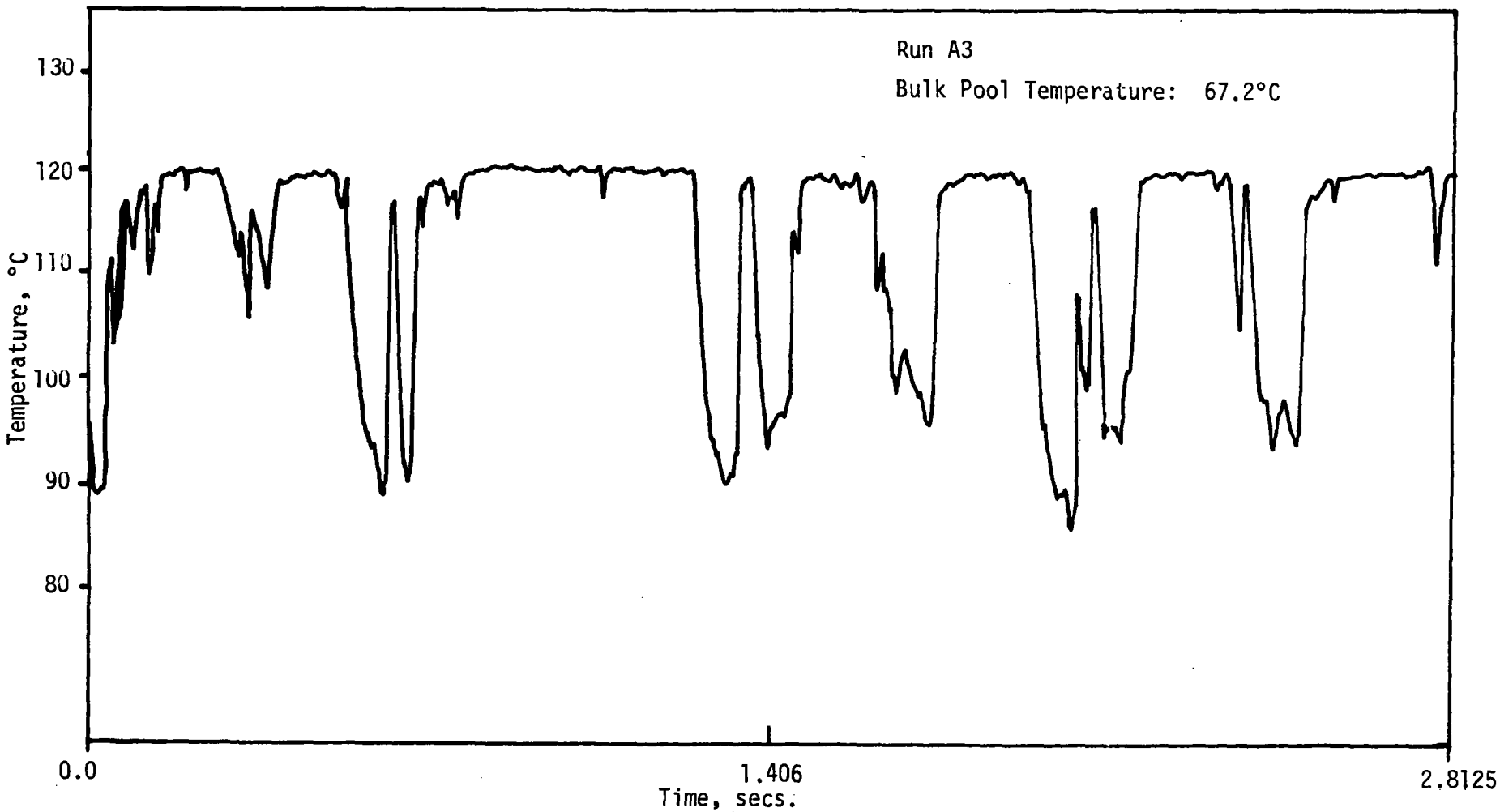

Figure 3.31 Vent Exit Temperature vs Time for Run A3

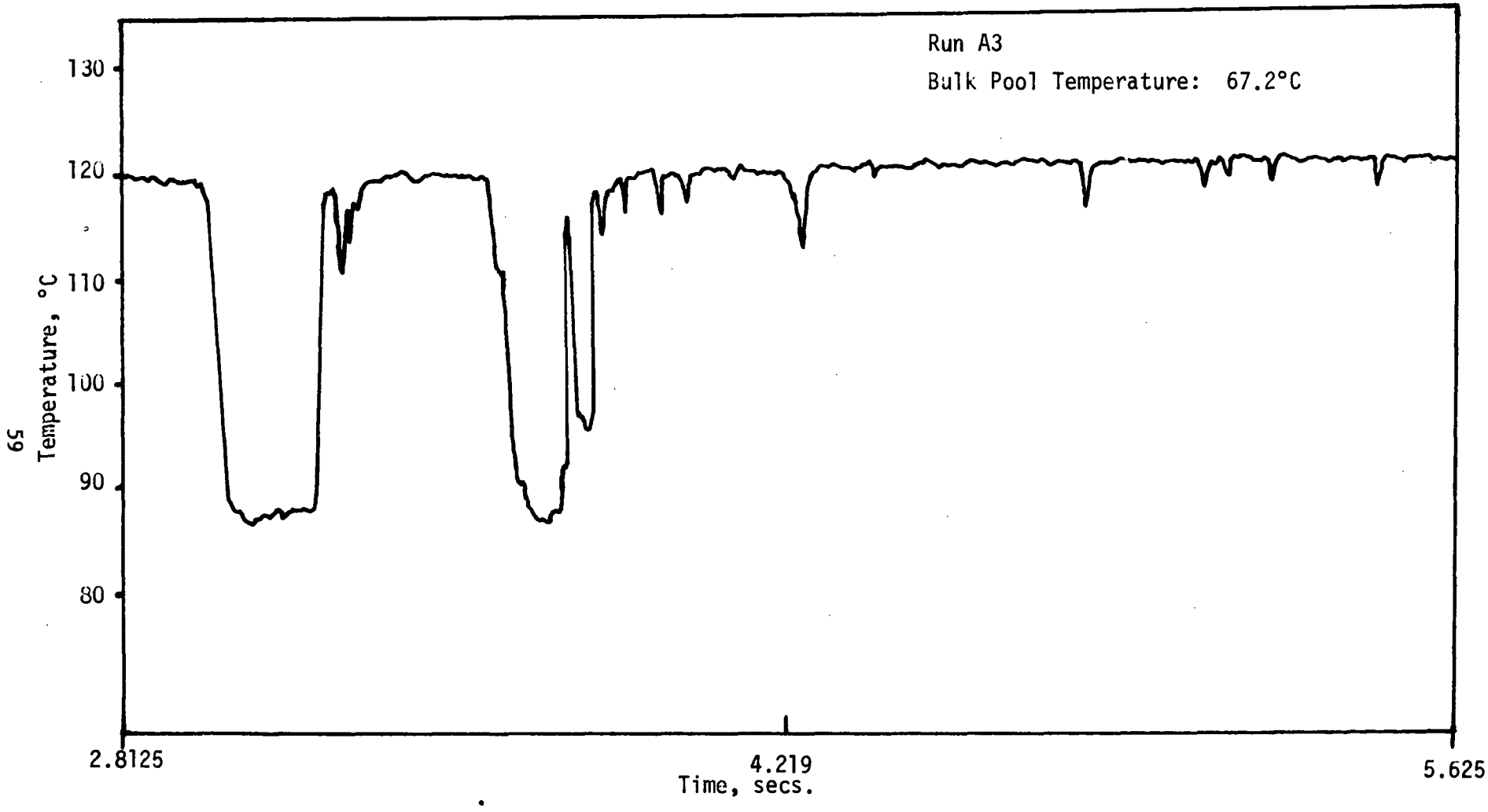

Figure 3.32 Vent Exit Temperature vs Time for Run A3

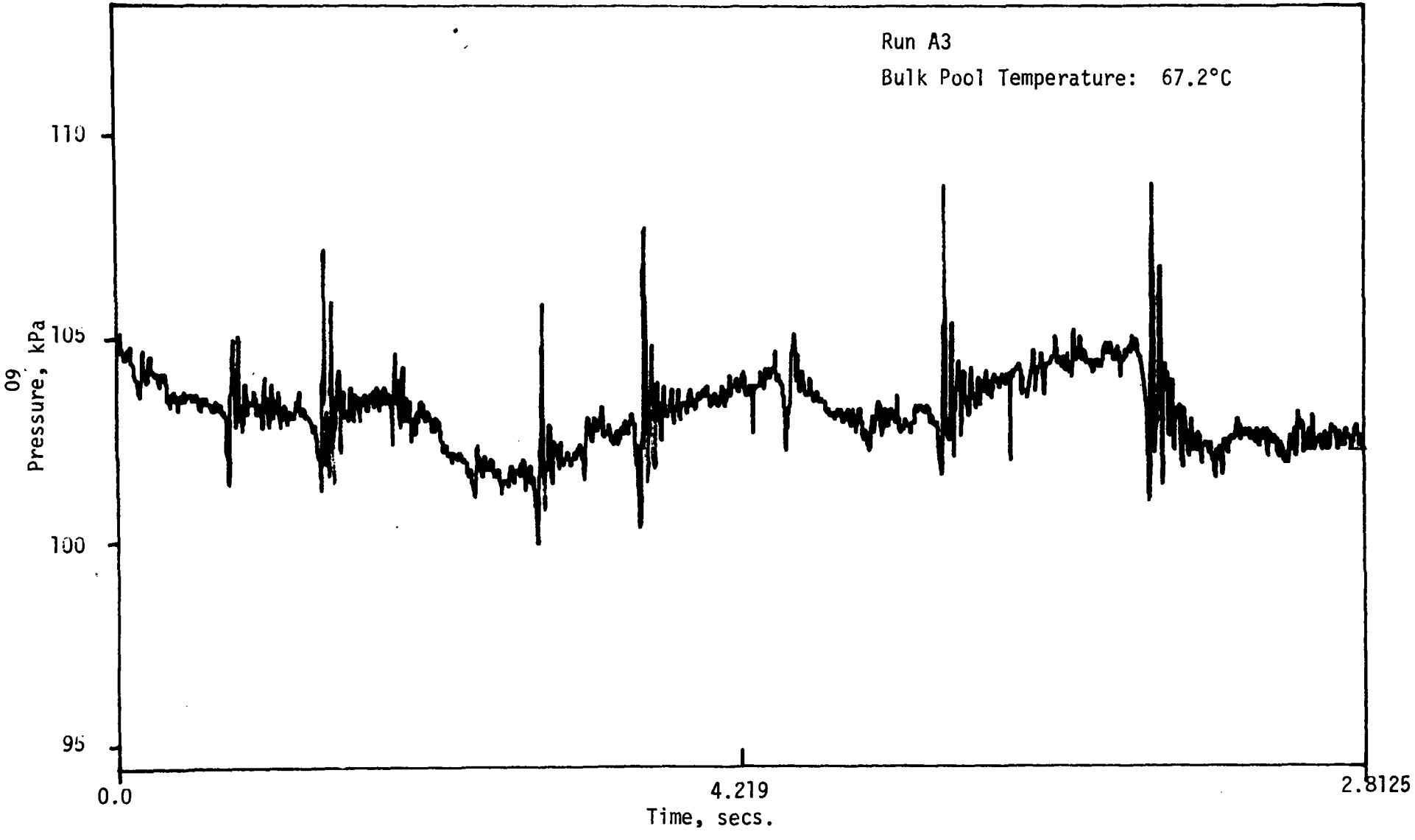

Figure 3.33 Bottom Pressure vs Time for Run A3

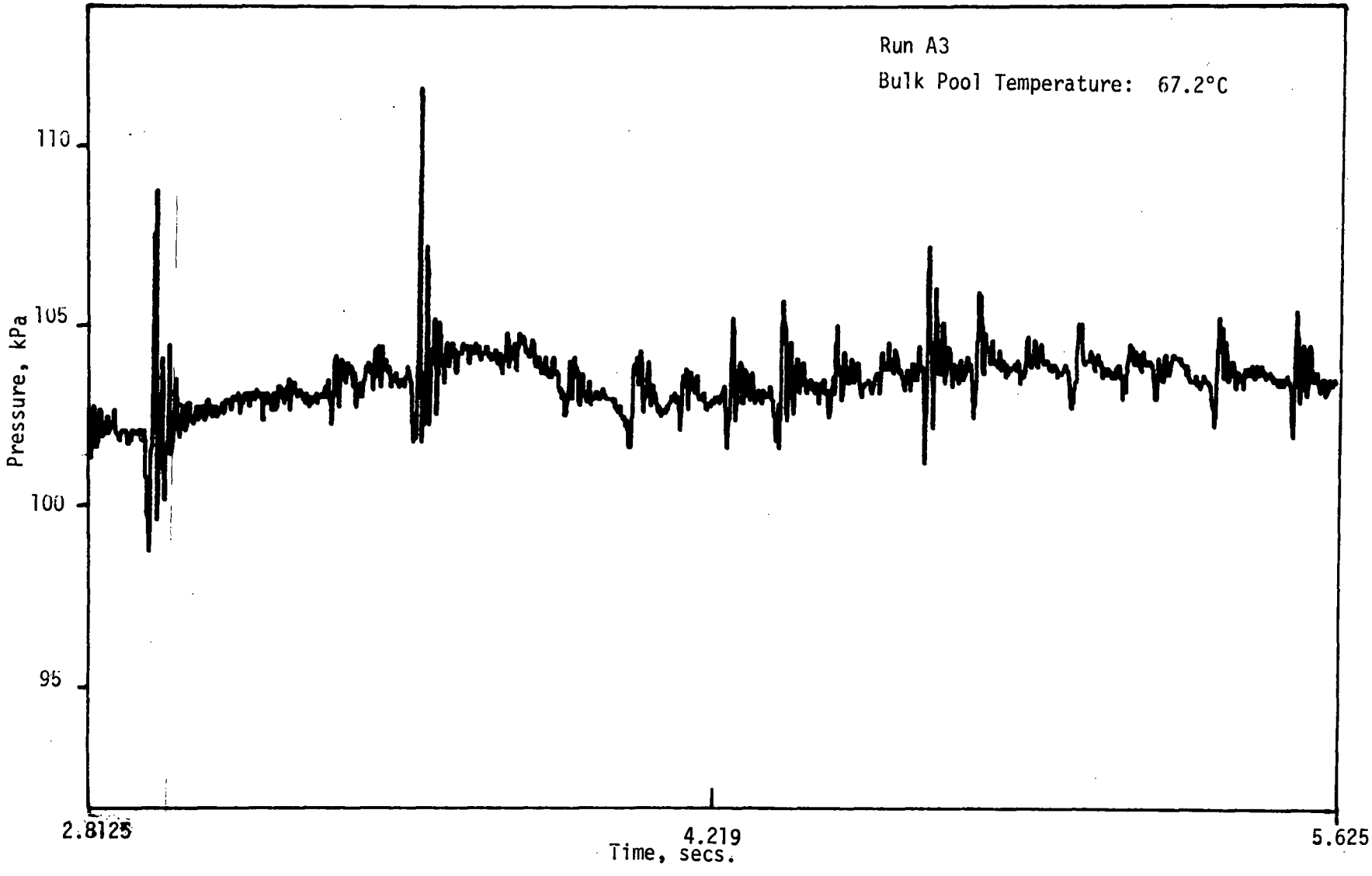

Figure 3.34 Bottom Pressure vs Time for Run A3

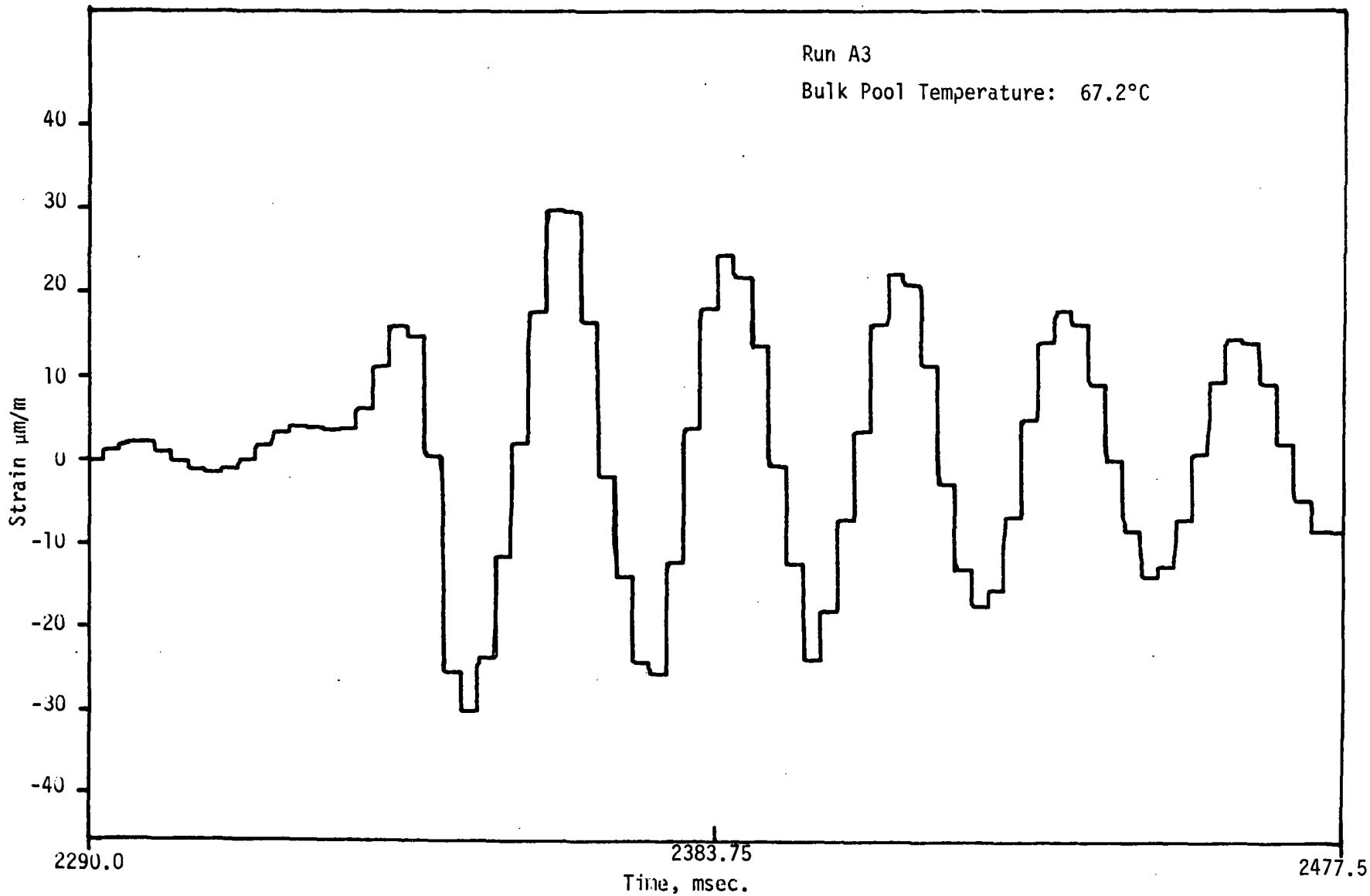

Figure 3.35 Detailed Strain (Gauge #1) vs Time for Run A3

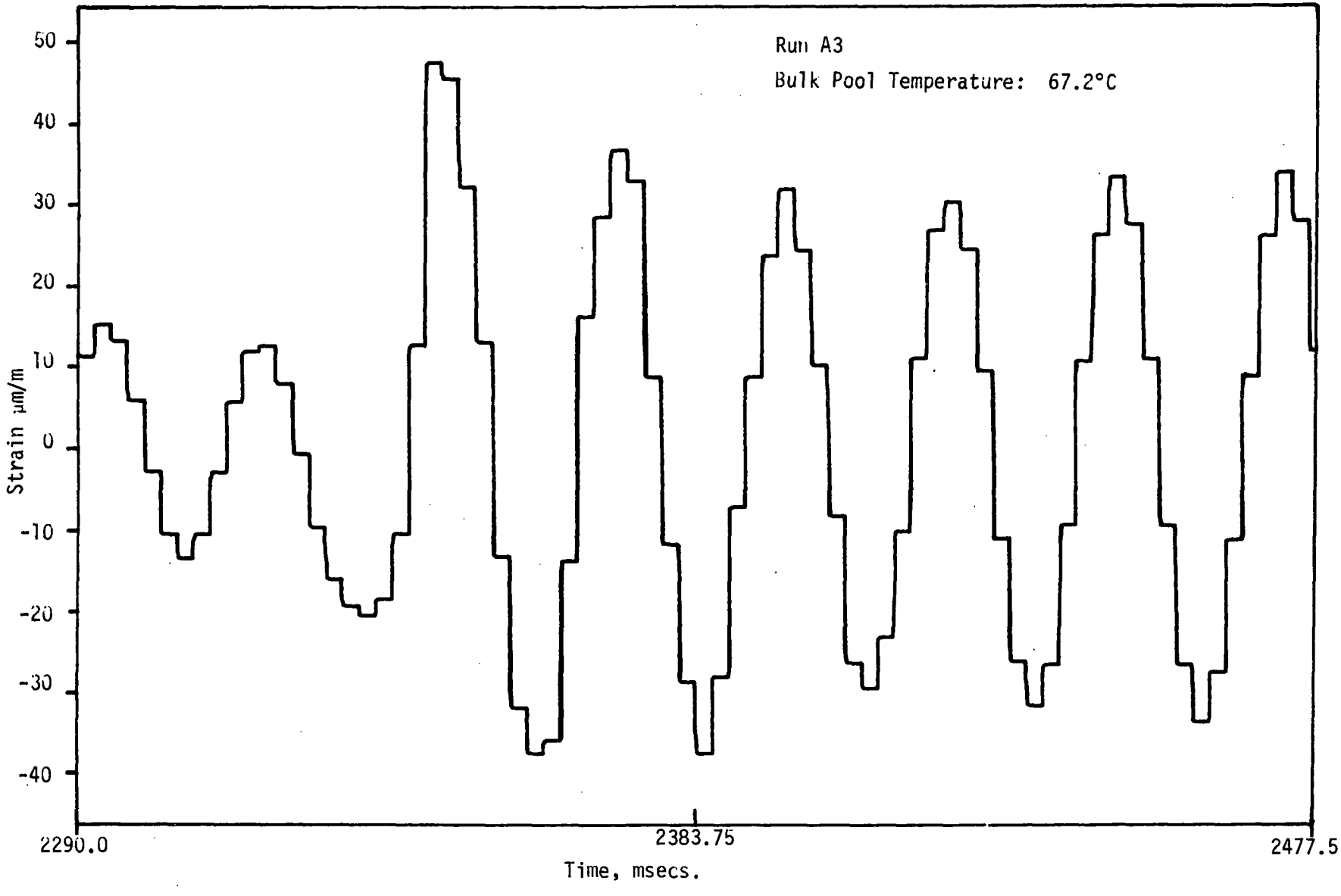

Figure 3.36 Detailed Strain (Gauge #2) vs Time for Run A3

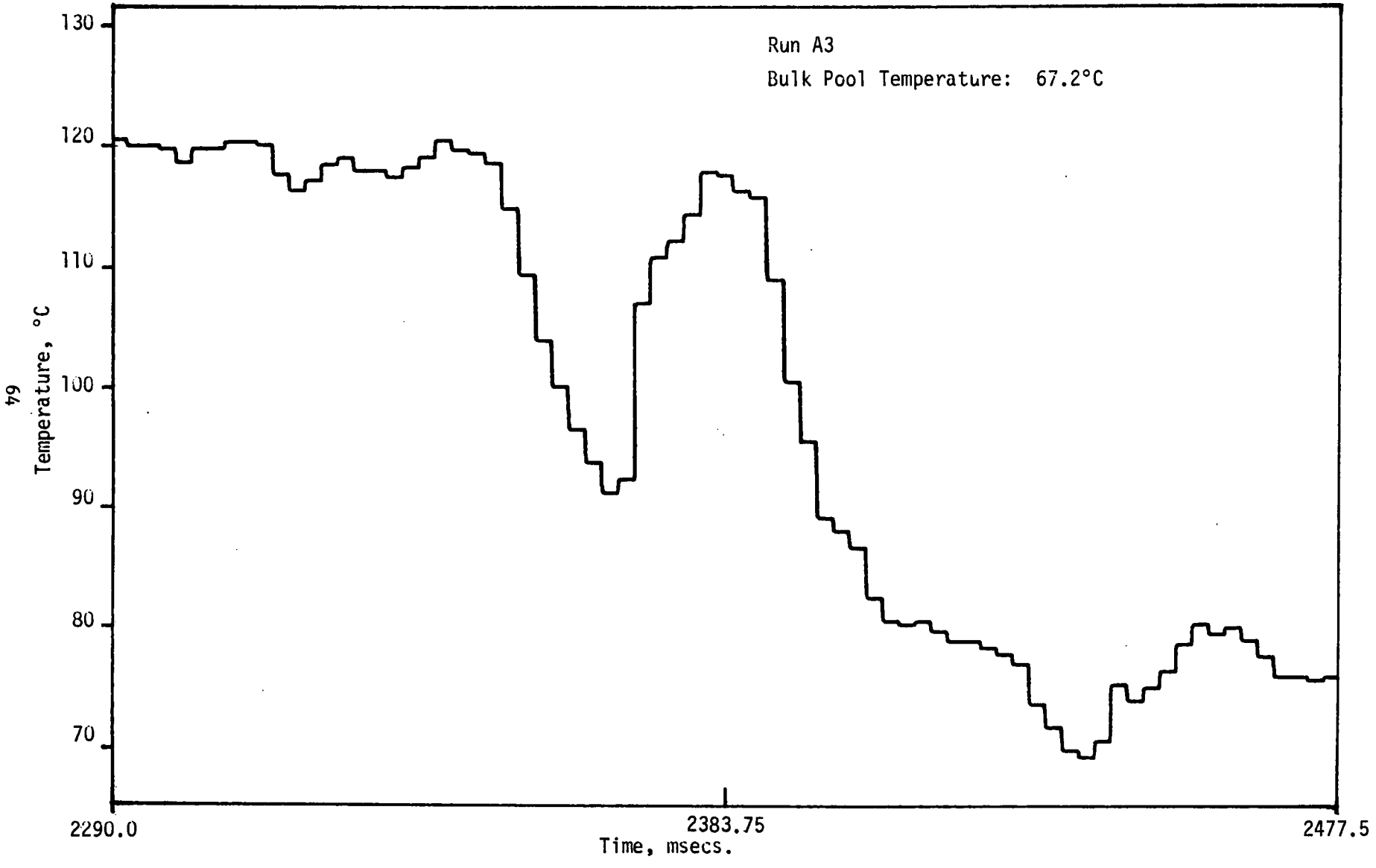

Figure 3.37 Detailed Vent Exit Temperature vs Time for Run A3

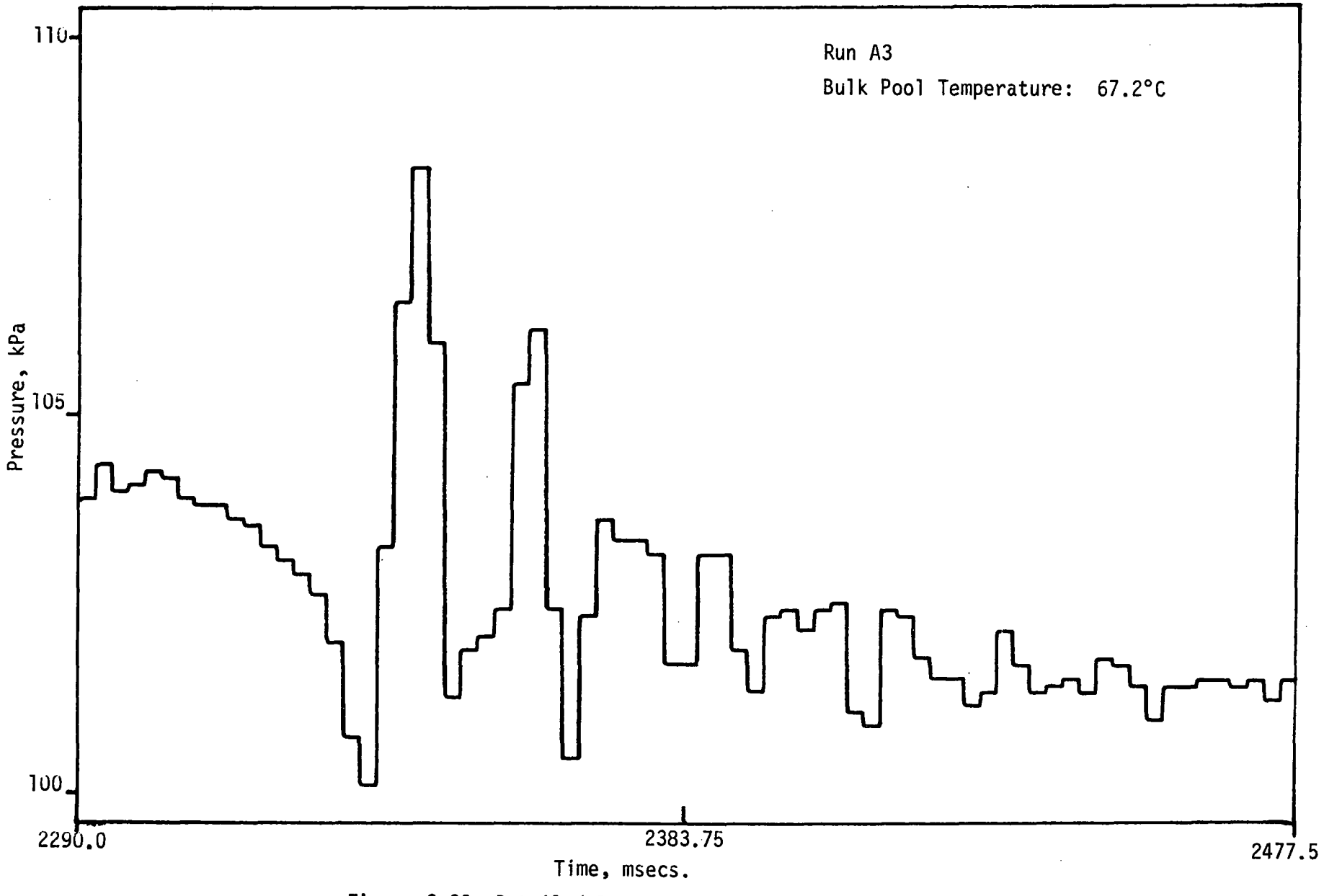

Figure 3.38 Detailed Bottom Pressure vs Time for Run A4

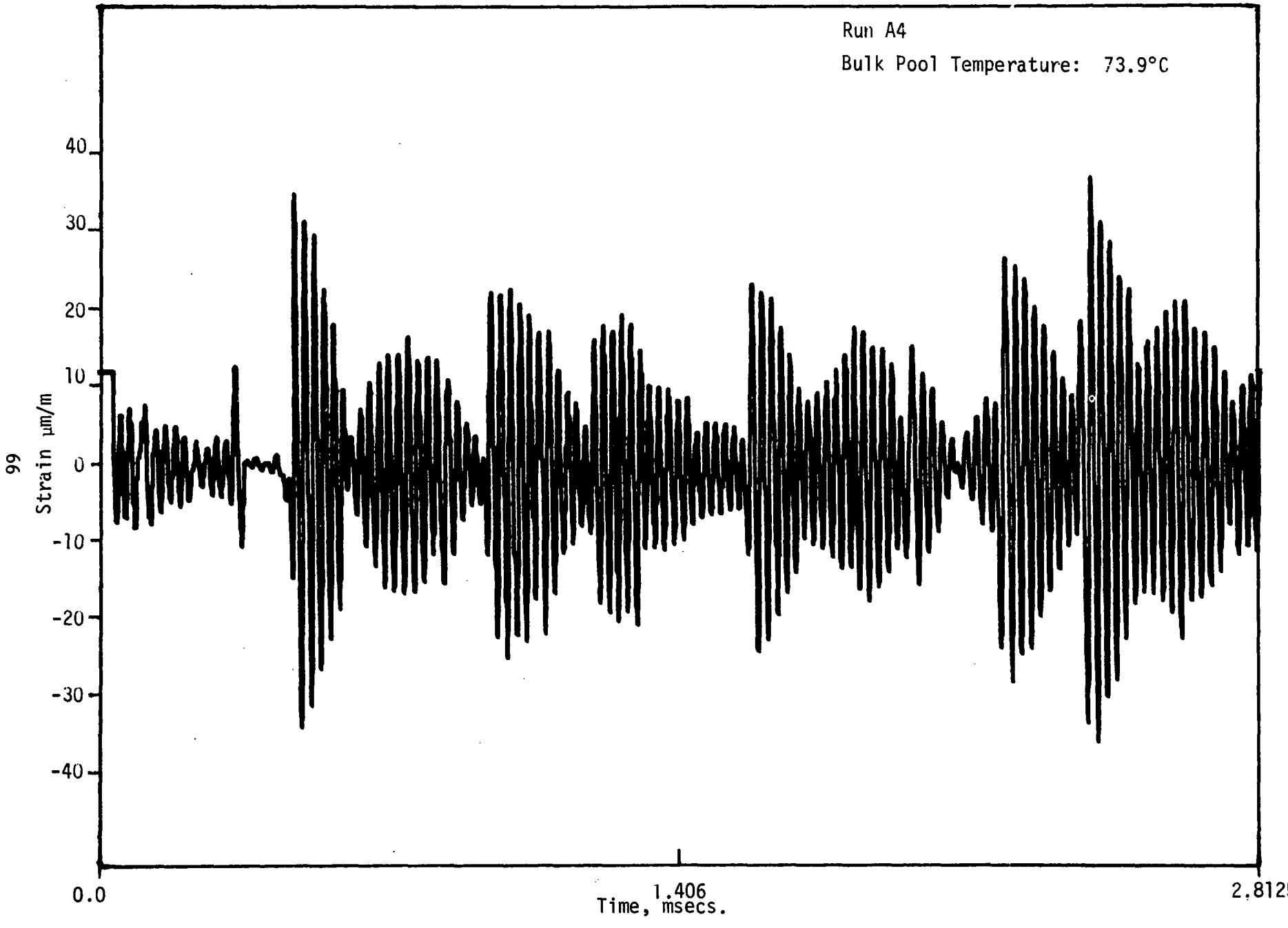

Figure 3.39 Strain (Gauge #1) vs Time for Run A4

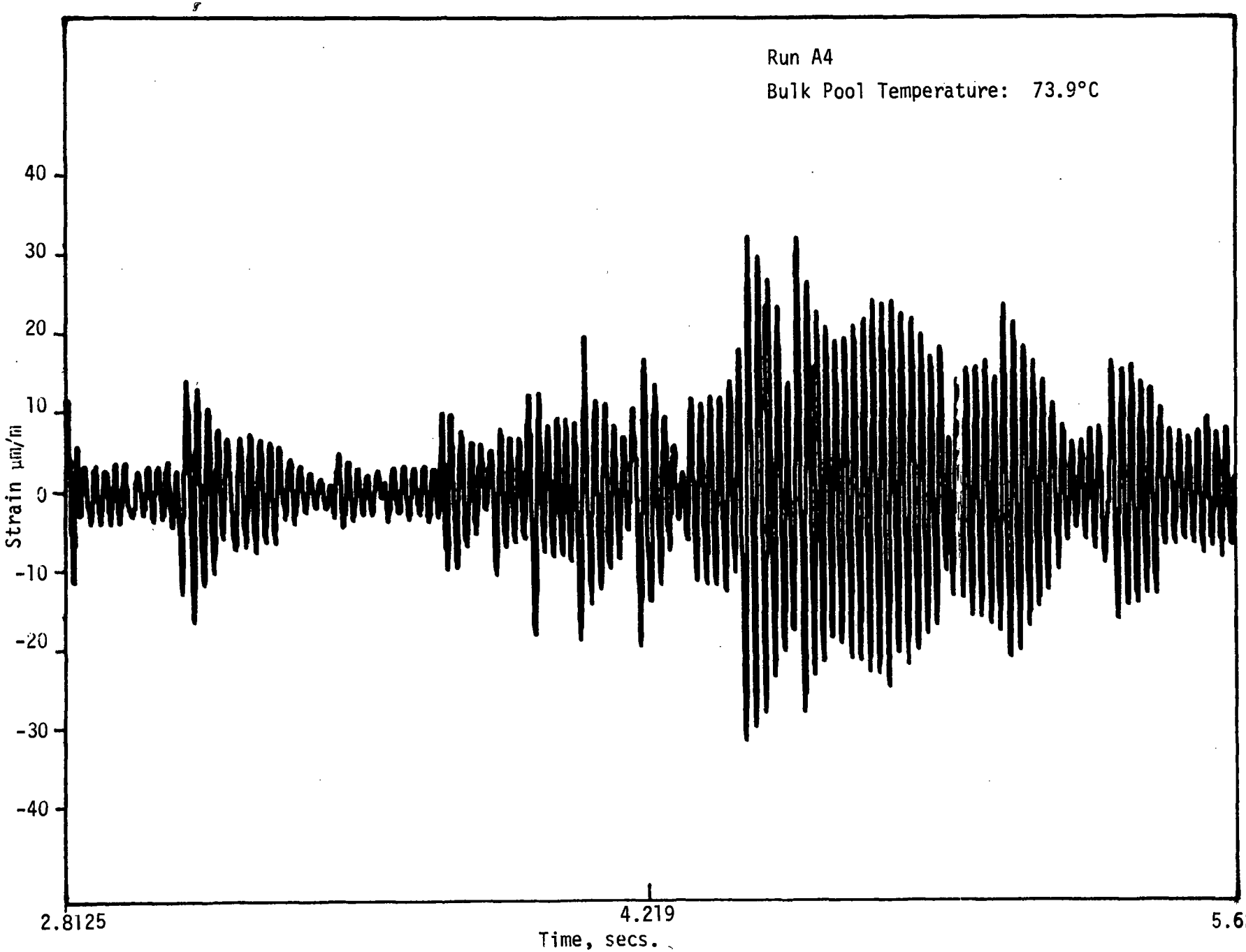

Figure 3.40 Strain (Gauge #1) vs Time for Run A4

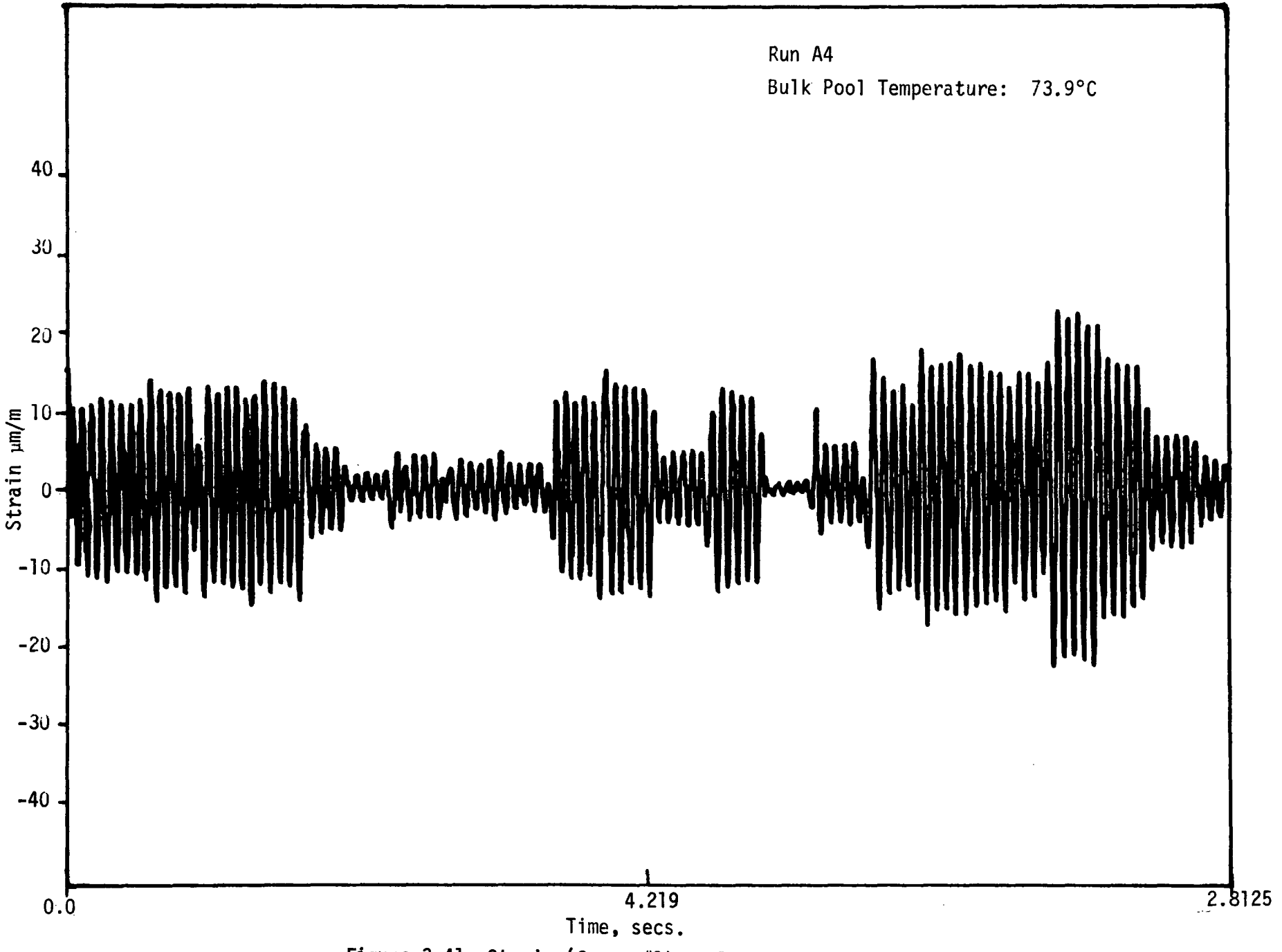

Figure 3.41 Strain (Gauge #2) vs Time for Run A4

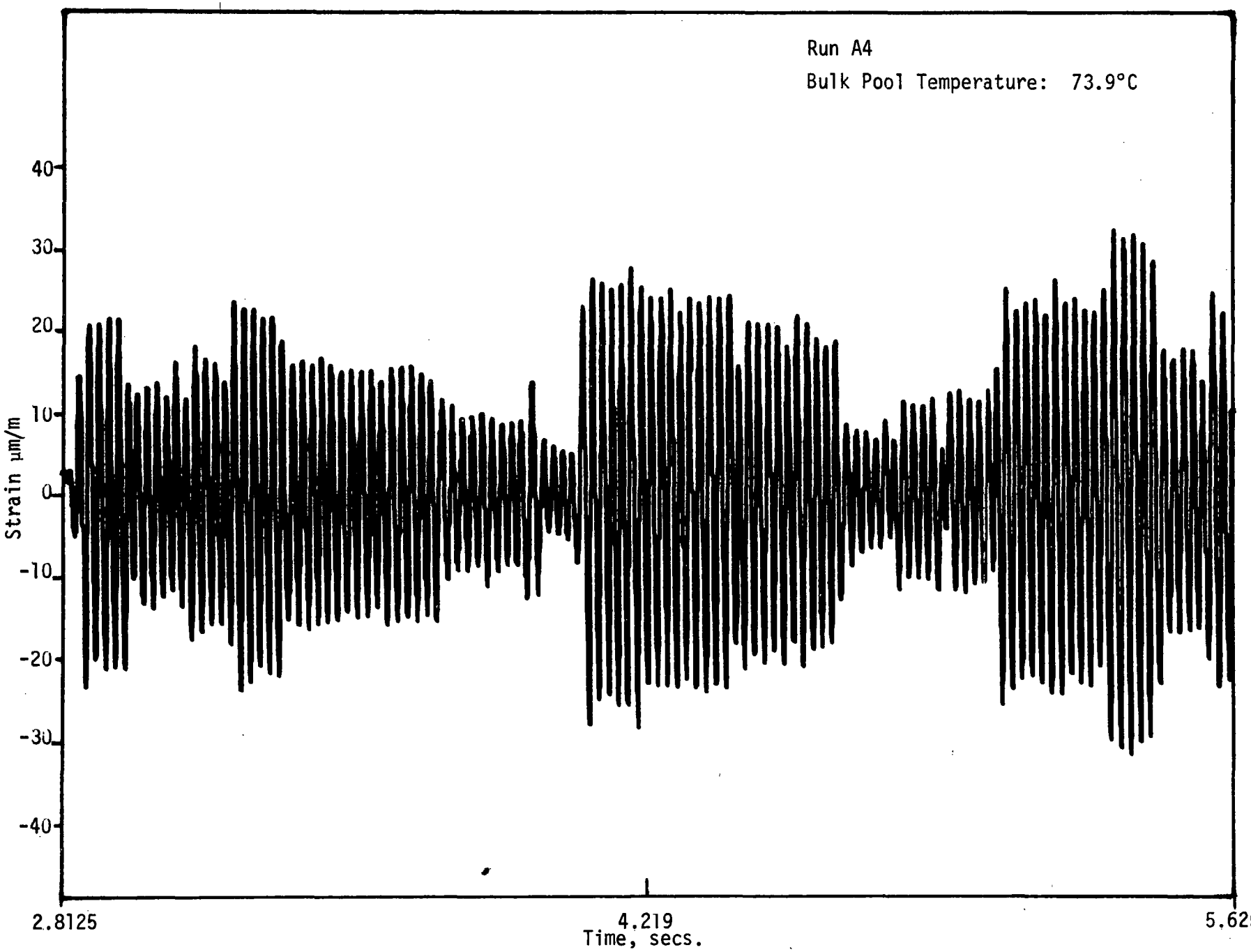

Figure 3.42 Strain (Gauge #2) vs Time for Run A4

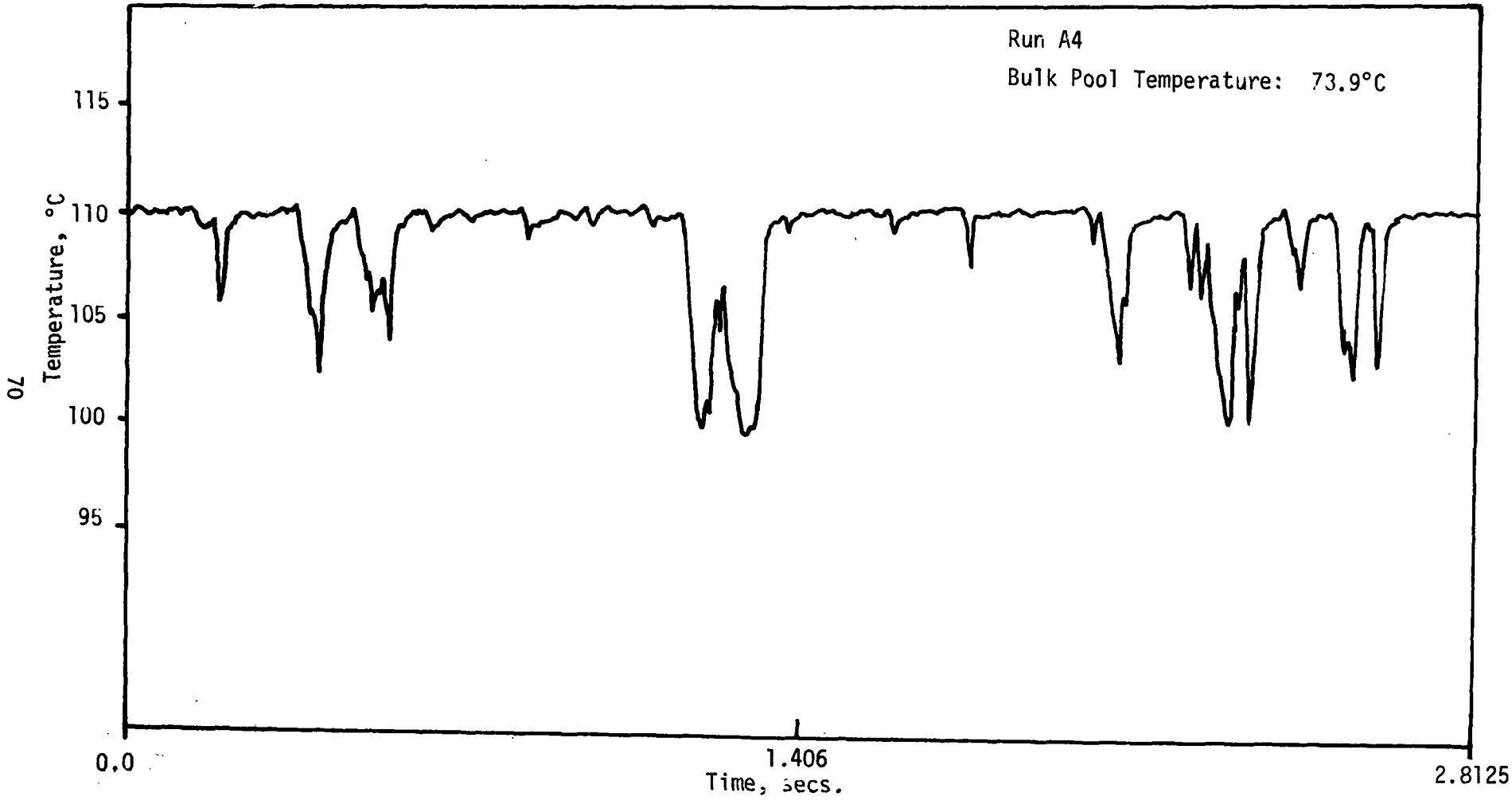

Figure 3.43 Vent Exit Temperature vs Time for Run A4

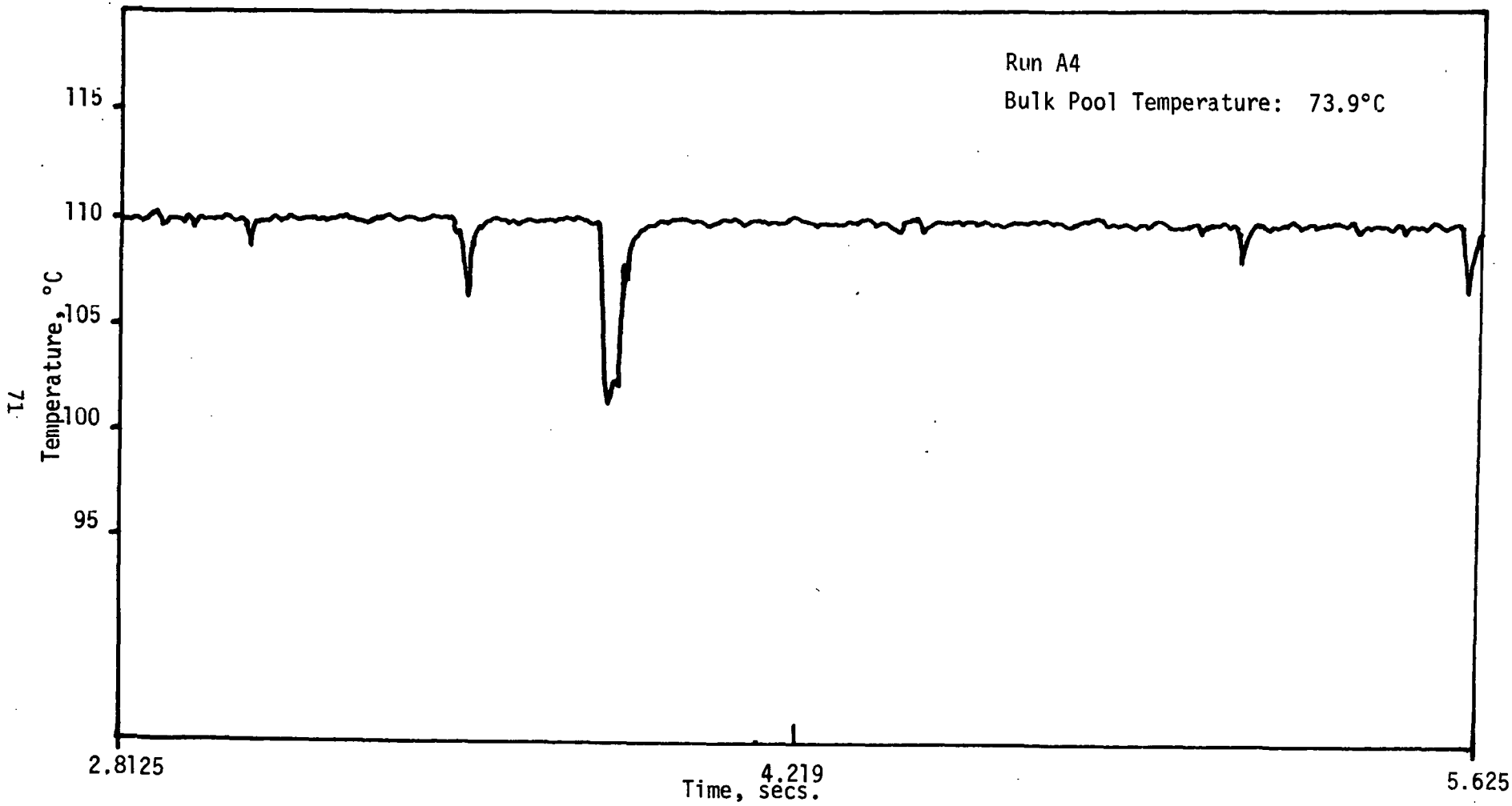

Figure 3.44 Vent Exit Temperature vs Time for Run A4

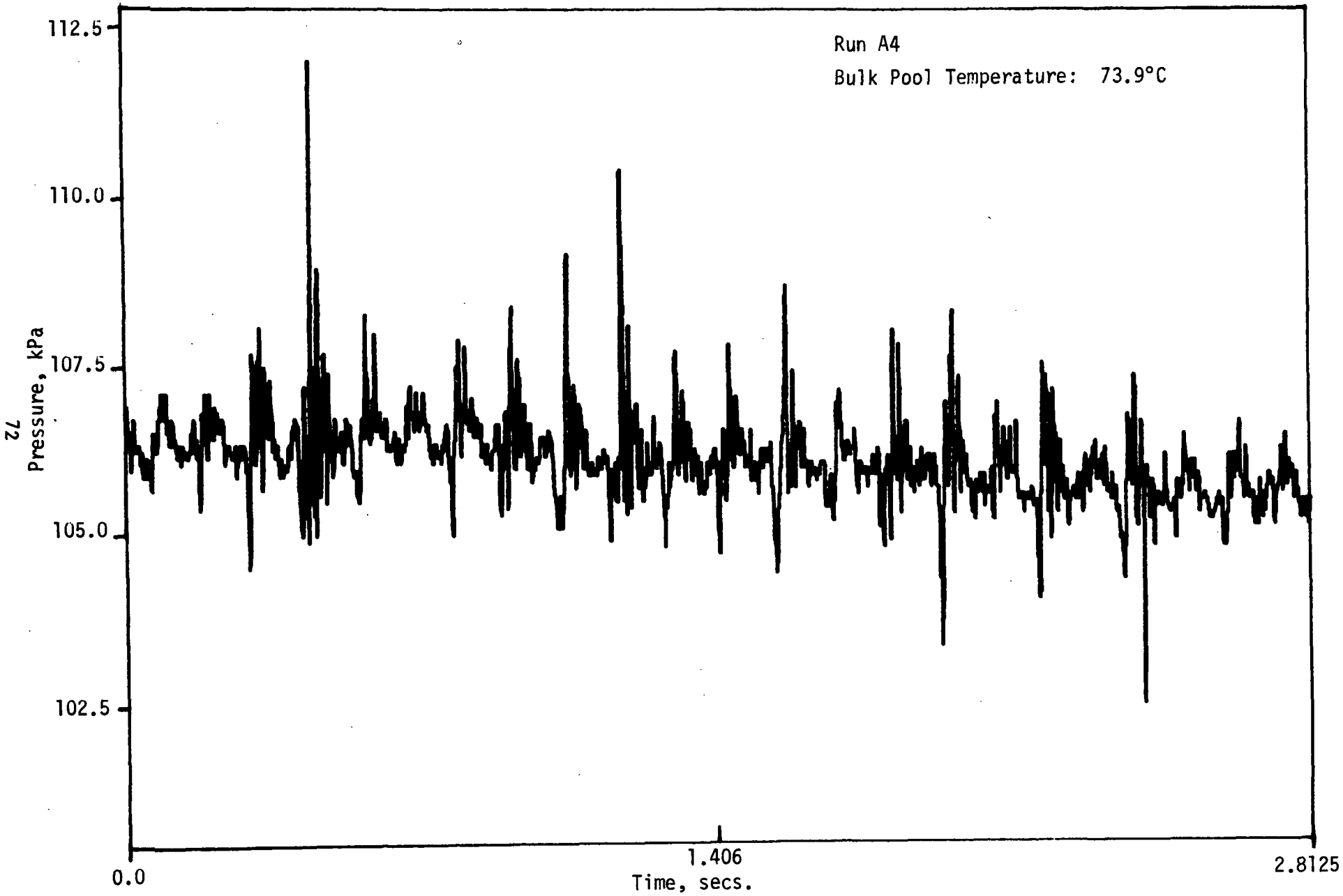

Figure 3.45 Bottom Pressure vs Time for Run A4

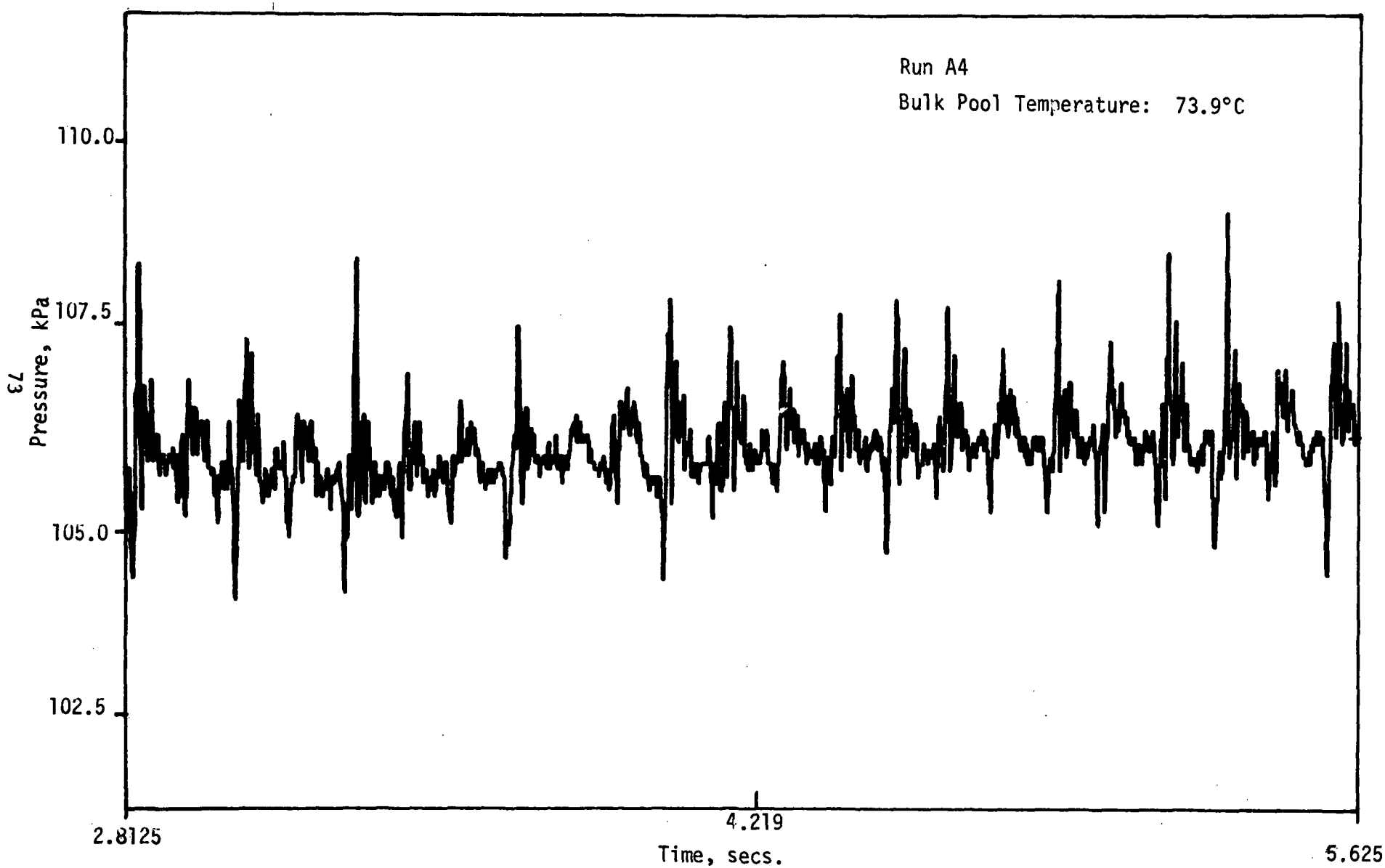

Figure 3.46 Bottom Pressure vs Time for Run A4

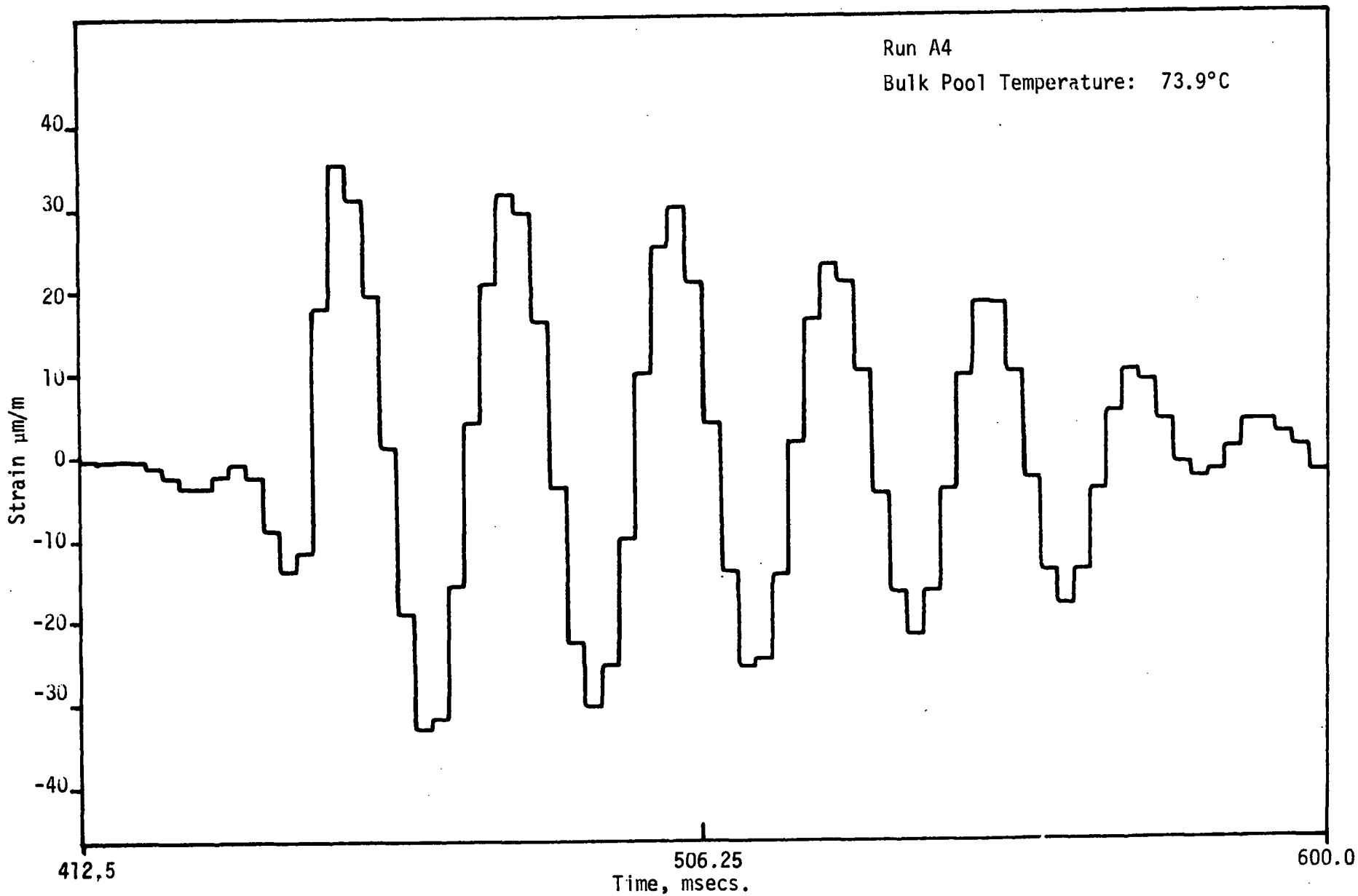

Figure 3.47 Detailed Strain (Gauge #1) vs Time for Run A4

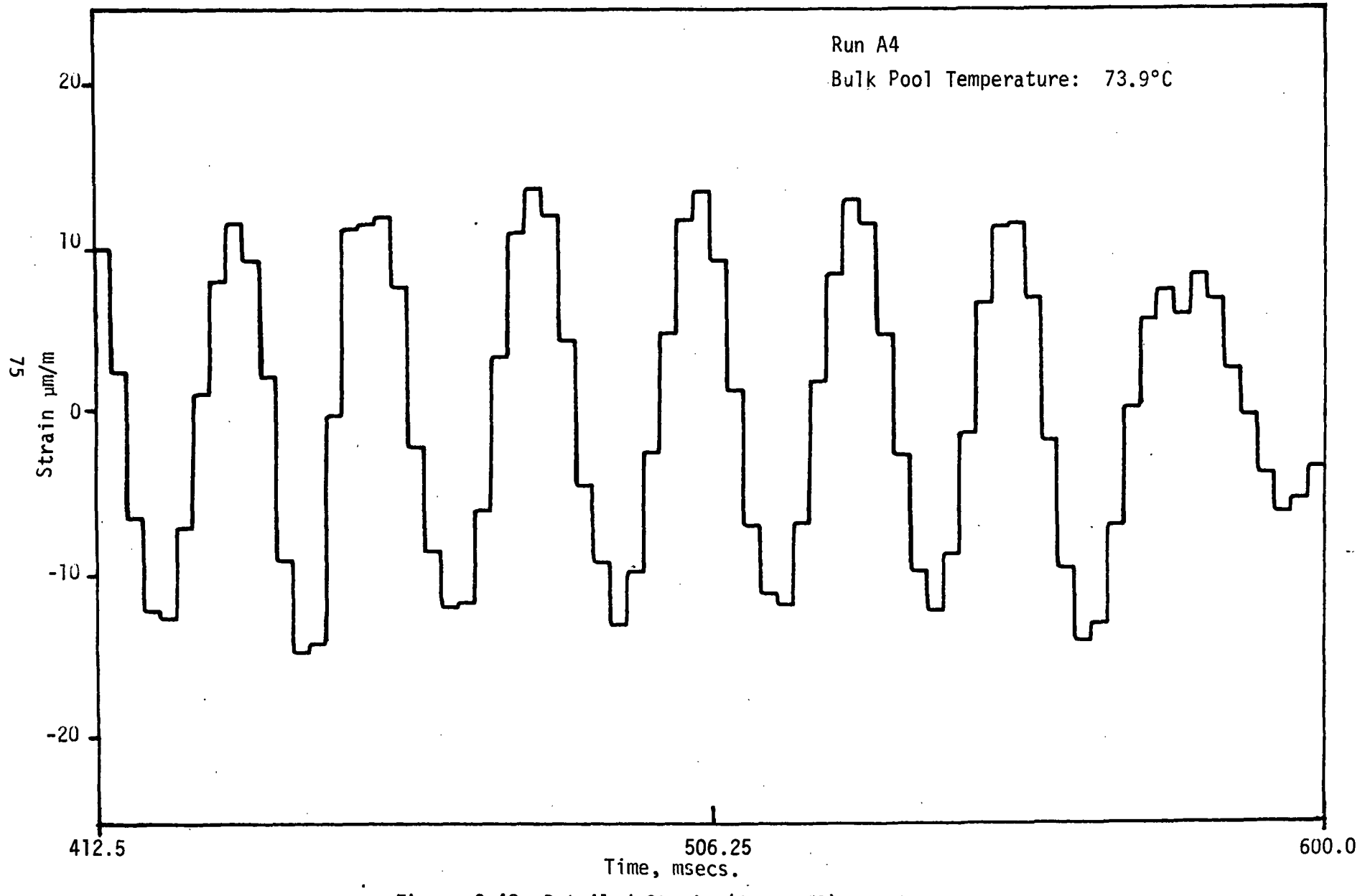

Figure 3.48 Detailed Strain (Gauge #2) vs Time for Run A4

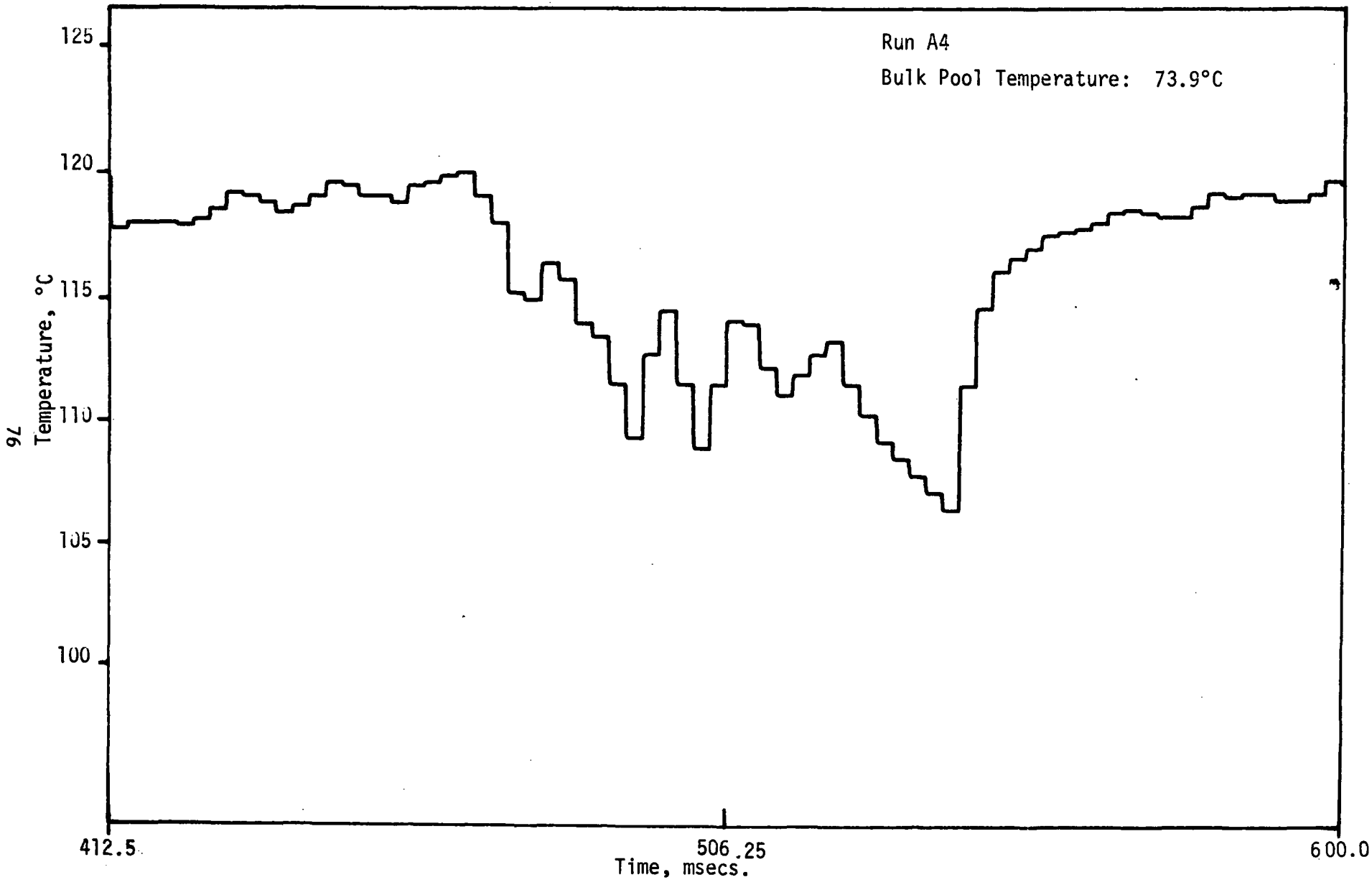

Figure 3.49 Detailed Vent Exit Temperature vs Time for Run A4

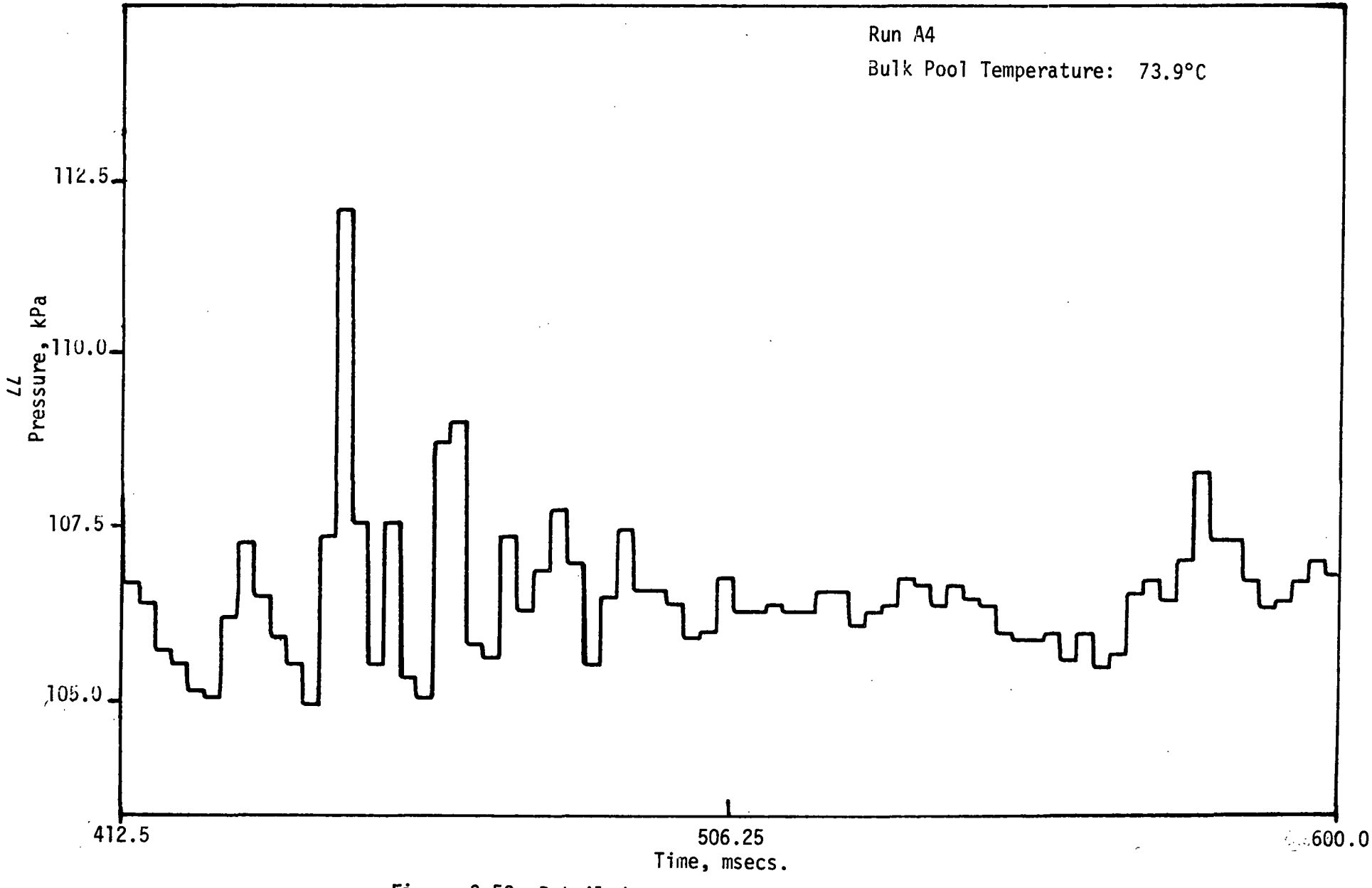

Figure 3.50 Detailed Bottom Pressure vs Time for Run A4

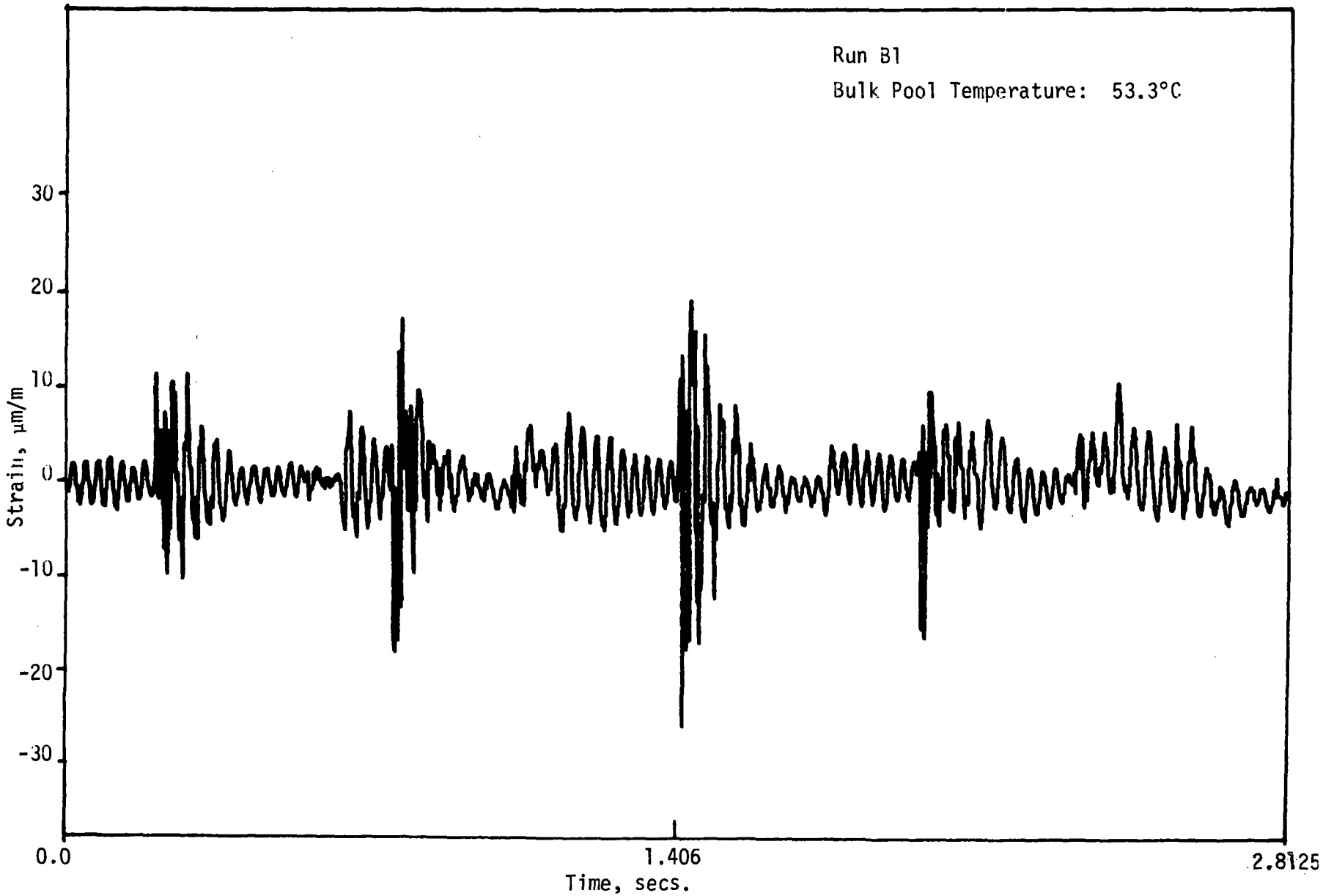

Figure 3.51 Strain (Gauge #1) vs Time for Run B1

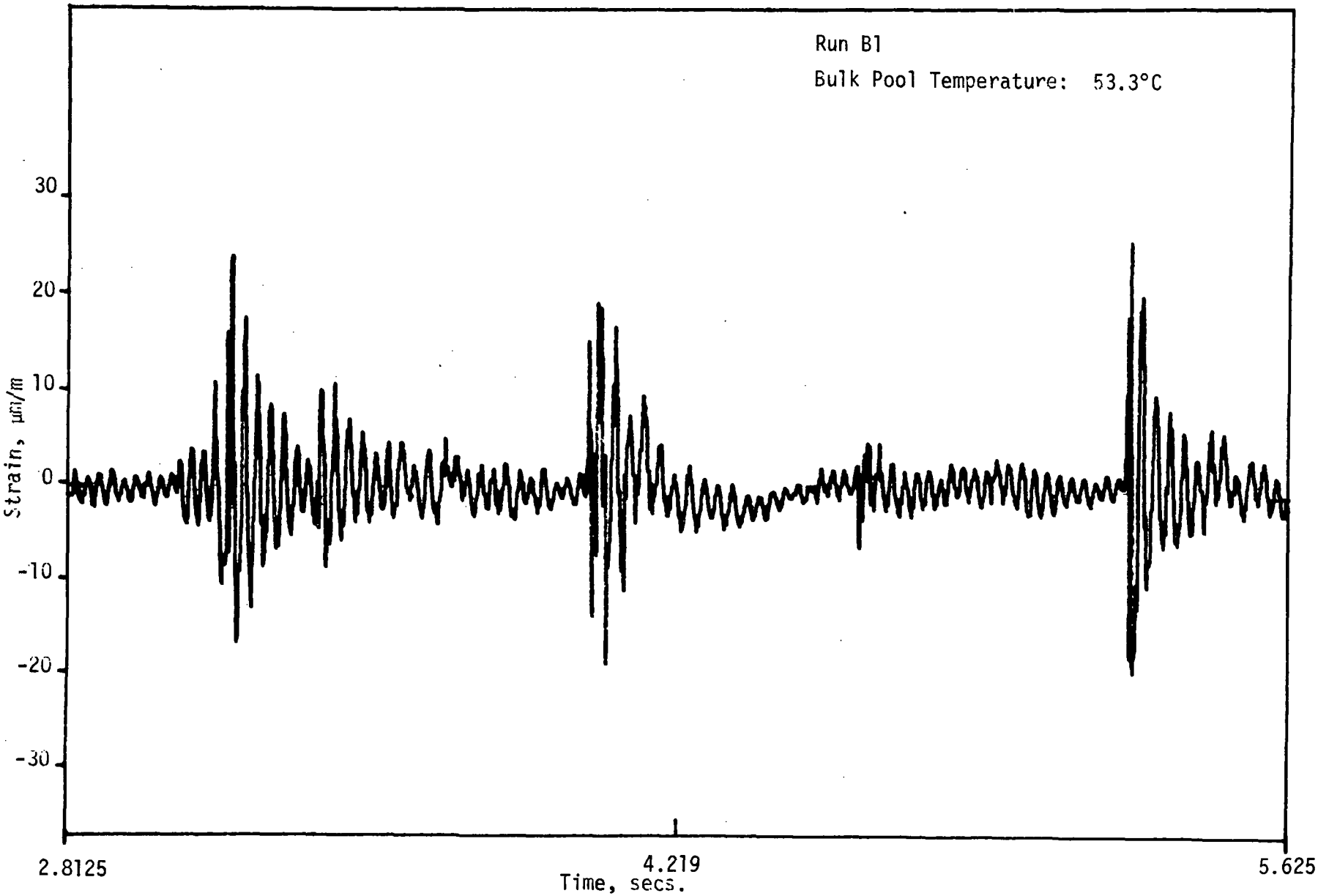

Figure 3.52 Strain (Gauge #1) vs Time for Run B1

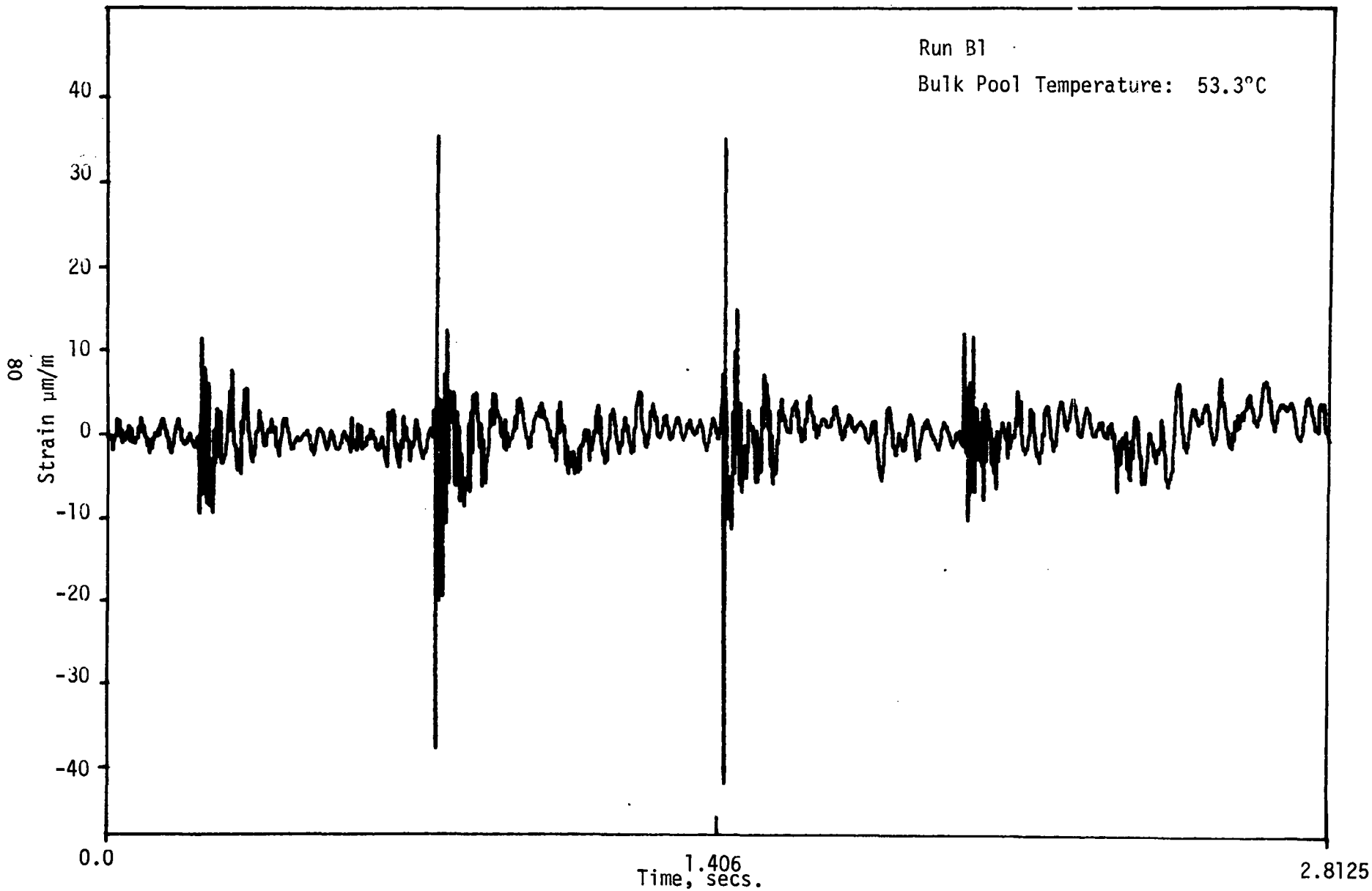

Figure 3.53 Strain (Gauge #2) vs Time for Run B1

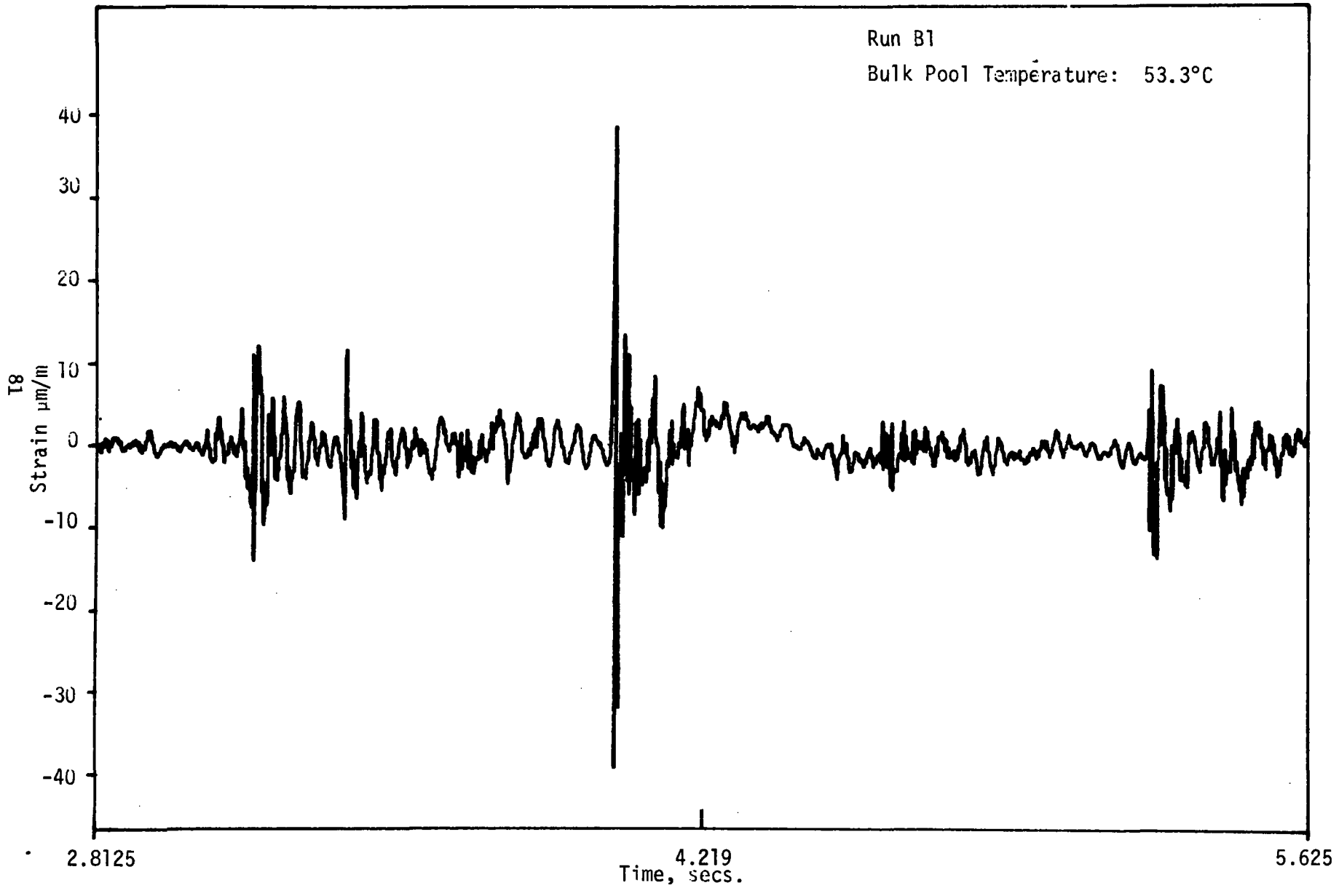

Figure 3.54 (Strain Gauge #2) vs Time for Run B1

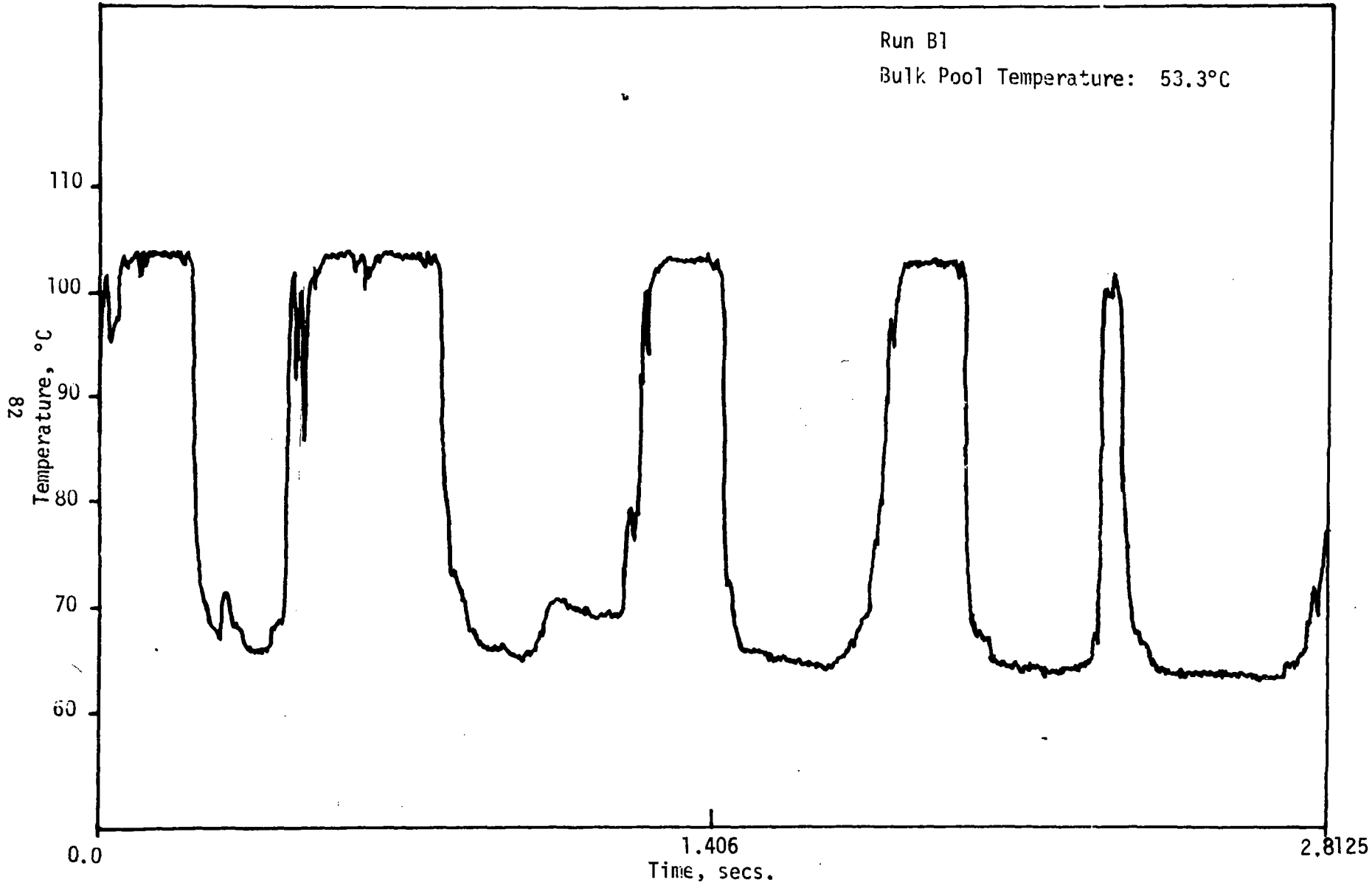

Figure 3.55 Vent Exit Temperature vs Time for Run B1

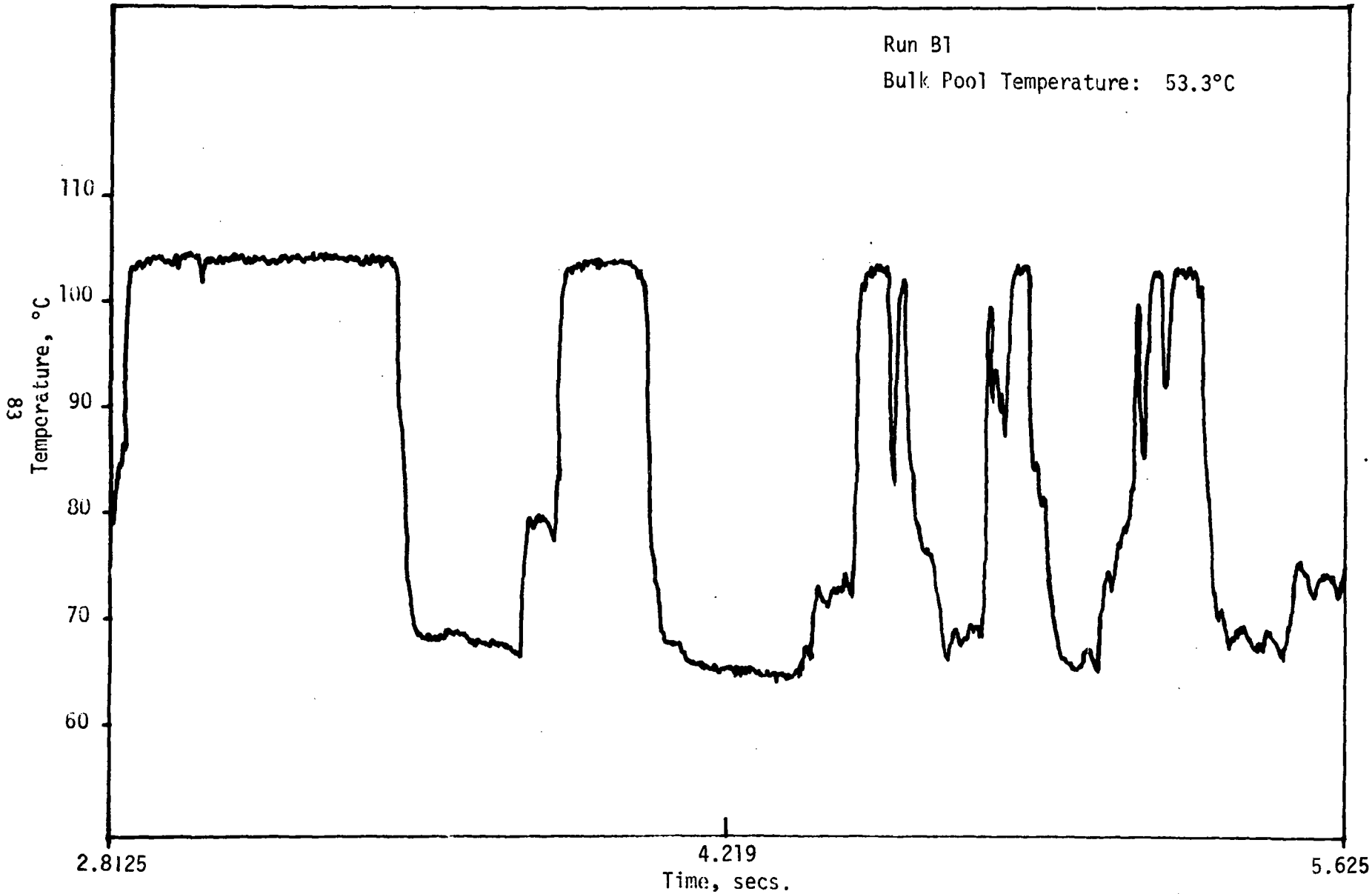

Figure 3.56 Vent Exit Temperature vs Time for Run B1

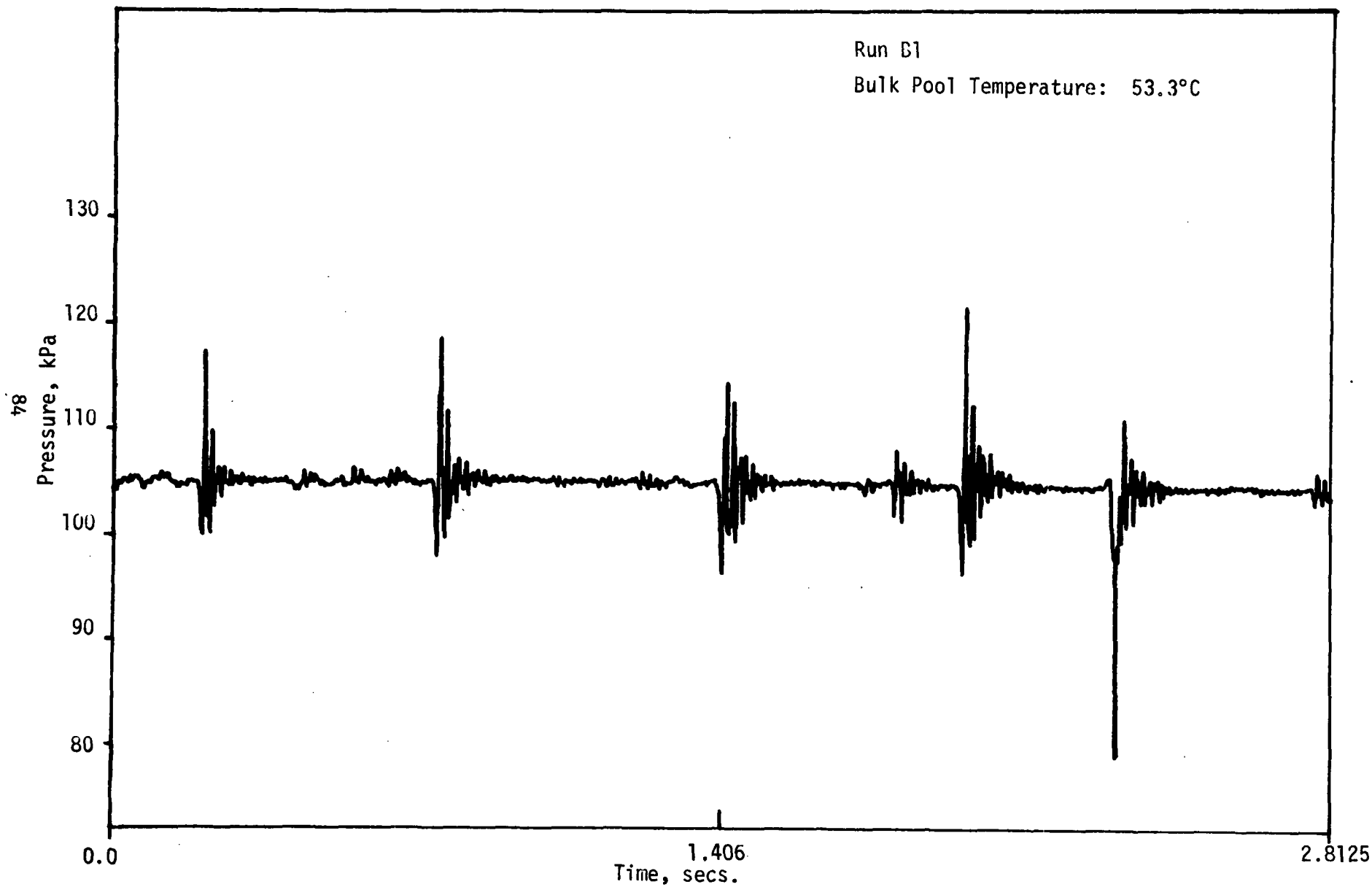

Figure 3.57 Bottom Pressure vs Time for Run B1

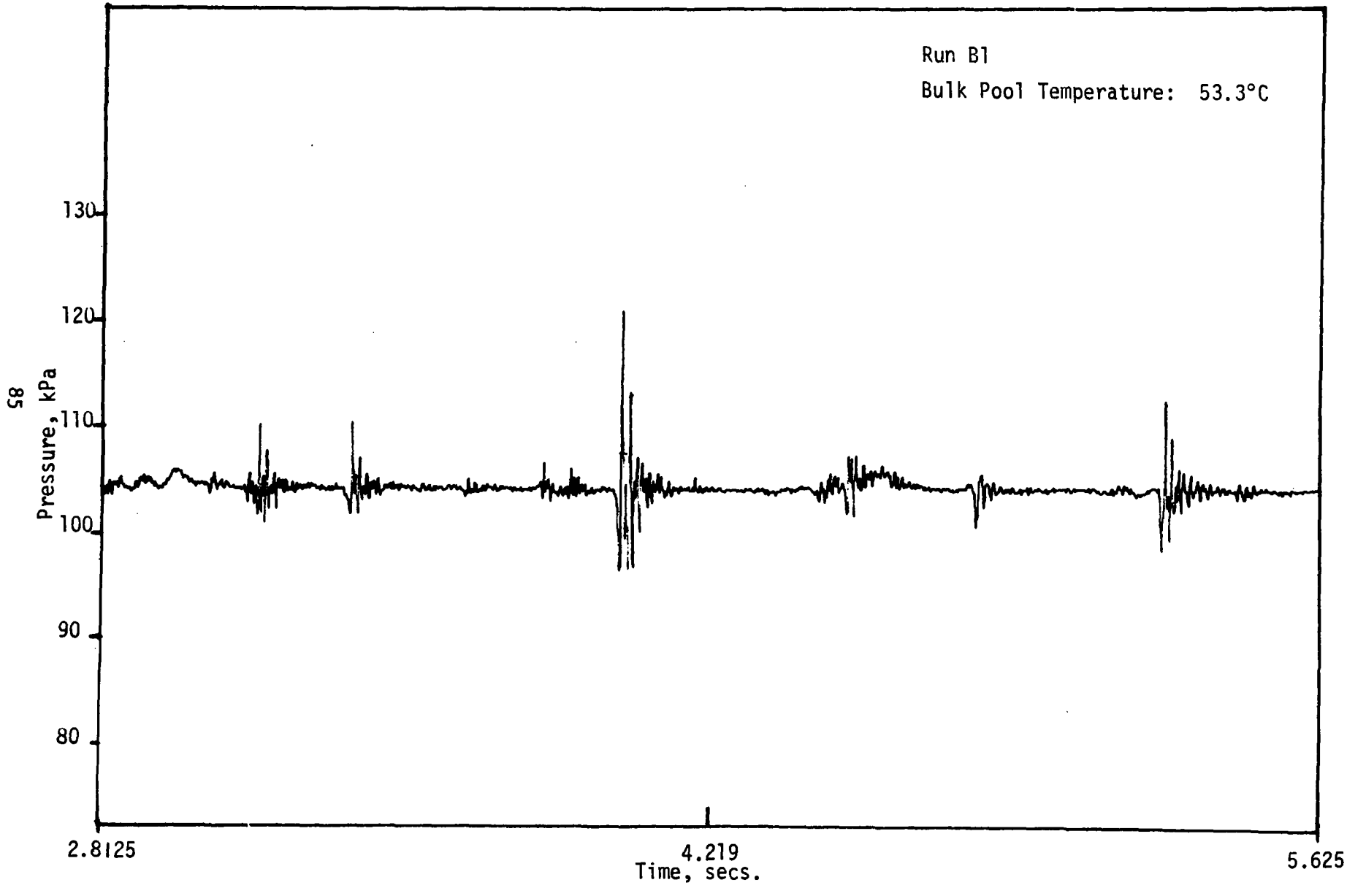

Figure 3.58 Bottom Pressure vs Time for Run B1

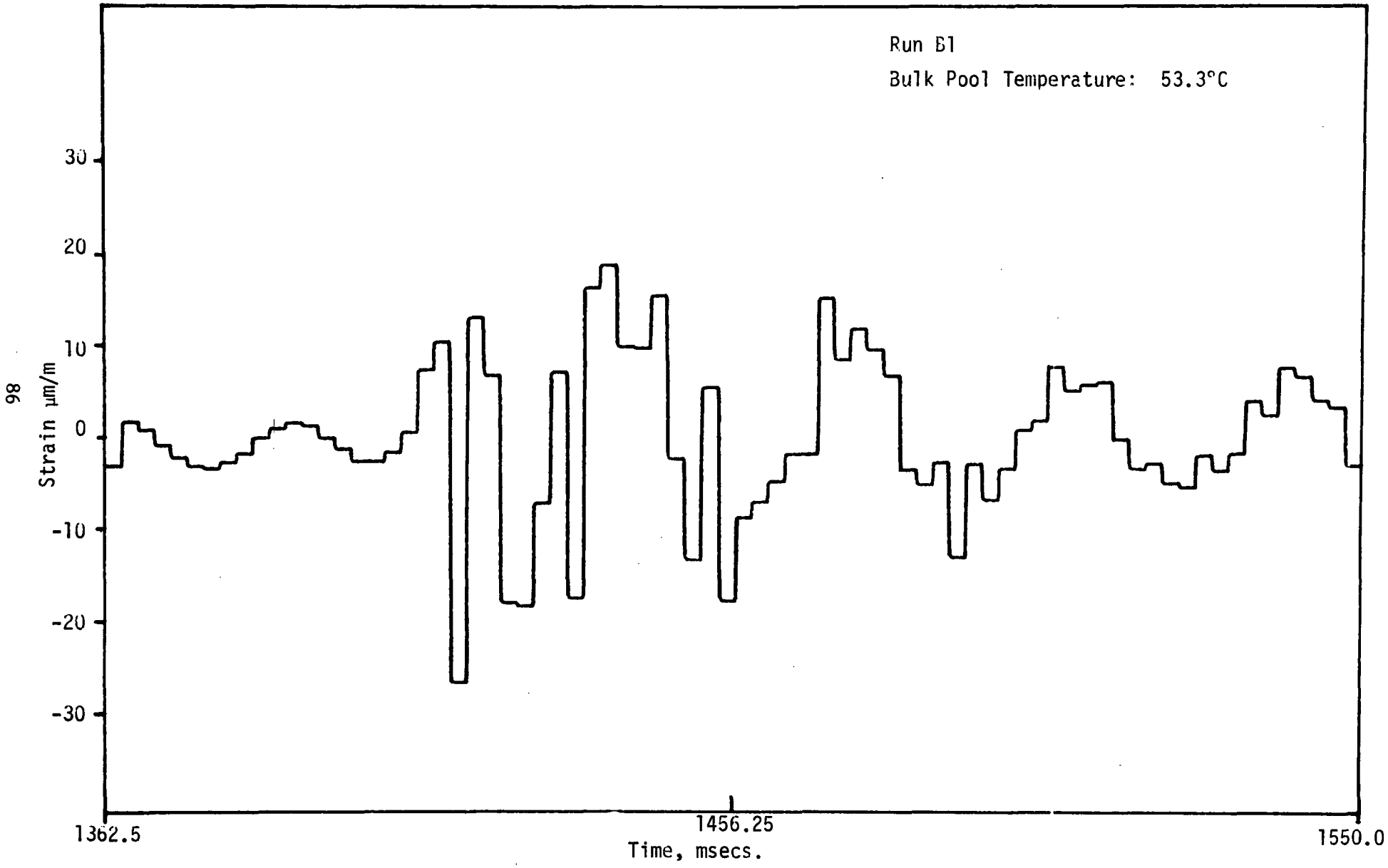

Figure 3.59 Detailed Strain (Gauge #1) vs Time for Run B1

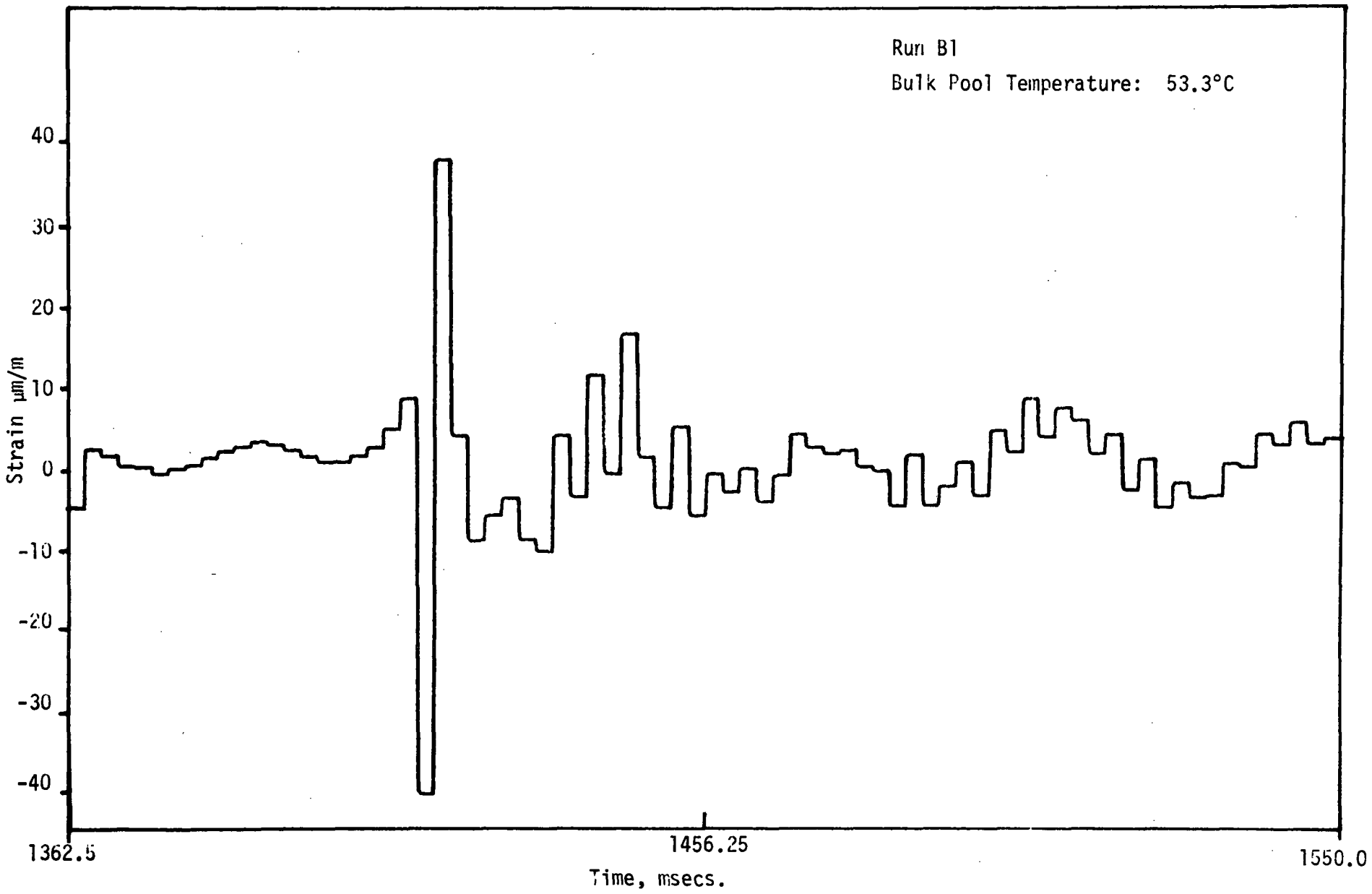

Figure 3.60 Detailed Strain (Gauge #2) vs Time for Run B1

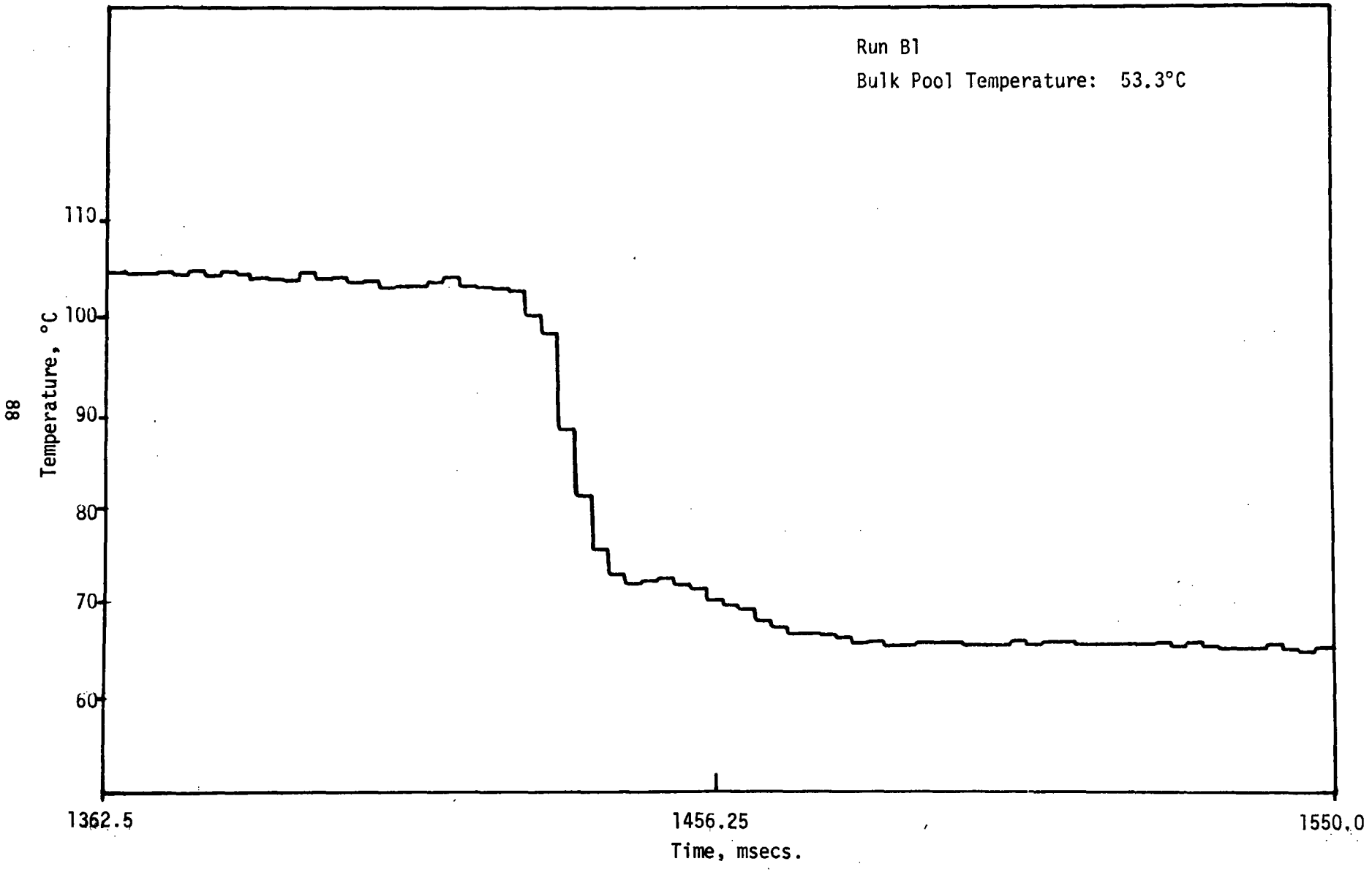

Figure 3.61 Detailed Vent Exit Temperature vs Time for Run B1

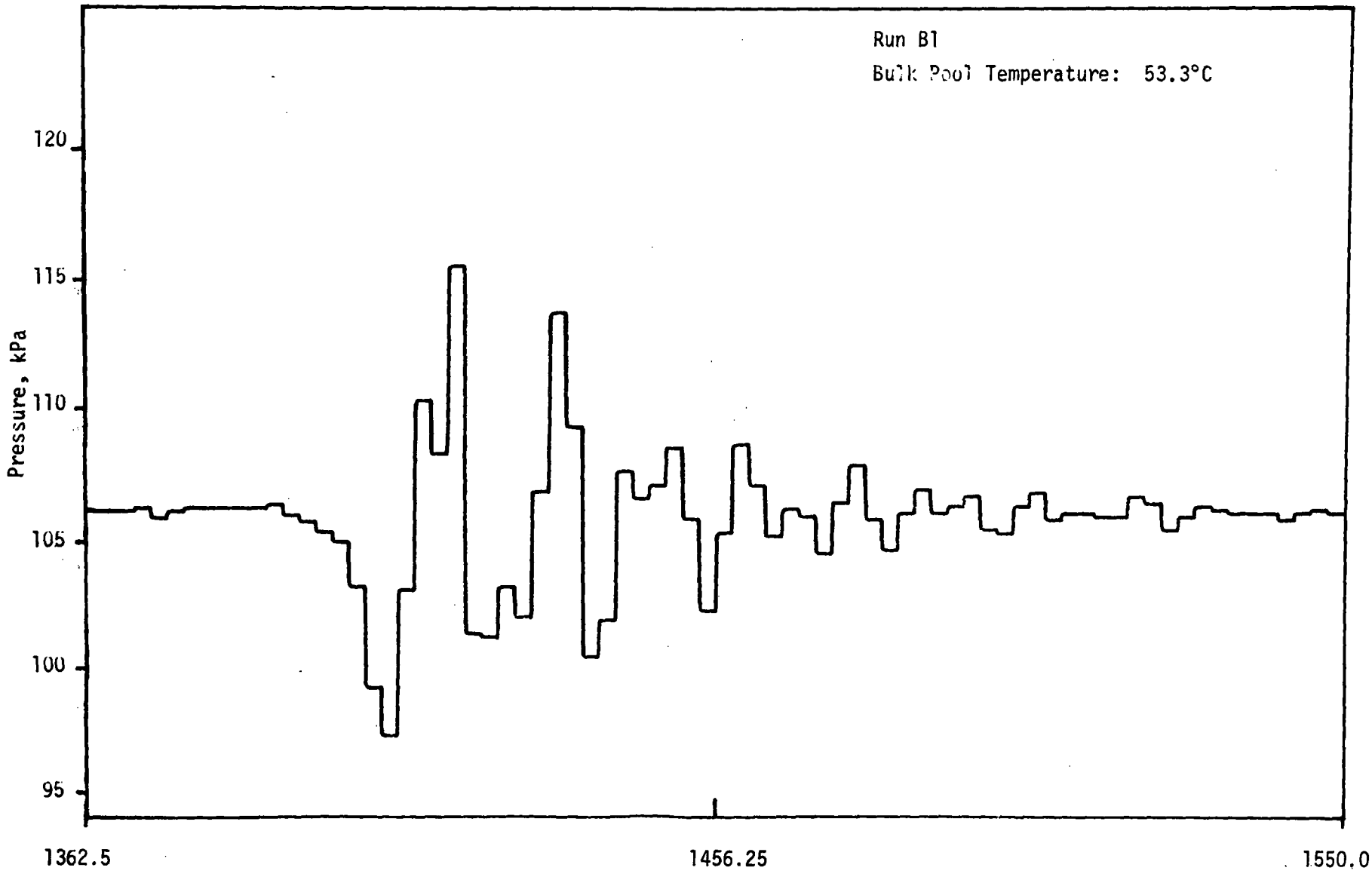

Figure 3.62 Detailed Bottom Pressure vs Time for Run B1

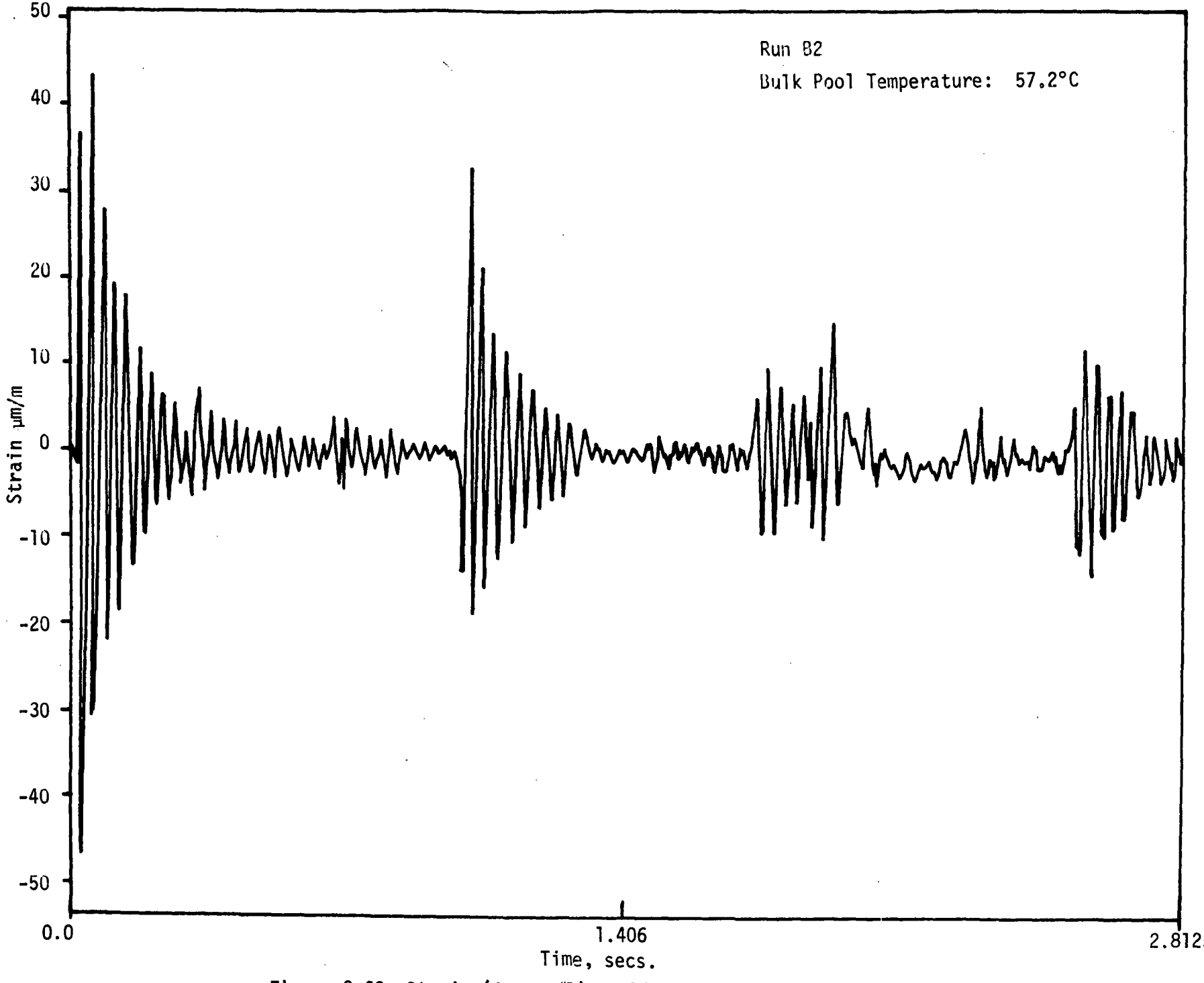

Figure 3.63 Strain (Gauge #1) vs Time for Run B2

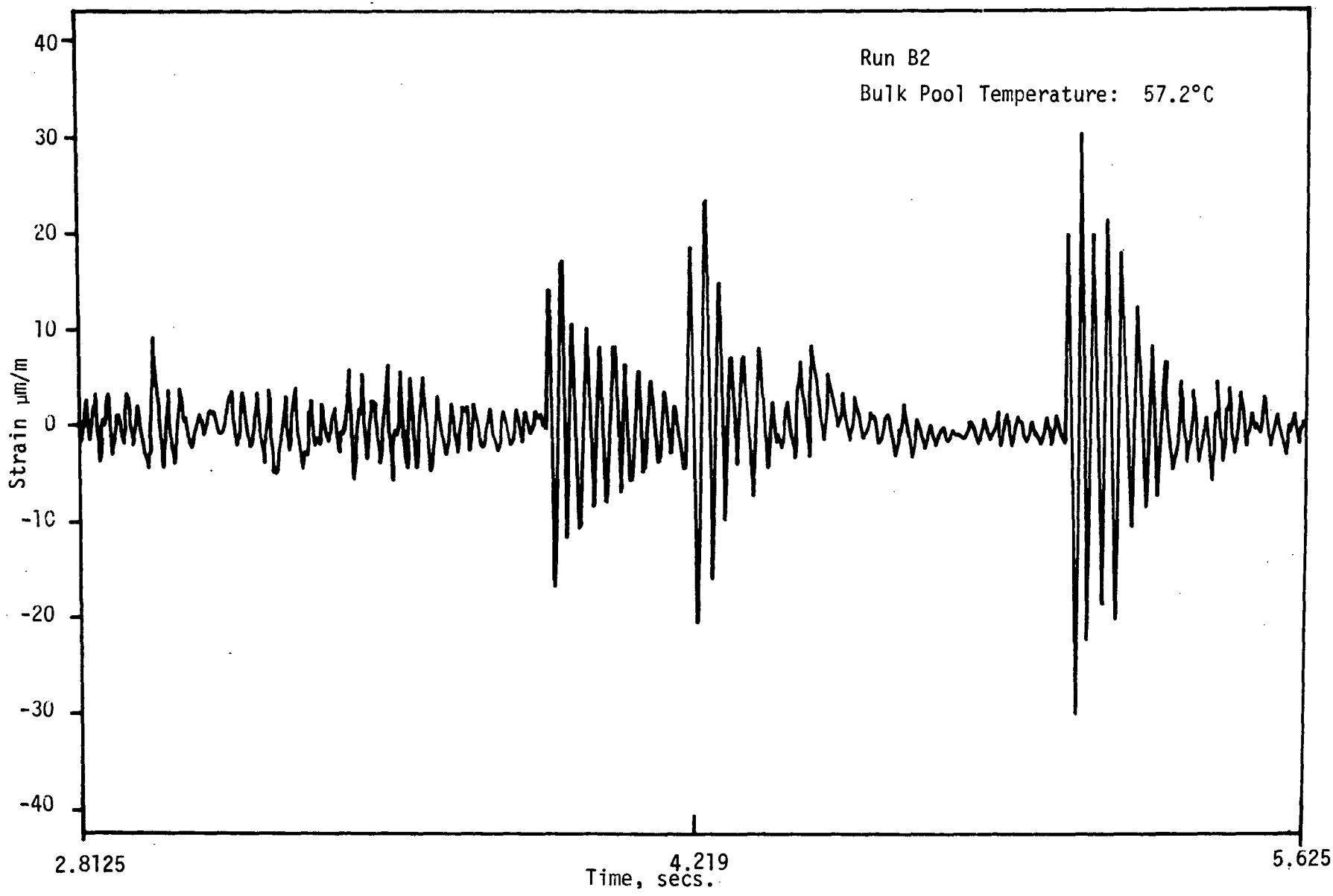

Figure 3.64 Strain (Gauge #1) vs Time for Run B2

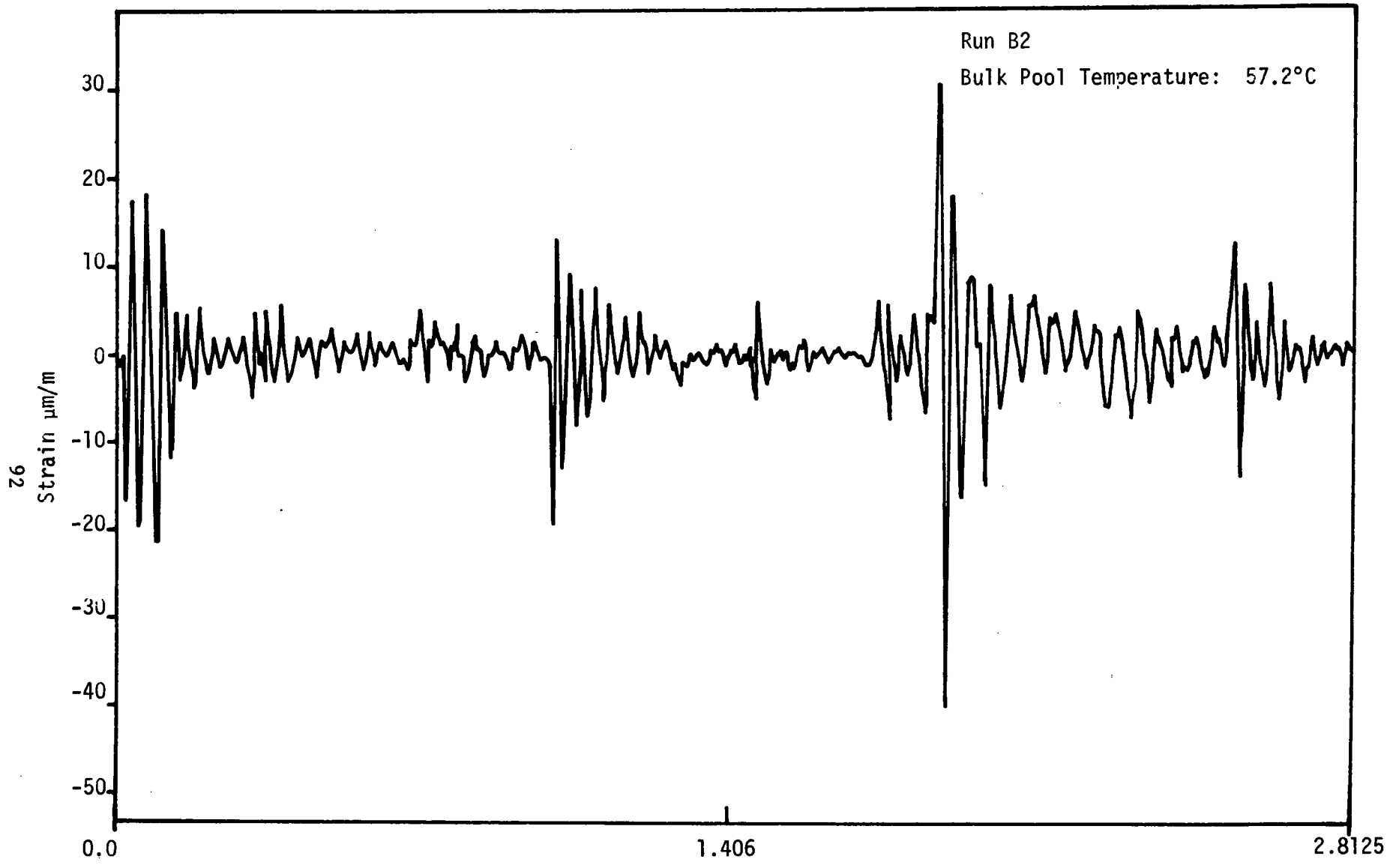

Figure 3.65 Strain (Gauge #2) vs Time for Run B2

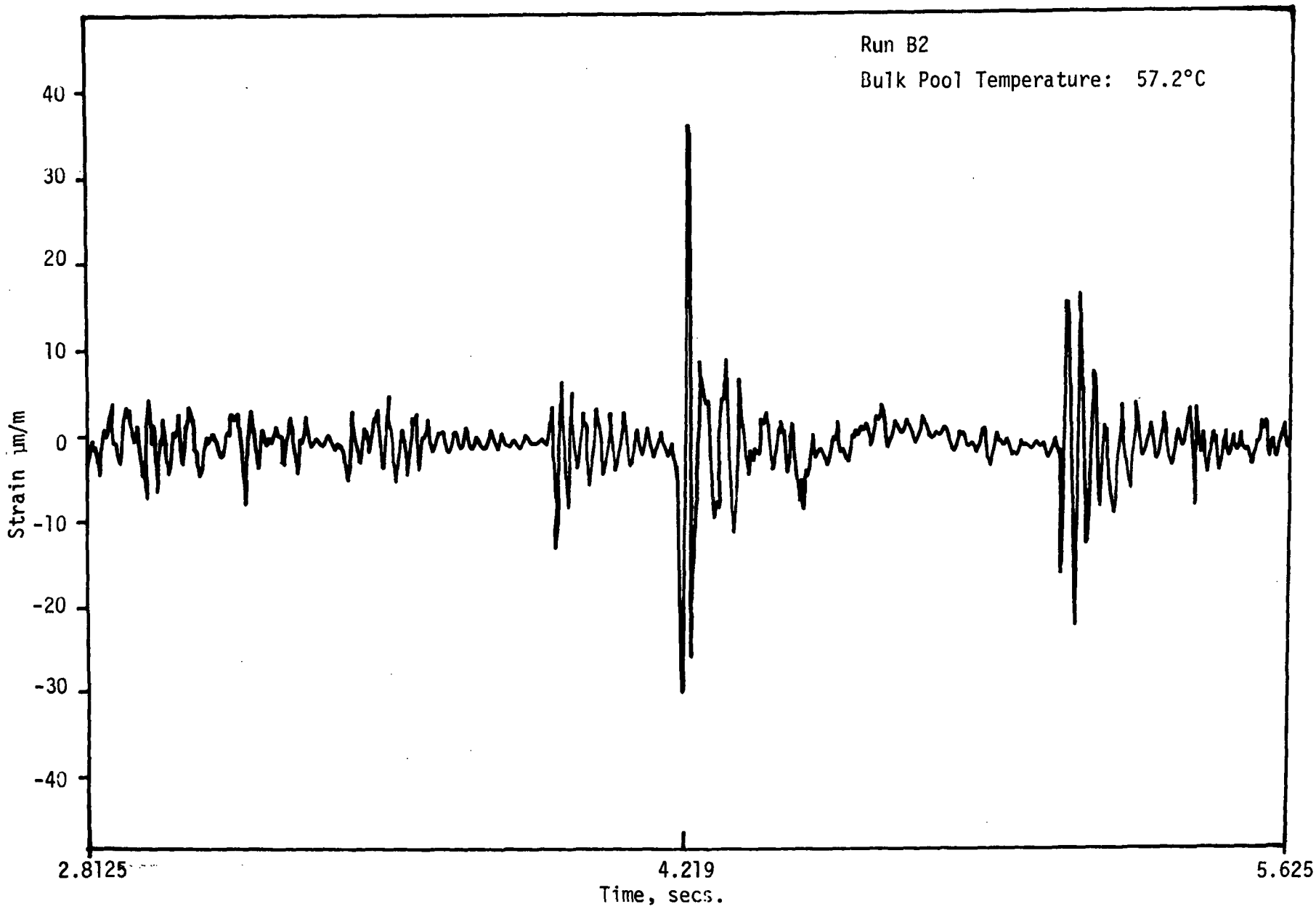

Figure 3.66 Strain (Gauge #2) vs Time for Run B2

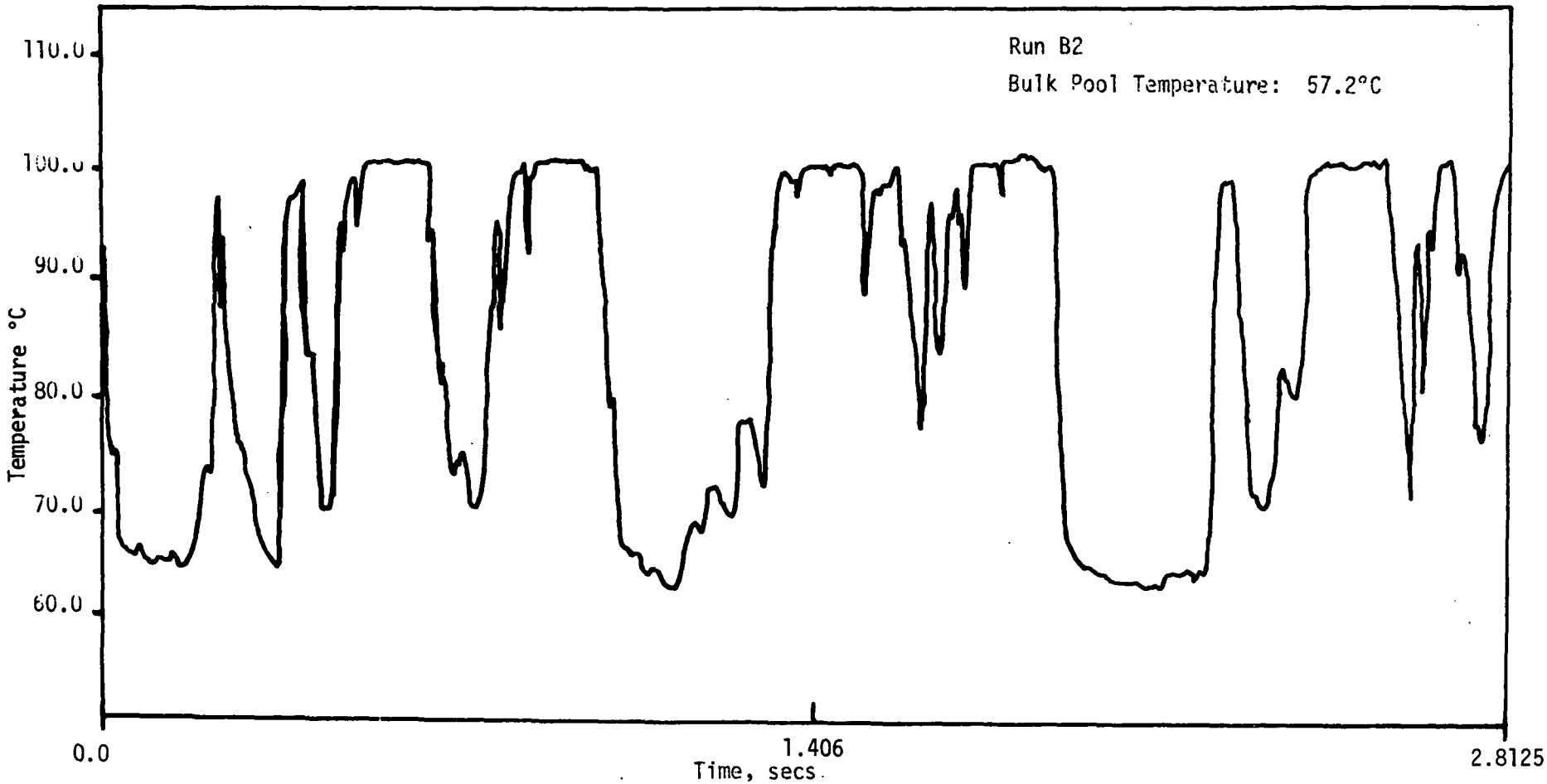

Figure 3.67 Vent Exit Temperature vs Time for Run B2

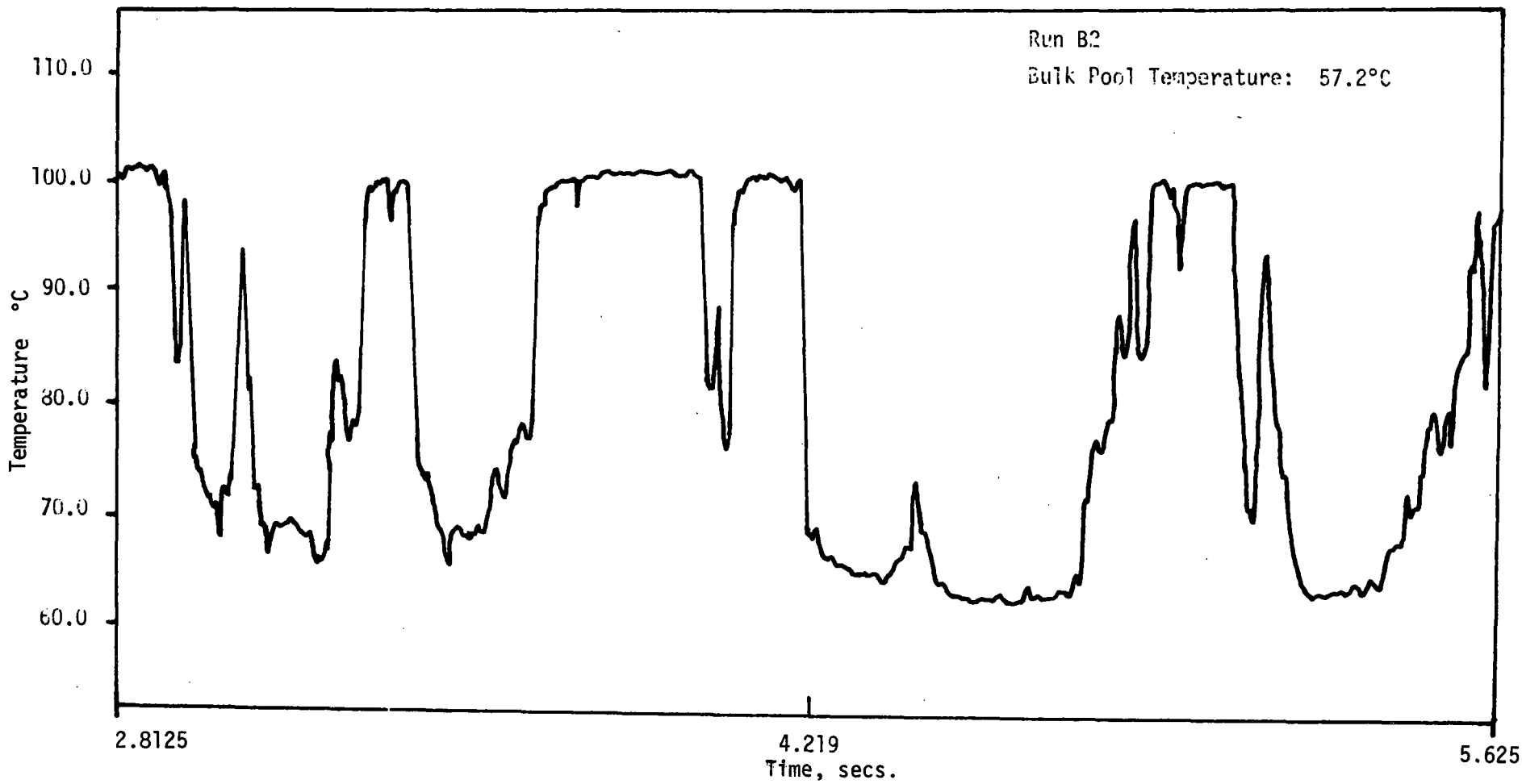

Figure 3.68 Vent Exit Temperature vs Time for Run B2

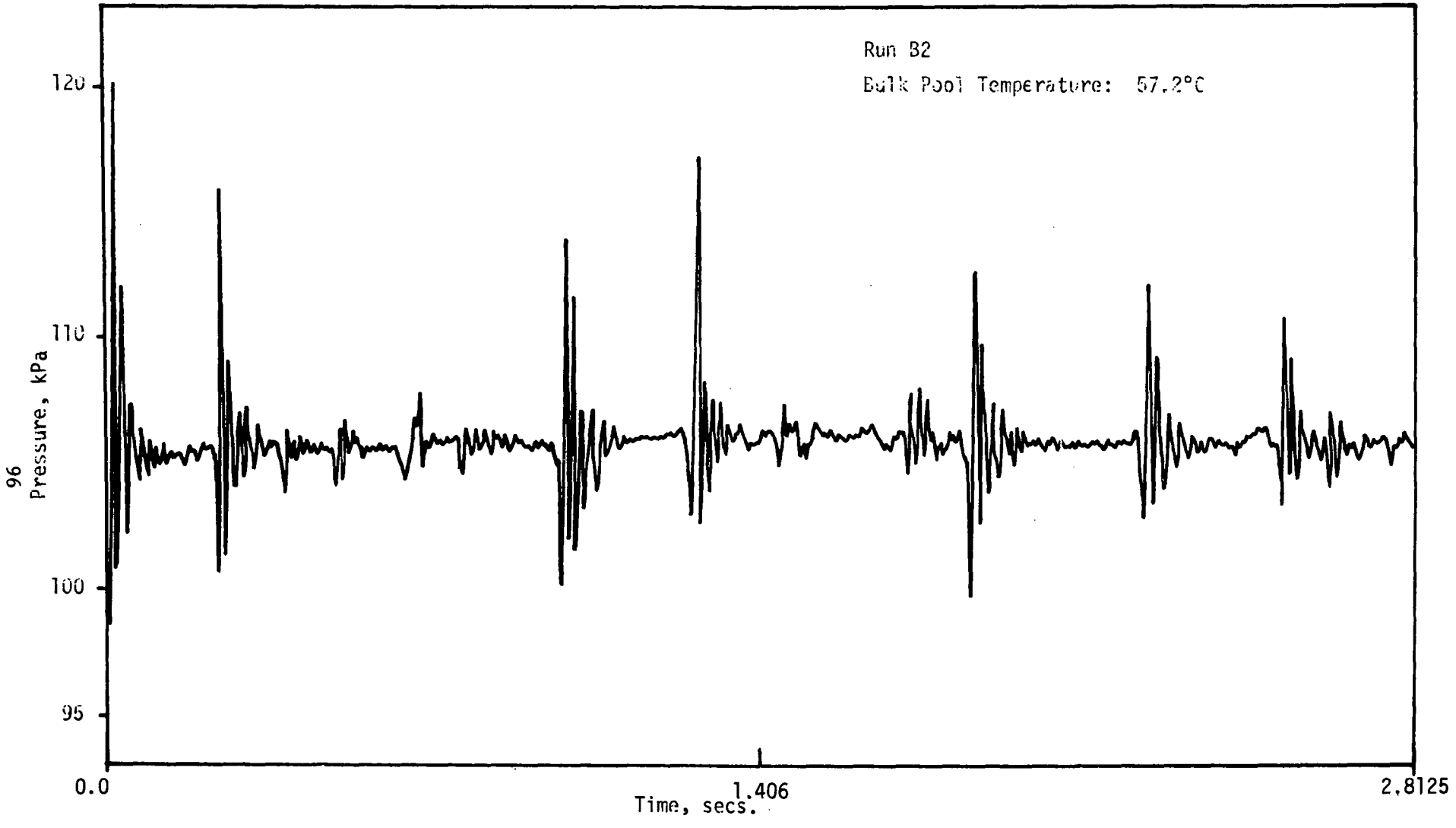

Figure 3.69 Bottom Pressure vs Time for Run B2

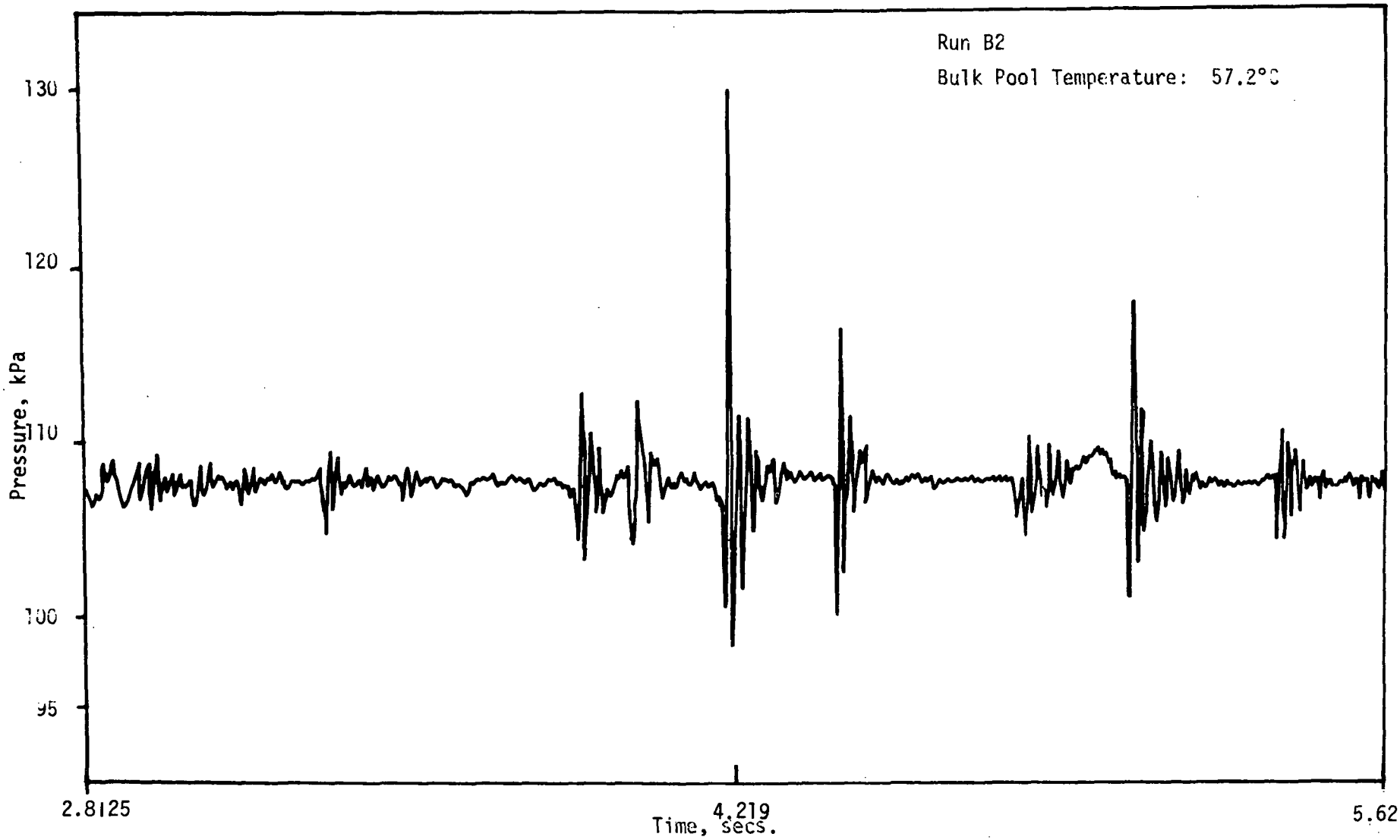

Figure 3.70 Bottom Pressure vs Time for Run B2

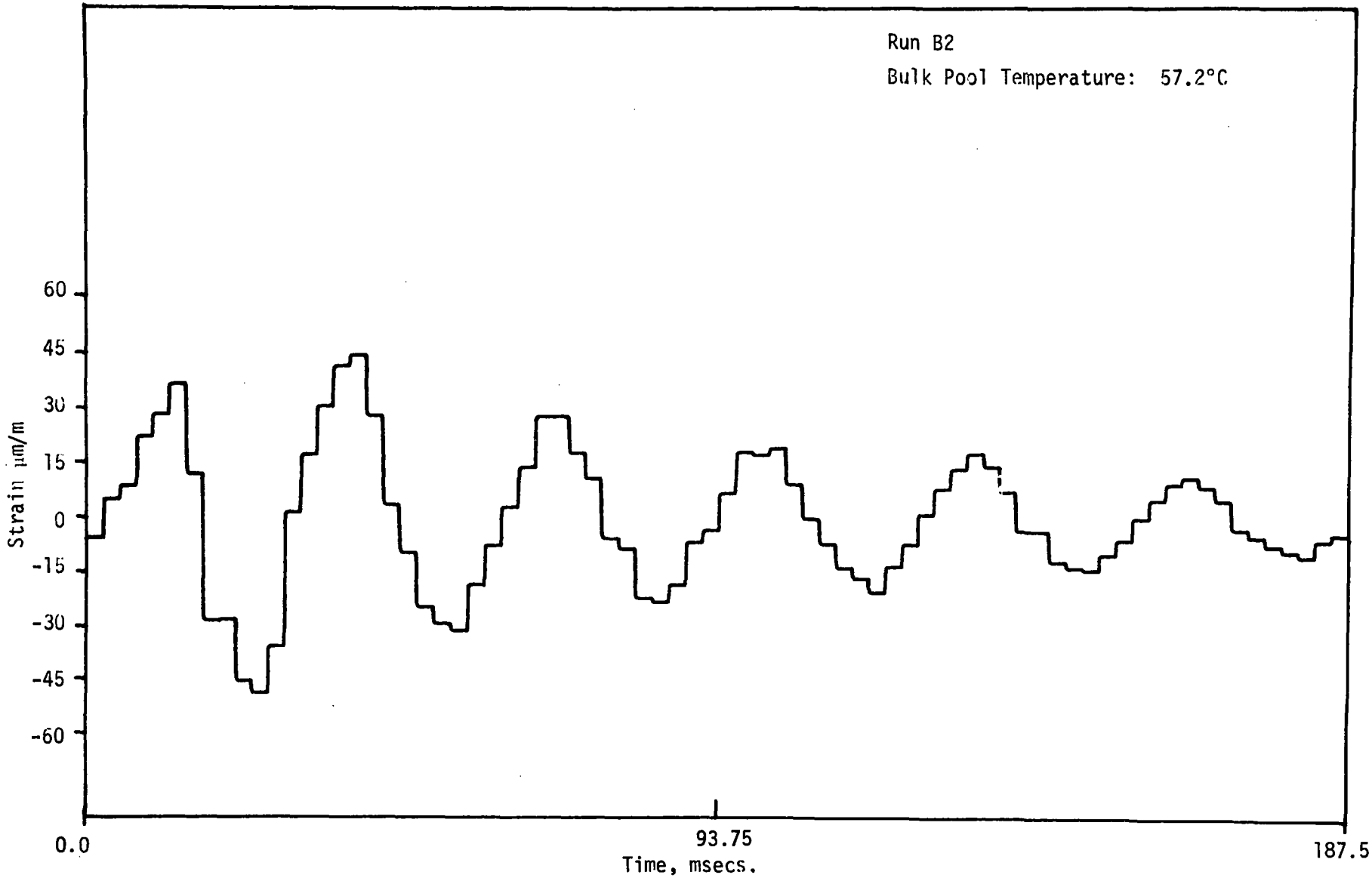

Figure 3.71 Detailed Strain (Gauge #1) vs Time for Run B2

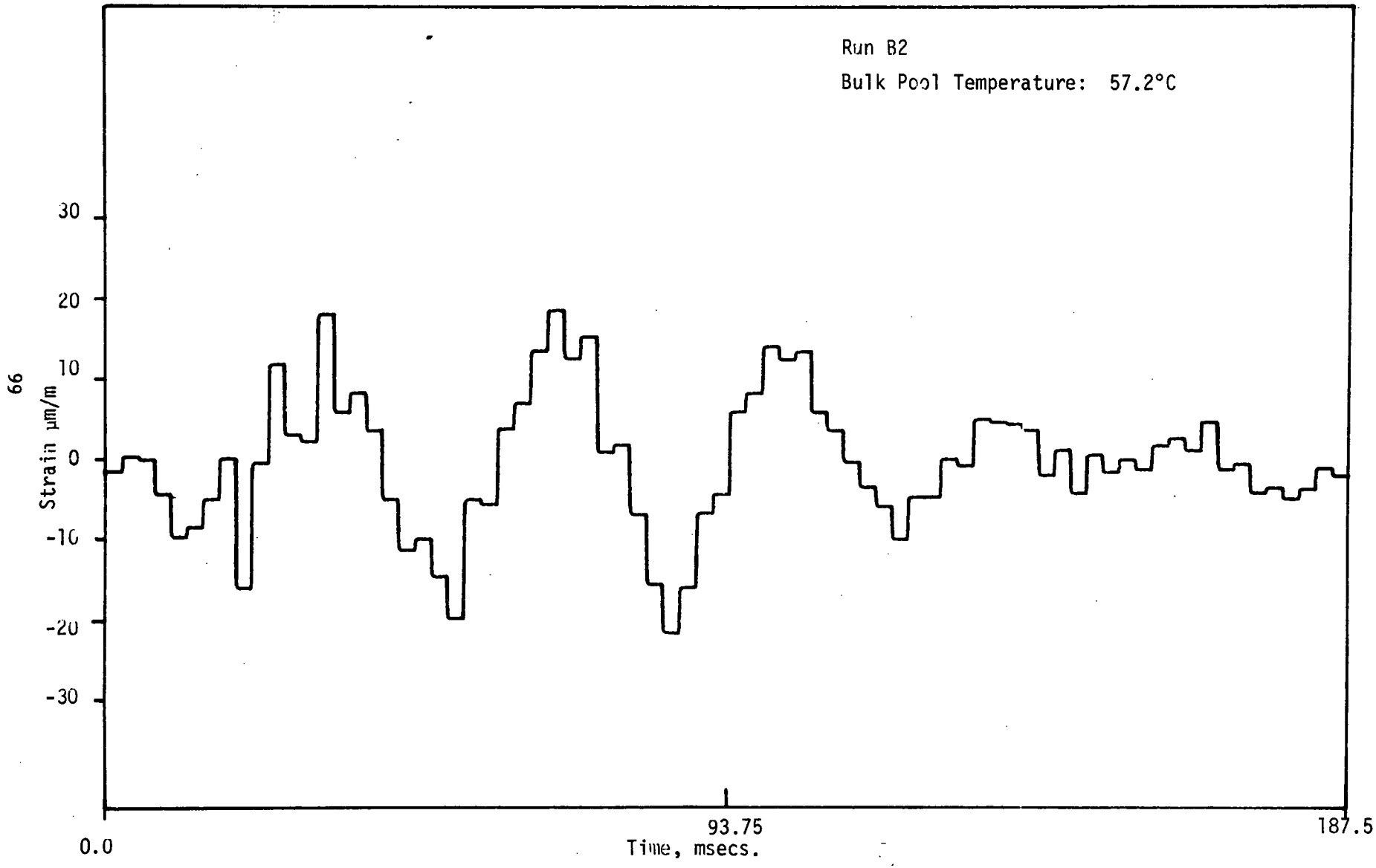

Figure 3.72 Detailed Strain (Gauge #2) vs Time for Run B2

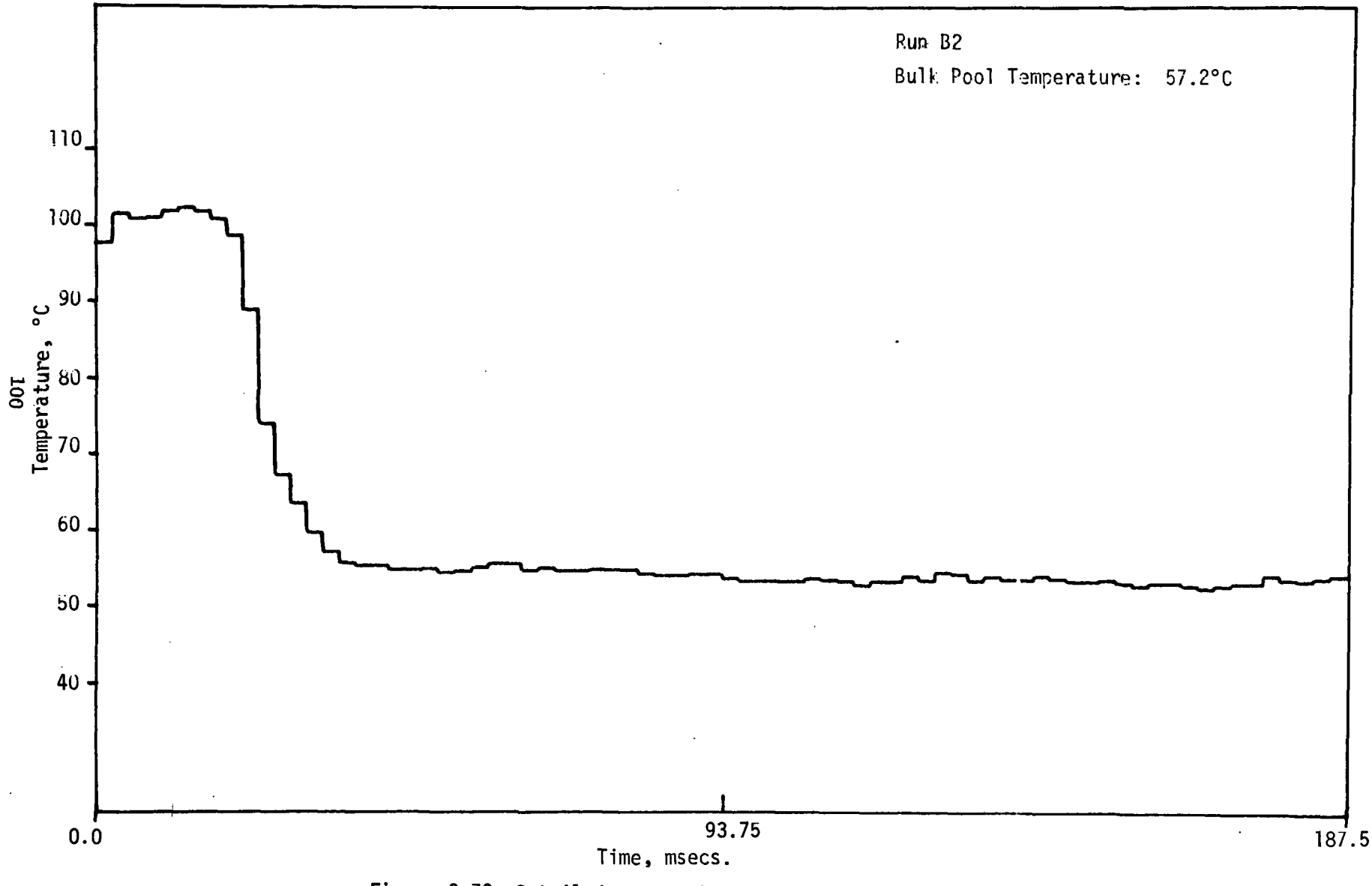

Figure 3.73 Detailed Vent Exit Temperature vs Time for Run B2

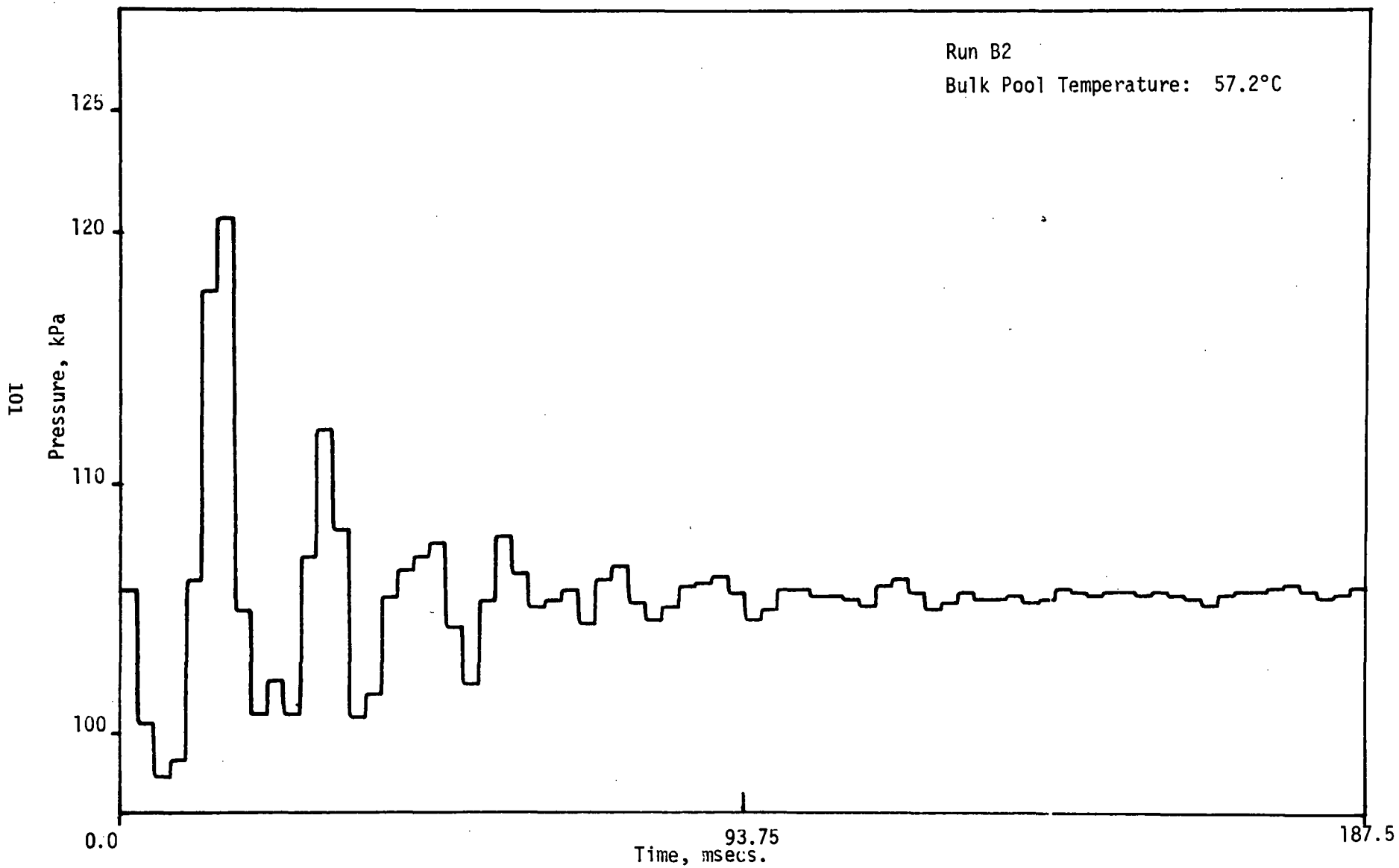

Figure 3.74 Detailed Bottom Pressure vs Time for Run B2

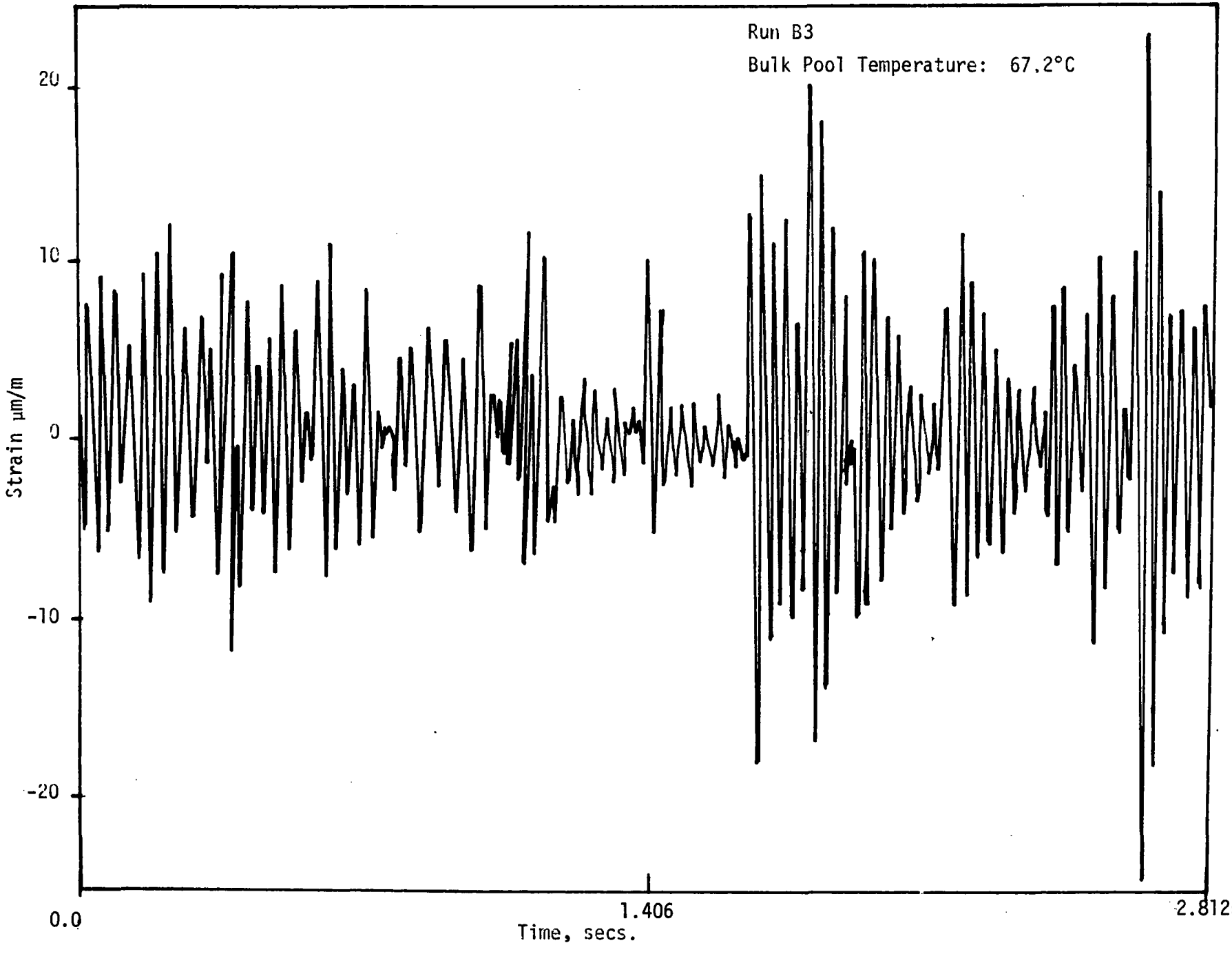

Figure 3.75 Strain (Gauge #1) vs Time for Run B3

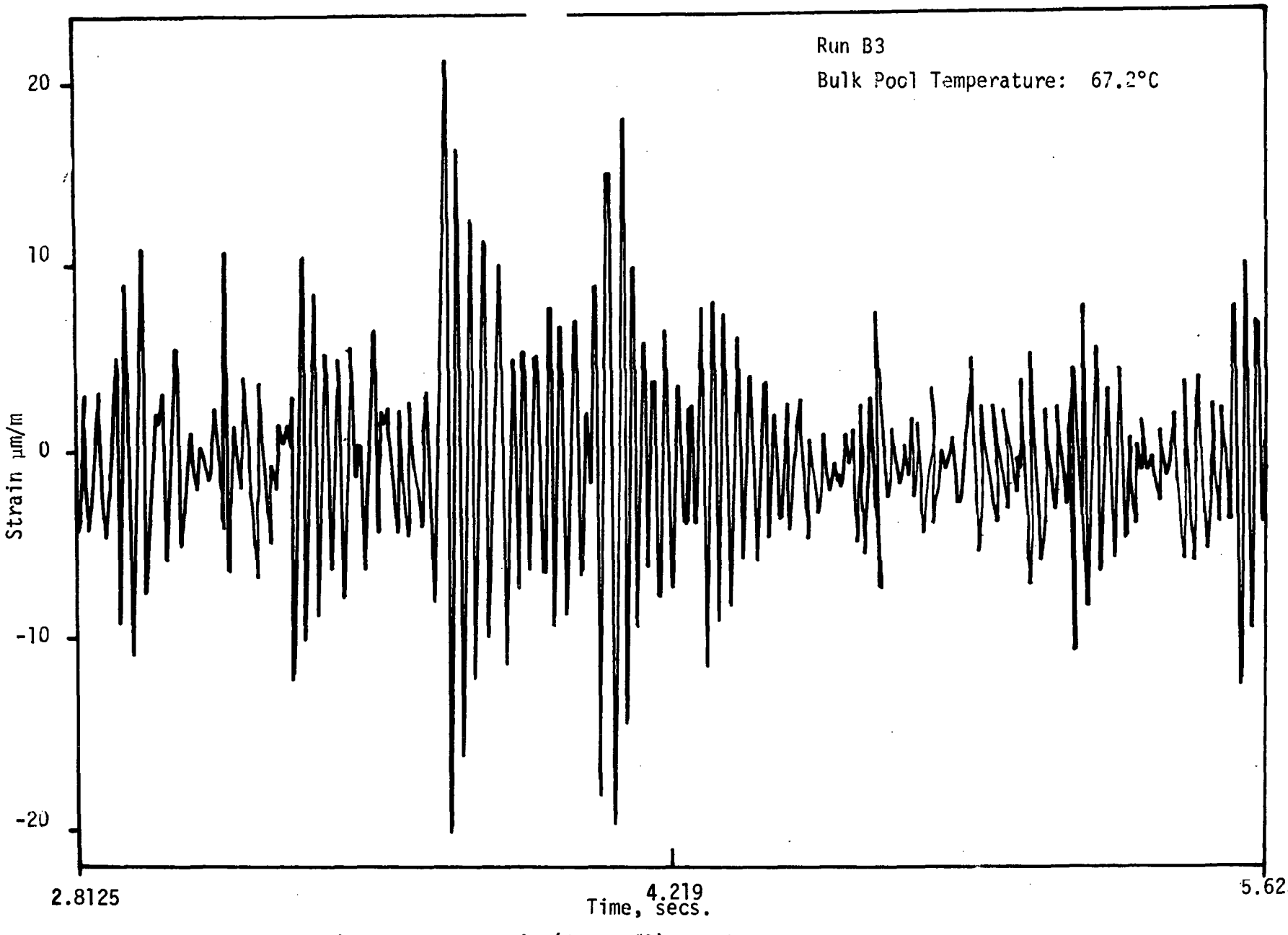

Figure 3.76 Strain (Gauge #2) vs Time for Run B3

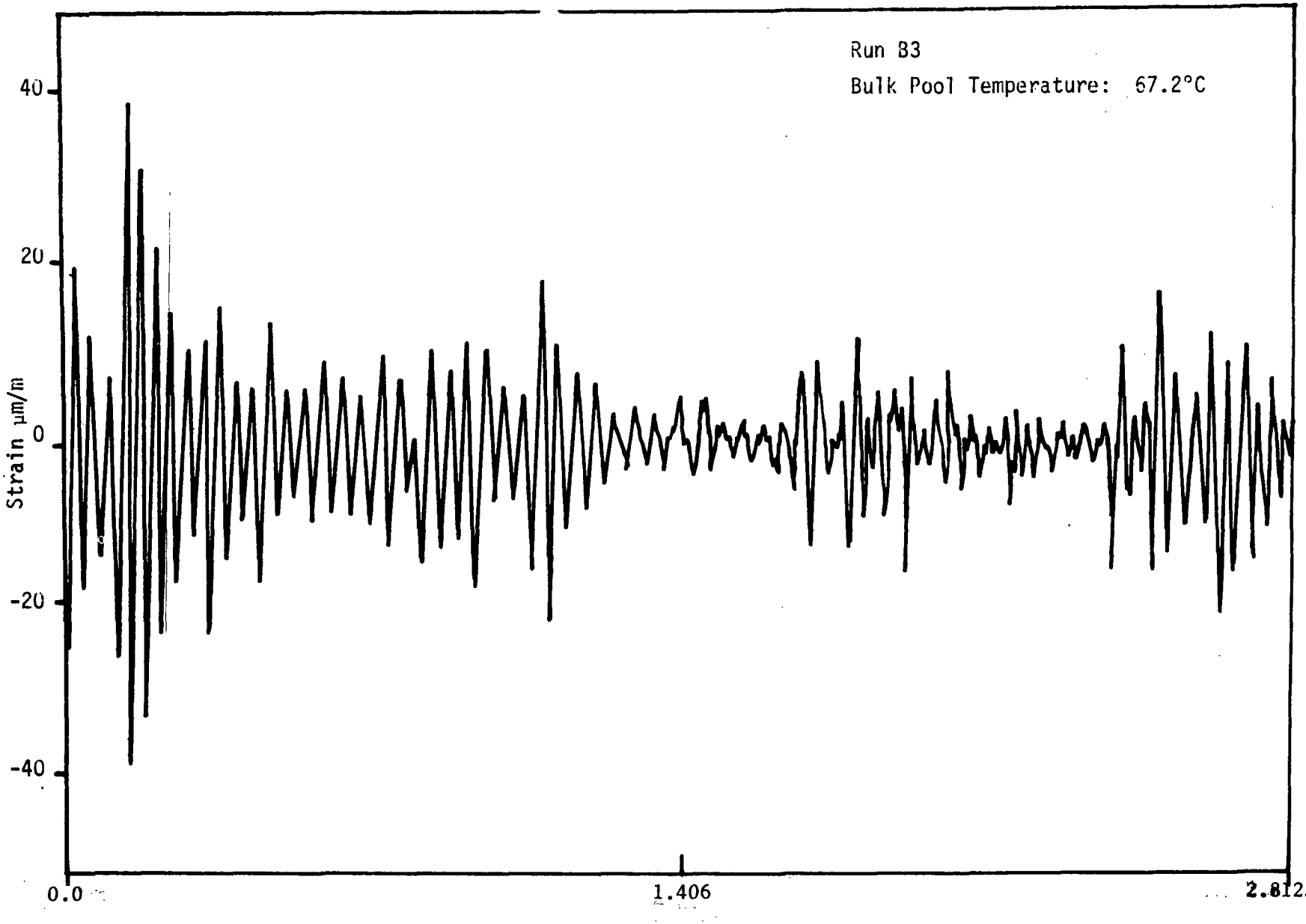

Figure 3.77 Strain (Gauge #2) vs Time for Run B3

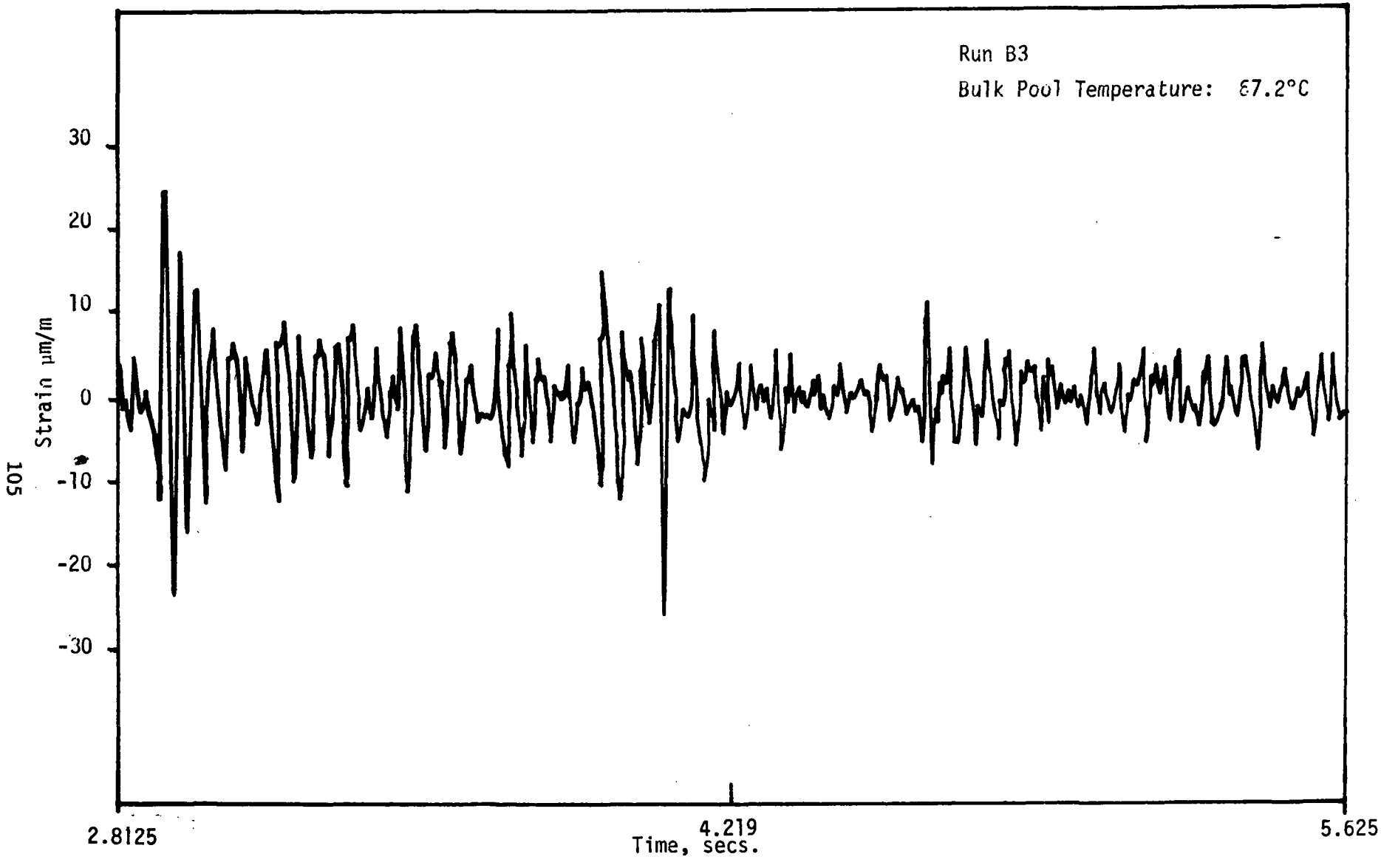

Figure 3.78 Strain (Gauge #2) vs Time for Run B3

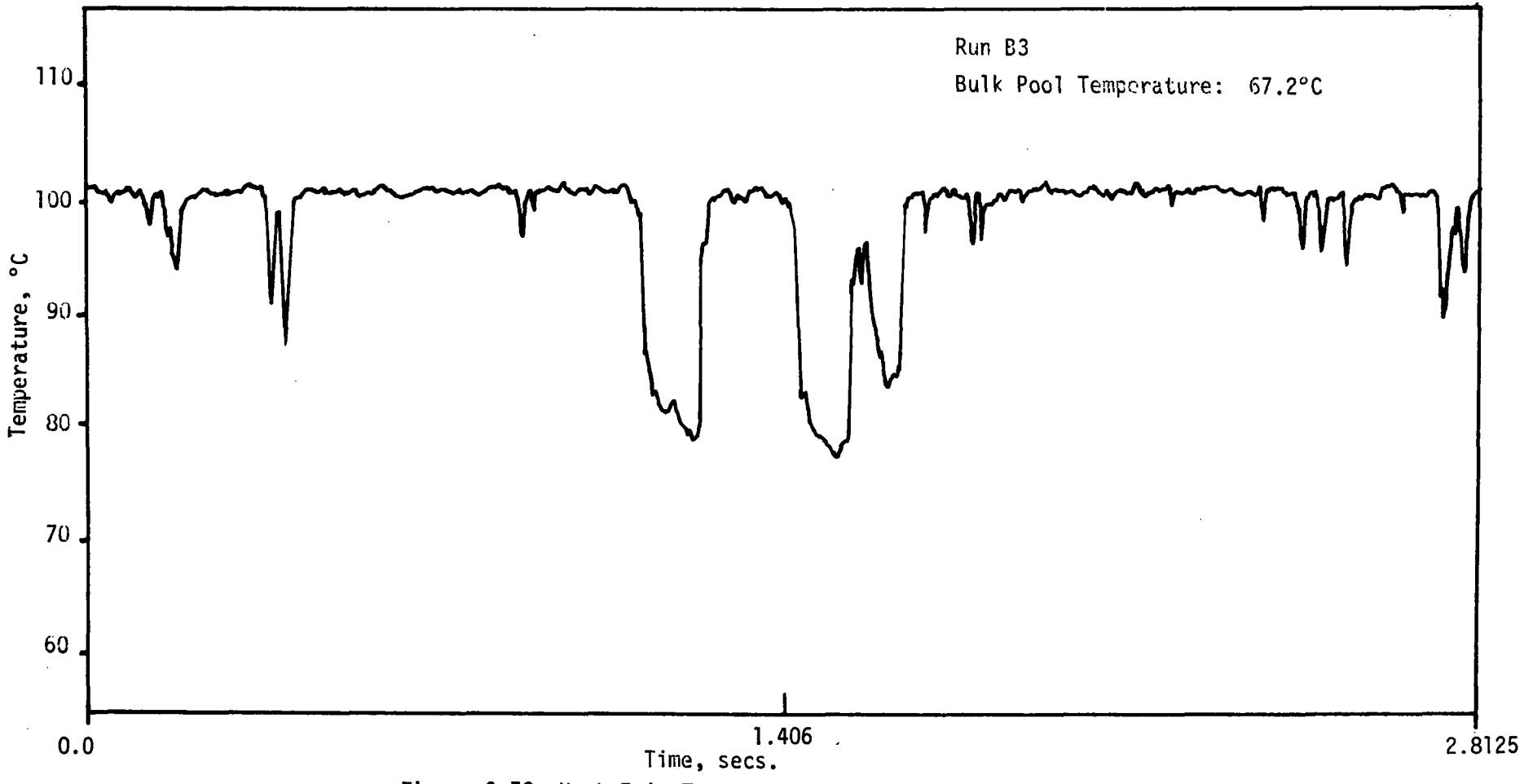

Figure 3.79 Vent Exit Temperature vs Time Run B3

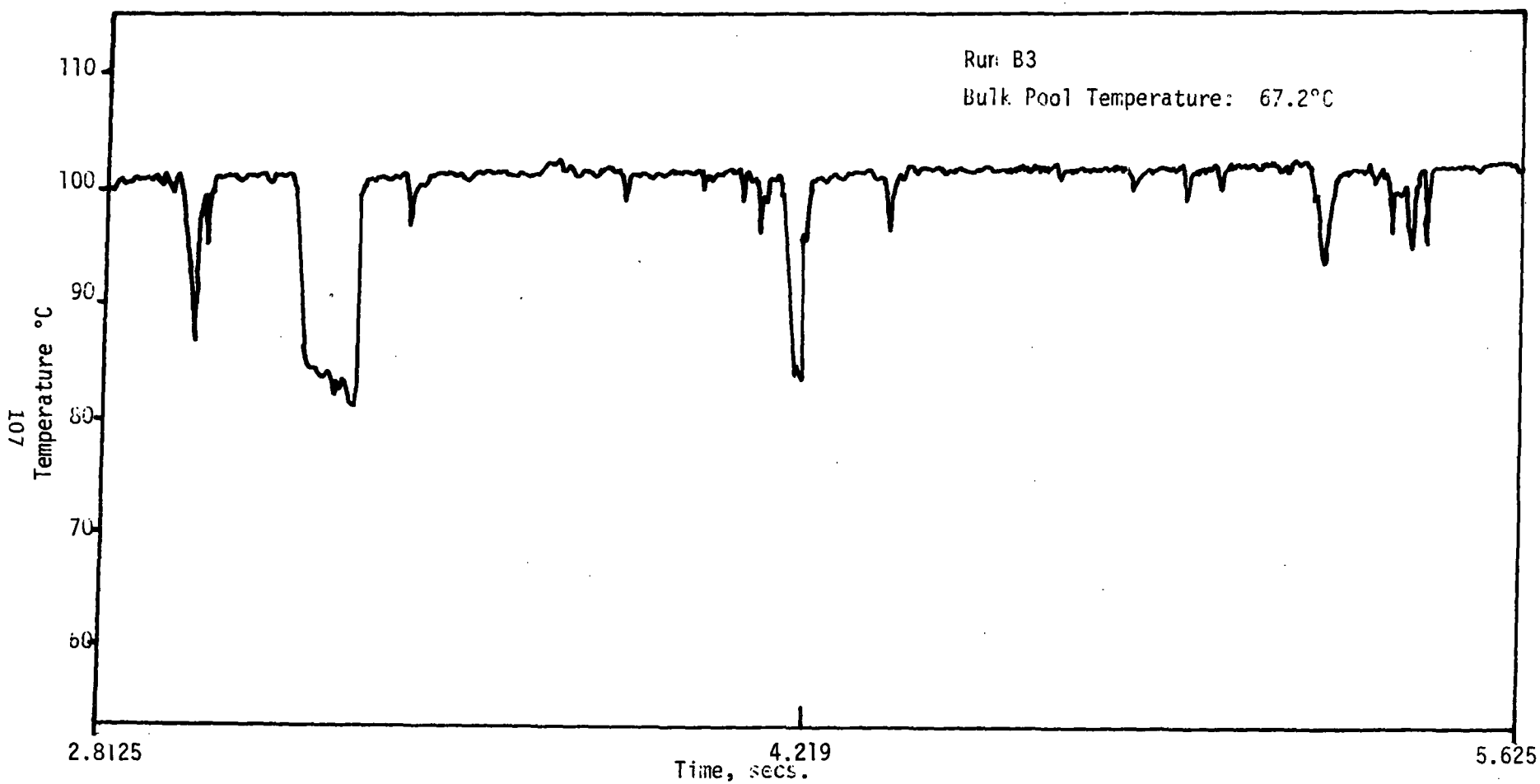

Figure 3.80 Vent Exit Temperature vs Time Run B3

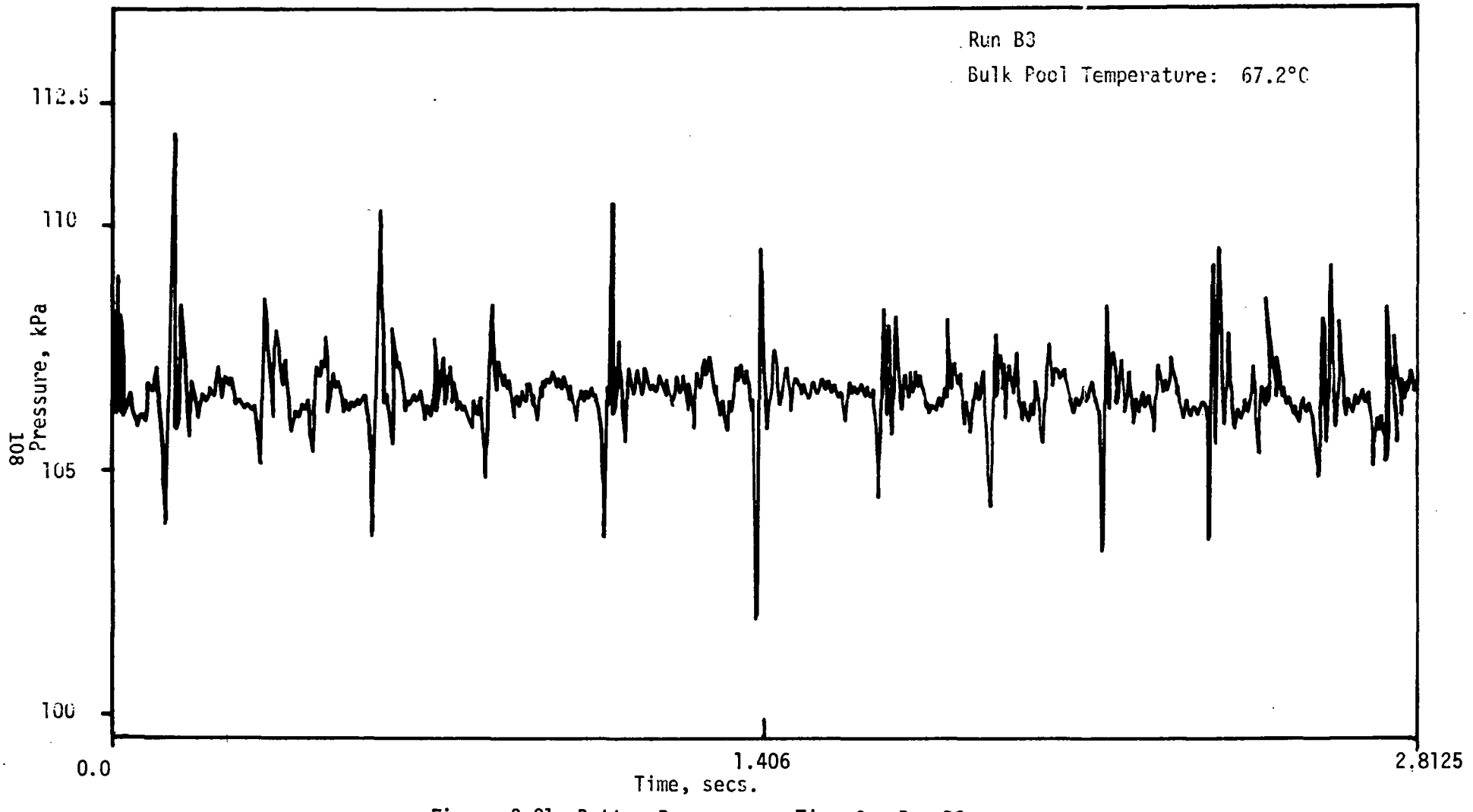

Figure 3.81 Bottom Pressure vs Time for Run B3

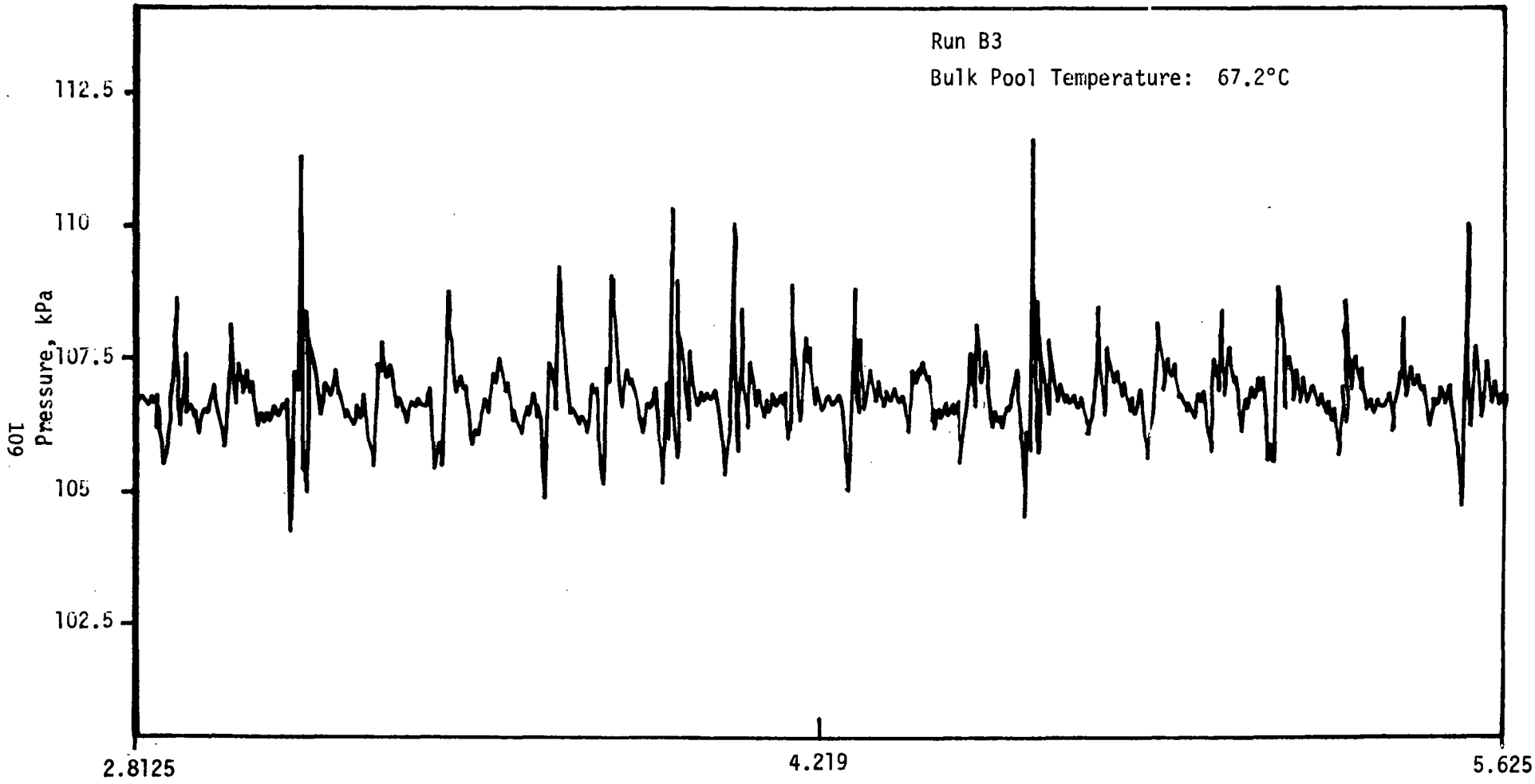

Figure 3.82 Bottom Pressure vs Time for Run B3

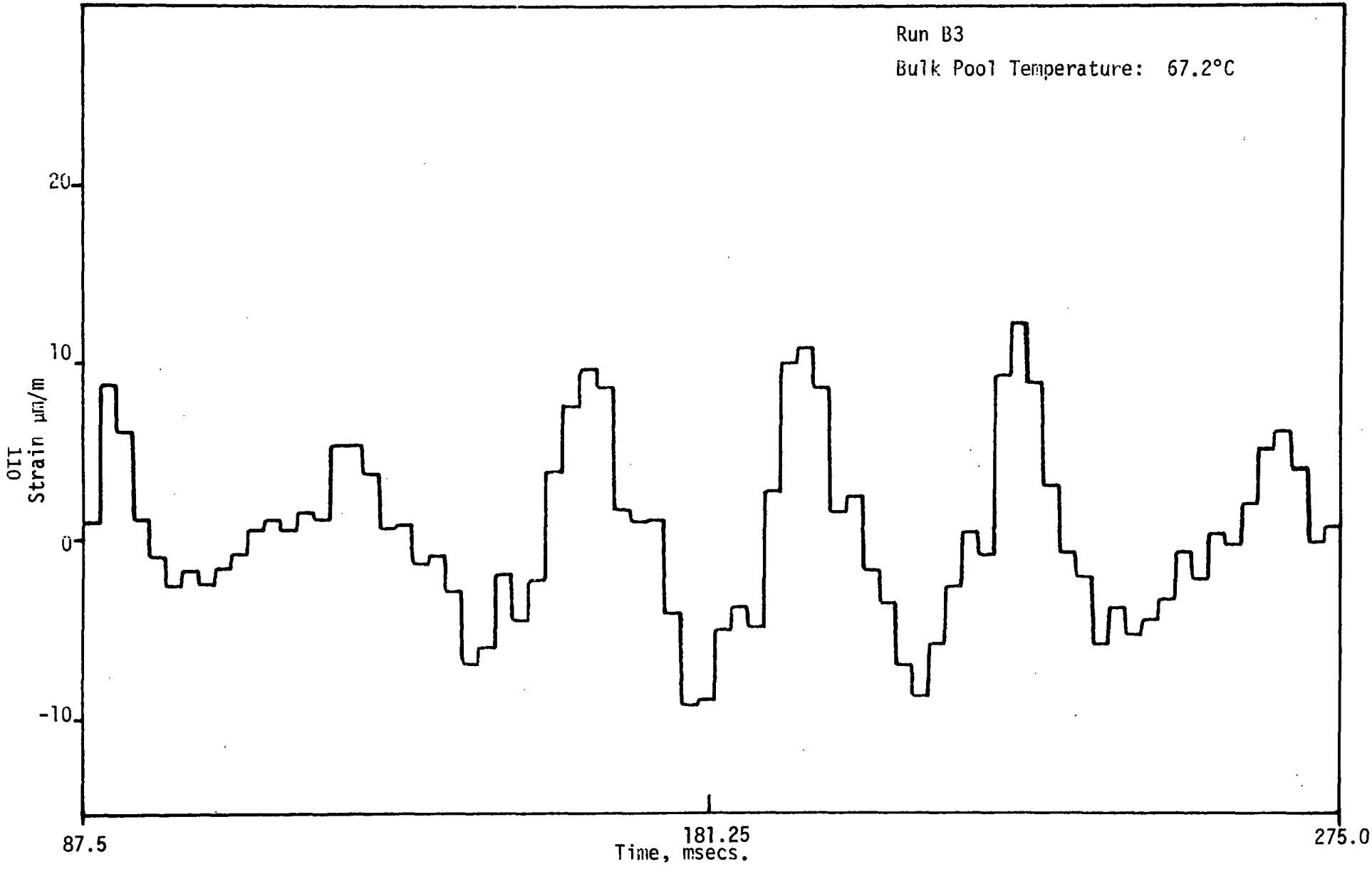

Figure 3.83 Detailed Strain (Gauge #1) vs Time for Run B3

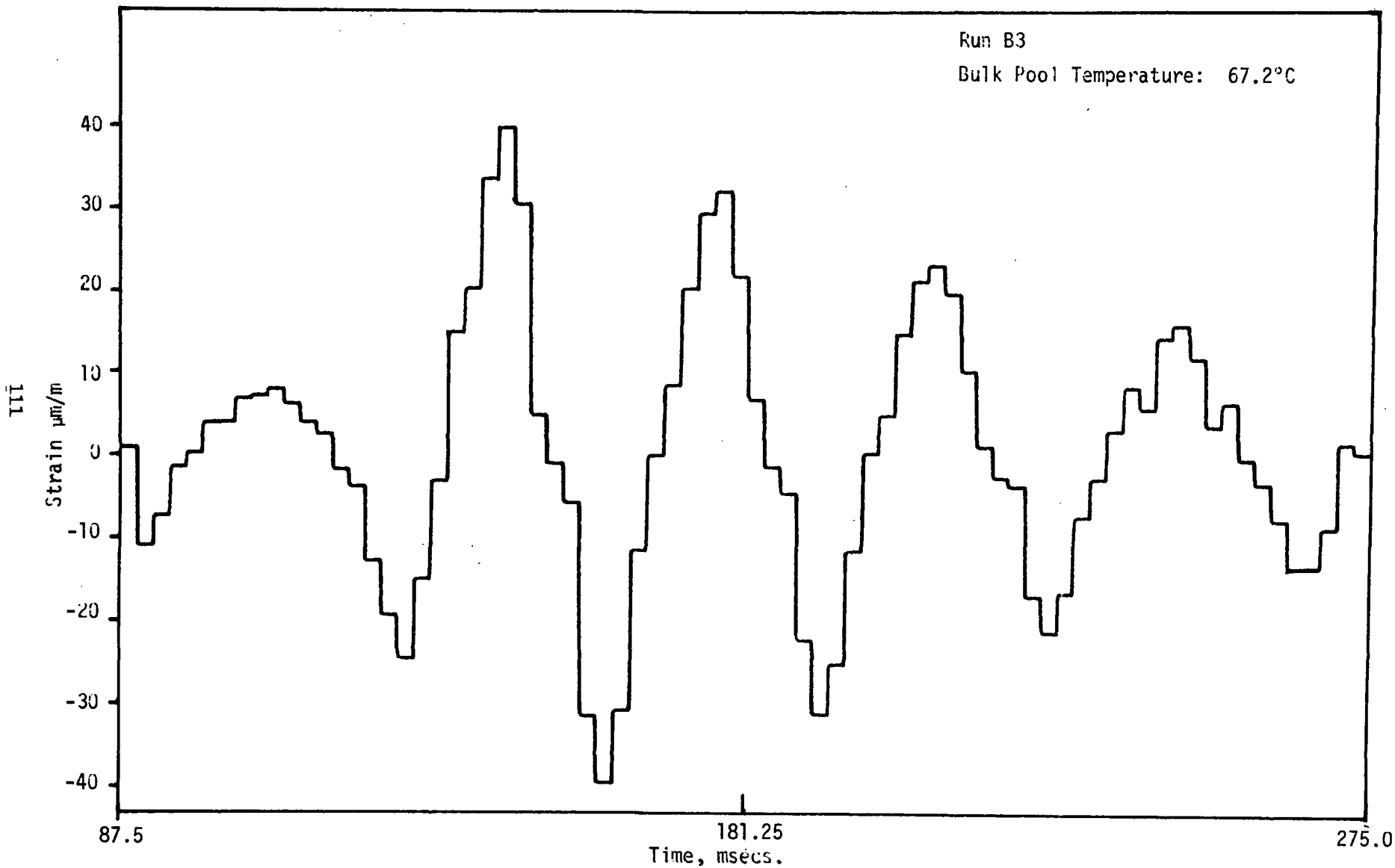

Figure 3.84 Deatiled Strain (Gauge #2) vs Time for Run B3

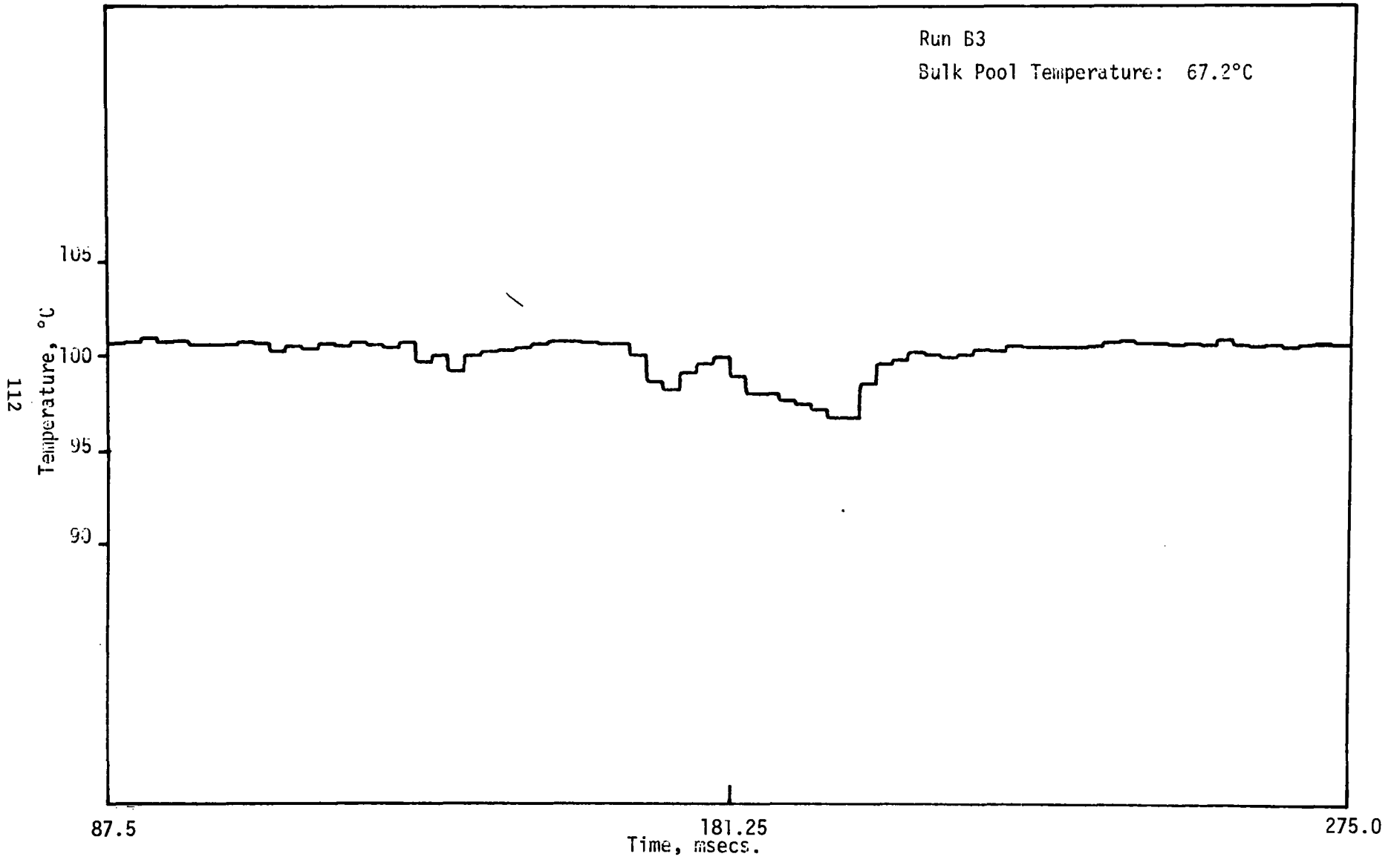

Figure 3.85 Detailed Vent Exit Temperature vs Time for Run B3

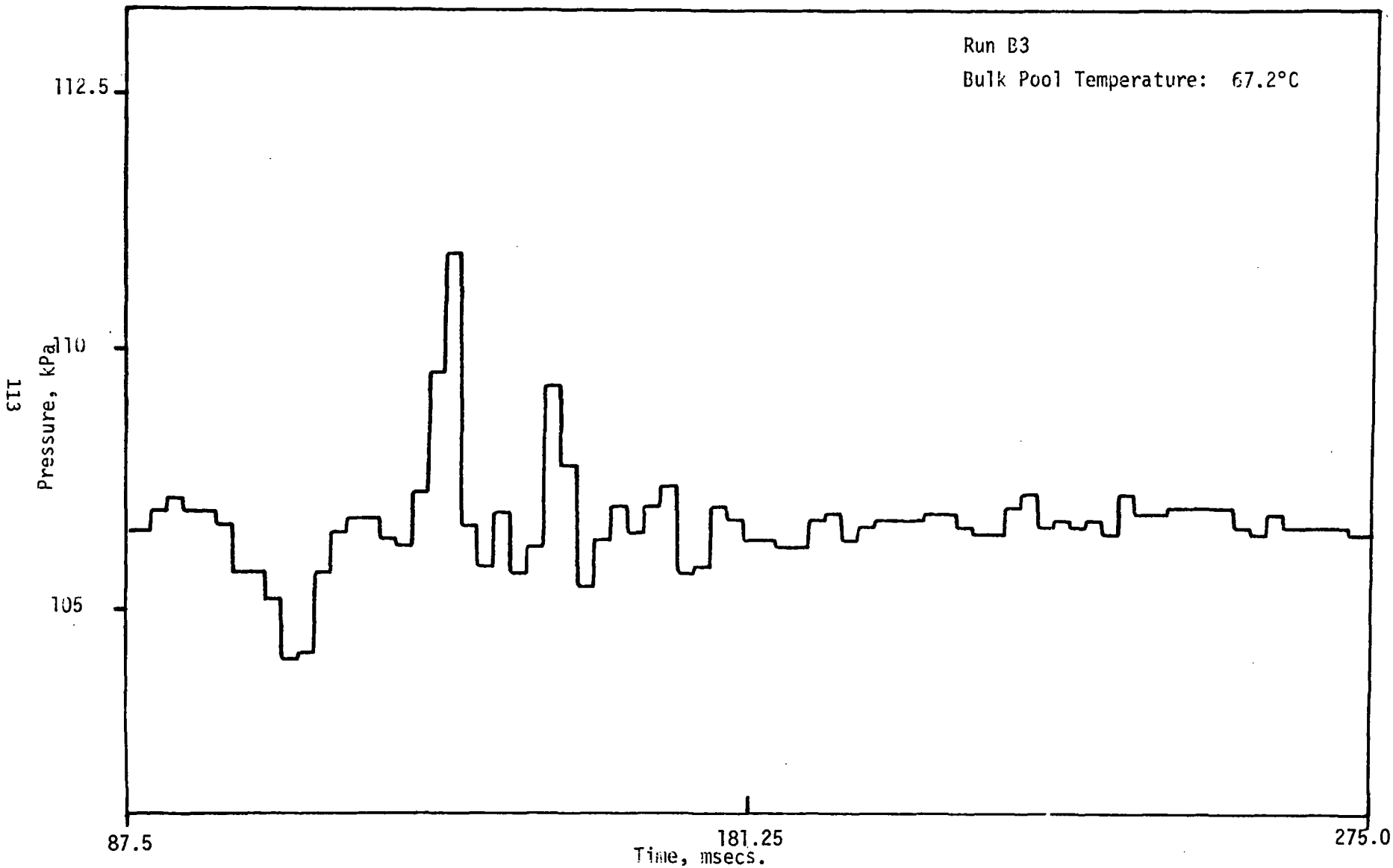

Figure 3.86 Detailed Bottom Pressure vs Time for Run B3

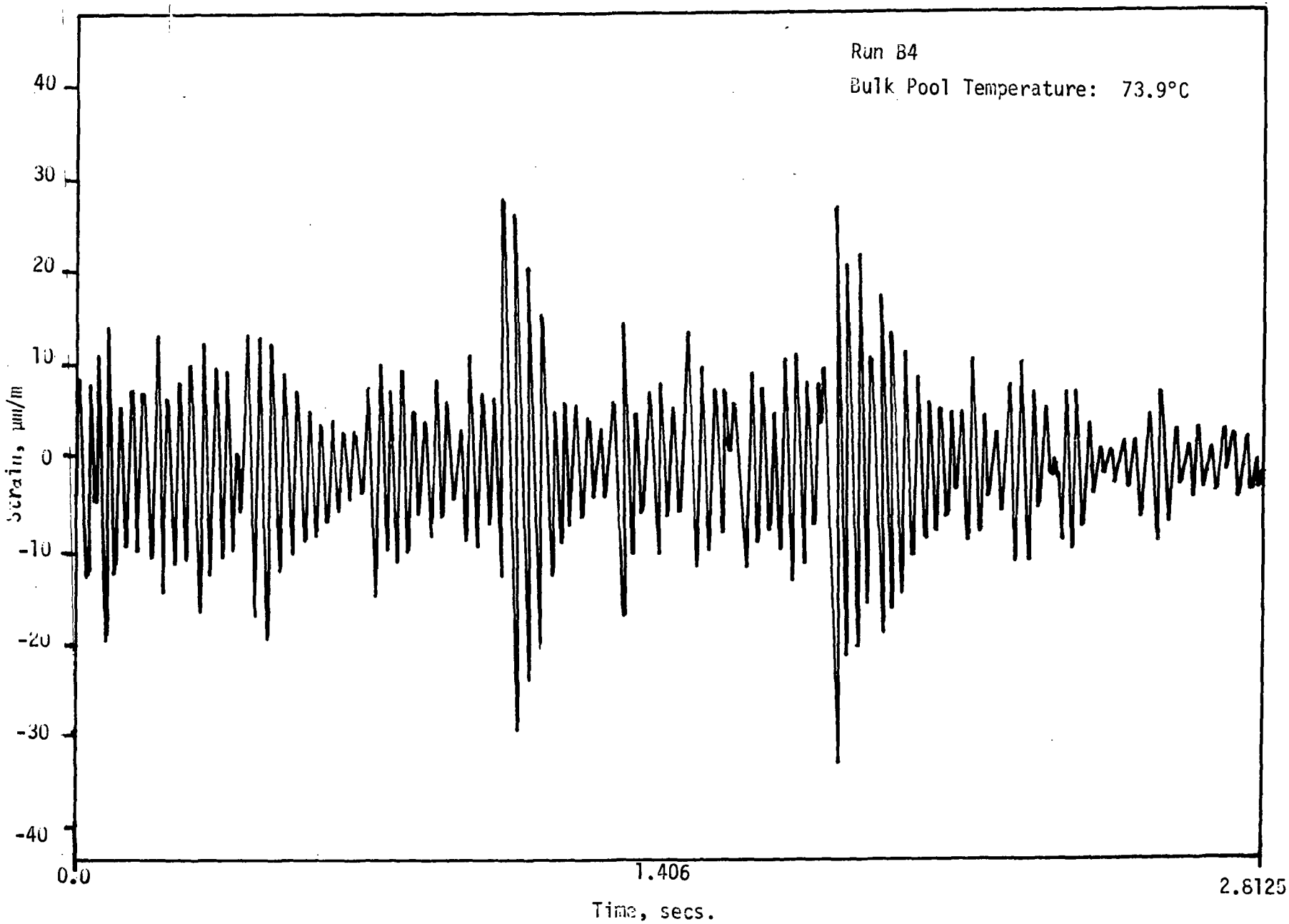

Figure 3.87 Strain (Gauge #1) vs Time for Run B4

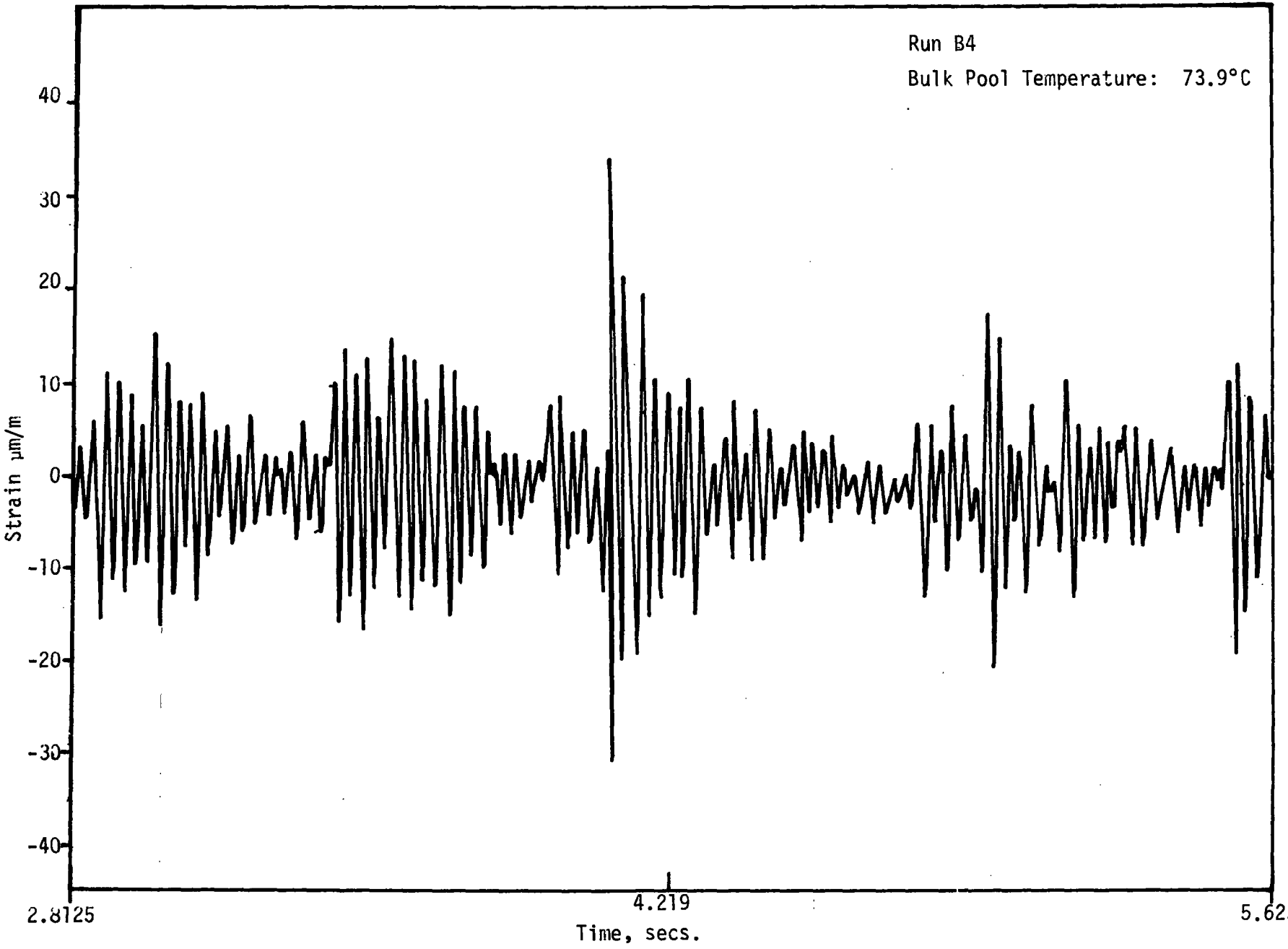

Figure 3.88 Strain (Gauge #1) vs Time for Run B4

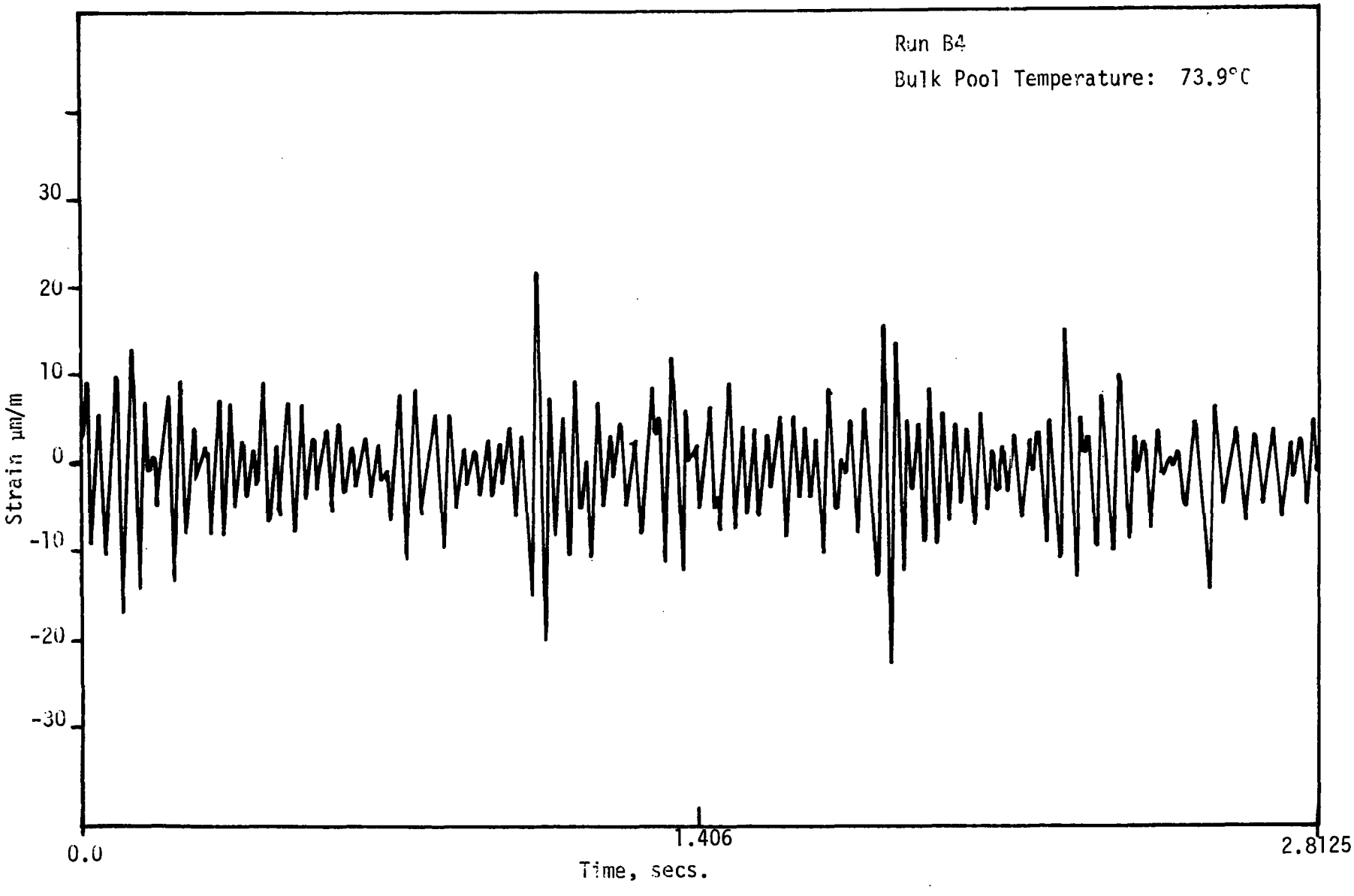

Figure 3.89 Strain (Gage #2) vs Time for Run B4

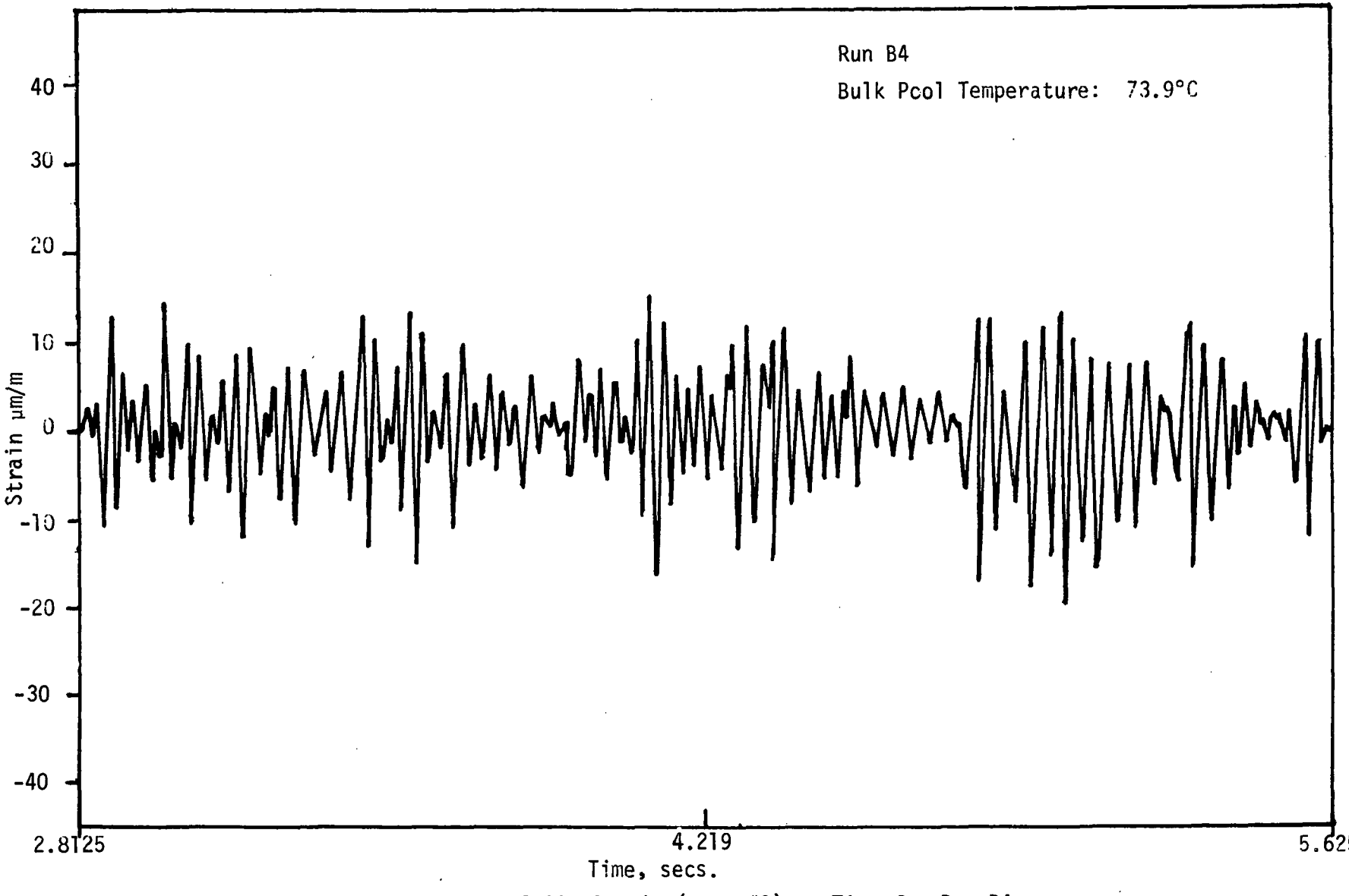

Figure 3.90 Strain (Gage #2) vs Time for Run B4

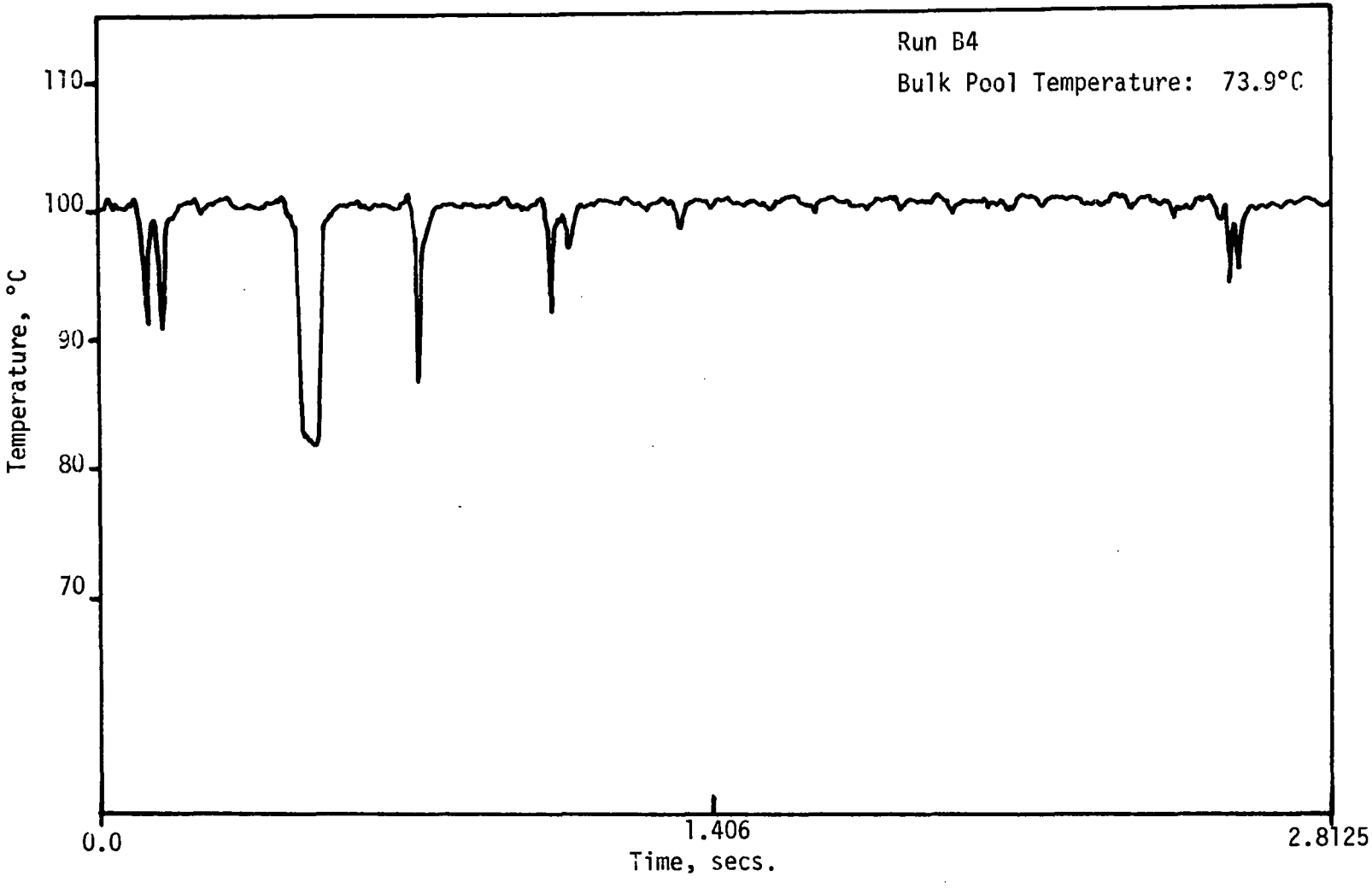

Figure 3.91 Vent Exit Temperature vs Time for Run B4

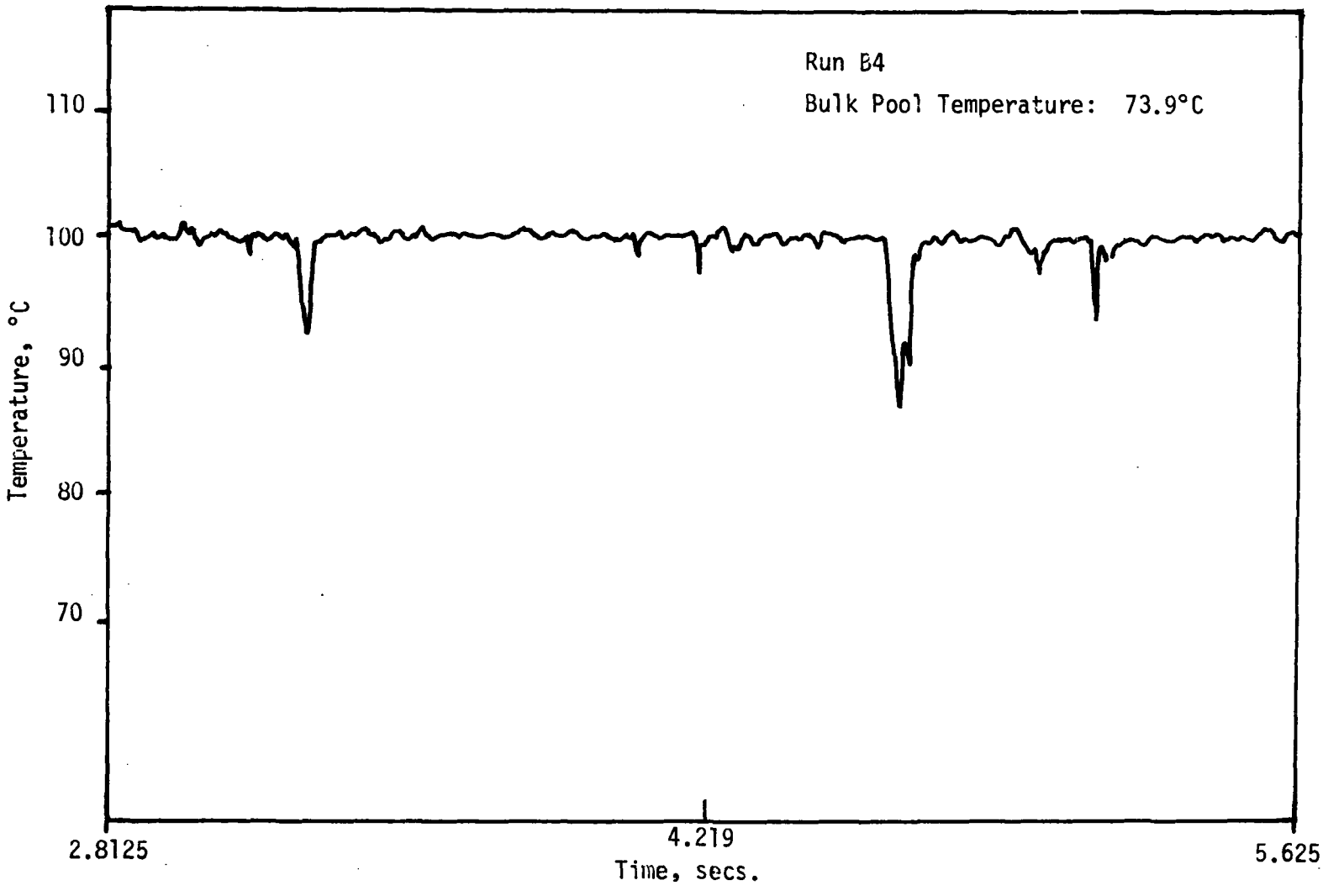

Figure 3.92 Vent Exit Temperature vs Time for Run B4

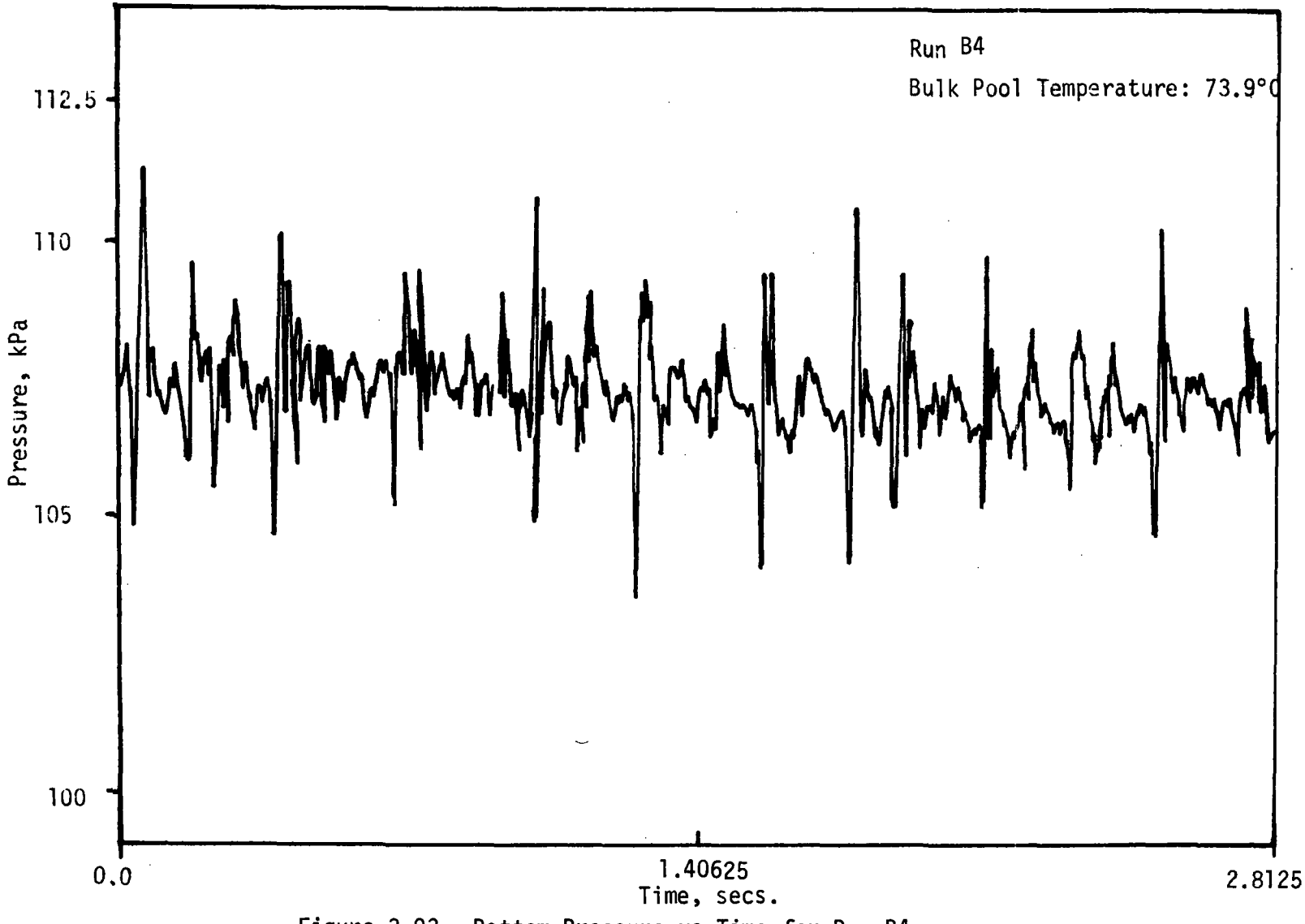

Figure 3.93 Bottom Pressure vs Time for Run B4

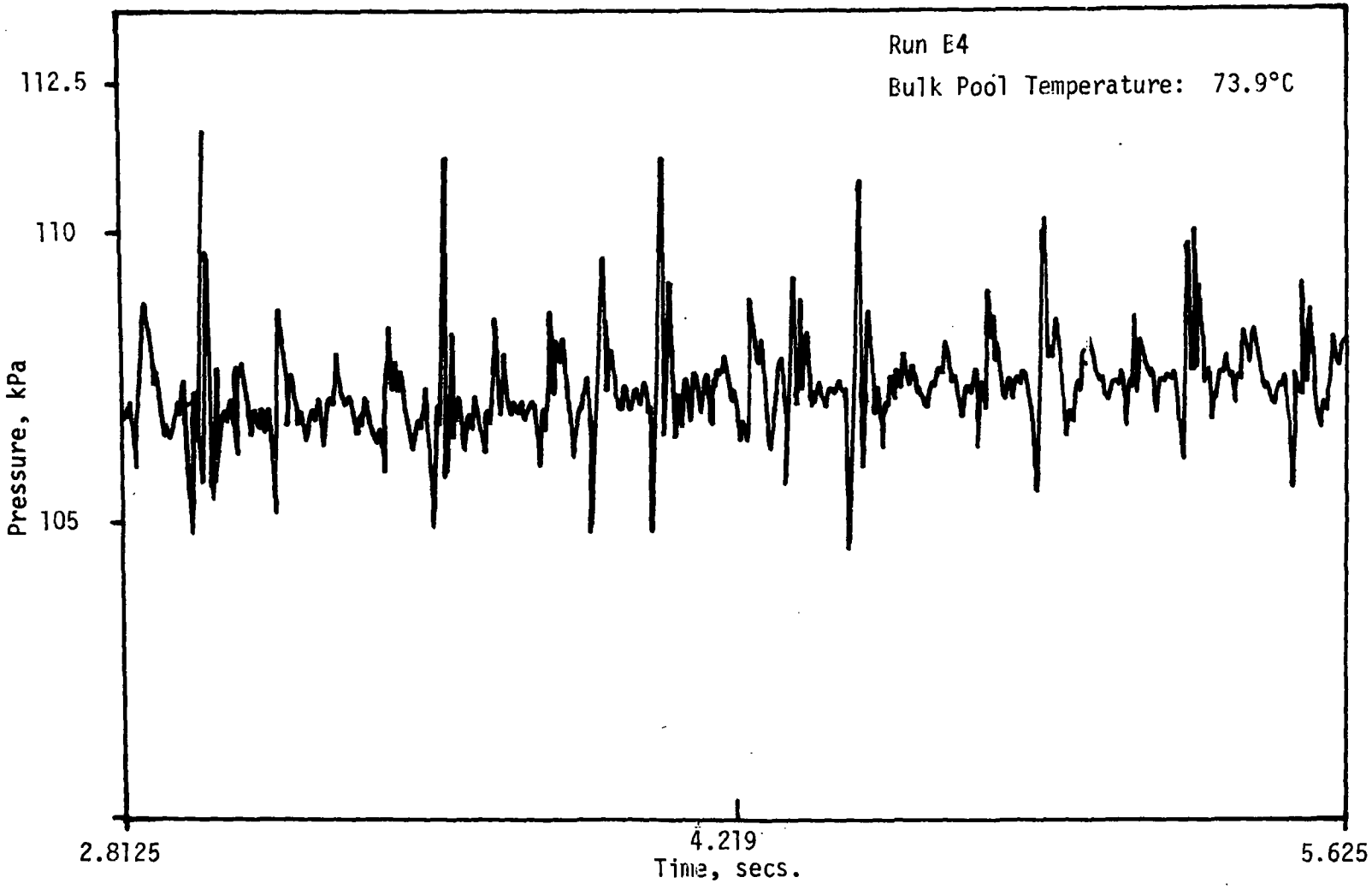

Figure 3.94 Bottom Pressure vs Time for Run B4

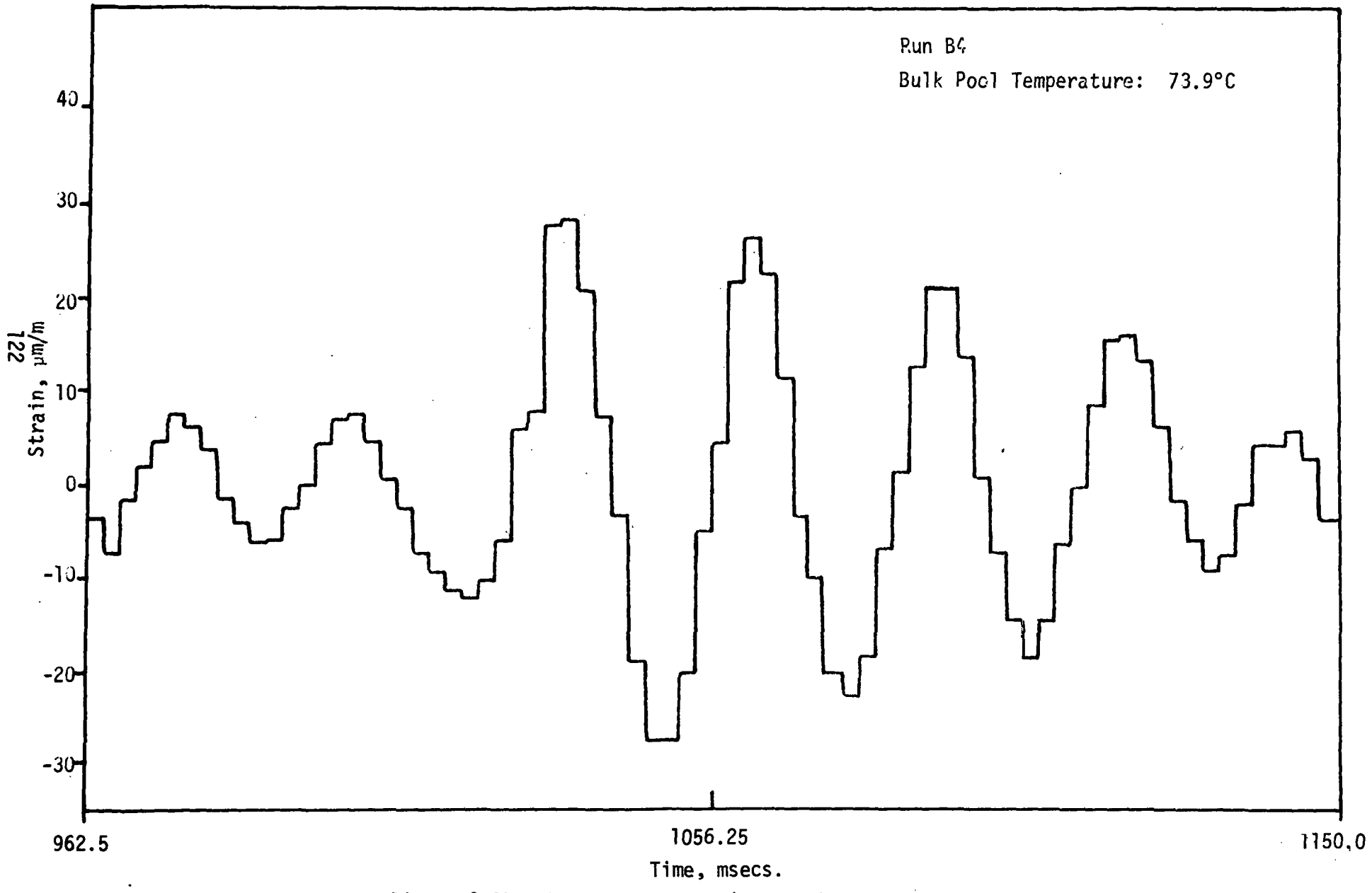

Figure 3.95 Detailed Strain (Gage #1) vs Time for Run B4

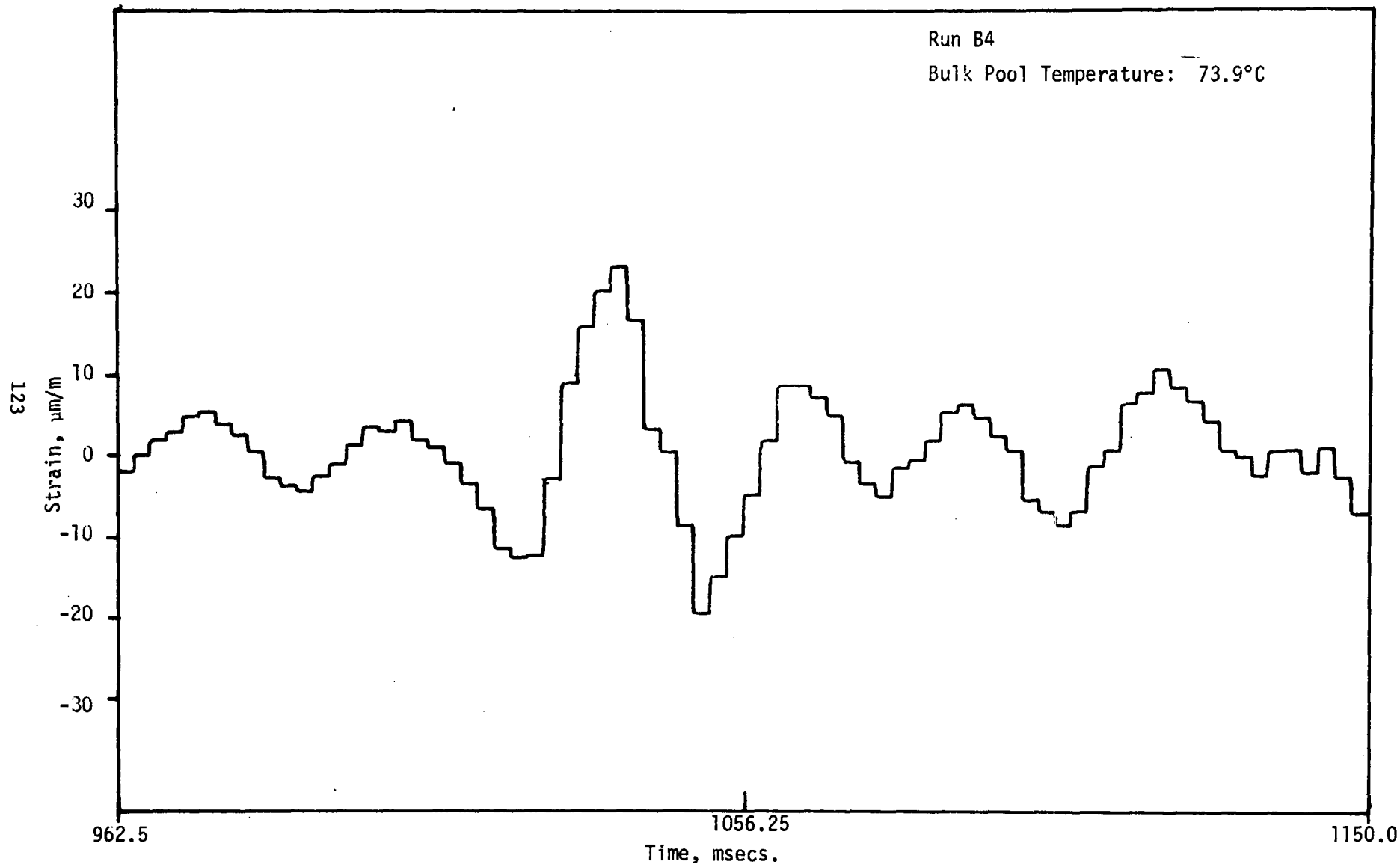

Figure 3.96 Detailed Strain (Gage #2) vs Time for Run B4

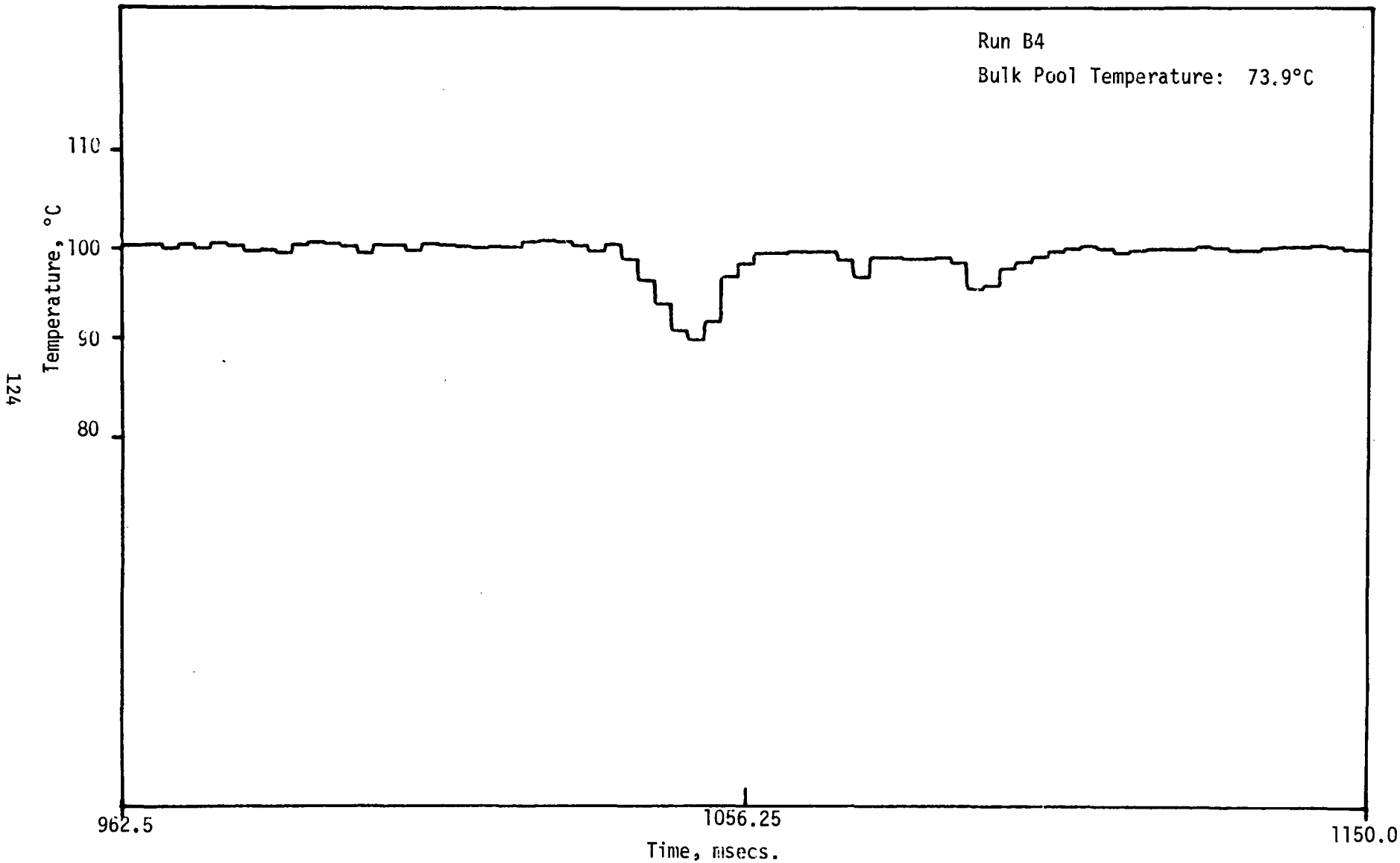

Figure 3.97 Detailed Vent Exit Temperature vs Time for Run B4

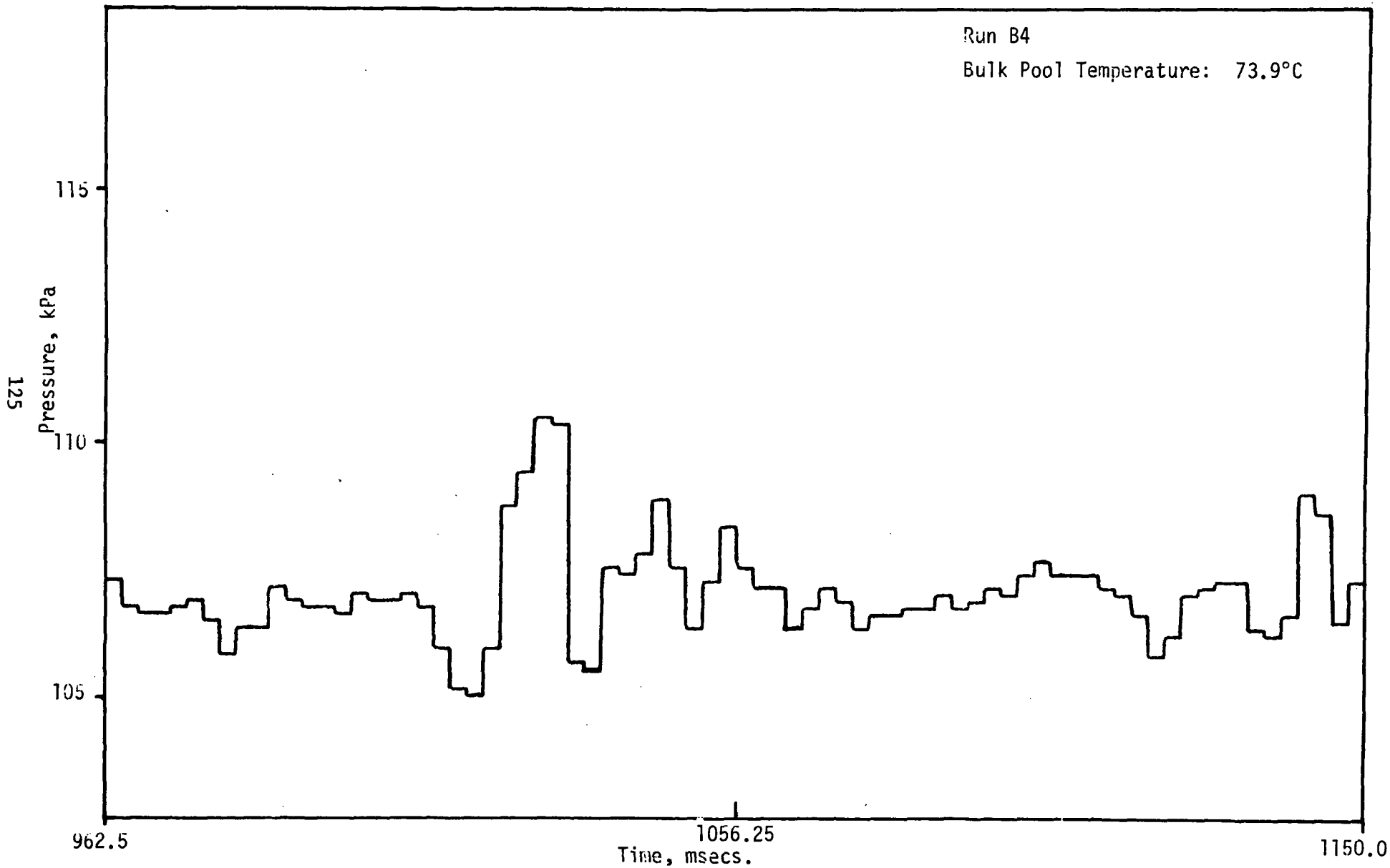

Figure 3.98 Detailed Bottom pressure vs Time for Run B4

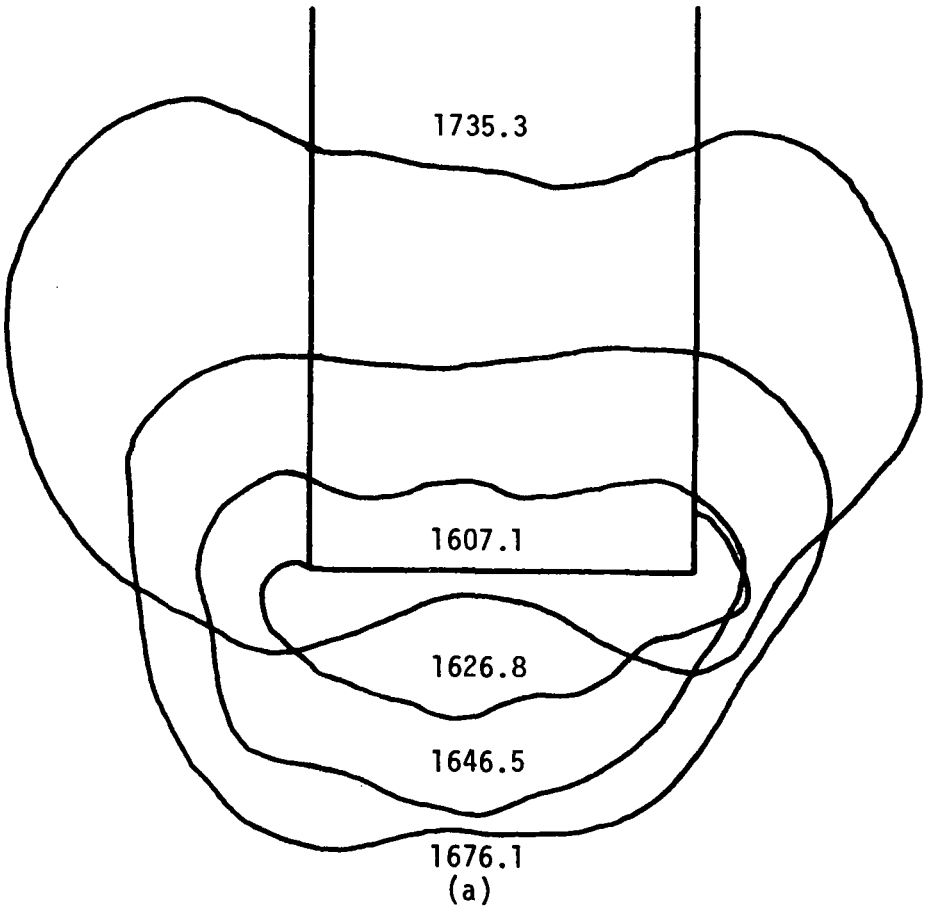

(a)

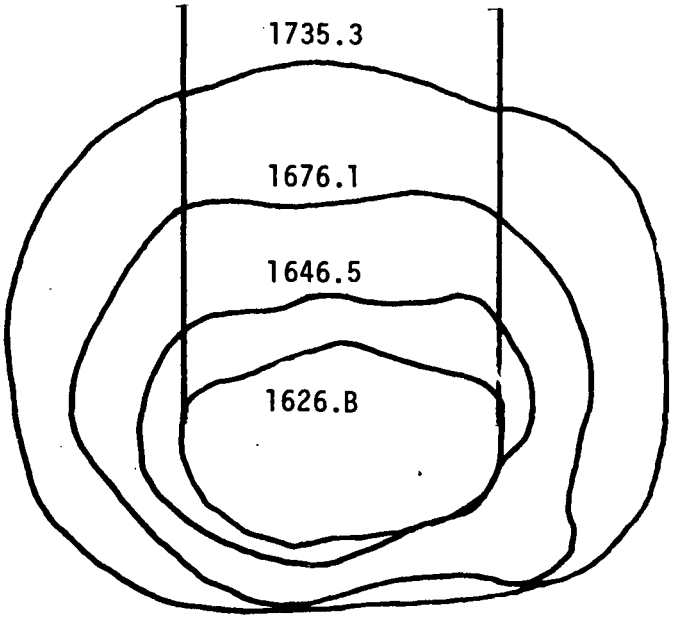

(b)

Figure 3.99 Interfacial History for Run A2

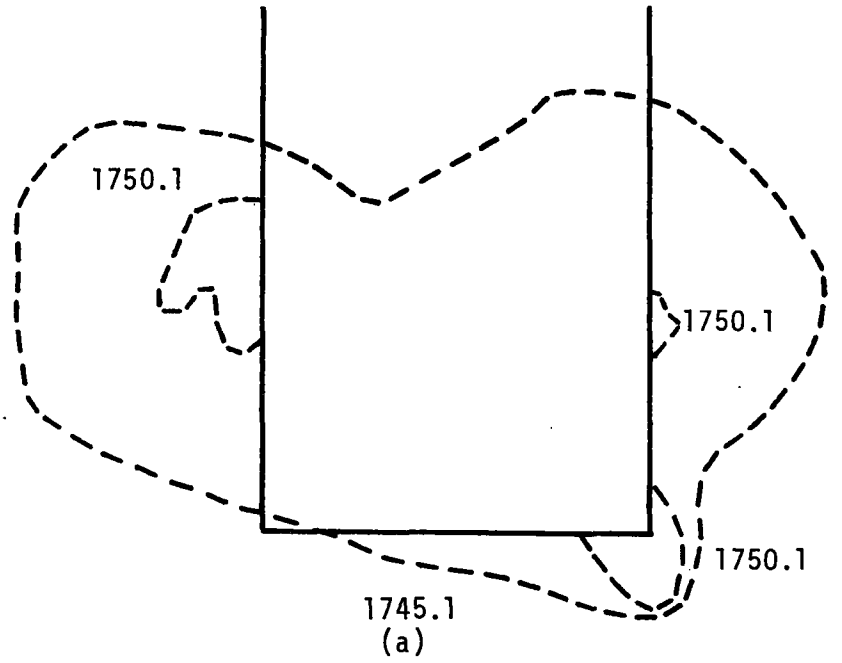

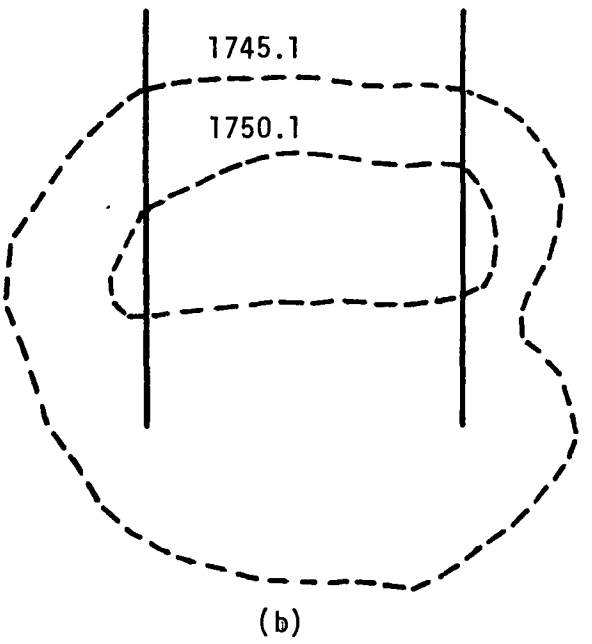

Figure 3.100 Interfacial History for Run A2

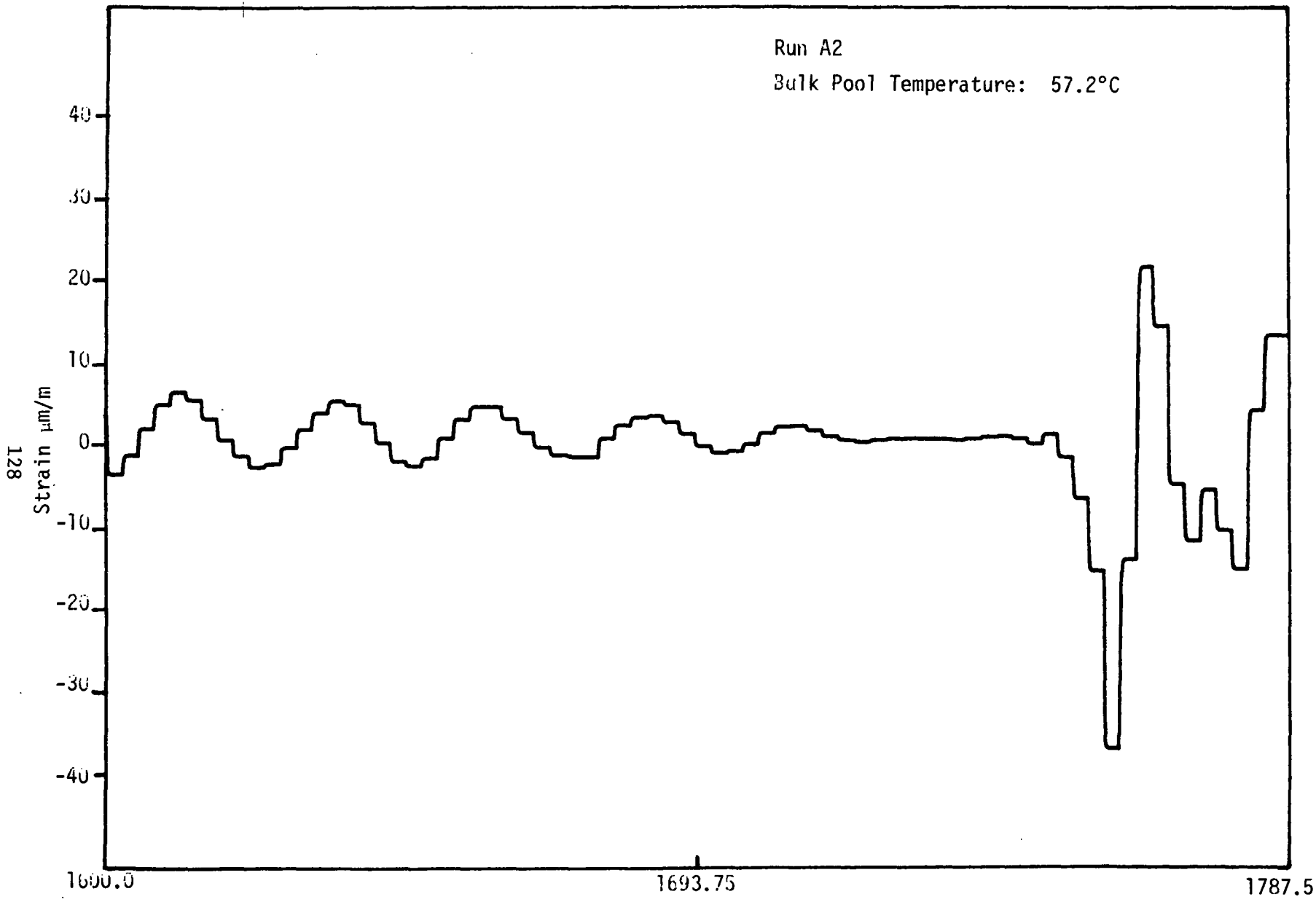

Figure 3.101 Detailed Strain (Gage #1) vs Time for Run A2

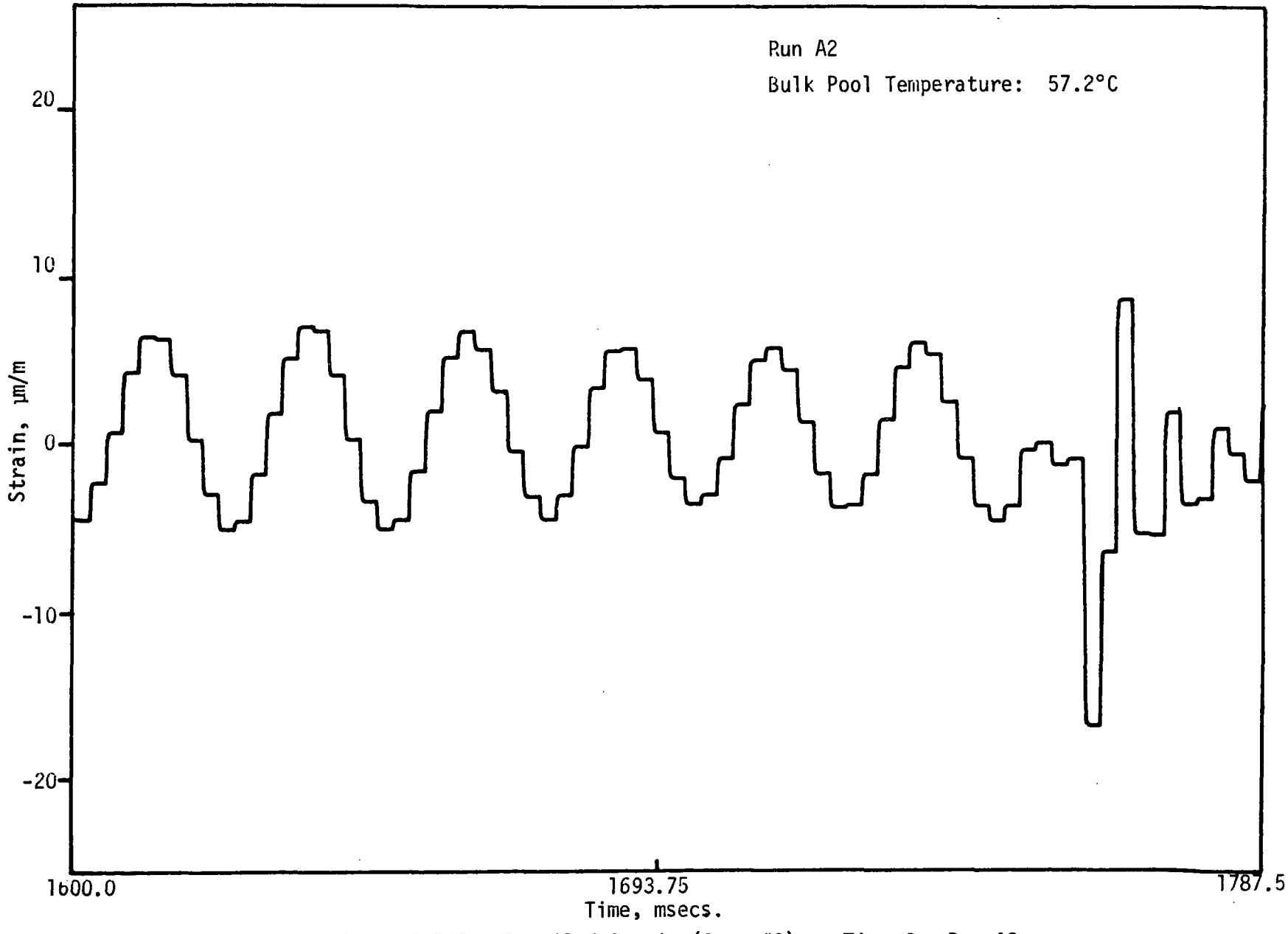

Figure 3.102 Detailed Strain (Gage #2) vs Time for Run A2

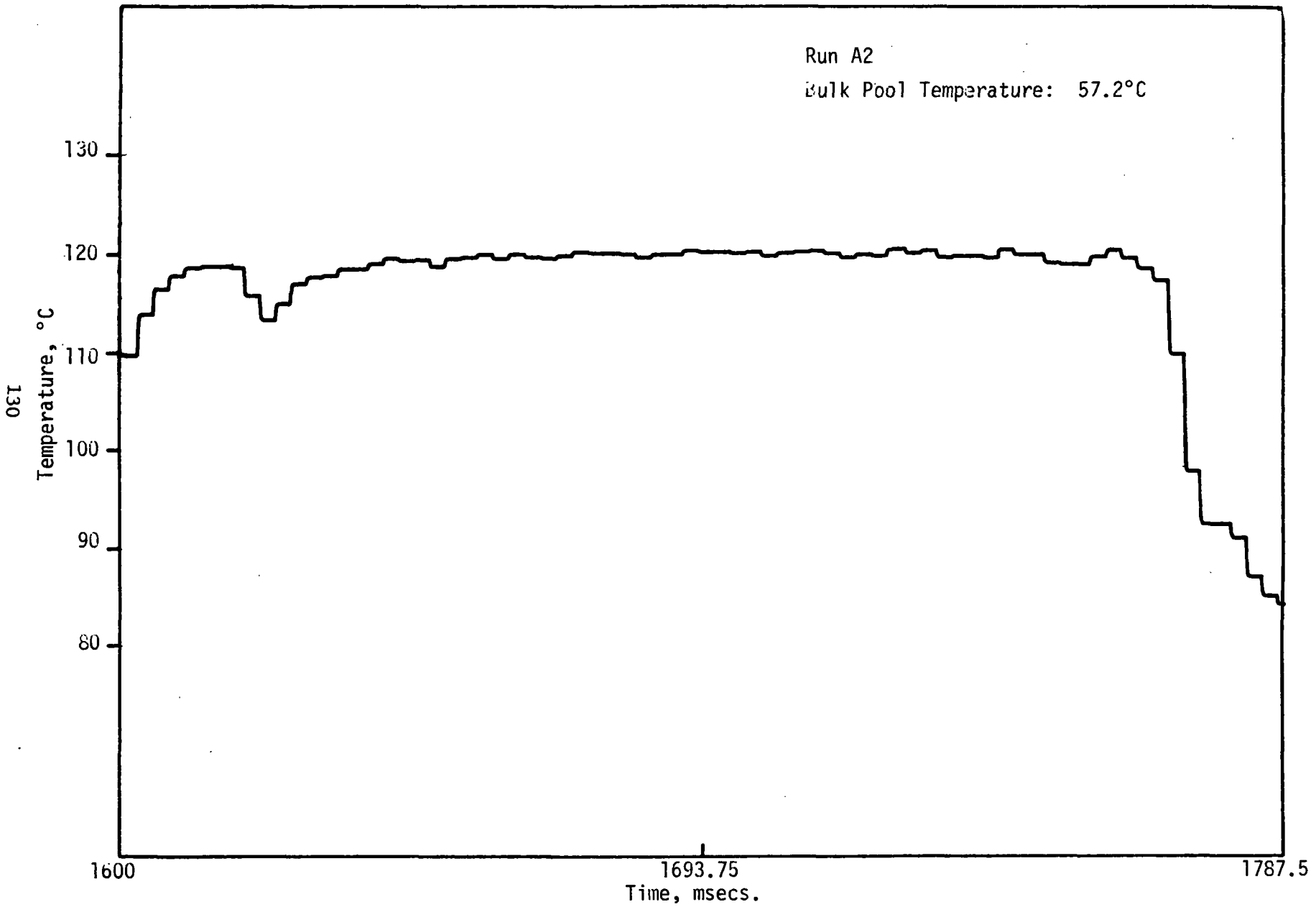

Figure 3.103 Detailed Vent Exit Temperature vs Time for Run A2

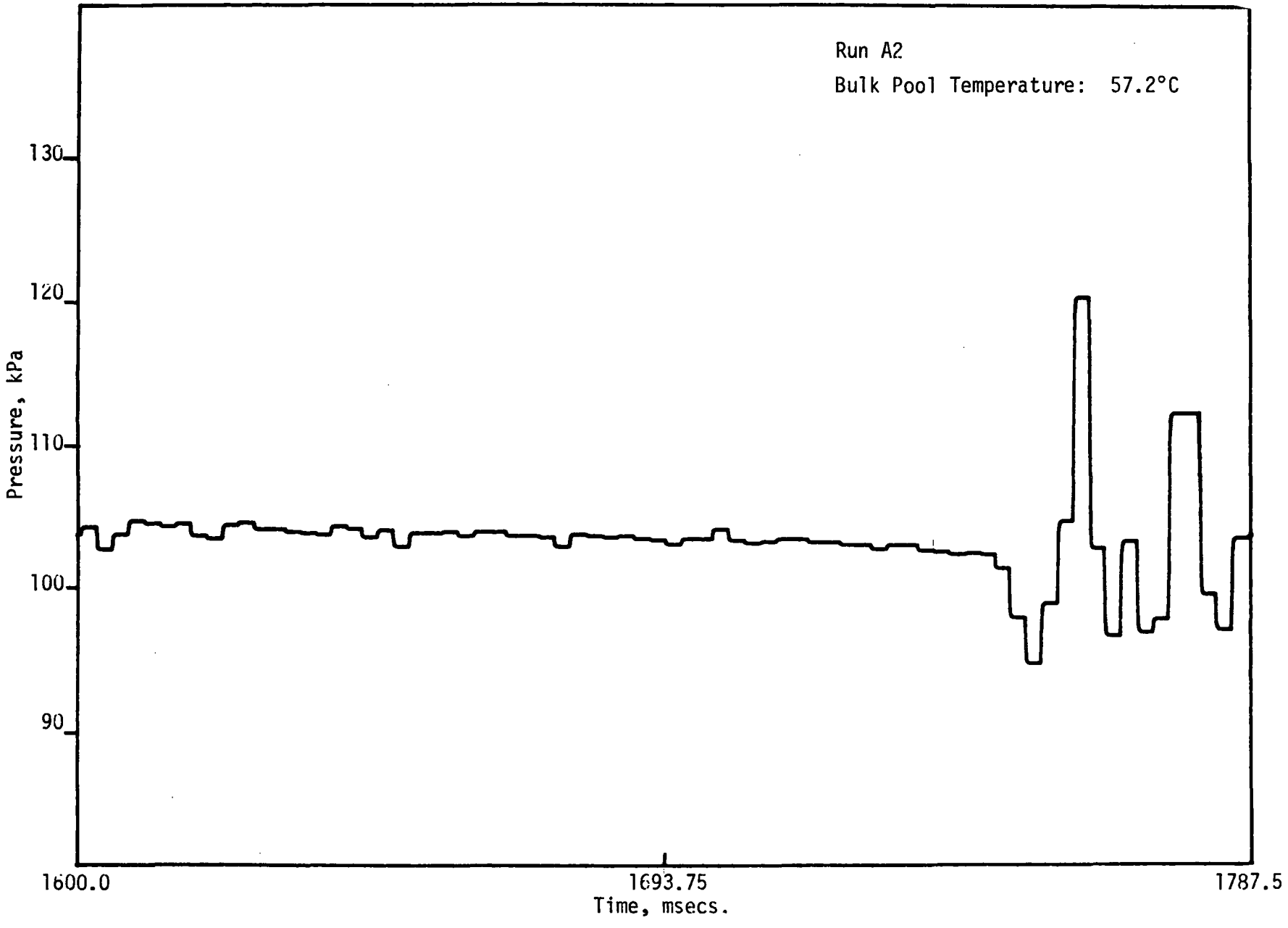

Figure 3.104 Detailed Bottom Pressure vs Time for Run A2

4. CONCLUSIONS

From the experimental results it can be concluded that pressure pulses recorded on the pool bottom, below the vent are generated by three different mechanisms. The first kind is bubble growth and bubble shape changes at the vent exit which generate only small pressure variations, on the order of a tenth of an atmosphere. The second kind is due to bubble collapse at the vent exit which generates large pressure pulses on the order of an atmosphere. The third kind is due to water slug motion inside the vent pipe. The magnitudes are typically a half to a third of an atmosphere. Only the second mechanism, bubble collapse, was seen to impose loading upon the downcommer. The loading was seen to occur simultaneously with the collapse. Bubble shape changes and water slug movement did not significantly affect loading on the downcommer.

From the experimental data it was observed that the magnitude and frequency of pressure were temperature dependent. At low pool temperatures (53.3°C) pressure pulses were characterized by high peaks at low frequencies. Representative peaks were between 115-125 kPa and occurred at a frequency of about 1.5 to 2.0 sec^{-1}. As pool temperature increased, magnitudes of pressure peaks decreased while pressure peak frequency increased. At pool temperatures of 73.9°C pressure peaks had decreased to 104-106 kPa with an increase in peak frequency to over 6.5 sec^{-1}. Unlike pressure pulses strain peaks were found to be nearly independent of pool temperatures. Comparison of the data recorded from the two strain gauges showed some differences in tube loading with respect to pool orientation. However, no preferential direction of injection tube loading was seen when the peak magnitudes of strain were examined.

Finally, the data gathered in this report represents only a small portion of the total possible data which could have been collected durring each experimental run. Data collection was principally constrained by the capacity of the data acquisition system. Equipment and software were not available at experimentation time which would allow for more than 9000 independent data points to be recorded, and a compromise between optimum run time and sample frequency was made. Future experimentation should be directed towards increasing the total data acquisition system capacity. Two purposes would be served. First a higher sampling frequency could be used which would more accurately record the magnitudes of transients durring chugging. Second a longer total run time would be achieved and the statistics of steam chugging could be better analyzed and understood.

REFERENCES

1. C. K. Chan et al., Suppression Pool Dynamics, Annual Report, July 1, 1976 - June 30, 1977, NUREG -0264-3, Feb. 1978.*

2. C. K. Chan et al., Suppression Pool Dynamics,Annual Report, July 1, 1977 - June 30, 1978.

3. E. W. McCauley and J. H. Pitts, Final Air Test Results for the 1/5-Scale Mark-1 Boiling Water Reactor Pressure Suppression Experiment, UCRL-52371, Oct. 31, 1977.

4. NEDO-13435, "Mark III Confirmatory Test Program One-Third Scale Three-Vent Air Test-Test Series 5806," General Electric Company.

5. Sonin, A. A., "MIT Program on Modeling of Pool Swell Hydrodynamics," Notes prepared for the Containment Code Review Group Meeting, Silver Springs, Jan. 6, 1977.

6. Archer, R. R. et al., An Introduction to the Mechanics of Solids, Second Edition, McGraw Hill, New York, 1972.

7. Holman, J. P. and Gajda, W. J. Jr., Experimental Methods for Engineers, Third Edition, McGraw Hill, New York, 1978.

*Available for purchase from the NRC/GPO Sales Program, U.S. Nuclear Regulatory Commission, Washington, DC 20555, and the National Technical Information Service, Springfield, VA 22161.

APPENDIX A

This supplemental section includes data expressed in numerical form collected from the experiments. For each run, the following parameters are given:

1) Bulk Pool Temperature - the average pool water temperature obtained at at the beginning of the run.

2) Approximate Pressure Pulse Frequency - the approximate total number of distinct pressure peaks divided by the entire length of the run.

3) Peak Values of Bottom Pressure and Pipe Strain

Maximum of values of pressure and strain recorded over about a 100 m sec interval after a pressure peak which occurred at the specified time (It should be emphasized that these values are not simultaneous reading observed but represent the largest recorded of each pulse).

Run A1

Bulk Pool Temperature 53.3°C

Approximate Pressure Pulse Frequency 1.42 sec^{-1}

	Peak Bottom Pressure (kPa)		Strain Gauge #1(μm/m)		Strain Gauge #2(μm/m)	
Time (ms)	Max P	Min P	Max ε	Min ε	Max ε	Min ε
535	118.6	97.3	28.13	-16.88	26.37	-34.20
149.75	120.3	97.8	30.88	-47.13	29.80	-27.92
2317.5	108.7	95.5	7.76	-13.79	10.00	-18.96
3135.0	114.1	96.8	12.77	-16.25	22.06	-16.49
4045.0	109.9	98.4	6.36	-8.19	11.13	-11.64
474.25	106.4	99.5	3.31	-1.15	8.25	-5.99
5120.0	109.5	97.6	4.92	-8.19	36.87	-37.17

Table A.1 Peak Bottom Pressure and Pipe Strain for Run A1

Run A2

Bulk Pool Temperature 57.2°C

Approximate Pressure Pulse Frequency 2.48 sec^{-1}

	Peak Bottom Pressure(kPa)		Strain Gauge #1(μm/m)		Strain Gauge #2(μm/m)	
Time (ms)	Max P	Max P	Max ε	Min ε	Max ε	Min ε
37.5	111.5	97.8	22.48	-20.91	38.00	-35.37
630.0	119.7	95.2	22.53	-23.80	22.56	-7.20
1282.5	111.6	98.6	6.15	-4.62	9.25	-7.37
1747.5	120.6	94.8	21.85	-37.84	8.54	-17.12
2382.5	111.7	98.1	5.13	-7.81	16.83	-13.23
3947.5	109.2	98.8	1.50	-3.52	8.79	-10.42
4555.0	117.6	99.0	63.46	-53.03	17.29	-21.68
4985.0	107.4	98.6	14.47	-14.25	11.89	-10.13
5150.0	107.7	100.9	4.54	-4.54	17.29	-17.08
5422.5	105.5	101.8	5.47	-4.28	8.29	-9.17

Table A.2 Peak Bottom Pressure and Pipe Strain for Run A2

Run A3

Bulk Pool Temperature 67.2°C

Approximate Pressure Pulse Frequency 3.38 sec^{-1}

	Peak Bottom Pressure(kPa)		Strain Gauge #1(μm/m)		Strain Gauge #2(μm/m)	
Approx. Time (ms)	Max P	Min P	Max ε	Min ε	Max ε	Min ε
252.5	104.6	100.6	13.02	-13.36	12.01	-12.26
465.0	107.0	100.4	12.01	-1370	26.79	-25.62
960.0	105.5	99.5	8.70	-9.33	18.25	-15.74
1175.0	107.7	100.3	31.77	-33.64	30.01	-33.65
1855.0	108.8	100.8	10.90	-9.33	35.41	-37.67
2950.0	108.7	98.6	18.41	-13.45	18.96	-18.67
3550.0	111.6	101.7	27.23	-24.35	56.00	-53.45
469.25	107.3	101.3	10.94	-11.62	41.48	-36.12

Table A.3 Peak Bottom Pressure and Pipe Strain for Run A3

Run A4

Bulk Pool Temperature 73.9°C

Approximate Pressure Pulse Frequency 6.40 sec^{-1}

	Peak Bottom Pressure (kPa)		Strain Gauge #1 (μm/m)		Strain Gauge #2 (μm/m)	
Approx. Time (ms)	Max P	Min P	Max ε	Min ε	Max ε	Min ε
437.5	112.1	105.0	35.72	-34.28	11.72	-14.81
910.0	108.4	105.5	22.78	-22.48	2.51	-3.04
1037.5	109.2	105.2	17.82	-22.06	3.21	-3.37
1150.0	110.4	105.0	18.45	-18.07	11.11	-10.61
1540.0	108.7	104.5	23.80	-24.26	12.59	-13.08
1947.5	108.3	105.7	15.65	-15.70	15.34	-16.33
2830.0	108.4	105.0	3.86	-2.25	20.24	-23.94
3330.0	108.5	105.0	3.44	-3.31	19.46	-15.67
3690.0	107.5	104.5	10.27	-9.52	11.93	-15.84
4037.5	107.9	104.0	11.88	-12.43	27.07	-28.71
4292.5	107.0	105.2	12.05	-11.41	24.06	-23.04
4542.5	107.9	104.4	32.79	-28.29	22.38	-21.60
4910.0	108.2	105.0	14.51	-13.45	13.00	-12.18
5297.5	109.2	104.5	16.84	-16.50	32.99	-30.69

Table A.4 Peak Bottom Pressure and Pipe Strain for Run A4

Run B1

Bulk Pool Temperature 53.3°C

Approximate Pressure Pulse Frequency 1.96 sec^{-1}

	Peak Bottom Pressure(kPa)		Strain Gauge #2(μm/m)		Strain Gauge #1(μm/m)	
Approx. Time (ms)	Max P	Min P	Max ε	Min ε	Max ε	Min ε
197.5	118.5	100.6	11.20	-9.67	11.70	-10.00
747.5	119.9	98.6	12.36	-37.94	17.69	-18.28
1400.0	115.8	99.0	14.96	-40.75	19.62	-26.53
1960.00	123.5	97.3	12.15	-10.37	9.70	-16.98
2320.0	110.2	79.5	2.31	-6.87	5.16	-2.82
3165.0	111.8	103.0	12.27	-13.8	24.91	-16.31
3397.5	108.6	103.1	3.64	-5.04	11.11	-8.73
3997.5	123.0	97.7	39.18	-39.5	20.03	-19.02
5250.0	114.6	99.9	10.04	-12.44	27.01	-19.81

Table A.5 Peak Bottom Pressure and Strain for Run B1

Run B2

Bulk Pool Temperature 57.2°C

Approximate Pressure Pulse Frequency 2.31 sec^{-1}

	Peak Bottom Pressure(kPa)		Strain Gauge #1(μm/m)		Strain Gauge #2(μm/m)	
Approx. Time (ms)	Max P	Min P	Max ε	Min ε	Max ε	Min ε
2.50	120.8	98.3	45.18	-47.64	17.69	-16.37
235.0	109.5	100.8	5.31	-5.16	1.61	-2.64
972.5	114.2	100.6	33.63	-19.43	13.22	-18.64
1257.5	118.2	103.3	3.16	-2.90	1.05	-3.35
1855.0	110.4	100.2	10.59	-9.03	31.49	-40.62
2232.5	112.8	103.1	3.08	-2.97	3.14	-6.74
2525.0	111.3	103.7	12.63	-10.44	14.96	-14.18
3875.0	109.3	103.5	16.95	-15.87	8.06	-12.32
4015.0	108.4	103.9	8.81	-6.17	4.13	-3.26
4190.0	116.5	98.6	18.95	-21.92	38.97	-29.92
4432.5	112.1	100.8	7.02	-3.94	2.44	-3.39
5065.0	113.1	100.8	30.80	-30.28	18.06	-20.72

Table A.6 Peak Bottom Pressure and Pipe Strain for Run B2

Run B3

Bulk Pool Temperature 67.2°C

Approximate Pressure Pulse Frequency 6.93 sec^{-1}

	Peak Bottom Pressure (kPa)		Strain Gauge #1(μm/m)		Strain Gauge #2 (μm/m)	
Approx. Time (ms)	Max P	Min P	Max ε	Min ε	Max ε	Min ε
105.0	111.8	103.8	9.48	-9.07	39.71	-32.94
315.0	108.4	105.0	10.44	-12.30	15.70	-22.61
565.0	110.2	103.5	7.80	-7.54	9.30	-9.71
800.0	108.3	104.7	4.87	-5.16	10.79	-12.03
1051.5	110.5	103.8	11.44	-7.99	18.84	-17.52
1328.5	109.5	102.0	10.03	-4.96	5.37	-3.80
1647.5	108.2	104.4	14.75	-18.50	10.00	-13.27
1785.0	108.0	106.0	19.99	-17.32	3.02	-12.23
2135.0	108.4	103.3	11.48	-9.33	4.67	-6.86
2360.0	109.2	104.0	7.80	-7.13	11.74	-13.68
2470.0	108.5	105.4	10.07	-11.00	18.10	-15.83
2602.5	109.3	104.5	23.11	-25.19	12.52	-18.68
3897.5	110.8	105.0	8.62	-9.55	14.30	-12.44
4635.0	111.8	104.2	8.36	-5.13	10.83	-7.11
5535.0	109.9	104.6	11.18	-11.59	4.09	-4.96

Table A.7 Peak Bottom Pressure and Pipe Strain for Run B3

Run B4

Bulk Pool Temperature 73.9°C

Approximate Pressure Pulse Frequency 6.60 sec^{-1}

	Peak Bottom Pressure (kPa)		Strain Gauge #1(μm/m)		Strain Gauge #2 (μm/m)	
Approx. Time (ms)	Max P	Min P	Max ε	Min ε	Max ε	Min ε
40.0	111.5	104.8	15.72	-19.17	13.39	-16.45
382.5	110.4	104.8	14.49	-15.53	9.96	-5.95
1012.5	110.7	105.2	29.47	-28.57	22.69	-20.21
1262.5	109.3	103.3	7.84	-7.13	9.09	-6.53
1777.5	110.6	104.4	28.72	-32.88	15.83	-23.56
2522.5	110.2	10.47	5.43	-5.39	7.48	-14.75
2865.0	108.7	105.7	11.96	-14.75	12.23	-12.40
2972.5	111.8	104.8	16.20	-15.61	13.93	-6.86
35325.5	111.5	104.8	16.28	-11.06	12.94	-16.37
4035.0	111.3	104.8	35.49	-24.95	14.22	-10.87
4497.5	111.3	104.6	5.95	-6.24	7.19	-7.23
4925.0	110.2	105.5	18.73	-19.14	10.79	-18.97

Table A.8 Peak Bottom Pressure and Pipe Strain for Run B4

NRC FORM 335 (7-77) U.S. NUCLEAR REGULATORY COMMISSION

BIBLIOGRAPHIC DATA SHEET

1. REPORT NUMBER (Assigned by DDC): NUREG/CR-1631

4. TITLE AND SUBTITLE (Add Volume No., if appropriate): Lateral Loads on Vent Pipe in Steam Chugging

2. (Leave blank)

3. RECIPIENT'S ACCESSION NO.

7. AUTHOR(S): I. Catton, C.K. Chan, V.K. Dhir, T. Risch

9. PERFORMING ORGANIZATION NAME AND MAILING ADDRESS (Include Zip Code)
School of Engineering and Applied Science
University of California, Los Angeles
Los Angeles, CA 90024

5. DATE REPORT COMPLETED: MONTH December, YEAR 1979

DATE REPORT ISSUED: MONTH August, YEAR 1980

6. (Leave blank)

8. (Leave blank)

12. SPONSORING ORGANIZATION NAME AND MAILING ADDRESS (Include Zip Code)
Division of Reactor Safety Research
Office of Nuclear Regulatory Research
U.S. Nuclear Regulatory Commission
Washington, DC 20555

10. PROJECT/TASK/WORK UNIT NO.

11. CONTRACT NO.: FIN B5875

13. TYPE OF REPORT: Final Report

PERIOD COVERED (Inclusive dates)

15. SUPPLEMENTARY NOTES

14. (Leave blank)

16. ABSTRACT (200 words or less)

The quasi-steady injection of steam into a pool of subcooled water was investigated. The resulting phenomenon was studied with emphasis on structural loading on the steam downcomer. From experimental data at a single steam mass flux it was found that pressure pulsations in the pool were temperature dependent. At low pool temperatures pressure pulsations were found to have high magnitudes and occur at low frequencies. At higher pool temperatures smaller, high frequency pressure pulses were observed.

Three types of pressure pulsations were observed to occur within the pool. Pressure pulsations from 1) bubble growth and bubble shape changes 2) bubble collapse and 3) water slug movement within the downcomer were observed and recorded. Loadings on the steam downcomer were seen to be influenced only by bubble collapse and the magnitudes were independent of pool temperature.

17. KEY WORDS AND DOCUMENT ANALYSIS

17a. DESCRIPTORS

17b. IDENTIFIERS/OPEN-ENDED TERMS

18. AVAILABILITY STATEMENT: Unlimited

19. SECURITY CLASS (This report): Unclassified

21. NO. OF PAGES

20. SECURITY CLASS (This page): Unclassified

22. PRICE: $

NRC FORM 335 (7-77)